Modification of pulse starch properties by nanoparticulation and phosphorylation techniques

by

Hongmin Dong

A thesis submitted in partial fulfillment of the requirements for the degree of

Doctor of Philosophy

in

Food Science and Technology

Department of Agricultural, Food and Nutritional Science
University of Alberta

Abstract

The global demand for plant-based protein is fast growing. This has resulted in significant expansion of pulse grain fractionation and value-added processing operations that primarily focus on protein refining. Pulse starches, as the major by-product of those operations, remain underutilized due to shortcomings in their functionalities, especially high retrogradation capacity after aqueous gelatinization. Therefore, modification of pulse starch to improve their properties is important for their wider use in food and industrial applications. This research mainly focused on improving the functionality of pulse starches by the application of nanotechnology and phosphorylation techniques. The objectives were: a) to define a sustainable and cost-efficient protocol for pulse starch nanoparticles (SNPs) preparation, b) to study physicochemical and rheological properties of SNPs produced from pulse starches in comparison to cereal starches, c) to investigate continuous approaches for the production of SNPs and their use in Pickering emulsions, and d) to investigate how phosphorylation, a popular chemical modification technique for starches, would influence the physicochemical and functional properties of pulse starches. The SNPs were prepared for the first time via a combination of ultrasonic-assisted dissolution of starch and subsequent rapid nanoprecipitation by using ethanol as an antisolvent. Different processing parameters were investigated, and an optimum protocol that is suitable to generate the smallest nanoparticles with the least amount of ethanol was identified. The results showed that SNPs from all starches were spherical in shape, where pulse SNPs had smaller and more uniform size than cereal SNPs. Pulse SNPs with higher amylose content showed greater relative crystallinity, enhanced short-range molecular order, and better thermal stability. Rheological studies confirmed that variations in the starch source as well as SNP morphology and thermal stability influence the viscoelastic properties of SNPs as a function of shear rate, frequency and temperature. Finally,

continuous nanoprecipitation techniques such as flash nanoprecipitation (FNP) and microfluidic nanoprecipitation (MNP) were investigated in comparison to batch nanoprecipitation (BNP) in order to demonstrate the potential for scale-up processing of SNPs. Under the same processing conditions, FNP yielded a more uniform spherically shaped SNPs with a particle size of ~100 nm, which was superior to all other techniques investigated. The Pickering emulsion produced using SNPs obtained by FNP had a smaller average droplet size of 3 μm when compared to emulsions produced without SNPs, which had an average size of 200 μm. With respect to phosphorylation of pulse starches and its impact on starch properties, the results indicated that this chemical modification significantly altered the thermal stability, crystallinity, flow behavior and amylase resistance of pulse starches. Overall, this research addresses the significant gap in the literature regarding pulse starch nanoparticulation and chemical modification/phosphorylation, and how these processing techniques would alter the physicochemical properties of native pulse starches. Developing such novel applications to pulse starches by nanoparticulation and chemical modification is expected to enhance the sustainability of the pulse grain processing industry.

Preface

Chapter 3 of this thesis has been submitted to the *Food Hydrocolloids* as Dong, H., Chen, L., Zhang, Q., Gao, J., Vasanthan, T. Effects of processing parameters on the morphology and characteristics of nanoparticles prepared by rapid nanoprecipitation of pea starch. I was responsible for the experimental work, data collection and analysis as well as the manuscript composition. Dr. Thava Vasanthan (supervisory author) assisted with concept formation, scientific discussions and manuscript editing and contributed to the composition. Dr. Qing Zhang and Jun Gao helped with data discussion and manuscript revisions. Dr. Lingyun Chen (University of Alberta) provided insightful experimental planning, manuscript revisions and analysis equipment.

Chapter 4 of this thesis has been submitted to the *Food Hydrocolloids* as Dong, H., Zhang, Q., Gao, J., Chen, L., Vasanthan, T. Production and characterization of nanoparticles from pulse starches by ultrasound-assisted dissolution and rapid nanoprecipitation as comparison with cereal starches. I was responsible for the experimental work, data collection and analysis as well as the manuscript composition. Dr. Thava Vasanthan (supervisory author) assisted with concept formation, scientific discussions and manuscript editing and contributed to the composition. Dr. Qing Zhang and Jun Gao helped with data discussion and manuscript revisions. Dr. Lingyun Chen (University of Alberta) provided insightful experimental planning, manuscript revisions and analysis equipment.

Chapter 5 of this thesis has been published as Dong, H., Zhang, Q., Gao, J., Chen, L., Vasanthan, T. (2021). Comparison of morphology and rheology of starch nanoparticles prepared from pulse and cereal starches by rapid antisolvent nanoprecipitation. *Food Hydrocolloids*, 119, 106828. I was responsible for the experimental work, data collection and analysis as well as the manuscript composition. Dr. Thava Vasanthan (supervisory author) assisted with concept formation, scientific discussions and manuscript editing and contributed to the composition. Dr. Qing Zhang and Jun Gao helped with data discussion and manuscript revisions. Dr. Lingyun Chen (University of Alberta) provided insightful experimental planning, manuscript revisions and analysis equipment.

Chapter 6 of this thesis has been submitted to the *Food Hydrocolloids* as Dong, H., Zhang, Q., Gao, J., Chen, L., Vasanthan, T. Preparation and characterization of nanoparticles from field pea starch by batch versus continuous nanoprecipitation techniques for use in food-grade Pickering emulsions. I was responsible for the experimental work, data collection and analysis as well as the manuscript composition. Dr. Thava Vasanthan (supervisory author) assisted with concept formation, scientific discussions and manuscript editing and contributed to the composition. Dr. Qing Zhang and Jun Gao helped with data discussion and manuscript revisions. Dr. Lingyun Chen (University of Alberta) provided insightful experimental planning, manuscript revisions and analysis equipment.

Chapter 7 of this thesis has been published as Dong, H. & Vasanthan, T. (2020). Effect of phosphorylation techniques on structural, thermal, and pasting properties of pulse starches in comparison with corn starch. *Food Hydrocolloids,* 109, 106078. I was responsible for the experimental work, data collection and analysis as well as the manuscript composition. Dr. Thava

Vasanthan (supervisory author) assisted with concept formation, scientific discussions and manuscript editing and contributed to the composition.

Chapter 8 of this thesis has been published as Dong, H. & Vasanthan, T. (2020). Amylase resistance of corn, faba bean, and field pea starches as influenced by three different phosphorylation (cross-linking) techniques. *Food Hydrocolloids*, 101, 105506. I was responsible for the experimental work, data collection and analysis as well as the manuscript composition. Dr. Thava Vasanthan (supervisory author) assisted with concept formation, scientific discussions and manuscript editing and contributed to the composition.

Acknowledgements

Table of Contents

List of Tables

List of Figures

List of symbols and abbreviations

Å	Angstrom
AFM	Atomic force microscopy
AL	Amorphous lamellae
AM	Amylose
AP	Amylopectin
AR	Amorphous growth ring
AR	Amylase resistance
AS/S	Antisolvent-to-solvent ratio
ATR-FTIR	Attenuated total reflectance-Fourier transform infrared spectroscopy
BNP	Batch nanoprecipitation
CIJM	Confined impinging jet mixer
CL	Chain length
CL	Crystalline lamellae
CNC	Cellulose nanocrystals
CR	Crystalline growth ring
DC	Degree of crosslinking
DLS	Dynamic light scattering
DMSO	Dimethyl sulfoxide
DP	Degree of polymerization
DSC	Differential scanning calorimetry
FACE	Fluorophore-assisted carbohydrate electrophoresis
FB	Faba bean
FE-SEM	Field emission scanning electron microscope
FNP	Flash nanoprecipitation
FP	Field pea
G'	Storage modulus
G''	Loss modulus

G*	Complex modulus
GBSS	Granule bound starch synthase
GOPOD	Glucose oxidase peroxidase
H_2SO_4	Sulfuric acid
H_3PO_4	Phosphoric acid
HCl	Hydrochloric acid
HMT	Heat moisture treatment
HNO_3	Nitric acid
HPAEC	High-performance anion-exchange chromatography
HPSEC	High Performance size exclusion chromatography
MALLS	Multi angle laser light scattering
MNP	Microfluidic nanoprecipitation
M_w	Weight average molecular weight
NaOH	Sodium hydroxide
O/W	Oil-in-water
$POCl_3$	Phosphoryl chloride
PSD	Particle size distribution
RC	Regular corn
RDS	Rapidly digestible starch
RI	Refractive index
RS	Resistant starch
RW	Regular wheat
SDS	Slowly digestible starch
SEM	Scanning electron microscopy
SHM	Staggered herringbone mixer
SNC	Starch nanocrystals
SNP	Starch nanoparticles
STMP	Sodium trimetaphosphate
STPP	Sodium tripolyphosphate

T_c	Conclusion temperature
T_c-T_o	Transition temperature range
TEM	Transmission electron microscopy
TGA	Thermogravimetric analysis
T_o	Onset temperature
T_p	Peak temperature
VSDS	Very slowly digestible starch
W/O	Water-in-oil
XRD	X-ray diffraction
γ	Shear rate
ΔH	Enthalpy of gelatinization
η	Viscosity
η^*	Complex viscosity
Θ	Theta
τ	Shear stress
ω	Angular frequency

Chapter 1: Introduction and objectives

1.1. Introduction

Plant-based protein refining is experiencing significant growth around the world due to rapidly growing consumer interest in plant protein-enriched foods. In many regions of the world, pulses are considered an important source of dietary protein and often represent a necessary supplement to other protein sources. Large quantities of pulse grains (~ 40 million metric tons), including field pea and faba bean, are produced annually worldwide (FAO, 2020). Thus, dry and/or wet processing operations, to produce value-added components from pulses, primarily protein concentrates and isolates, are growing quickly. These operations unavoidably generate bulk amounts of crude starch as by-product (yield > 60%; purity 65-85%) (Tyler and others 1981) that are currently channeled into animal feed or ethanol industries, competing with low priced feed-grade wheat and barley (i.e., ~$180/Mt) (Alberta Pulse Growers 2019). Not only is this dumping practice not economically appealing to the emerging pulse value-added processing industry, but it is also missing an opportunity to realize a greater process value. Considering the relatively higher price of raw materials, where cleaned de-hulled and split pea and faba beans are $250/Mt (Alberta Pulse Growers 2019), and the lack of flexibility in marketing the by-product starch, the pulse fractionation processing operation has become very sensitive to raw-material price fluctuations and to the scale of operation that raise sustainability concerns. Developing new applications for pulse starches is therefore very important to ensure long term sustainability of this growing industry.

Starch is a carbohydrate that exists in plants as micron-sized granules of different shapes. It is composed of two different molecules known as amylose (mostly linear) and amylopectin (highly

branched), both of which are polymers of alpha-D-glucose (Gallant and others 1997). It is extensively used as a food and non-food ingredient due to its renewable and biodegradable nature, vast abundance, and low price. However, starch in its native form has many limitations such as poor solubility, high retrogradation, limited digestibility and poor functional properties. For these reasons, various physical, chemical, and enzymatic modifications have been employed to improve starch properties and functionalities. In most commercial applications, chemical modifications, such as cross-linking and substitution, play a significant role for improving the functional properties of native starches. Over the past decade, research in starch nanotechnology has been gaining momentum in the food and biomaterial industries. Starch nanoparticles (SNPs), produced by both "top-down" and "bottom-up" approaches, have been documented in the literature (Bel Haaj and others 2013; Perez Herrera and others 2016; Dai and others 2018; Jeong and Shin 2018). Isolation of SNPs from native starch granules by selectively hydrolyzing the amorphous regions by enzyme and/or acid in order to concentrate the crystalline regions is regarded as a "top down" approach (Kim and others 2015). The *in vitro* synthesis of SNPs from starch molecules is a "bottom-up" approach. In this approach, the native starch granules are initially solubilized in a solvent by heating techniques (boiling, autoclaving, etc.). Subsequently, smaller particles are formed from the solubilized starch molecules by anti-solvent precipitation, also called as nanoprecipitation. The nanoprecipitation process involves the gradual addition of an anti-solvent (miscible with the solvent) into the solubilized starch solution or vice versa (Chin and others 2011; Martínez Rivas and others 2017; Saari and others 2017). Nanoprecipitation, although a new technique, has become an important strategy for nanoparticle formation in pharmaceutical, agricultural, food and cosmetic industries due to its advantages such as simplicity, cost-efficiency,

ease of scalability, good reproducibility, and the production of particles with a narrow size distribution.

To date, most of the application studies on SNPs have focused on polymer nanocomposites, bioplastics and paper/paper board products (Le Corre and others 2010; Salam and others 2013; Le Corre and Angellier-Coussy 2014). These studies have used SNPs prepared by "top-down" methods from high amylopectin (waxy) corn and potato starches, where only a narrow range of SNPs has shown promising results. This initial success presents both a challenge and an opportunity to improve SNPs working materials and the way they are made, not only for industrial applications, but also for the less investigated areas of food and related applications such as food rheology/texture, packaging, and nutraceutical carrier technologies. The SNPs formation using starches that are non-waxy and contain higher amylose, such as those from pulses through nanoprecipitation, has received scant attention. The relationship between molecular structure and characteristics of SNPs, in particular in amylose-containing starches, is not well understood. Furthermore, very limited information is available with respect to scale up processing of SNPs through continuous nanoprecipitation, although vast amount of research has been conducted for other biopolymers. Moreover, since the chemically modified starch is commercially used, it is important to understand the effect of chemical pre-treatments such as crosslinking and substitution, to pulse starches, and how that would influence the physicochemical characteristics of SNPs. Therefore, before SNPs can be used as an ingredient in different food and industrial applications, more research is needed to determine how the starch source and molecular characteristics of SNPs influence their physicochemical and functional properties. This thesis research is geared towards understanding how variations in the starch molecular composition and botanical origins (pulses vs

cereals) influence SNPs characteristics and thus provide a guideline for selecting the appropriate starch type for a target functionality.

1.2. Research objectives and hypothesis

The overall objective of this thesis was to define a sustainable and cost-efficient protocol for pulse SNPs formation and obtain SNPs with various characteristics by a combination of physical and chemical technologies. Since cereal starches have been widely researched and commercially used in many food and non-food applications, the objective was further extended to compare the properties of pulse SNPs to those of corn and wheat counterparts prepared in the similar manner. This knowledge can lead to new and novel applications for pulse starch in the food industry compared to the use of micro-scale native or modified starch granules. The main objectives of this research are as follows:

<u>Objective 1</u>: To define a sustainable "bottom-up" protocol for the production of pulse SNPs

Hypothesis: The combination of heating/gelatinization and ultrasonication will promote the dissolution of starch molecules; SNPs could be produced using rapid nanoprecipitation of starch with ethanol as the anti-solvent; the size of particles obtained using rapid nanoprecipitation can be affected by changing the process parameters.

Specific objectives: to investigate the effect of dissolution conditions of starch granules (i.e., gelatinization and ultrasonication conditions) on the formation of SNPs; to evaluate the effect of antisolvent-to-solvent (AS/S) ratios and the effect of starch concentration on the formation of SNPs; to determine the effect of addition techniques (i.e. antisolvent to starch solution or vice versa) on the formation of SNPs; to investigate the effect of separation and drying procedures on

the re-dispersibility and stability of SNPs; and to understand the possible mechanisms of the rapid nanoprecipitation process and the formation of SNPs (Chapter 3).

Objective 2: To characterize and compare the physicochemical properties of SNPs produced from pulse and cereal starches

Hypothesis: The molecular characteristics of native starch significantly differ between pulse and cereal starches, which behave differently upon heating and ultrasonication; the different amylose content, molecular characteristics and starch types will influence the formation of SNPs as well as their properties.

Specific objectives: To compare the effect of AS/S ratios and starch concentration on particle size of SNPs produced from native starches of different botanical origins (cereal: corn and wheat, pulse: faba bean and field pea); to investigate the molecular composition and structure of SNPs obtained from pulse and cereal starches; and to compare the morphology, crystalline structure, molecular order, and thermal properties of SNPs obtained from pulse starches to those from cereal starches (Chapter 4).

Objective 3: To compare the rheological properties of SNPs produced from pulse and cereal starches

Hypothesis: The starch source, morphology and molecular characteristics of SNPs will significantly influence the thermal stability of SNPs and their viscosity and viscoelastic behavior in aqueous suspension.

Specific objectives: To compare the temperature effect on particle size of SNPs produced from native starches of different botanical origins (cereal: corn and wheat, pulse: faba bean and field pea); to understand the static and dynamic rheological properties of aqueous SNPs suspensions as a function of shear rate, frequency and temperature (Chapter 5).

Objective 4: To investigate continuous nanoprecipitation technologies for scale-up processing and for their use in Pickering emulsion

Hypothesis: SNPs could be produced using rapid nanoprecipitation of starch with ethanol as the anti-solvent by mixing either starch solution into ethanol or ethanol into starch solution; and thus, SNPs could be produced by mixing starch solution into ethanol simultaneously using continuous micromixers by adjusting starch concentration, AS/S ratio, and flow rate. SNPs can be used to produce Pickering emulsions with a smaller droplet size than emulsions produced from native starch granules of the same botanic source, and thus reduce the creaming tendencies of such emulsions.

Specific objectives: To investigate the optimum levels of starch concentration and AS/S ratio using rapid batch nanoprecipitation (R-BNP) method with rapid injection of anti-solvent and solvent to each other; to evaluate the effect of flow rate on the formation of field pea SNPs using continuous micromixers; to compare the batch process (BNP) to continuous processes (FNP and MNP) for the production and characterization of field pea SNPs; to produce Pickering emulsions using the resultant SNPs (Chapter 6).

Objective 5: To evaluate how food grade chemical modifications influence the functionalities of pulse starch

Hypothesis: Chemical modifications could improve the functionalities of pulse starch, such as thermal stability and amylase resistance.

Specific objectives: To investigate the effects of three different phosphorylations on the structural, thermal, pasting properties and amylase resistance of starch (Chapters 7 and 8).

Chapter 2: Literature review

2.1. Pulse grain composition and fractionation

Pulses are leguminous crops that are harvested for dry grain, thereby excluding crops harvested green when they are used as vegetables such as green peas and green beans (Hoover and others 2010). Other dried legumes used for oil extraction, such as soybean and groundnut, and sowing purpose (i.e., seeds of clover and alfalfa) are not classified as pulses (FAO, 2020). There are thousands of pulse varieties grown worldwide, including dry edible beans, peas, lentils, and chickpeas. Pulse grains are an excellent source of protein, carbohydrates, dietary fiber, vitamins, minerals and phytochemicals. Large number of people in the world consumes pulses as staple food in combination with cereals to meet their protein requirement. Traditional sources of proteins including animal were considered superior both nutritionally and functionally; however, utilizing animals as a source of proteins raised many ethical issues. Moreover, it cannot be continued to be used as a sole source of protein to meet the growing need for proteins due to increasing population. Therefore, interest in pulses due to their high protein content compared to cereal grains is growing. These are the second most consumed food crop after cereals in the world.

Cereal grains are characteristic of a composition which is high in carbohydrates and low in protein, while pulses have a significantly higher protein content. Pulse are composed of carbohydrates, mainly starches (55-65%), proteins (~25%), fiber (2-13%), and lipids (1-4%) and minor amounts of vitamins and minerals (Hall and others 2017). Fig. 2.1 shows FE-SEM images of the pulse flour, faba bean and field pea, where starch is embedded in a protein and fiber matrix. A variety of dry and wet processing technologies for refining starch from plant materials have been developed and currently are being used by the grain processing industry. Dry processing technologies such as
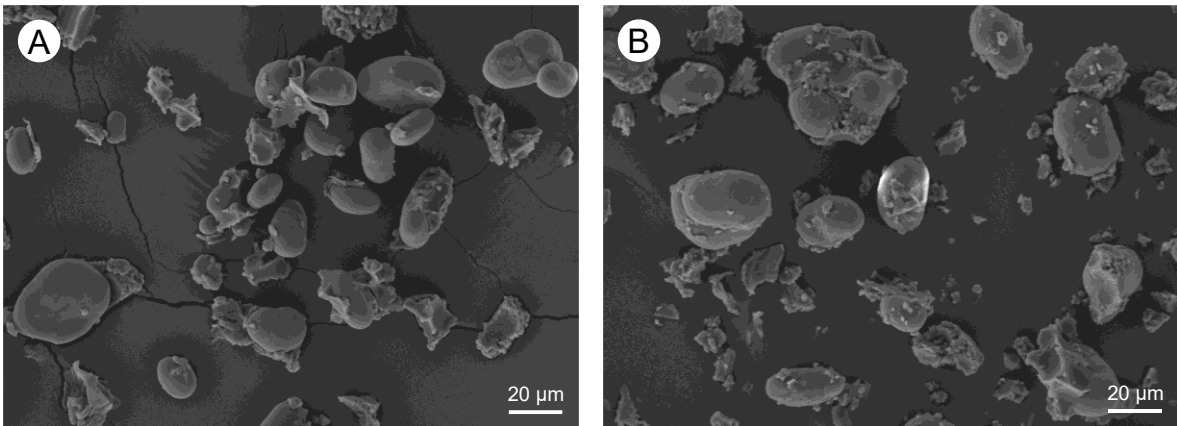
Fig. 2.1 FE-SEM images of the pulse flour: (A) Faba bean; and (B) Field pea.

"milling and sieving" or "milling and air-classification" are relatively robust and cost efficient but result in low purity starch concentrates (less than 75%, dry basis) with inferior functional properties due to contaminants such as dietary fiber, protein and minerals. The term "dry processing" refers to the use of processing steps which do not include the use of water or other solvents. Wet processing technologies yield starch isolates with greater purity (up to 99%, dry basis) and better functional properties. The term "wet processing" refers to the use of processing steps which include the use of water or other solvents such as ethanol. In the wet approach, the dehulled pulse seeds are soaked and then milled in a wet state. The protein in the suspension can be isolated using different methods, such as alkaline extraction-isoelectric precipitation, acid extraction, water extraction, salt extraction-heat precipitation and ultrafiltration. The starch remaining in the suspension can be purified by additional washing to remove protein residue and filtration through a screen of a certain pore size (e.g., 70 μm) to remove fiber residue, which is followed by recovering and drying to obtain isolated starch (Gao and others 2009). The

shortcomings in the wet processing technologies are primarily attributed to a lack of robustness due to fiber hydration and consequent requirement for large volume of water at commercial scale; a lack of process cost efficiency due to multiple processing steps such as high shear mixing, centrifugation, membrane filtration and spray drying; a large capital cost for equipment setup; alkaline and acid chemical usage to improve starch recovery. In the dry milling and air-classification, the dehulled pulse grains are usually milled using a pin mill or impact mill and followed by air classification. The major fraction from the air classification process is the coarser and denser starch-rich fraction which is separated from the finer and lighter protein-rich fraction during the process based on their different densities and particle sizes. However, air classification cannot separate the starch from the protein matrix completely even after repeated milling and air classification. Thus, the purity of pulse starches obtained by air classification is lower than that obtained by wet milling.

2.2. Starch

Starch is a carbohydrate that exists in plants as micron sized granules of different shapes. It is composed of two different molecules known as amylose (mostly linear) and amylopectin (highly branched), both are polymers of alpha-D-glucose (Gallant and others 1997). The unique architecture of these two molecules within the starch granule leads to the semi-crystalline nature of the starch granules (Gallant and others 1997). In addition to amylose and amylopectin, the starch granule contains very small amounts of protein, lipid and phosphorous. Some proteins are only loosely associated with the granule surface, whereas others are firmly bound inside the granules, in the form of enzymes such as granule-bound starch synthase I (GBSSI). Lipids are associated with amylose molecules to form amylose-lipid complexes. Phosphorus is covalently bound to the amylopectin molecules as phosphate monoesters (Pérez and Bertoft 2010). Over the past several

decades, starch chemistry and technology research has made enormous progress toward understanding the native starch granular architecture at the molecular level (Zobel 1988; Baldwin and others 1998; Pérez and Bertoft 2010). Consequently, multiple applications in the food and non-food areas have emerged, mostly focusing on modifying starch by physical, enzymatic and/or chemical means at the granular and molecular levels.

2.2.1. Granule morphology

Starch occurs in the form of granules in cereal and pulse grains (Fig 2.2A-C), as well as in most tubers and roots. These discrete granules have distinct morphology in different plants, ranging from round, oval, ogival or elongated to flat, lenticular or polygonal, and a wide range of sizes (1-100 μm). The starch granules of pulses, such as field pea, are generally oval, kidney and irregular shapes with some grooves on the surface and have sizes in the range of 10-40 μm (Fig. 2.2 A). In some cereals, typically wheat, rye, and barley, granules have a bimodal size distribution with small and large granules; the diameter cut-off being approximately at 10 μm (Naguleswaran and others 2012). For example, wheat starch consists of small round and large lenticular starch granules (Fig. 2.2 B). The granules of corn starches show polygonal, irregular, and spherical shapes (Fig. 2.2 C). The sizes of corn starch granules vary from 5 μm to 20 μm, usually smaller than those of pulse starches. Corn starch granules have pores on their surface, leading to channels to a central cavity in the starch granules (Shrestha and others 2012). Tuber starch granules, such as potato starch, had a characteristic ranging from round (small particles) to ellipsoidal (large particles) in shape with smooth surface (Fig. 2.2 D), and had sizes (10-60 μm) larger than those of pulse starches.
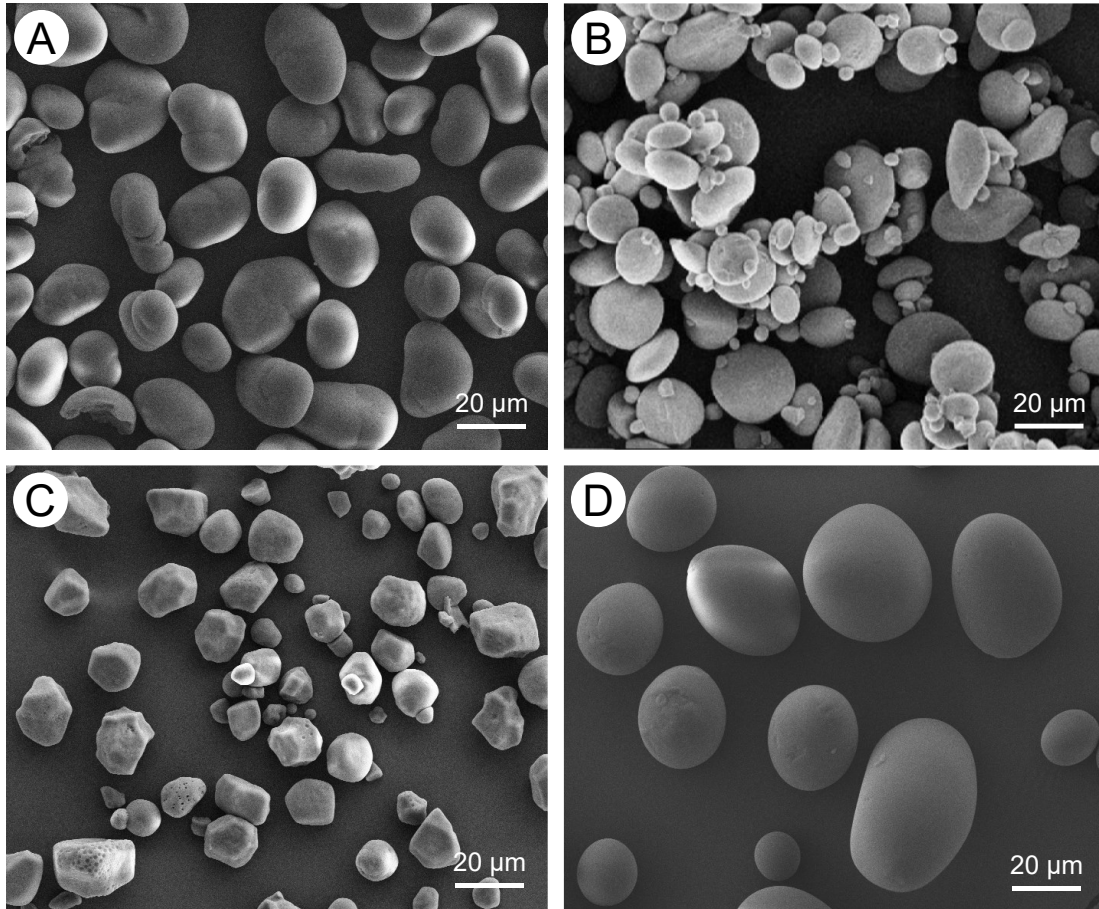
Fig. 2.2 Scanning electron microscopy images of native starch granules from (A) pea, (B) wheat, (C) corn and (D) potato. Image of wheat starch granules is adapted from (Naguleswaran and others 2012), with permission of Elsevier Ltd.

2.2.2. Granule architecture

Hierarchical arrangement of amylopectin and amylose that from the architect the native starch granule structure is presented in Fig. 2.3 (Hizukuri 1986; Pilling and Smith 2003; Pérez and Bertoft 2010). Fig. 2.3A shows the native starch granules (up to100 μm) that represent a unique molecular architecture that is composed of less ordered amorphous growth ring (AR) and highly ordered crystalline growth ring (CR) (Fig. 2.3B) alternatively at different nanoscales. The CR (120-500 nm) is composed of many blocklets (Fig. 2.3C) that are interconnected by amylose molecules (Fig. 2.3D). Amylose molecules are mostly present in the amorphous regions of starch granule as random coil, amylose lipid complex or exist as co-crystalized within amylopectin crystals (Pérez and Bertoft 2010), where the extent of co-crystallization is likely proportional to the amylose content and their degree of polymerization (DP). Each blocklet (20-100 nm) is composed of many amorphous lamellae (AL) and crystalline lamellae (CL) alternatively (Fig. 2.3E). The formation of the CL and AL is primarily attributed to the unique branching structure of amylopectin (Fig. 2.3F) and its cluster model (Hizukuri 1986; Pérez and Bertoft 2010). Intermolecular associations among the shorter chains (A and B1 chains) of amylopectin molecule and consequent double helix formation as well as their packing into unit cells are primarily responsible for the crystallinity of native starch (Hizukuri 1986; Zobel 1988; Pérez and Bertoft 2010). Depending on the variations in the arrangement of double helices in the unit cell, as identified by x-ray crystallographic technique, starch crystals are classified into three types: A-type (present in cereal starches except in high amylose types), B-type (tubers and high amylose cereal starches) and C-type (present in pulses) (Buléon and others 1998). These crystals differ in their molecular and physicochemical properties.

A

*Native starch granules (Diameter = 1-100 μm)

B

*Cross section of a starch granule showing alternative layers of crystalline growth ring (CR) & amorphous growth ring (AR)

C

*Many of the semi-crystalline blocklets form the crystalline growth ring (CR) (Diameter = 120-500 nm)

CR

AR

D

*Blocklets in CR connected by amylose molecules that run through or between blocklets (Blocklet diameter = 20-300 nm)

G

*The unique branching pattern of amylopectin showing long chains (C, B2) and short chains (A, B1)

AL CL AL CL AL CL AL CL

*Cluster model

F

CL CL CL CL

AL AL AL AL

E

*Each blocklet is composed of many Crystalline lamella (CL) & amorphous lamella (AL) alternatively; (CL diameter = 9-12 nm)

Fig. 2.3 The hierarchical arrangement of amylopectin and amylose that from the architect starch granule. (B) Adapted from (Pilling and Smith 2003), with permission of American Society of Plant Biologists. (C, D) Adapted from Perez Herrera and others (2016), with permission of John Wiley and Sons. (G) Adapted from Ball and others (1996), with permission of Elsevier Ltd. (F) Adapted from Pérez and Bertoft (2010), with permission of John Wiley and Sons.

13

2.2.3. Molecular structures of amylose and amylopectin

Amylose and amylopectin are two major components of starch granule. The ratio of amylose and amylopectin varies among starch sources. Regular starches, such as regular corn, wheat, and potato, consist of about 20-30% amylose and 70-80% amylopectin. Waxy starches have around 0-5% amylose, whereas high amylose starches (i.e., ae mutants) contain greater than 40% (Tester and others 2004). Amylose can be considered as a linear molecule with few branches (less than 1%) and long chains with degree of polymerization (DP) varying from 700 to 6500 (Fig. 2.4A). The molecular weight of amylose has been shown to range from 10^5 to 10^6 (Mua and Jackson 1997; Tester and others 2004). Amylose is not stable in aqueous solutions and forms double-helices that readily precipitate. These precipitates are crystallites of the B-polymorph type (Gidley 1989). Single amylose molecules also form helical complexes with iodine, lipids, and different alcohols (Godet and others 1993). These left-handed helices are more compact than the double-helices and crystallizes into V-polymorph pattern (Pérez and Bertoft 2010). X-ray crystallographic result of many starch granules, especially from cereals, show a characteristic peak at 20° 2θ, which is attributed to V type amylose-lipid complexes (Waduge and others 2010). However, it should be noted that the peak near 20° 2θ may not only be attributed to lipid-amylose complexes because it is also found in waxy starches (Varatharajan and others 2010). Generally, amylose is classified into lipid-complexed amylose and free amylose. The well-known blue-color reaction of starch with iodine is due to the amylose-iodine complex and is commonly used to quantitatively measure amylose content in starch. However, lipid-amylose complex interferes with the measurement (particular in cereal starches) and therefore only apparent amylose is detected. To achieve a measurement of the total amylose content, the sample has to be defatted completely. The structure of pulse amylose has not been well characterized.
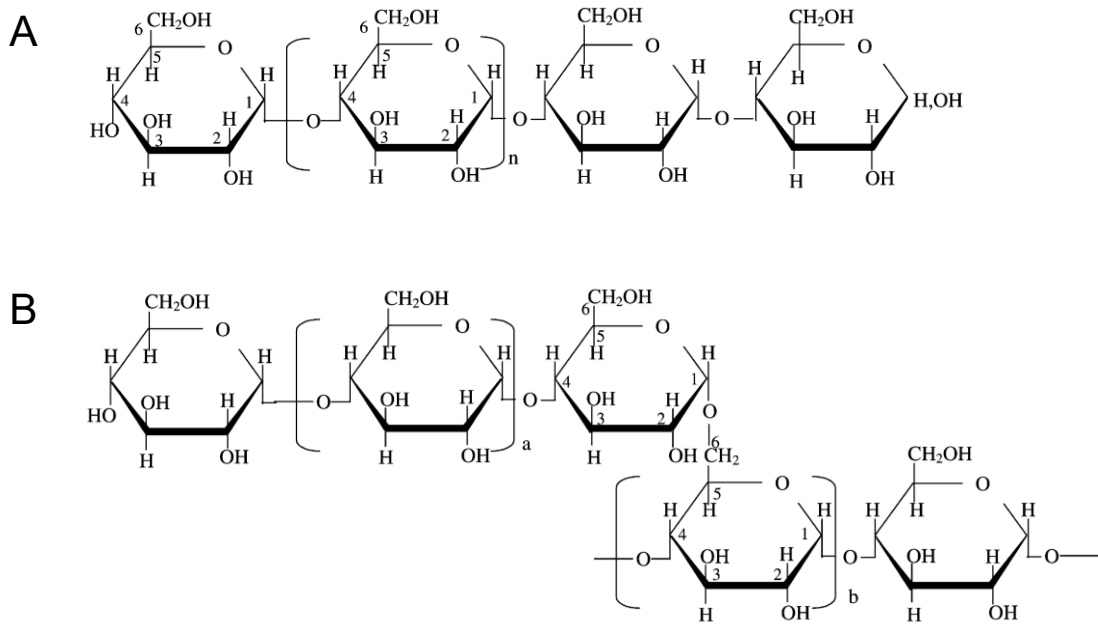
Fig. 2.4 Structure of (A) amylose and (B) amylopectin. Adapted from Tester and others (2004), with the permission of Elsevier Ltd. Amylose: α-(1→4)-glucan; average n=ca.1000. The linear molecule may carry a few long chain branches linked by α-(1→6). Amylopectin: α-(1→6) branching points. For exterior chains, a = ca. 12-23. For interior chains, b = ca. 20-23. Both a and b vary among starch sources.

Amylopectin is the major, highly branched component of all starches with a weight average molecular weight of the order 10^7-10^9 (Hizukuri 1986). Amylopectin consists of α-D glucopyranose units linked by α- (1→4) linkages with a greater proportion (5-6%) of α- (1→6) linkages, which results in a branched molecule (Fig. 2.4B). This branched structure renders amylopectin soluble in cold water. Amylopectin consists of numerous chains that are much shorter than the chain in amyloses. Hizukuri (1986) has classified the amylopectin unit chains as A, B and C (Fig. 2.5). The A-chains are the shortest (DP 6-12) and are linked to other chains (B- or C-) by their reducing ends through α-D-(1→6) linkages. B-chains are classified into B1 (DP 13-24), B2 (DP 25-36), B3 (DP > 36) and even longer chains, which are linked to another B-chains or a C-chain. A-chains are completely external, whereas all B-chains have one external chain (B1) and the rest of the chain is internal. Those most external chains (A and B1) contribute to double helices within the native granules, which are packed into lamellae crystallites. Each amylopectin molecule has only one C-chain, thus the length of the C-chain greatly varies among individual molecules. The size-distribution of the chains can be determined after debranching by either size exclusion chromatography (SEC), high-performance anion-exchange chromatography (HPAEC), or fluorophore-assisted carbohydrate electrophoresis (FACE). The average branch chain length of amylopectin varies with the source and maturity of the starch and the location of molecules in the granule. In general, amylopectin molecules of A-type starches, such as corn and wheat, have both long and short chains that are smaller than those of the B-type starch (i.e., potato starch), and have a larger proportion of the short-chain fractions than that of B-type starch (Table 2.1). C-type starches, such as pulse starches, faba bean, field pea, and lentil consist of mixtures of A- and B-type x-ray patterns and A- and B-type branch chain patterns and have both very long and very short chains. However, there is limited information on the fine structure of amylose and

amylopectin of pulse starches, and therefore, it is difficult to make meaningful comparisons with

the structure of amylose and amylopectin of cereal and tuber starches.
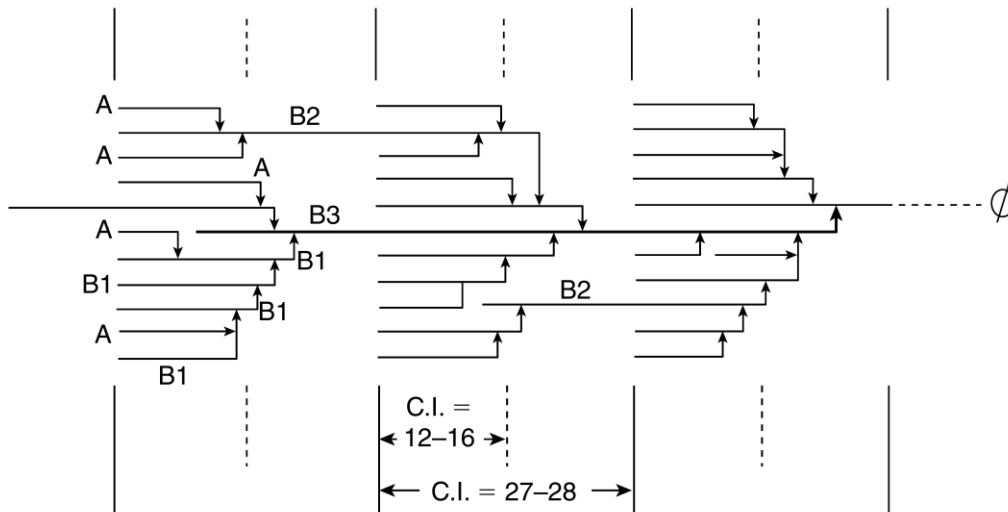
Fig. 2.5 A cluster model of amylopectin proposed by Hizukuri with A, and B1-B3 chains. The chain carrying the reducing end (Ø) is the C chain. Horizontal lines represent (1→4) linkages, perpendicular lines (1→6) linkages. C.I. (chain length). Adapted from Hizukuri (1986), with the permission of Elsevier Ltd.

Table 2.1 Apparent amylose content and amylopectin chain length distribution (%) of starch from different sources.

Starch source	Apparent amylose content (%)	Distribution (%)*			
		DP 6-12	DP 13-24	DP 25-36	DP > 36
Regular corn [a]	21.6-30.0	15.0-31.6	41.3-55.3	12.1-15.5	0-21.4
Wheat [b]	23.0-30.0	19.0-54.0	40.9-50.4	4.5-18.0	0.4-23.4
Potato [c]	22.0-36.0	12.3-23.8	43.3-56.8	15.2-16.6	6.4-28.9
Faba bean [d]	17.0-42.0	19.3-21.7	53.1-56.0	12.8-15.5	9.7-12.1
Field pea [e]	24.0-49.0	16.2-25.4	48.5-59.9	13.1-16.1	9.5-19.4
Lentil [f]	23.5-38.9	22.1-26.9	55.0-58.4	13.6-16.2	9.4-9.9

*DP (Degree of polymerization)

[a] (Jane and others 1999; Wang and Wang 2001; Perera and others 2001; Chung and others 2009; Chung and others 2009; Ai and others 2011; Wang and others 2017; Li and others 2019)

[b] (Jane and others 1999; Franco and others 2002; Ao and Jane 2007; Blazek and Copeland 2008; Singh and others 2009; Gomand and others 2011; Naguleswaran and others 2012; Wang and others 2017)

[c] (Jane and others 1999; McPherson and Jane 1999; Wang and Wang 2001; Guo and others 2019)

[d] (Morrison and Laignelet 1983; Haase and Shi 1991; Gunasekera and others 1999; Ambigaipalan and others 2011; Li and others 2019)

[e] (Ratnayake and others 2001; Huang and others 2007; Chung and others 2008; Chung and others 2010; Li and others 2019)

[f] (Hoover and Ratnayake 2002; Huang and others 2007; Chung and others 2008; Chung and others 2010; Li and others 2019)

2.2.4. Gelatinization and retrogradation characteristics

Native starch granules are insoluble in cold water due to their compact and semicrystalline structure. However, starch, when heated in excess water, undergoes an order–disorder phase transition called gelatinization where starch solubilization takes place. A number of techniques, including differential scanning calorimetry (DSC), X-ray diffraction (XRD), Fourier transform infrared spectroscopy, light scattering, and optical microscopy have been used to analyze the phase transition and structural changes during gelatinization. A summary of the phase transition resulting during starch gelatinization in the presence of excess water has been shown in Fig. 2.6 based on the observation from previous studies (Donovan 1979; Hoover and Hadziyev 1981; Waigh and others 2000; Iida and others 2008). The scheme is as follows: the diffusion of water into the granule, water absorption by the amorphous region, hydration and swelling of the starch granules upon heating, loss of crystalline order, dissociation of double helices, loss of birefringence, disruption of the granule and amylose leaching. Once the contents are released, the granular surface, often called granular ghosts, collapses, and frequently remains intact in solution. The gelatinization transition temperature [onset temperature (T_o), peak temperature (T_p), conclusion temperature (T_c)] and enthalpy of gelatinization(ΔH) have been found to be influenced by the molecular architecture of crystalline region rather than the proportion of the crystalline region (i.e., amylose to amylopectin ratio). In general, for regular starches, the A-type polymorph, such as corn and wheat starch, melt at a higher temperature than the B-type (i.e. potato) which means the A-type polymorph has greater crystalline stability than the B-type (Fannon and others 2004; Cai and others 2014). According to previous research, in the granules of C-type pulse starches, such as pea starch, the B-type polymorphs are located in the inner layer of starch granules and surrounded by the A-type polymorphs (Bogracheva and others 1998). During the heating in an aqueous medium, the

19

gelatinization of C-type pulse starch granules is initiated from the central hilum area, and the B-type polymorphs are melted at a substantially lower temperature range than the A-type polymorphs because of the loose packing of the former type (Jane and others 1999). Therefore, C-type pulse starches show relatively lower gelatinization temperatures compared with the A-type cereal starches (Li and others 2019). However, the crystalline stability of starch granules cannot be only predicted based on the polymorphic pattern, because the packing of the double helices in the crystalline lamellae is influenced by the nature of the branching pattern (distance between the branching points and number of chains in the building blocks) and the chain length. In addition to the crystalline structure, other factors that have been shown to affect the gelatinization parameters are the lipid and phosphorus contents, as well as starch damage.
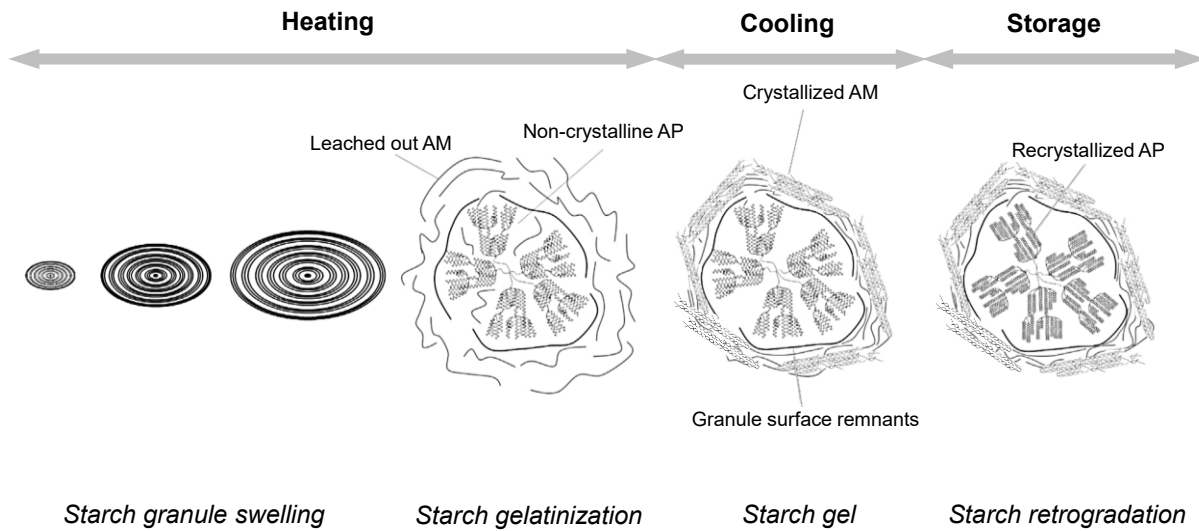
Fig. 2.6 Schematic representation of changes that occur in a starch-water mixture during heating, cooling and storage. AM (amylose), AP (amylopectin). Adapted from Joye (2019), with the permission of Elsevier Ltd.

Upon cooling and storage of a gelatinized starch paste, the starch chains (amylose and amylopectin) reassociate through hydrogen bonding, leading to the formation of a more ordered structure. These molecular reassociations are called retrogradation. Since linear amylose chains can reassociate at a faster rate than the highly branched amylopectin molecules, starch with higher amylose content (i.e., pulses) has generally been associated with a greater retrogradation tendency. Research has shown that starches with longer amylopectin chains retrograde more quickly than those with short chains (Silverio and others 2000). During storage, retrogradation alters the molecular order, crystallinity, gel strength, and the gel network. In general, the degree of retrogradation is time and temperature dependent and vary depending on the starch source and composition. Retrograded starch exhibits a B-type crystalline pattern (Hoover 1995). Retrograded amylose molecules melt at higher temperatures between 130-160 °C, whereas retrograded amylopectin molecules melt at lower transition temperatures than their native counterpart (Eerlingen and Delcour 1995).

2.3. Starch nanoparticles

Starch has attracted extensive attention in various applications due to its renewable and biodegradable nature, vast abundance, and cheap price. However, starch in its native form has many limitations such as poor solubility, retrogradation, and poor functional properties. For this reason, various physical, chemical, and enzymatic modifications have been employed to improve starch properties and functionality. Currently, research in starch nanotechnology is suggesting that more diversity and predictable outcomes and utilities can be achieved by manipulating crystalline/amorphous structures of native starch granules and solubilized starch molecules at nanoscale (Kim and others 2008; Le Corre and Angellier-Coussy 2014; Kim and others 2015). Nanoparticles refer to particles that have at least one dimension smaller than 1000 nm but are larger than a single molecule or atom. However, the size range varies with the material source and

is not universally applicable. Because of the extremely small size, light weight, large surface area, low cost, abundance, renewability and biodegradability, starch-based nanoparticles have attracted a lot of attention in various applications, including biodegradable composites, bioplastics and paper/paper board products, hydrogels, aerogels, emulsion stabilization, fat replacement and drug delivery (Salam and others 2013; Li and others 2014; Kim and others 2015; Chen and others 2019).

The terms, starch nanocrystals (SNCs) and starch nanoparticles (SNPs), are used interchangeably in the literature. However, it is important to note that a structural difference exists between these two. SNCs are defined as the crystalline nano-blocklets resulting from the disruption of the amorphous and semi-crystalline structure of starch granules by acid hydrolysis, whereas SNPs are defined based on size and structure include amorphous material, however neither SNC nor SNPs are 100% crystalline (Angellier-Coussy and others 2009). The structural difference and ultimately the size of the particle is primarily due to the degree of acid hydrolysis, or due to the processing methods. For these reasons, the term, SNPs, is chosen here based on size and must define the degree and nature of the crystallinity specifically for each type of SNPs. In this literature review, the terms SNC and SNPs will be used according to how they were presented by the original authors and may in some cases be used interchangeably.

To date, the production of SNCs using acid hydrolysis has been reviewed (Le Corre and others 2010; Lin and others 2012; Dufresne 2014), with a focus on the preparation of SNC using different acid hydrolysis conditions, chemical modifications, their characterization, and applications. More recently, different methods for preparing SNPs have been reviewed (Kim and others 2015; Sun 2018). The authors also describe the physicochemical characteristics of SNPs and their potential

use in food and biomedical applications. Most of the application studies on SNPs have been focused on polymer nanocomposites, bioplastics and paper/paper board products (Le Corre and others 2010; Salam and others 2013; Le Corre and Angellier-Coussy 2014).

These studies have used SNCs prepared by acid hydrolysis from high amylopectin (waxy) corn and potato starches , where only a narrow range of SNPs has shown promising results. This initial success presents both a challenge and an opportunity to improve SNPs working materials and the way they are made, not only for industrial applications, but also for the less investigated areas of food and related applications such as food rheology/texture, packaging, nutraceutical carrier technologies, etc. The SNPs formation using starches that are non-waxy and contain higher amylose such as those from pulses through nanoprecipitation has received scant attention.

In this section, the preparation of nanoparticles from starch was discussed in detail, which can be classified into "top-down" (i.e., acid hydrolysis, ultrasonication, high-pressure homogenization, etc.) and "bottom-up" (i.e., self-assembly, nanoprecipitation, microemulsion) approaches. The characterization of nanoparticles using morphology, particle size distribution (PSD), long-range crystalline and short-range molecular order, molecular structure and composition, and physicochemical properties in terms of starch source and processing methods were discussed. Finally, the potential utilization of SNPs in the fields of nanocomposites, as emulsion stabilizer, and as delivery carriers was discussed based on their characteristics.

2.3.1. Preparation methods

SNPs have been prepared through both "top-down" and "bottom-up" approaches (Bel Haaj and others 2013; Perez Herrera and others 2016; Qiu and others 2016; Dai and others 2018; Jeong and Shin 2018). In "top down" approach, SNPs can be produced from native starch granules through

various techniques including hydrolysis by enzyme and/or acid, mechanical treatments using high-pressure homogenization, irradiation, and ultrasonication. The *in vitro* synthesis of SNPs from dissolved starch molecules or linear chains is a "bottom-up" approach, such as self-assembly and nanoprecipitation. Currently, the commonly used method for the isolation of SNC and SNPs is the acid hydrolysis process, however, this method lacks cost efficiency and sustainability, where acid is used with longer treatment times and achieves a low yield (<15%) of SNPs. Also large volumes of water are required to wash away the acid. Recently, new technologies and environmental awareness have led to the rise of enzymatic and physical techniques such as ultrasonication, high-pressure homogenization, nanoprecipitation, enzyme debranching with a controlled recrystallization and microemulsion. These methods have the advantage of producing higher yields of SNPs (up to 90%) with little to no waste compared to acid hydrolysis.

2.3.1.1. Top-down approach

During acid hydrolysis, the nanoscale crystalline lamellae of amylopectin are resistant to acid hydrolysis and are concentrated by selective hydrolysis of the amorphous region. Thus, according to starch granular architecture discussed earlier (Fig. 2.3), SNPs produced by acid hydrolysis could be a group of few blocklets, a single blocklet or a portion of a blocklet. Currently, SNCs are usually produced by treating starch slurry with diluted HCl or H_2SO_4 at 25-55 °C for a long period (5-40 days). Fig. 2.7 shows the transmission electron micrographs (TEM) of SNCs obtained from waxy maize starch by HCl and H_2SO_4 hydrolysis, respectively (Putaux and others 2003; Angellier and others 2004). SNCs were composed of 5-7 nm thick nanoplatelets with 60-65° acute angles a length of 20-40 nm and a width of 15-30 nm. TEM observations confirmed the presence of the crystalline lamellae and individual platelets which separated after hydrolyzing the amylopectin

branching points. LeCorre and others (2011) investigated the influence of the botanic origin and

amylose
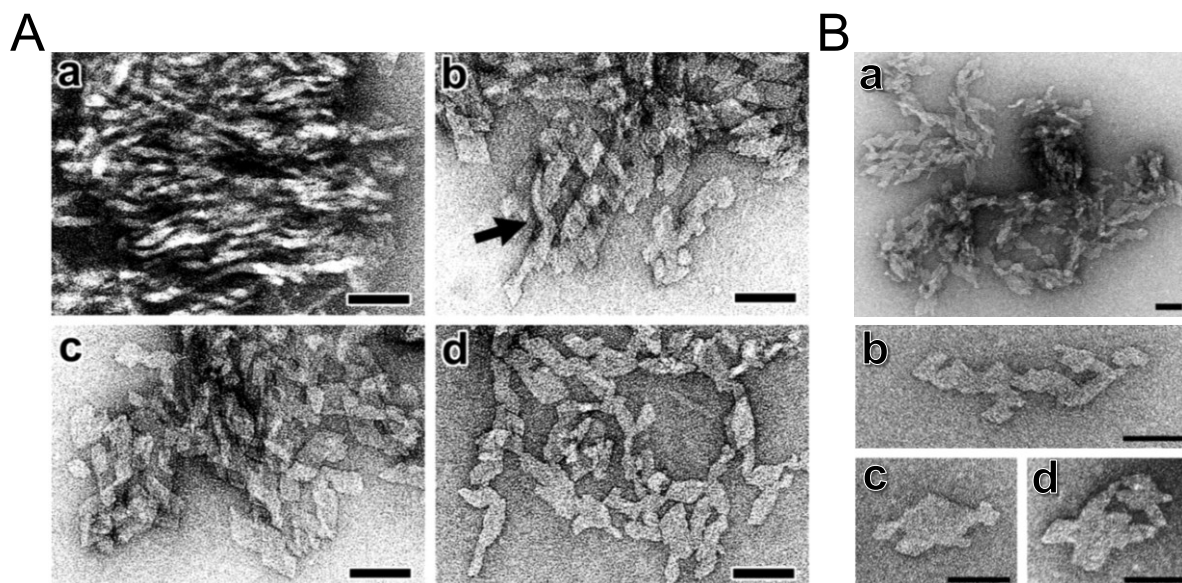
Fig. 2.7 TEM micrographs of negatively stained waxy maize starch samples: (A) a-c fragments of waxy maize starch granules after 2 weeks of 2.2 N HCl hydrolysis at 36°C. In a, a lamellar organization is clearly revealed with the platelets lying parallel to the incident electron beam. In b and c, parallelepipedal platelets are seen lying flat on the carbon film. The arrow in b indicates a pyramidal stack of crystals. d. Individual waxy maize starch nanocrystals obtained after 6 weeks of hydrolysis. Adapted from Putaux and others (2003), with permission of American Chemical Society. (B) Nanocrystals obtained after 3.16 M H_2SO_4 hydrolysis of waxy maize starch granules for 5 days, at 40 °C, 100 rpm and with a starch concentration of 14.69%. a-d. Aggregates of nanocrystals and organizations of nanoplatelets. Scale bar: 50 nm. Adapted from Angellier and others (2004), with permission of American Chemical Society.

content on the morphology of SNCs prepared by acid hydrolysis. SNCs were prepared from waxy, regular and high amylose corn, potato and wheat, which covered both A- and B-type starches and three corn starches differing in amylose content [waxy (<5%), regular (25%), and high amylose (70 %) (LeCorre and others 2011). This study demonstrated only a moderate influence of the botanic origin on the particle size and thickness, while difference was more pronounced on the particle shape. SNCs produced from A-type starches rendered square-like particles, while those from B-type starches rendered round-like particles, which could be explained by the different packing configurations of amylopectin chains for A- and B-type starches. The degree of crystallinity of SNCs was significantly related to amylose content while no difference was observed when comparing starches from different botanic origins but with similar amylose contents. Furthermore, due the high amylopectin content (> 95%) in waxy starch, most of the studies on acid hydrolysis have been performed using this starch source such as waxy corn, waxy potato and waxy rice starches (LeCorre and others 2011; Bel Haaj and others 2013; Perez Herrera and others 2016; Qiu and others 2016; Dai and others 2018; Jeong and Shin 2018).

Other commonly used "top-down" approaches are mainly physical treatments, including ultrasonication, high pressure homogenization, extrusion, gamma irradiation, and steam jet cooking. Compared to acid hydrolysis, these methods are more environmentally sustainable and with greater production efficiency. During ultrasonication, high energy is released and converted to high pressure and high temperature, and consequently resulting in the production of nanoparticles with reduced size and polydispersity from native starch granules. For example, the ultrasonication of a waxy corn starch slurry in a water bath at 8 °C is necessary in order to prevent gelatinization and it is 75 min at 20 kHz with a horn with a tip diameter of 13 mm. SNPs between

30-100 nm were obtained, however these had lower crystallinity than those obtained by acid hydrolysis. Similar results were observed for high pressure homogenization, the SNPs produced via reactive extrusion were also almost completely amorphous. Furthermore, the effect of combining physical treatments, such as ultrasonication, heat-moisture treatment, and homogenization, and acid hydrolysis were investigated (Park and others 2016; Kim and others 2017; Shabana and others 2019). However, the combination with physical treatments also reduced the long-range crystallinity of starch granules compared to those obtained by acid hydrolysis alone.

2.3.1.2. Bottom-up approach

Regarding "bottom-up" process, the commonly used methods of SNPs preparation are nanoprecipitation, enzyme debranching and recrystallization, and microemulsion. Among those methods, nanoprecipitation, also known as anti-solvent precipitation, has gained increased interest due to its simplicity and scalable potential. In this approach, the native starch granules are initially dissolved in a solvent such as DMSO, alkali solution, or solubilized in water by heating techniques (boiling, autoclaving, etc) followed by high shear homogenization and/or ultrasonication technologies. Subsequently, smaller particles are formed from the solubilized starch molecules by antisolvent nanoprecipitation. Usually, an antisolvent that is miscible with water, such as ethanol, propanol, etc., is gradually added into the solubilized starch solution or vice versa. The mixing of antisolvent and solvent leads to supersaturation, nucleation, and nucleus growth and thereby formation of nanoscale particles (Chin and others 2011; Dong and others 2015; Barreras-Urbina and others 2016) (Fig. 2.8). This process essentially changes the starch state during change in solvent composition. Thus, solute concentration, mixing method, and antisolvent/solvent (AS/S) ratio may exert various effects on the supersaturation, nucleation, and nuclei growth and therefore the properties of resultant particles, such as particle size, particle size distribution (PSD), and
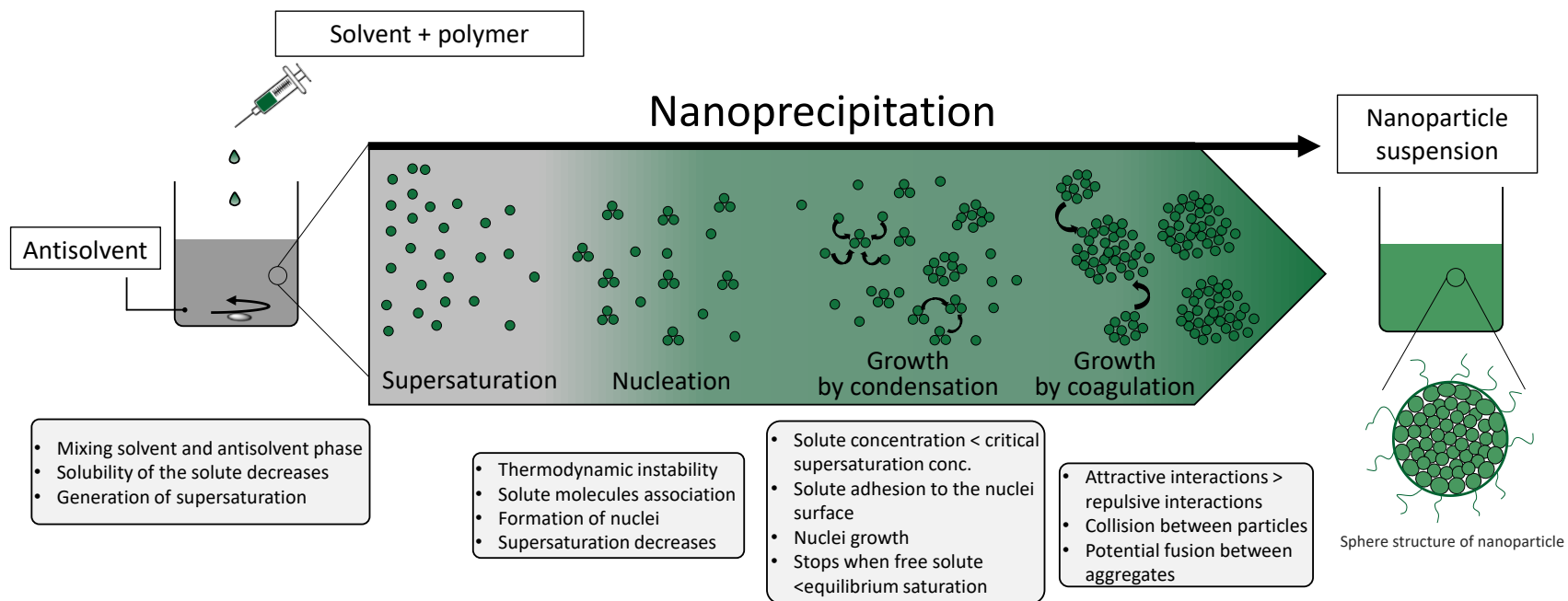
Fig. 2.8 Schematic illustration of nanoprecipitation process. Adapted from Martínez Rivas and others (2017), with permission of Elsevier Ltd.

morphology characteristics (Fig. 2.9). For example, low starch concentration, or a large AS/S ratio lead to a smaller particle size (Chin and others 2011; Dong and others 2015). In the case of using water as the solvent and organic solvent as the anti-solvent, the sizes of the resultant SNPs produced ranked in order with the following solvents: Acetone > methanol > ethanol (Sadeghi and others 2017). Qin and others (2016) produced normal corn, waxy corn, high amylose corn, tapioca, potato, sweet potato and pea starch nanoparticles by nanoprecipitation with the dropwise addition of ethanol into dilute solution of gelatinized starch under stirring. They reported that the particle size of SNPs was between 30 and 75 nm which was much smaller than the size of SNPs reported in previous publications. Tan and others (2009) prepared waxy corn starch acetate nanoparticles with nanoprecipitation process by the dropwise addition of water to acetone solution of starch acetate. They found that it is an efficient method for the production of SNPs and the size of SNPs can be controlled by the concentration of starch solution. Despite the advantages of nanoprecipitation treatment, it has some limitations such as the large amount of antisolvent (i.e., AS/S ratio of 10:1, 20:1, 30:1) and longer processing time (due to slow dropwise addition) to produce a unit quantity of SNPs. These factors hinder the industrial production and application of SNPs. In recent years, extensive efforts have been made to overcome these limitations. In a series of studies (Chang and others 2017a; Chang and others 2017b), SNPs were prepared from pure amylose and potato starches respectively, by nanoprecipitation with the dropwise addition of ethanol into a potato starch solution after dissolution combined with ultrasonication treatment. Their results suggested that ultrasonication was effective in the production of nanoparticles with less antisolvent. In another study, Saari and others (2017) prepared waxy corn starch nanoparticles by autoclaving and nanoprecipitation with direct addition of ethanol into starch solution at once (rapid nanoprecipitation) for the production of SNPs with a greater efficiency and less cost.
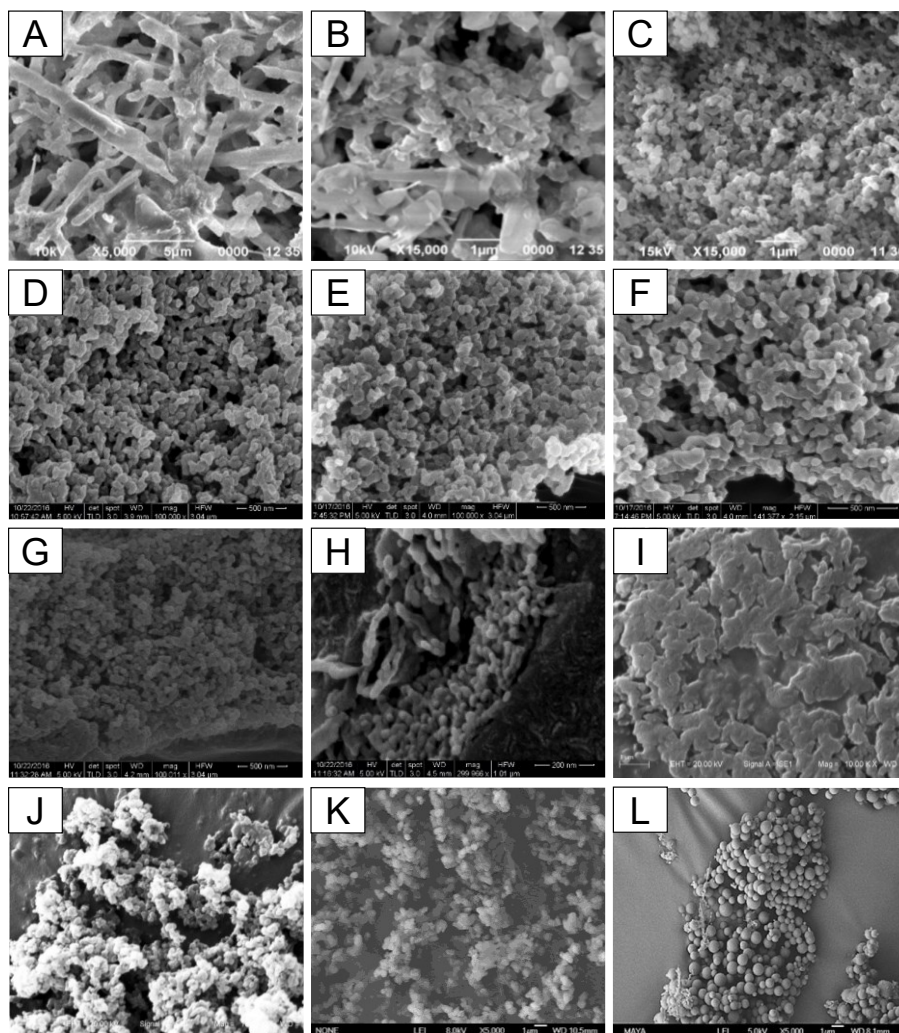
Fig. 2.9 SEM images of starch nanoparticles (SNPs) produced by nanoprecipitation: (A-C) Sago SNPs prepared by addition of 1 mL of 10 mg/mL starch solution (0.8% NaOH and 1% urea as solvent) into absolute ethanol dropwise at AS/S (antisolvent-to solvent) ratio 5:1, 10:1 and 20:1.From Chin and others (2011), with permission of Elsevier Ltd.; (D-F) waxy corn, regular corn, high amylose corn SNPs obtained by addition of 10 mg/mL starch solution (0.8% NaOH and 1% urea as solvent) into absolute ethanol dropwise at AS/S ratio 10:1. From Sadeghi and others (2017), with permission of Elsevier Ltd.; (G, H) regular corn SNPs obtained by addition of 10 mg/mL starch into methanol and acetone dropwise at AS/S ratio 10:1. From Sadeghi and others (2017), with permission of Elsevier Ltd.; (I-J) SNPs obtained by using 3% potato starch paste (water as solvent) without ultrasonic treatment and using the one with 30 min ultrasonic treatment at AS/S ratio 2:1. Starch was added into absolute ethanol dropwise. From Chang and others (2017b), with permission of Elsevier Ltd.; (K) Amylose nanoparticles obtained by precipitating 10 mg/mL amylose solution (90% DMSO/10% water mixture as solvent) with same volume ethanol under ultrasonication. From Dong and others (2015), with permission of John Wiley and Sons; (L) Waxy corn SNPs prepared from 0.8mg/mL autoclaved starch solution by directly mixing absolute ethanol into starch solution at AS/S ratio 1:1. From Saari and others (2017), with permission of Elsevier Ltd.

However, both larger particles and aggregates of nanoparticles were observed. According to those studies, the dissolution methods and addition techniques might play a crucial role on the nanoprecipitation results. In addition, SNPs produced through "bottom-up" approach usually show more amorphous structure (i.e., low crystallinity), here the amylopectin SNPs show lower crystallinity than amylose SNPs. Therefore, Qiu and others (2016) produced SNPs with controllable particle size between 20-100 nm using short-chain starch molecules from debranched waxy corn starch by nanoprecipitation. In general, most of those studies are using waxy corn and potato as starch sources, other sources especially pulses were rarely investigated.

Another commonly used method is enzyme debranching and recrystallization method, which involves the preparation of linear chain molecules by enzyme debranching and the sequential formation of SNPs by retrogradation of the linear chain at low temperature. The SNPs formed usually show high crystallinity when compared to those produced by other "bottom-up" processing. For example, after pullulanase debranching and recrystallization of waxy corn starch with a concentration of 15%, the SNPs produced had a spherical shape with particle sizes between 60 and 120 nm and degree of crystallinity up to 55.41% (Sun and others 2014). Microemulsion method involves the preparation of water-in-oil (W/O) or oil-in-water (O/W) microemulsion consisting of water droplets dispersed in an oil phase or oil droplets dispersed in an aqueous phase, respectively (Gutiérrez and others 2020). Moreover, SNPs could be produced by the combination of microemulsion with cross-linking reactions and physical treatments such as high-pressure homogenization and ultrasonication (Shi and others 2011).

2.3.2. Characterization

Based on their physical and chemical properties, the characterization of nanoparticles is performed using a variety of analytical techniques. It is necessary to characterize SNPs in order to understand their structure and their interaction with each other and with the surrounding environment. The influence of physical properties, such as size, shape, crystallinity, state of dispersion and surface properties, affects the performance of SNPs in food system. The morphology and PSD of SNPs has been investigated using SEM, FE-SEM, transmission electron microscopy (TEM), and dynamic light scattering spectroscopy (DLS). Their long-range crystalline structure and short-range molecular order have been determined by XRD and ATR-FTIR, respectively, using the same methods as their native counterpart. There is scarce information related to molecular structure and composition of SNCs and SNPs. The molecular size distribution of SNCs and SNPs obtained from a few starch sources such as waxy corn, regular corn, and high amylose corn, and potato, mungbean was investigated by size-exclusion chromatography (SEC) (Kim and others 2012; Perez Herrera and others 2017; Chang and others 2017b), while fewer studies were focused on their molecular structure/profile (Perez Herrera and others 2017). In addition, thermal properties of SNPs have been demonstrated by differential scanning calorimetry (DSC) and thermogravimetric analysis (TGA). Moreover, the rheological properties of SNPs from a few starch sources including potato starch (Shi and others 2012a; Shi and others 2012b; Shi and others 2013), waxy corn (Jiang and others 2016), regular corn, wheat, oat and barley (Perez Herrera and others 2017), have been documented in the literature.

2.3.2.1. Morphology and particle size distribution

The morphology and size distribution of SNPs could be characterized by SEM, TEM, atomic force microscopy (AFM), DLS, etc. By using different formulation methods and controlling the

preparation conditions, SNCs, SNPs, vesicles, and micelle morphologies of SNPs with the size of 10-700 nm with different shapes such as lamellar, spherical, rod-like, and irregular, was formulated (Kim and others 2015). With acid hydrolysis, the shape of the SNPs represents the original structures present in native starches, for example, SNC from A-type starches showed a square shape while those from B-type starches were round. SNPs from B- and C-type starches were larger than those from A-type starches which was in agreement with their resistance to acid hydrolysis. With other methods, such as nanoprecipitation, the morphology (shape and size) can be controlled by altering the formulation conditions. Chin and others (2011) reported that the nanoprecipitated sago starch particles had fibrous shape when the AS/S ratio 10:1 (v/v) was used (Fig. 2.9A) and a mixture of spherical starch nanoparticles and elongated fiber-like particles were formed when the AS/S ratio was changed to 15:1 (Fig. 2.9B). However, when the AS/S ratio was further changed to 20:1, the SNPs were mainly spherical with smaller particle size. Although there are some differences in the morphology of SNPs, it is obvious that the SNPs obtained from both "top-down" and "bottom-up" approaches tend to self-aggregate forming microscale agglomerates. This is possibly due to the presence of a large number of hydroxyl groups on the surface of SNPs, which readily participate in the formation of hydrogen bonding or van der Waals attraction between SNPs. This aggregation behavior limited their application. For example, in the production of nanocomposites with SNPs, blending a homogenous aqueous SNPs suspension with a matrix solution is required, which is critical to achieve desirable mechanical properties of the nanocomposites. To avoid the aggregations, facile physical treatment such as sonication or homogenization was performed to disperse SNPs in aqueous suspension. In addition, the recovery and drying methods can influence the morphology and dispersibility of SNP. Different observations existed in previous studies, for examples, Uzun and Kokini (2014) reported that corn

SNPs were spherical in shape after vacuum oven drying, while lost their shape and formed fibrous structure after freeze-drying. In another study, authors found drying procedures both oven-drying and freeze-drying had no obvious effect on the appearance of the amylose nanoparticles (Yan and others 2017). This might due to the different drying conditions such as temperature, humidity, drying time, as well as starch type used (Uzun and Kokini 2014; Yan and others 2017).

2.3.2.2. Molecular composition

Molecular weight distributions of SNPs could be analyzed using a high-performance size-exclusion chromatograph (HPSEC) equipped with a refractive index (RI) detector. However, little information is available with regards to the molecular profile of SNC and SNPs. Angellier-Coussy and others (2009) investigated the molecular composition of SNC by H_2SO_4 hydrolysis of waxy corn starch granules and found they were mostly composed of low degree of polymerization (DP) chains in the range of 9-22 and the average DP of 14.2 when subjected to debranching enzymes (isoamylase and pullulanase). The authors attributed the average DP to the thickness of the crystalline lamellae, thus concluding that nanocrystals correspond to the crystalline lamellae present in the native starch granules. Therefore, acid hydrolysis of native starch granules leads to the disruption of the amorphous regions and thus the isolation of the crystalline lamellae. The chain length distribution of SNPs from waxy, normal, high amylose corn, potato and mungbean was also investigated using gel permeation chromatography (Kim and others 2012). These authors reported a decrease in the proportion of long amylopectin chains resulting from acid hydrolysis of long amylose and amylopectin chains in the amorphous regions of native starches. The short (B1 and A) chains are more resistant to acid hydrolysis than long chains because they are present mostly in the crystalline lamellae. The molecular characteristics before and after isoamylase debranching of SNPs isolated by H_2SO_4 hydrolysis from waxy, normal, high amylose corn were investigated

by high performance size exclusion chromatography coupled with online multi-angle laser light scattering (HPSEC-MALLS) (Perez Herrera and others 2017). The SNPs from high amylose starches are comprised of both low Mw linear and short A + B amylopectin chains, while SNPs from waxy and normal (A-type) starches are comprised primarily of short A + B amylopectin chains. This study suggested the involvement of amylose in A- and B-type crystals of SNPs.

The molecular structure of the SNPs produced by enzyme debranching and recrystallization method was also reported by previous studies (Liu and others 2016; Lee and others 2019). SNPs produced by this method contained a large amount of small molecular weight fractions of chain length at DP 9-16, indicating the SNPs were formed by the short linear chains. Starch paste treated with pullulanase produced lotus seed starch nanoparticles with smaller molecular weight than those treated with β-amylase and α-amylase. In addition, Chang and others (2017b) investigated the molecular size distribution of potato starch paste after ultrasonic treatment in order to produce SNPs from starch paste by nanoprecipitation. They found molecular weight of starch molecules decreased gradually with an increase in ultrasonic treatment time. Based on the increase in amylose fraction, the authors concluded that the degradation of the amylopectin primarily occurred at the α-1, 6-glycosidic linkages (i.e., the branching points) and the α-1, 4-glycosidic linkages of the long inner amylopectin C chains. Based on the above findings, reducing the molecular weight of starch molecules by enzyme debranching or mechanical fragmentation can provide a route to prepare nanoparticles from starch with greater production efficiency.

2.3.2.3. Long-range crystalline structure

The crystallinity of starch and SNPs could be characterized by the X-ray diffraction (XRD) technique. As identified by XRD, starch crystals are classified into three types: A-type (present in

cereal starches except in high amylose types), B-type (tubers and high amylose cereal starches) and C-type (present in pulses). Generally, the crystalline structure of SNPs produced by acid hydrolysis are consistent with the native starch, such as waxy corn SNPs (A-type), corn SNCs (A-type), potato SNPs (B-type), etc. SNPs obtained from C-type starch behave differently, for example, SNPs hydrolyzed from native field pea starch was mainly A-type polymorph (Chen and others 2008). Field pea starches are C-type polymorphs and contain both A- and B-type polymorphs in varying proportions (Hoover and Ratnayake 2002). During the acid hydrolysis process, in addition to the amorphous areas, which are more rapidly hydrolyzed than the crystalline ones, B-type polymorph disappeared ahead of the A-type polymorph (Putaux and others 2003). This could be explained by the relatively less amount of B-type polymorph in the starch granules as well as the distribution of them where B-type polymorphs may be located in the outer layer while A-polymorph may be in the inner layer (Putaux and others 2003). Although the SNPs can be obtained by acid hydrolysis with the inherent crystallinity, some problems remain to be solved: the long duration (longer than 5 days) and low yield (less than 20%) for practical utilization. Therefore, recent studies have been focusing on the preparation of SNPs using alternative processes such as physical treatments (e.g., ultrasonication, high pressure homogenization, and extrusion) (Shi and others 2011; Song and others 2011; Bel Haaj and others 2013). Compared to the acid hydrolysis, these physical treatments generate SNPs in shorter periods with greater yields. However, most SNPs prepared using physical treatment exhibited amorphous structure because physical treatment such as high shear may cause the breakdown of crystalline structure of the starch granules.

For most "bottom-up" approaches, since the crystalline structure of starch granules were disrupted to obtain dissolved starch molecules, SNPs produced from those methods were not related to the crystalline type of native starches. For examples, SNPs produced by nanoprecipitation show V-type diffraction pattern with mostly amorphous structure. Moreover, according to the previous reports (Qiu and others 2016; Qin and others 2016), there is a high positive correlation between the amylose content of starch and the relative crystallinity of SNPs. Qiu and others (2016) prepared SNPs by nanoprecipitation using fractionated amylose and amylopectin from potato starch. Both amylose and amylopectin SNPs exhibited V-type diffraction pattern. The relative crystallinity of amylose SNPs was 30.2%-45.6% compared to native potato starch (36.9%), whereas that of amylopectin SNPs decreased substantially in the range of 8.6-9.2%. SNPs prepared by enzyme debranching and recrystallization led to a formation of A-or B- + V-type polymorphs with a larger relative crystallinity (up to 60.1%) depending on the enzyme incubation temperature and degree of debranching (Sun and others 2014; Liu and others 2016). The crystallinity of SNPs is influenced by the properties of starch such as botanical source, amylose content of starch, crystalline structure, as well as the processing techniques and conditions for SNPs production such as hydrolysis temperature, ultrasonic power, level and time as well as the type of enzyme used.

2.3.2.4. Short-range molecular order

ART-FTIR is used to monitor the change in the short-range molecular order and functional groups of SNPs. Similar to native starches, SNCs and SNPs show a typical spectrum absorption band at 3700-3000 cm^{-1}, which is attributed to the -OH stretching vibration and its width indicates the extent of formation of inter- and intra-molecular hydrogen bonds (Shi and others 2012c; Qin and others 2016). Ahmad and others (2020) observed the peaks of -OH stretching shifted to longer wavelengths for SNPs produced by nanoprecipitation using starch molecules obtained through

mild alkali hydrolysis and ultrasonication process when compared to their native counterparts. The bands at around 2926, 1045, and 1370 cm^{-1} ascribes to the asymmetric stretching of C-H and bending modes of the methylene (Shi and others 2012c). Qiu and others (2016) found that the band at 2926 cm^{-1} of the SNPs produced by nanoprecipitation using short linear chains was reduced and the band at 1400 cm^{-1} was enhanced significantly. The absorption at around 1640 cm^{-1} ascribes to adsorbed water (i.e., H-O-H bending vibrations on the amorphous regions of starch), which is a typical characteristic absorption band of starch. The peak intensity of this band decreased significantly in SNPs produced by nanoprecipitation as observed in previous studies (Gutiérrez and others 2020; Ahmad and others 2020). The peaks at 1150, 1080, and 990 cm^{-1} are mainly attributed to the stretching vibration of the C-O bond, C-O-H and C-O-C groups in the anhydrous glucose ring, respectively (Hebeish and others 2014; Qin and others 2016; Ahmad and others 2020). The characteristic peaks at range of 850-870 cm^{-1} associate with the existence of β-glycosidic bonds in SNPs due to C1-H1 stretching vibration (Ahmad and others 2020).

Although it has been proposed that FTIR is not related to XRD and is unable to differentiate starch long-range order characteristics and polymorphism, the spectrum variation of starch is interpreted in terms of the level of short-range order structure present on the edge of starch granules. The band at around 1047 cm^{-1} is sensitive to the amount ordered or crystalline structure; the band at 1022 cm^{-1} is related to the amorphous structure; the band at 995 cm^{-1} is related to hydrogen bonding of the hydroxyl group at C-6 (van Soest and others 1995). Therefore, the absorbance ratio of 1047/1022 can be used to measure the change of ordered starch to amorphous starch, and the absorbance ratio 995/1022 can be used as a measure of the degree of double helices. A greater absorbance ratio at 1047/1022 indicated a greater degree of order/crystallinity and a greater ratio

of absorbance at 995/1022 indicates a greater degree of double helix. Ahmad and others (2020) reported that the ratio of absorbance bands at 1047/1018 and 995/1018 decreased after SNPs formation indicating decrease in crystalline structure of starch and generation of its amorphous phase. It is clear that isolation/formation of SNPs from starch is accompanied by some changes in the physico-chemical structure of starch.

2.3.2.5. Thermal stability

The thermal characteristics of native starch, SNC or SNPs have been analyzed by DSC. LeCorre and others (2012) investigated the thermal properties of waxy, normal, high amylose corn, wheat and potato SNCs produced by acid hydrolysis. SNCs showed two thermal transitions when heated in excess water as well as in the dry state, contrary to native starches which only had one transition. In excess water, the two endothermic peaks were attributed to the two stage of crystalline melting, one from unpacking of the double helices and the other from unwinding of the double helices. SNCs from B-type starches showed more thermal stability than those from A-type starches as they consist of more rigid crystallites. In the dry state, the peaks were attributed to crystallites melting, with a direct transition from packed helices to unwound helices; and the presence of two peaks was attributed to the heterogeneity in crystallite quality (Thielemans and others 2006; LeCorre and others 2012).

For SNPs produced by nanoprecipitation, it has been reported that DSC curves of those SNPs in excess water were flat with very small endothermic peaks due to the smaller particle size with less swelling capacity/viscosity of SNPs in water (Qin and others 2016; Gutiérrez and others 2020). The melting temperature and enthalpy vary according to starch source and the processing parameters. Qin and others (2016) found that the higher the amylose content of native starch, the

higher enthalpy change of SNPs was observed. For example, the enthalpy changes of high amylose corn SNPs, regular corn SNPs, and waxy corn SNPs was about 6.16, 4.21, and 0.96 J/g, respectively. Compared with amylopectin SNPs, amylose SNPs exhibited higher melting temperature and enthalpy (Qiu and others 2016). There is limited information of thermal properties of SNPs in dry state reported in the literature. A more recent study (Ahmad and others 2020) found the transition temperature ranges of SNPs were broader than their native counterparts, which was in good agreement with another study on SNPs produced by enzyme debranching and recrystallization (Sun and others 2014). The broad melting range of SNPs could be attributed to the heterogeneity of the SNPs in which amorphous and crystalline phases were in mixture, the more amorphous structure, the broader transition temperature range of SNPs.

2.3.2.6. Rheological properties

Rheological measurements have recently been applied to characterize starch nanoparticles or microparticles suspensions (Shi and others 2012; Jiang and others 2016; Perez Herrera and others 2017). The starch source, concentration, and thermal stability of the SNPs, as well as how they are produced played a significant role in the viscosity and viscoelastic properties of SNP. LeCorre and others (2011) found a positive correlation between the viscosity and concentration of SNC from different starch sources produced by acid hydrolysis and all SNC suspensions showed a shear-thinning behavior for a given concentration ranging from 5% to 10% (w/v). The drying methods, such as spray-drying and freeze-drying, also influence the rheology of SNC in aqueous suspensions. Shi and others (2012b) reported the effect of spray-drying and freeze-drying on the rheological properties of aqueous suspensions containing SNP prepared by emulsion cross-linking technology. They found suspensions containing freeze-dried SNP show a greater viscosity and stronger shear thinning, while the suspensions containing spray-dried SNP had more stiffness

and a greater tendency to recover from deformation. They also investigated the effect of NaCl concentration on the rheological properties of SNP obtained by those two drying methods (Shi and others 2012a; Shi and others 2013). The presence of NaCl enhanced the thermal stability of all SNP suspensions as determined by the dynamic rheological properties as a function of temperature (25-90 °C). However, the viscosity of SNP obtained by the two drying methods displayed opposite trends, where viscosity increased in a suspension containing freeze-dried SNP. Jiang and others (2016) compared the rheological properties of SNC obtained from waxy maize starch by acid hydrolysis with SNP produced by the self-assembly of short-chain amylose. They found the viscosity of SNC was greater than that of SNP; here the viscosity of SNP did not change noticeably with increase of concentration. Moreover, the presence of NaCl enhanced the viscosity of the SNC, while there was no influence on the viscosity of the SNP even at high ionic strengths (10.5-256.0 mM). In a more recent study (Perez Herrera and others 2017), the rheological behaviors of SNP isolated by acid hydrolysis from different botanical origins (wheat, oat, barley and potato) with comparable amylose contents but different crystalline polymorph types were determined. Variations in the PSD, thermal stability and concentration among the SNP influenced their rheological properties. Rheological measurements are important in determining the dispersion microstructure of the nanoparticles suspension, and can be divided into four types: isotropic structure, biphasic structure of isotropic and liquid crystalline, liquid crystalline structure, and gel-like structure (Shafiei-Sabet and others 2012; Perez Herrera and others 2017). Since measuring the viscoelastic behavior is a nondestructive process it can provide information on the structure and elasticity, and the storage stability of a material. Previous studies have indicated that the rheological behavior of SNC/SNP suspensions and the critical concentrations for the phase

transition from one dispersion microstructure to another were dependent on processing techniques (i.e., drying methods), characteristics of SNC/SNP (i.e., particle size and surface charge), and post-treatment (i.e., addition of NaCl) (Shi and others 2012; Jiang and others 2016; Perez Herrera and others 2017).

Although some information on the rheological properties of SNP is available, systematic data on the morphology-rheology relationships are very limited, especially for those SNP produced by nanoprecipitation. Most of the previous studies have focused on the rheological behavior of SNP produced by acid hydrolysis, or have solely dealt with individual SNP suspensions (Shi and others 2012; Shi and others 2013; Jiang and others 2016; Perez Herrera and others 2017). Furthermore, most of those studies used cereal and tuber starches, such as corn, wheat, rice, oat, potato, and tapioca. To date, there is no comprehensive comparative investigation on the static and dynamic rheology of pulse SNP suspensions.

2.3.3. Current uses and potential applications

2.3.3.1. Pickering emulsion

Particle-stabilized emulsions, usually referred to as Pickering emulsions, have attracted considerable research interest in the past decade due to their unique properties. Compared to surfactant-stabilized emulsions, Pickering emulsions tend to be more stable against Ostwald ripening and coalescence and forming an emulsion with long-term stability. Various plant derived solid particles such as starch and cellulose have been used to stabilize emulsions. Li and others (2012) reported that the addition of waxy corn SNC above 0.02 % (w/v) stabilized the emulsion for longer than 2 months storage without the coalescence of oil droplets. During heating, the emulsion was stable at temperatures less than 60 °C whereas at 80 °C the emulsion became phase

separated possibly due to SNC gelatinization at high temperature. Ge and others (2017) investigated the characteristics of Pickering emulsions stabilized by SNPs from 4 types of starches (regular corn, tapioca, sweet potato, and debranched waxy corn) prepared by nanoprecipitation. They found emulsions using sweet potato and regular corn SNP with a diameter ranged from 100-220 nm have better stability than those with a diameter either less than 100 nm or more than 220 nm. More recently, Bu and others (2020) concluded that emulsions co-stabilized by SNPs and Tween 80 had enhanced stability and maintained good performance under harsh conditions such as high temperature, salt ion and acid conditions. However, SNP made from anti-solvent nanoprecipitation may be more porous and deformable than SNCs produced by acid hydrolysis, and therefore creating less stable Pickering emulsion. SNCs with the amorphous region largely removed may have the greatest degree of rigidity, resulting in a thicker adsorbed layer around the droplet conferring an excellent barrier for more stable emulsions. In order to improve the performance of SNPs, SNPs produced with different modification, such as octenylsuccinic anhydride esterification (Lu and others 2016; Saari and others 2017), carboxymethyl (Xiao and others 2020), citric acid crosslinking (Sufi-Maragheh and others 2019), have been successfully investigated as an emulsion stabilizer in recent studies. It should also be point out that starch-based Pickering emulsions may have some potential limitations for practical applications. SNCs produced by acid hydrolysis show disadvantages due to the acid used, low recovery, and large amount of waste produced. Moreover, chemical modifications of SNP may not appeal to consumers in the increasing market of clean label ingredients. Nevertheless, starch-based nanoparticles can be used as emulsion stabilizer in Pickering emulsions for a range of potential applications in food, cosmetics and pharmaceuticals.

2.3.3.2. Food bioactive ingredients and drugs carriers

Starch is an abundant, nontoxic, biodegradable, and biocompatible polymer. Thus, it is an excellent candidate for use as carriers for food bioactive ingredients and drug delivery. Recently, SNPs have gained great attention in this application field due to their submicron size and mobility, as well as large surface-to-volume ratio. SNCs and SNPs have been used a delivery carrier for antioxidants and anti-cancer drugs, such as curcumin (Chin and others 2014; Li and others 2016), polyphenols (Liu and others 2016; Qiu and others 2016), doxorubicin hydrochloride (an anti-cancer drug) (Yang and others 2017), and Triphala Churna (an ayurvedic drug) (Nallasamy and others 2020). Through SNPs as the nanocarrier, the bioactive ingredients or drugs encapsulated may not only increase their bioavailability and bioactivities but also become more stable than free ingredients under high temperature, ionic strength, and ultraviolet radiation. Moreover, Qiu and others (2016) found that the adsorption amounts of polyphenols (procyanidins, epicatechins, and catechins) on amylopectin SNPs were dramatically greater than those of amylose SNPs. Therefore, similar as in a Pickering emulsion, branched structure of SNPs played a key role on the performance of SNP in drug loading capacity. However, the linear chain played a more important role in the SNP formation. Thus, the amylopectin to amylose ratio may be a main factor influencing the formation of SNPs as well as their performance in various applications. To better encapsulate or adsorb drug molecules, chemically modified SNPs were also reported to be used in drug delivery systems. For example, sodium tripolyphosphate cross-linked SNPs that had been loaded with diclofenac sodium showed enhanced entrapment efficiency, which was up to 95.01% (El-Naggar and others 2015). Hydroxyethyl SNPs with size of 160 nm were effective in encapsulating two chemically distinct drugs having varying hydrophobicities (Narayanan and others 2015). The release behavior was influenced by their chemical nature and drug-matrix interactions. Acetylated corn SNPs also have

been shown to have a large encapsulation efficiency when using ciprofloxacin as a model drug (Mahmoudi Najafi and others 2016). In a more recent study (Miskeen and others 2021), citric acid modified SNPs that had been loaded with beta-carotenes as a model hydrophobic material showed enhanced effectiveness in encapsulation of hydrophobic compound.

2.3.3.3. Nanocomposites

"Nanocomposites" refer to polymeric composite materials that are filled with nanosized rigid particles. Compared with conventional composites, these nanocomposite materials show superior mechanical, barrier, and thermal properties at low levels of addition as well as their recyclability, transparency, and low weight. SNCs and SNPs are obtained from an inexpensive and abundant source and when compared to other synthetic nanomaterials, they are biodegradable and non-toxic. For these reasons, research focus on the use of SNCs and SNPs has dramatically increased over the past decade. In particular, starch based nanosystems have been used as reinforcement filler in the composite polymeric films, as they have shown the capability to improve mechanical, barrier and electrical properties of the films (Le Corre and Angellier-Coussy 2014). SNC-based nanocomposites are primary prepared by casting and water evaporation since SNCs are initially available in aqueous suspensions after processing (Le Corre and Angellier-Coussy 2014). A wide range of natural and synthetic polymers have been investigated for the composites with SNP, including natural rubber (Angellier and others 2005), polylactic acid (Yu and others 2008), pullulan (Kristo and Biliaderi 2007), soy protein isolate (Zheng and others 2009), polyvinyl alcohol (Chen and others 2008), polybutylene succinate (Lin and others 2011), cellulose acetate (Danilovas and others 2014), poly(butylmethacrylate) (Bel Haaj and others 2016). According to the above-mentioned studies, incorporation of SNP significantly improved mechanical and barrier properties of films and reduced water vapor and oxygen permeability through the film. However,

most of those studies were focused on the SNCs produced through acid hydrolysis. Bel Haaj and others (2016) compared the reinforcing potential of SNCs isolated from waxy corn through acid hydrolysis with those of SNPs obtained through ultrasonication. They found SNCs performed better in reinforcing a polymer film, while SNPs reduced the transparency of the nanocomposite films to a lesser extent than the SNCs due to their smaller size. Although SNPs exhibited less of a reinforcing potential compared to that brought by SNCs, the easier method to produce SNPs with a more environmentally sustainable approach, such as ultrasonication, nanoprecipitation, without the addition of any chemical additive or further purification steps, should arouse interest regarding applications for this class of SNPs. In addition, compare to inorganic and metal nanoparticles, such as clay, carbon, and silver nanoparticles, starch-based nanoparticles are biodegradable, renewable and compatible with many other materials. However, carbon/silver nanoparticles play an important in the antimicrobial nanocomposite. In this case, starch-based nanoparticles can be used not only as carriers of active antimicrobial nanoparticles but also as polymer matrices for biodegradable nanocomposites (Jung and others 2018). Other examples of applications of SNCs/SNPs in various fields are summarized in Table 2.2.

Table 2.2 Applications of starch nanoparticles.

Application fields	Roles of SNPs/SNCs	References
Food applications		
Emulsion stabilizer	Stabilization of oil-in-water emulsion against coalescence	(Ge and others 2017)
Fat replacer	Useful fat replacer/stabilizer for an O/W model emulsion due to the formation of nanocrystal network in the continuous phase	(Javidi and others 2019; Kaur and others 2019)
Food packaging	Improvement in the properties such as mechanical properties, thermal stability, moisture resistance, oxygen barrier property, and biodegradability.	(Le Corre and Angellier-Coussy 2014)
Non-food applications		
Composites filler	Reinforcement of polymeric matrix	(Angellier and others 2005)
Biomedical materials	Drug release regulator for drug delivery system	(Qiu and others 2016)
Fluorescent agent	Improvement of biocompatibility and cell uptake behavior of fluorescent organic nanoparticles as a precursor.	(Liu and others 2015)
Adsorbent agent	Absorbents for the removal of dissolved organic pollutants from water or other system	(Abidin and others 2018)
Paper binding and coating	Decrease of paste viscosity, increase of binding capability	(Kim and others 2015)
Thermo-responsive conducting	Improvement of thermo-responsive electrical conductivity by acting as crosslinker and nanofiller	(Valodkar and Thakore 2010)
Purification of targeted enzyme	Starch-coated nanoparticles to improve the efficiency of magnetic nanocarrier for the purification of targeted enzyme	(Paul and others 2015)

To date, SNPs have not been incorporated into any commercial food products, however based on their functional properties they are an excellent candidate as a thickening, bulking, and texturizing agent, fat replacer, emulsion stabilizer, etc. SNPs have been produced with sizes in range 10-700 nm and shapes of lamellar, spherical, rod-like, and irregular, through either "top-down" or "bottom-up" approaches from various starch sources including waxy corn, regular corn, high amylose corn, potato, wheat, barley, oat, rice or pea. Most of these application studies have used SNP produced by acid hydrolysis of the amorphous parts of native starch granules and most commonly used starches are waxy corn and potato starches. To prepare SNPs in large scale, anti-solvent nanoprecipitation of starch or recrystallization of short chain glucan are the most promising. In the future, SNPs produced through those very productive methods may be utilized as a novel way to control the rheological properties and texture of foods in the formulation of products with low fat, salt or sugar. Prior to the use of SNPs in food systems, more research will be required to better understand how these nano-sized ingredients influence human health.

Chapter 3: Effects of processing parameters on the morphology and characteristics of nanoparticles prepared by rapid nanoprecipitation of pea starch

3.1. Introduction

Starch is a natural biopolymer, which is abundant in nature, renewable and biodegradable. It exists in plants as micron sized granules composed of two different molecules known as amylose (mostly linear) and amylopectin (highly branched) (Gallant and others 1997). It is extensively used as a food and non-food ingredient for various applications including thickening, gelling, stabilizing, fat replacement, nutraceutical carrier, bioplastic, paper coating, and reinforcing agent (Hoover and others 2010). However, starch in its native form has many limitations such as poor solubility, retrogradation, limited digestibility and poor functional properties. For this reason, various physical, chemical, and enzymatic modifications have been employed to improve starch properties and functionality. Currently, starch nanoparticles (SNPs) are gaining more interest for their improved quality and high potential in different applications (Kim and others 2008; Le Corre and Angellier-Coussy 2014; Kim and others 2015).

There are various techniques for SNP production including acid and/or enzyme hydrolysis, anti-solvent nanoprecipitation, microemulsion, enzyme debranching and recrystallization, and mechanical treatments using extrusion, high pressure homogenization, ultrasonication, irradiation. Among various such methods, anti-solvent nanoprecipitation is a simple, fast, and reproducible method to produce SNPs with desired size. The nanoprecipitation process involves a dropwise addition of a dilute starch solution into an anti-solvent or vice versa which leads to supersaturation of starch molecules, nucleation, and nucleus growth and thereby formation of nanoscale particles (Chin and others 2011; Dong and others 2015; Barreras-Urbina and others 2016).

This process essentially changes the starch state during the change in solvent composition. Thus, solute concentration, mixing method, and antisolvent/solvent (AS/S) ratio may exert various effects on the supersaturation, nucleation, and nucleus growth and therefore the properties of resultant particles, such as particle size, particle size distribution (PSD), and morphology characteristics. However, this technique has some limitations such as large amount of antisolvent (i.e., ethanol, isopropanol, acetone) and longer processing time (due to slow dropwise addition) to produce a unit quantity of SNPs, which hinder the industrial production and application of SNPs. In recent years, extensive efforts have been made to overcome these limitations. In a series of studies, Chang and others (2017a; 2017b) prepared SNPs from pure amylose and potato starches, respectively, by nanoprecipitation with dropwise addition of ethanol into a potato starch solution after dissolution combined with ultrasonication treatment. Their results suggested ultrasonication was effective in the production of nanoparticles with less antisolvent. In another study, Saari and others (2017) prepared waxy corn starch nanoparticles by autoclaving and nanoprecipitation with direct addition of ethanol into starch solution at once (rapid nanoprecipitation) for the production of SNPs with higher efficiency and lower cost. However, both larger particles and aggregates of nanoparticles were observed. According to those studies, the dissolution methods and addition techniques might play a crucial role on the nanoprecipitation performance. Thus, in this study, the combination of ultrasonication and rapid nanoprecipitation was investigated for the production of SNPs.

Pulse grains are rich in nutritionally superior protein (25%-30%, w/w) (Hoover and others 2010). The fast-increasing demand for plant protein has triggered many pulse grain fractionation and refining operations across the world. Pulse starch would be a good candidate for the production of

SNPs because it is an undervalued byproduct of expanding pulse protein refining. Therefore, in this study, field pea starch was used as a model sample to produce SNPs using novel methodology involving ultrasound-assisted dissolution followed by rapid nanoprecipitation. This technique is simple and convenient in terms of safety, cost and can give better yield with desired particle size. The aim of the study was to define a sustainable and cost efficient "bottom-up" protocol for pulse SNPs processing with the following specific objectives: 1) to evaluate how processing parameters, including dissolution conditions (i.e., gelatinization and ultrasonication conditions), and nanoprecipitation conditions (i.e., AS/S ratio, dilute starch concentration, addition techniques) on the particle size and morphology; 2) to investigate how to recover SNP and how separation and drying procedures affect the re-dispersibility and stability of SNPs; and 3) to understand the possible mechanisms of the rapid nanoprecipitation process and the formation of SNPs.

3.2. Materials and methods

3.2.1. Materials

Faba bean (low tannin) and field pea grains were obtained from Tomtene Seed Farms, Birch Hills, SK, Canada. A lab scale grinding mill (Model ZM 200, Retsch, Haan, North Rhine-Westphalia, Germany) installed with a 0.5 mm screen was used to produce flour from field pea grains. Starch isolation (> 95% purity) from field pea flour was performed according to the method of Gao and others (2009). Regular corn starch was obtained from Ingredion Inc, Bridgewater Township, NJ, USA. Regular wheat starch, potato starch, pure amylose and amylopectin from potato starch was obtained from Millipore Sigma Canada Co, Oakville, ON, Canada. Milli-Q water was used for all experiments as a solvent phase; absolute ethanol was used as an antisolvent phase. All other chemicals were of analytical grade.

3.2.2. Preparation of SNPs

SNPs were prepared by a rapid nanoprecipitation technique from the dissolved starch. Fig. 3.1A illustrates the SNPs preparation scheme and the parameters evaluated in this study. Starch solution was prepared by heating/gelatinization and subsequent ultrasonication according to methods previously described (Iida and others 2008; Chang and others 2017b). Briefly, native field pea starch was dispersed in milli-Q water with a series of concentrations of 10, 50, and 100 mg/mL and gelatinized in boiling water bath for 30 min with stirring on a vortex mixer every 5 min for 30 s to achieve sufficient gelatinization. The gelatinized starch paste was then sonicated for 5-30 min using a 20 kHz ultrasonic processer (FS-1200 N, Shanghai Sonxi Ultrasonic Instrument Co., Ltd., Shanghai, ZJ, China) equipped with a probe transducer and a flat tip of 1/2" (13 mm). The probe was immersed into the samples during ultrasonication, carried out at specified amplitudes (10%, 20%, 30%, 40%, 50%, 60%, and 70%) and 5/2 s on/off pulses were applied to minimize heat generation. The homogenous starch solution was then diluted to concentrations of 5, 10, 15, 30, 50, and 100 mg/mL before nanoprecipitation. The starch solution prepared without ultrasonication was used as control. The starch granular structure changes upon gelatinization and ultrasonication were observed using light microscopy.

For rapid nanoprecipitation, all experiments were completed using water and absolute ethanol as solvent (S) and antisolvent (AS), respectively. The nanoprecipitation was performed by pouring the absolute ethanol rapidly into the diluted starch solution in a stirring reactor (Fig. 3.1A). The starch concentration and AS/S ratio (v/v) ranged from 5 to 100 mg/mL and from 0.3:1 to 10:1, respectively. The resultant colloidal suspensions in ethanol-water system were stirred (500 rpm) for 1 h. Slow nanoprecipitation by gradually adding ethanol into starch solution dropwise under

Fig. 3.1 A) A schematic diagram showing the experimental setup in this study for starch nanoprecipitation; B) The methods and experimental conditions used to determine the influence of various process parameters on SNP formation. Grey shading indicates the fixed method/conditions chosen for all experiments. AS/S (antisolvent-to-solvent ratio).

selected conditions was also investigated for comparison. In order to eliminate the effect of separation and collection process on the particle characteristics, the resultant particles in ethanol-water system were directly used for the measurement of particle size. These processes were demonstrated to cause broad PSD and thus a greater heterogeneity of nanoparticles. Moreover, some particles could not be redispersed and strongly adhered onto the bottom of tube after centrifugation, suggesting a decreased production efficiency. Thus, after mixing, an aliquot of the colloidal suspension obtained was diluted with Milli-Q water for the analysis of the particle size, particle size distribution (PSD), and polydispersity index (PDI) by dynamic light scattering (DLS, see Section 2.4).

SNPs were separated from the colloidal suspension in ethanol-water system by using following three methods : a) high speed centrifugation at $48000 \times g$ for 20 min, discarding supernatant and redispersing the pellet nanoparticles in Milli-Q water; b) solvent evaporation by a rotary evaporator (IKA RV 10 digital, Staufen, Germany) under the conditions of 50 °C and vacuum with a rotating speed of 100 rpm and the concentrated SNPs were resuspended in Milli-Q water; and c) shear induced recovery method by using a homogenizer (Heidolph Diax 900, Schwabath, Bavaria, Germany) to promote the settling of fine particles at 8,000 rpm for 1 min. Sediments were collected by centrifugation and redispersed in Milli-Q water. Separation conditions of each method were selected after a series of preliminary trials, where an optimal yield of SNPs (> 90%) was achieved. The redispersed colloidal SNPs in Milli-Q water were frozen at −20 °C overnight in a freezer. The frozen samples were then freeze dried (FreeZone 12, Labconco Corp., Kansas, MO, USA) at a sublimating temperature of −45 °C for 4-5 days. Oven-dried SNPs were also prepared at 40 °C

overnight with an air convection oven (Thermo Scientific Heratherm™ General Protocol Oven, Thermo Scientific, Waltham, MA, USA) and used for a comparison.

3.2.3. Redispersion of SNPs

Ten micrograms of the dry SNPs was redispersed in 10 mL Milli-Q water and stirred for 2 h, then the dispersions were diluted to 0.2 mg/mL with Milli-Q water and the particle size, PSD, and PDI were measured by DLS as mentioned in section 3.2.4.

3.2.4. Measurements of particle size, PSD, PDI, and zeta-potential of SNPs

The particle size, PSD, and PDI of the SNPs were determined by dynamic light scattering (DLS) using a Zetasizer (Nano S, Malvern Instruments, Malvern, Worcestershire, UK). The samples were prepared by dispersing the SNPs in Milli-Q water and diluting to a concentration of about 0.2 mg/mL. All measurements were conducted at a scattering angle of 173° in a temperature regulated cell at 25 °C. Fifteen measurements were determined for each run and the mean ± standard deviation of 3 runs were reported. PSD can also be reflected by PDI values from 0 to 1; the smaller PDI values indicate a narrower the size distribution. Monodispersed particles have a PDI of 0. The zeta-potential of the SNPs in ethanol-water mixture were determined in a U-shaped cuvette. All measurements were carried out at 25 °C in triplicates.

3.2.5. Field emission scanning electron microscopy (FE-SEM) images

The morphology and the size of SNPs were observed using FE-SEM (Zeiss Sigma 300 VP-FESEM, Zeiss, Oberkochen, Germany) at an accelerating voltage of 5 kV. SNP samples were mounted on a circular aluminum stub with a double-sided sticky tape and coated with carbon. ImageJ software was used to determine particle diameter from the microscopy images. The diameters of 200 particles (n = 200) from each sample were measured.

3.2.6. Stability analysis

SNP stability as a function of temperature and storage time were investigated. SNP suspensions of 0.2 mg/mL in Milli-Q water before and after freeze-drying were prepared for the stability tests. For stability as function of storage time, the SNPs suspensions were storage at room temperature for 0 h, 0.5 h, 1 day, and 2 days. For the stability as function of temperature, the SNPs suspensions were incubated at 25, 40, and 60 °C for 0.5 h and then gradually cooled to room temperature. The particle size distribution of the samples was measured by DLS at 25 °C.

3.2.7. Statistical analysis

All experiments were done in at least three replicates. Results are presented as mean ± SD (standard deviation). Analysis of variance was performed, and the mean comparisons were performed by Tukey's HSD test with a OriginPro software (OriginPro 9.0.0, OriginLab, Northampton, MA, USA).

3.3. Results and discussion

Preparation of SNPs commonly uses organic solvents such as dimethyl sulfoxide and acetone, or an alkali solution. For food and nutraceutical applications, utilization of more biocompatible solvents is required to ensure the safety of the final products. Thus, water was selected as a solvent and ethanol as an antisolvent to prepare SNPs in this study. The method development was based on two previous studies on starch dissolution (Chang and others 2017b) and nanoprecipitation (Saari and others 2017). In order to reduce the amount of antisolvent and solvent used in this study, the effects of dissolution parameters, such as starch stock concentration, ultrasonication amplitude and duration time on the particle size, were demonstrated with starch dilution concentration of 10 mg/mL at the antisolvent/solvent (AS/S) ratio of 1:1. The two important nanoprecipitation parameters investigated were the AS/S ratio and the starch concentration. The mechanism of starch

nanoprecipitation was elucidated by studying the generation of SNPs from the ethanol-water mixture. Finally, the methods of SNPs separation and drying on the particle properties were investigated. Based on this screening process the final method and condition were optimized and finalized, as shown in Fig. 3.1.

3.3.1. The effect of dissolution parameters on the formation of SNPs

Starch samples were mixed with water and solubilized by heating/gelatinization and subsequent ultrasonication according to previous studies (Iida and others 2008; Chang and others 2017b) where ultrasonication decreased the viscosity of starch solution after gelatinization to facilitate SNP preparation. In Fig. 3.2A, the light microscopy images show the microstructural changes during starch gelatinization and ultrasonication in excess water (100 mg/mL). Native field pea starch granules were round and oval in shape with a particle size of 6-43 µm (Fig. 3.2A1). During gelatinization, starch granules mainly undergo three steps as following: a) swelling with increasing temperature due to hydration increases granule size; b) further increases in temperature disrupted the granule and thereby leaching starch molecules from the granules; c) the starch granular surface collapsed and remained in the solution (Fig. 3.2A2). Swollen starch granules (primarily composed of amylopectin network) are responsible for the viscosity of the gelatinized starch and hinder nanoparticle formation during nanoprecipitation. This disruption of the network and possible depolymerization caused by ultrasonication can lead to loss of viscosity as well as complete molecular dispersion (Fig. 3.2A3). The decrease in viscosity of the starch solution was also visually evident by a change from an opaque and gel-like solution to a more clear and runny liquid solution. Therefore, the ultrasonic process was expected to render the starch molecules dissolved completely in the solution, thus affect the size of SNPs prepared via nanoprecipitation of starch. It

was important to investigate the effect of ultrasonic treatment on the starch solutions with respect to the size of SNPs formed by nanoprecipitation.
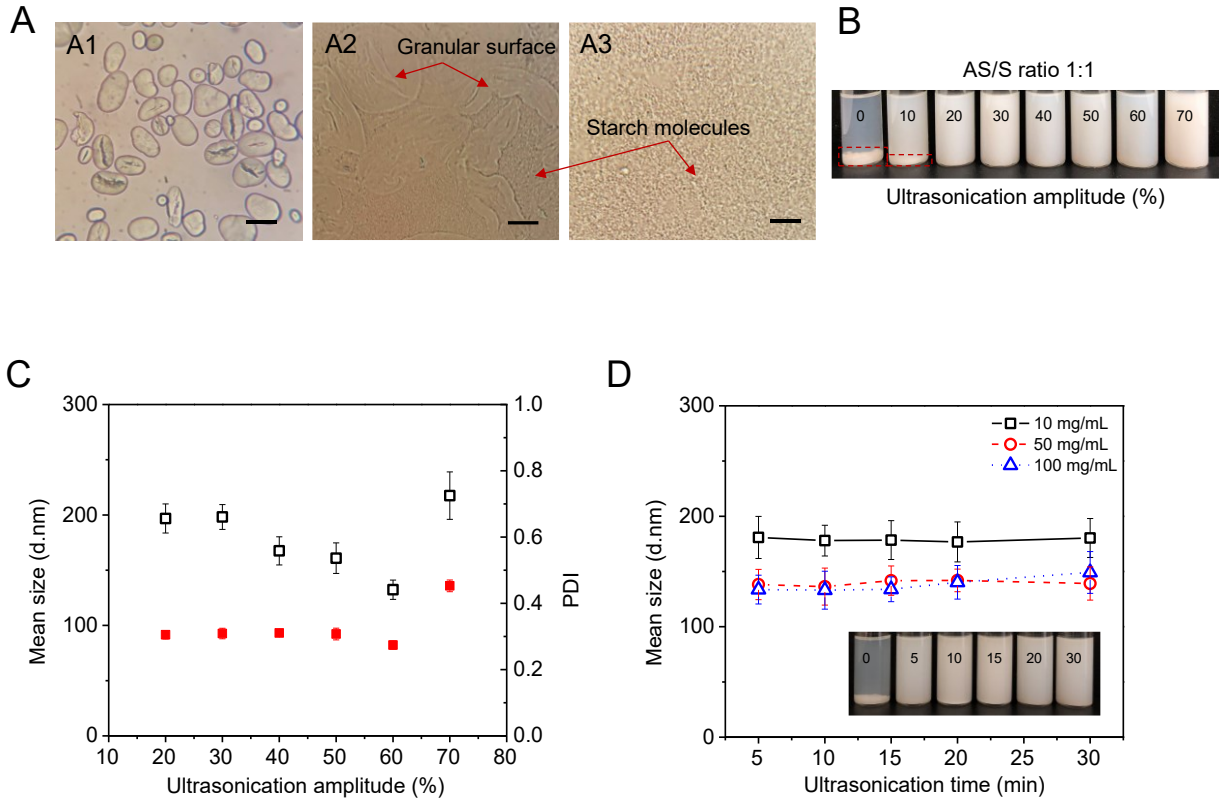
Fig. 3.2 The effect of starch dissolution parameters on SNP formation. A) Light microscope images of (A1) native starch, (A2) gelatinized starch and (A3) ultrasound treated starch solution of 100 mg/mL stock (scale bar: 20 µm); B) Photograph of the suspensions formed after mixing ethanol with starch solution; C) Mean size (open square) and PDI (polydispersity index, solid square) of SNP prepared by using starch solution with 10 min ultrasonication at various amplitudes; D) Mean size of SNP prepared from starch solution with different stock concentrations and ultrasonication time (insert photograph of the suspensions formed after mixing). All experiments were performed at starch dilution concentration of 10 mg/mL, AS/S (antisolvent-to-solvent) ratio 1:1.

Adding ethanol into starch solution changed the appearance of the suspensions from transparent (diluted starch solution 10 mg/mL) to opaque (starch in ethanol-water system). Fig. 3.2B shows the photograph of particle suspensions in ethanol-water system (AS/S ratio 1:1) without ultrasonication or with ultrasonication at varying sonication amplitudes (ranging from 0-70%). SNPs obtained from starch solution with ultrasonication amplitude above 20% exhibited a colloidal suspension without any visible aggregation, while those less than 20% resulted in two phases, colloidal supernatant and starch sediments, respectively. When measuring the mean sizes and PDI of the samples redispersed in Milli-Q water by DLS (Fig. 3.2C), those samples produced with ultrasonication at amplitudes less than 20% showed large PDI values close to 1, which were not suitable for a DLS measurement, suggesting that the samples had a broad particle size distribution and likely contained large particles and aggregates. A large PDI value in the range of 0.7-1 indicates poor quality samples with a broad size distribution (Zetasizer Software for the Nano. APS and mV, Version 7.01, Malvern Instruments). Therefore, only the mean sizes and PDI values of samples with ultrasonication at an amplitude of more than 20% are presented in Fig. 3.2C. The mean sizes initially decreased with increasing amplitude from 20% to 60%, exhibited a minimum, and then increased when further increase in the amplitude from 60% to 70%. The PDI values remained unchanged with increasing amplitude from 20% to 50%, while significantly decreased beyond 50% and then increased from 60%. As the amplitude increased, the disruption of starch network improved and rendered the uniform dispersion of starch molecules in solution. This increased the distribution efficiency of the starch solution into ethanol and led to the formation of smaller particles with a narrow PSD. However, when the amplitude exceeded 60%, the mean particle size increased from 130 to 220 nm with a broad PSD (PDI 0.45). The reason was that the induced depolymerization by ultrasonication at a larger amplitude resulted in a large number of

molecules being present in the ethanol-water mixture, leading to particle overgrowth (i.e., generation of larger particles with a broad PSD). Fig. 3.3 shows FE-SEM images of freeze-dried samples obtained from starch solution without ultrasonication (Fig. 3.3A and B) and with 10 min ultrasonication at an amplitude of 60% (Fig. 3.3C and D). Large particles existed in the sample produced without ultrasonication treatment due to the incomplete dissolution of starch (i.e., granular surface remained in the starch solution), which is in agreement with the result observed by light microscopy as shown in Fig. 3.2A. The SNPs produced with ultrasonication were more discrete and their surface were smoother and more regular.
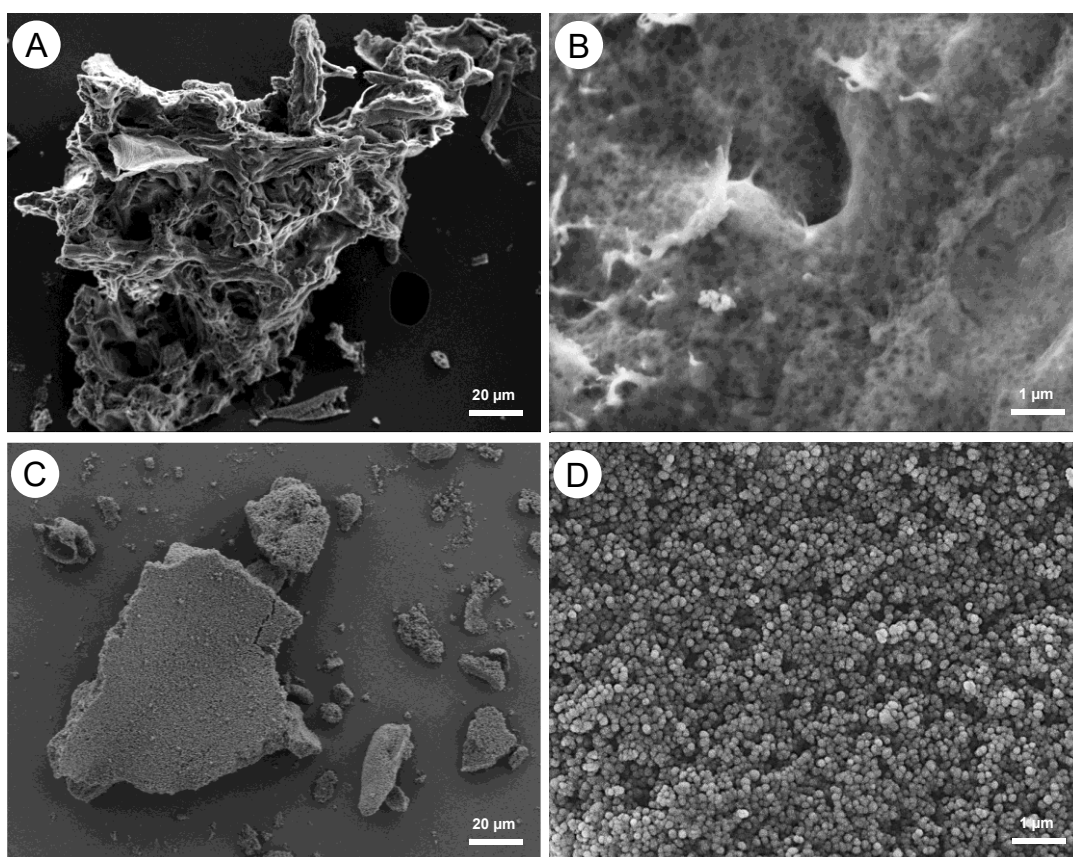
Fig. 3.3 FE-SEM images of freeze-dried samples produced from starch stock solution (100 mg/mL) without ultrasonication (A, B); and the one with ultrasonication for 10 min at an amplitude of 60% (C, D). All samples were obtained by nanoprecipitation with 10 mg/mL diluted starch solution at AS/S ratio 1:1.

Fig. 3.2D shows the mean size of SNPs prepared by nanoprecipitation (diluted starch concentration 10 mg/mL, AS/S ratio 1:1) using starch stock solutions of different concentrations treated by ultrasound for various periods of time. The data in Fig. 3.2D indicated that the mean particle size of SNPs was affected by the concentration of stock solution. Under identical nanoprecipitation conditions, the mean particle size of SNPs produced from a 10 mg/mL stock solution was significantly greater than those from a 50 or 100 mg/mL stock solution. However, there was no significant difference in mean particle size between SNPs produced from 50 and 100 mg/mL stock solutions. This indicates that the effect of ultrasound on SNP formation is more significant for starch stock solution of greater concentrations (i.e., 50-100 mg/mL). Therefore, it is beneficial to form smaller particles by using greater concentrations of starch as stock solution for starch dissolution, followed by dilution to the desired concentration for nanoprecipitation, instead of using a lesser concentration stock solution directly. However, starch solutions of even greater concentrations, such as 150-200 mg/mL were not effectively treated by ultrasonication due to the formation of a firm gel. According to previous studies (Iida and others 2008; Chang and others 2017b), the effect of ultrasound on the viscosity of starch was dependent on the starch source and concentration. Chang and others (2017a) investigated the effect of ultrasound on the viscosity of amylose solution and found the viscosity of 10 mg/mL amylose solution only decreased by 50% after 30 min ultrasonication, while there was a 99.9% decrease in viscosity of the 50 mg/mL amylose solution. The results in Fig. 3.2D also indicated that ultrasonication time (from 5-30 min) did not affect the size of the SNPs. The mean particle size of SNPs was not changed significantly with increasing ultrasonication time. However, this result is inconsistent with a previous study (Chang and others 2017b), in which mean particle size of potato SNPs decreased with increasing ultrasonication time. This could be due to markedly decreased viscosity of field pea starch paste

after ultrasonication within 5 min under the test conditions (at an amplitude of 60%). As discussed earlier, besides the disruption of the starch network, starch molecules in solution may undergo depolymerization (chain scission) during ultrasonication, which could also lead to the decrease in starch viscosity. The change in molecular weight of starch in SNPs was evaluated and shown in Chapter 4. In general, ultrasonication promoted the generation of discrete of starch molecules, facilitating a better nanoprecipitation process for the production of more uniform SNPs.

3.3.2. The effect of nanoprecipitation parameters on the formation of SNPs

3.3.2.1. The effect of AS/S ratios

The AS/S ratio exhibited an important effect on particle size and PSD, as shown in Fig. 3.4A. Within the range of AS/S ratios from 0.8:1 to 2:1, the particles were uniformly dispersed in the suspension without any visible aggregation, while particles gradually precipitated during mixing at AS/S ratios less than 0.8:1 as well as above 2:1. This may be attributed to the initial rapid supersaturation of molecules triggered by a rapid molecular dehydration under a large AS/S ratio (Chin and others 2011; Qiu and others 2016). According to previous studies (Saad and Prud'homme 2016; Lee and others 2020), larger molecules showed a faster nucleation and a greater growth rate since their solubility decreased faster than that of smaller molecules. Thus, starch molecules with a low solubility could be precipitated at low AS/S ratios. Fig. 3.4B shows the mean size and PDI of the SNPs produced by rapid nanoprecipitation with 10 mg/mL starch solution at various AS/S ratios. There was a distinct point at the AS/S ratio of 1:1, below which the mean particle size and PDI increased sharply. This is in agreement with observations from Fig. 3.4A. With increasing the AS/S ratio from 1:1 to 10:1, the mean size decreased slightly, but the decrease was not significant. The mean size for SNPs obtained at the AS/S ratios of 10:1, 5:1, 3:1, and 1:1 was 115, 110, 120, and 130 nm, respectively. The influence of the AS/S ratio on the size
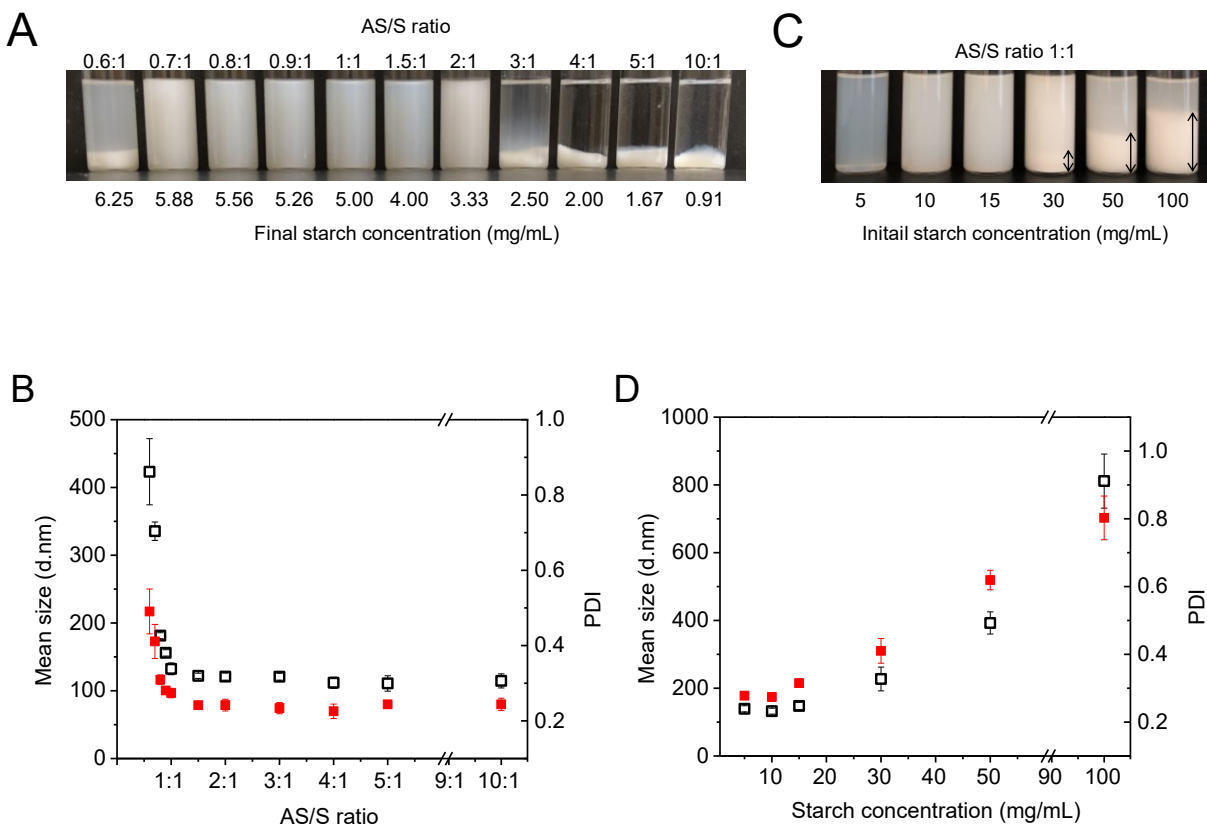
Fig. 3.4 The effect of nanoprecipitation parameters on SNP formation. A) Photograph of the suspensions formed after mixing ethanol with starch solution at different AS/S ratios; B) Mean size (open square) and PDI (polydisperse index, solid square) of SNP prepared by rapid nanoprecipitation with starch concentration of 10 mg/mL at different AS/S ratios; C) Photograph of the suspensions formed after mixing ethanol with starch solution at different starch concentrations; D) Mean size (open square) and PDI (solid square) of SNP prepared by rapid nanoprecipitation with different starch concentrations at AS/S ratio of 1:1; All experiments used starch solutions diluted from 100 mg/mL stock solution after ultrasonication for 10 min at an amplitude of 60%.

of SNPs was insignificant at AS/S ratios from 1:1 to 10:1, suggesting SNPs could be produced with less ethanol with a ratio as low as AS/S 1:1. This is possibly due to the ultrasound-assisted dissolution of starch in water that improved the starch molecular dissolution and uniformity, facilitating homogeneous kinetics during nanoprecipitation. This is in agreement with previous studies (Chang and others 2017a; Chang and others 2017b), in which the authors also reported the effect of AS/S ratio on the formation of nanoparticles was insignificant after using ultrasonication. They produced nanoparticles from pure amylose and potato starch by the slow addition of starch solution dropwise into ethanol at the AS/S ratio ranges of 3:1-10:1 and 2:1-10:1, respectively. However, in the present study, this ratio was reduced to 1:1 for field pea starch. This is very likely due to the different starch type as well as modified nanoprecipitation technique used (i.e., rapid addition as opposed to slow addition). The results of our research indicate that the combination of ultrasonication and rapid nanoprecipitation may be a better approach to produce SNPs at lower cost since less ethanol required.

3.3.2.2. The effect of starch concentration

A freshly prepared starch solution (i.e., stock solution, 100 mg/ml) was diluted to different concentrations of 5, 10, 15, 30, 50, and 100 mg/mL. The effect of starch concentration on the SNPs mean particle size and PDI was investigated at a fixed AS/S ratio 1:1 (v/v). As shown in Fig. 3.4C, sedimentation of particles was visually observed beyond 30 mg/mL starch concentrations. The mean particle size and PDI of SNPs, determined by DLS in Milli-Q water, increased with increasing starch concentration in a nonlinear fashion (Fig. 3.4D). Increasing the starch concentration from 5 to 10 mg/mL led to a slight decrease in the mean particle size from 140 nm to 130 nm. This can be attributed to the enhanced molecular supersaturation and consequent greater nucleation rate. There was no significant change in the PDI (both values <0.3) with

increasing starch concentration from 5 to 10 mg/mL, indicating SNPs formed were more uniform (i.e., narrow PSD) in nature. However, the mean particle size remarkably increased from 130 to more than 800 nm with a further increase in starch concentration from 10 to 100 mg/mL, where the PDI correspondingly increased up to 0.8, suggesting that the PSD became broad. At a starch concentration of 100 mg/mL, 60% of the obtained particles had submicron size, whereas the remaining 40% were micrometer scale. The PDI value of 0.8 also indicates the existence of large particles or aggregates in the sample. A similar result was observed in the nanoparticles from pure amylose prepared by slow addition of ethanol dropwise into amylose solution (Dong and others 2015).

According to previous studies (Wang and others 2010; Dong and others 2015), the increase in the mean size of nanoparticles with an increase of solute concentration may be due to the following two factors: a) the influence of starch concentration on viscosity; b) the number of starch molecules in the ethanol-water system. The greater viscosity of solution with increasing starch concentration may have hindered the diffusion between starch solution and ethanol. This led to non-uniform molecular supersaturation, nucleation, and growth, resulting in larger particles with broader PSD. Besides, the number of nuclei formed in the ethanol-water system increased with increasing starch concentration, which led to particle aggregates to form larger particles. This phenomenon can also be explained by increasing starch concentrations leading to an increase in inter-molecular associations, meaning more starch molecules associated and precipitated prior to SNP formation. However, the results of this study indicated that, through ultrasonication and rapid nanoprecipitation, smaller particles can be obtained by using a high concentration of starch solutions (i.e., 50 mg/mL). Similar results were reported when producing potato SNPs by using

ultrasonication and slow nanoprecipitation (Chang and others 2017); here a large concentration potato starch solution (up to 50 mg/mL) with 30 min ultrasonication was used to form small particles by the slow addition of starch solution to ethanol at the AS/S ratio of 10:1. This was probably because the ultrasonication could break the interaction of starch molecules and possibly depolymerization, reducing the chain entanglement during nanoprecipitation. The discrete and smaller molecules thus formed small nuclei and then grew into small particles.

In addition, nanoprecipitation could control the growth of particles by rapid addition and mixing of ethanol with the starch solution (i.e., rapid nanoprecipitation); this was more efficient than slow dropwise addition technique (i.e., slow nanoprecipitation). Fig. 3.5 shows FE-SEM images of samples produced by both techniques with starch concentrations of 10 mg/mL and 50 mg/mL at the AS/S ratio of 1:1. FE-SEM images show that particles prepared by rapid nanoprecipitation were spherical and relatively uniformly distributed, while those by slow nanoprecipitation were less uniform with small nuclei and formed large aggregates. As the starch concentration increased to 50 mg/mL, FE-SEM images of the samples produced by rapid nanoprecipitation still showed spherical particles, whereas there were only starch aggregates observed in images of samples produced by slow nanoprecipitation. This could be explained by molecular association with a high starch concentration during slow nanoprecipitation, when the ethanol concentration was gradually increased from 0 to 50%. Therefore, a careful selection of starch concentration and addition technique is important to precisely control molecular supersaturation, nucleation and growth rates to produce SNPs with desirable particle characteristics. The rapid nanoprecipitation technique provides not only an approach to prepare smaller SNPs, but also a strategy to improve the production efficiency.
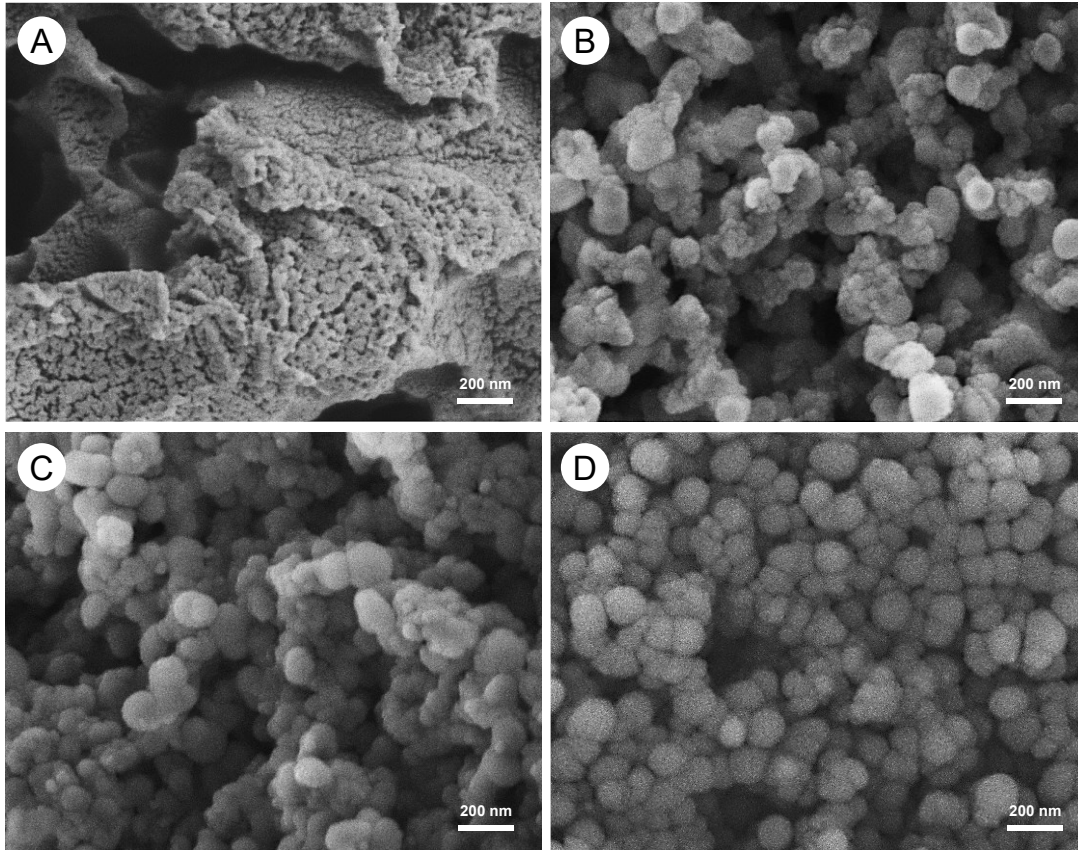
Fig. 3.5 FE-SEM images of samples produced by: A, B) slow nanoprecipitation (dropwise addition of ethanol into starch solution), and C, D) rapid nanoprecipitation (rapid pouring of ethanol into starch solution) with starch concentration of 50 mg/mL (A, C) and 10 mg/mL (B, D), respectively, at AS/S ratio 1:1.

3.3.3. Mechanism of SNP formation by nanoprecipitation

The observed effects of AS/S ratio, starch concentration and addition methods (directly pouring or dropwise) on the formation of SNPs indicated a kinetically controlled syneresis. According to previous studies, nanoprecipitation was proposed to involve a molecular weight related nucleation-growth mechanism (Aubry and others 2009). In this mechanism, a few critical nuclei of solute are formed when the solution is sufficiently supersaturated, and then these nuclei grow by capturing solute molecules from the surrounding solution (this procedure also called condensation). The number of nuclei varies exponentially with the level of supersaturation, which is mainly controlled by the AS/S ratios; here the greater AS/S ratios translate to a greater supersaturation. Starch contains amylose and amylopectin. Amylopectin exhibits better solubility than amylose due to its highly branched structure, although the latter has relatively lower molecular weight. Upon addition of ethanol into the starch solution with an increasing AS/S ratio, the particle formation is initiated by the supersaturation of starch molecules depending on their solubility. It was expected that amylose molecules were to reach supersaturation and nucleation earlier than amylopectin at the low AS/S ratio (i.e., low ethanol concentration) due to their lower solubility. To test this, the amylose content of sedimented starch fractions generated at different AS/S ratios was determined. Table 3.1 shows the yields of sedimented starch fractions and their amylose contents. Without adding ethanol, no solid fraction separated from the starch solution upon centrifugation (at 5000 × g), due to the complete dissolution of starch molecules. A molecular-type dependent (AM or AP) fractionation was observed with increasing AS/S ratios from 0.3:1 to 0.6:1 (Table 3.1). Compared to the total amylose content (41%, w/w) of starch, the sedimented fraction consisted of a greater percentage of amylose (i.e., 77%) in the sediments obtained from AS/S ratio of 0.3:1. With increasing AS/S from 0.3:1 to 0.6:1, the yield of sedimented fraction increased from ~ 27% to

Table 3.1 The yield, amylose and amylopectin contents of the sedimented fraction obtained from fractionation of starch in ethanol-water system at different AS/S ratios

Samples	Sedimented fraction (% of starch) [x]	Amylose (%) [y]	Amylopectin (%) [z]
Native starch	-	41.1 ± 0.1 g	58.9 ± 0.1a
Starch solution	-	-	-
0.3:1	26.9 ± 1.5 d	76.6 ± 1.1 b	23.4 ± 1.1 f
0.4:1	55.8 ± 3.5 c	51.6 ± 0.4 c	48.4 ± 0.4 e
0.5:1	80.8 ± 4.2 b	45.4 ± 0.3 ef	54.6 ± 0.3 c
0.6:1	94.0 ± 2.7 a	42.4 ± 0.5 fg	57.6 ± 0.5 ab
0.7:1	75.6 ± 4.5 b	44.1 ± 0.2 e	55.9 ± 0.2 bc
0.8:1	28.8 ± 3.8 d	47.8 ± 0.4 d	52.2 ± 0.4 d
0.9:1	17.3 ± 1.8 de	99.2 ± 0.6 a	0.8 ± 0.6 g
1:1	7.3 ± 0.7 e	99.3 ± 0.4 a	0.7 ± 0.4 g

Data are means ± standard deviation (n = 3). Means within columns not sharing a common letter are significantly different at $p < 0.05$.
[x] Sedimented fraction was obtained from the ethanol-water mixture by centrifugation at 5000 × g;
[y] Amylose contents were measured by using iodine-blue technique (Chrastil 1987)
[z] Amylopectin (%) =100-Amylose (%)
- Not detected.

~ 94% (w/w) and their amylose contents decreased from 77% to 42%, indicating the gradual enrichment of amylopectin, because the solubility of amylopectin decreased with the increase in AS/S ratios. At the AS/S ratio of 0.6:1, almost all starch molecules were sedimented (~ 94%, w/w). This fractionation of starch in ethanol-water mixture at the AS/S ratio ≤ 0.6:1 indicated the non-uniform nucleation and growth of starch molecules due to the different solubility of starch molecules as well as the lower level of supersaturation. With a further increase in the AS/S ratio to 0.8:1, 0.9:1, and 1:1, the amount of the sedimented fraction decreased to 29%, 17% and 7% with amylose contents of 48%, 99% and 99%, respectively. After centrifugation (5000 $\times g$), most of the particles were well dispersed in the ethanol-water mixture due to their smaller particle size. According to previous studies (Brick and others 2003; Aubry and others 2009), high levels of supersaturation are required to initiate homogeneous nucleation, which is beneficial for the formation of small particles. At low supersaturation, particles can grow faster than they nucleate, resulting in particles with a larger PSD. However, at higher supersaturation levels, nucleation dominates particle growth, finally resulting in smaller particles. The results observed in the present study suggested an increase in supersaturation levels for starch was accompanied by an increase in nucleation and a decrease in growth rates (i.e., less sediments). Therefore, in order to obtain SNPs of less than a few hundred nanometers in size, nucleation should be favoured over growth. When growth is favoured over nucleation, few nuclei form and will likely grow into micrometer sized particles. The greater amylose content in sediments of AS/S 0.9:1 and 1:1 also indicated the large particles formed here were mainly amylose nuclei aggregates, which was in agreement with the premise that amylose molecules reach supersaturation and nucleation faster than the amylopectin molecules.

Based on the accumulated observations in the present study, a mechanism was proposed for the nanoprecipitation of starch molecules in ethanol-water mixtures (Fig. 3.6A) to form SNPs. As could be anticipated from the distinct visual appearance of SNPs in ethanol-water mixture (Fig. 3.4A), clear differences were observed in the particle size at different AS/S ratios (Fig. 3.4B and 3.6B). At low supersaturation, upon addition of ethanol into starch solution, the particle formation is initiated by the molecular type-dependent supersaturation of starch, from AM to AP gradually (Table 3.1). The nuclei formed initially from amylose and further grew through capturing starch molecules, resulting in the formation of large particles and subsequent sedimentation. This sedimentation tendency of SNPs was prevalent especially at lower AS/S ratios as well as higher starch concentrations that did not result in stable colloidal dispersions (Fig. 3.4C and Fig. 3.5C). According to previous studies (Brick and others 2003; Aubry and others 2009), if the supersaturation is less, nucleation is more difficult, a small number of nuclei will be formed, and the resulting particles will be large because they evolve by collecting all the available solute molecules (i.e., all the solute molecules in excess of their solubility limit). When there is more solute (i.e., high solute concentration), the supersaturation is greater, which yields more nuclei, but there are also more molecules to feed the growth of these nuclei. This could also explain the increased amount of sediments at low AS/S ratios (i.e., AS/S 0.3:1-0.6:1) (Table 3.1); with an increase of AS/S ratio the supersaturation increases, and more molecules reach their solubility threshold to feed the growth of nuclei. For example, at very low AS/S ratio of 0.3:1, nuclei mainly formed from amylose and further grew by collecting all available starch molecules (i.e., supersaturated amylose and amylopectin molecules), which resulted in 27% sediment (i.e., large particles) with 77% amylose in the sediment while other molecules (i.e., mainly amylopectin) remained dissolved in the solution. At the AS/S ratio of 0.6:1, there was ~94% sediment probably

because most of the starch molecules were in excess of their solubility limit. This led to a fast

growth of nuclei by collecting more starch molecules, resulting in the formation of larger particles.
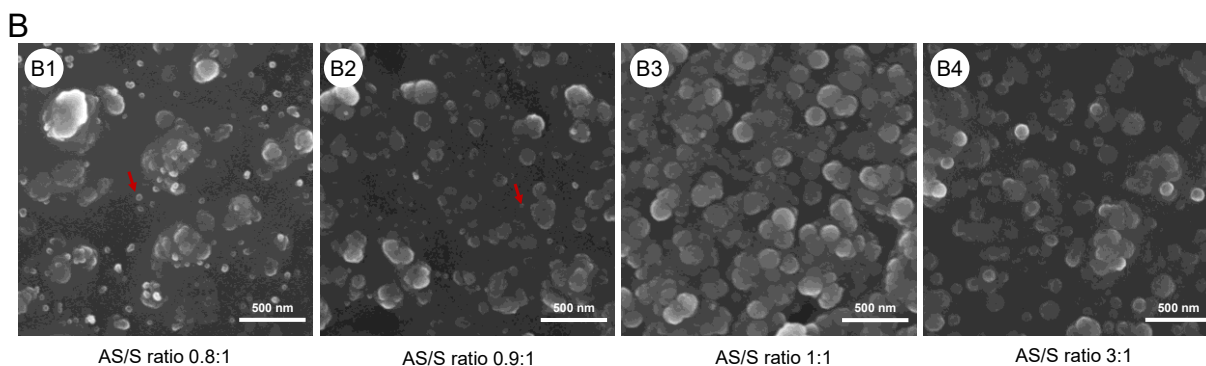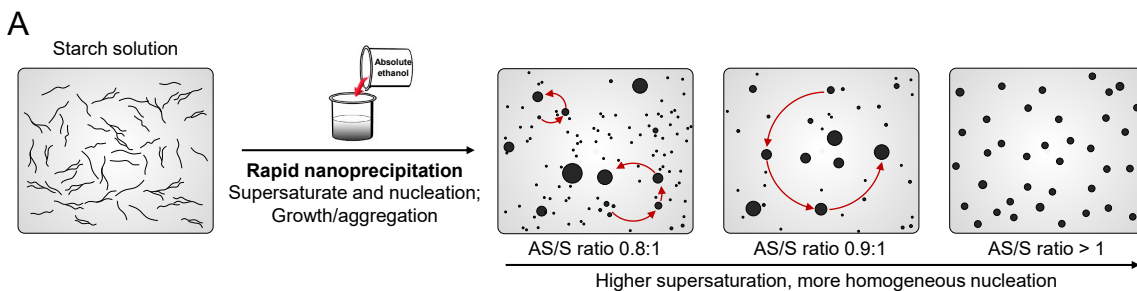
Fig. 3.6 SNP formation in ethanol-water system. A) Schematic mechanism of nanoprecipitation. Growth of the nuclei of 10-50 nm and their fusing with larger particles lead to the growth of nanoparticle spheres. Spherical colloidal starch particles form upon growth of large number of small nuclei when AS/S ratio is more than 1:1. Adapted and modified from previous reports (Barreras-Urbina and others 2016; Sipponen and others 2018); B) FE-SEM images of SNP dispersions at varying AS/S ratios. Both large and small particles (red arrow) presented at lower AS/S ratios due to lower level of supersaturation and inhomogeneous nucleation.

According to the nucleation-growth/aggregation model, high level of supersaturation (i.e., high

AS/S ratio) is required to initiate homogeneous nucleation process (Brick and others 2003). At a

low AS/S ratio (i.e., 0.8:1), the PSD of SNPs was found to be broader with greater value of PDI

(Fig. 3.4B). As shown in FE-SEM images (Fig. 3.6B), non-uniform particles i.e., a mixture of

small and large SNPs, were present in two SNPs samples produced at the AS/S ratios 0.8:1 and

0.9:1 (Fig. 3.6B1 and B2, respectively). In those samples, the observed small particles ranged in size between 20-50 nm. At the AS/S ratio of 0.8:1, the presence of the small particles was more prevalent with the mean size of 35 ± 5 nm (FE-SEM image analysis). These small particles may further grow by aggregation to form larger particulates (i.e., > 200 nm). This is evident from FE-SEM images (Fig. 3.6B1) showing the presence of many small particles on the surface of larger aggregates. Thus, it seems plausible that nucleation-growth mechanism occurs in parallel to particle aggregation and growth. It was observed that when increasing the AS/S ratio above 1:1, the resulting aggregates were much smaller and uniform with smoother surface area (Fig. 3.6B2). This may be attributed to high levels of supersaturation at AS/S ratios above 1:1 (Fig. 3.6B3 and B4) that leads to rapid and homogeneous nucleation of amylose and amylopectin molecules. At the AS/S ratio of 1:1, there were only few small particles (< 50 nm), with most particles in the size range of 70-200 nm (Fig. 3.5 D and 3.6 B3). In addition, according to the result from Table 3.1, there was 7% sediment with 99% amylose, indicating those large particles were formed by the aggregation of particles formed mainly from amylose, which also supports the influence of starch molecular type on the nucleation-aggregation mechanism of starch nanoprecipitation. At very high supersaturation (AS/S ratio > 3:1), the nucleation-growth model predicts that the number of the nuclei should increase rapidly and consequently leading to particles of small size. However, this is in conflict with the behavior observed here at high supersaturation. Indeed, under such conditions (AS/S ratio > 1:1), the mean particle size was independent of AS/S ratios (Fig. 3.4B). For this high supersaturation regime, the nucleation-aggregation mechanism may dominate. In nucleation-aggregation mechanisms, the number of nuclei is so large that they have frequent encounters, thus resulting in the aggregation of those nuclei, which hinders the further reduction in particle size with an increase in AS/S ratio (Aubry and others 2009). Finally, rapid addition of

ethanol into starch solution to a desired AS/S ratio (i.e., 1:1), could avoid the non-uniform nucleation and growth of SNPs during slow nanoprecipitation when ethanol was gradually added into the starch solution (rapid vs slow nanoprecipitation).

SNP formation via a supersaturation-nucleation-and-growth route has been proposed in earlier research, but this research has given further insight. Here the nucleation is possibly initiated by precipitation of amylose molecules as precursors for the critical nuclei. SNPs then form via aggregation and collection/fusion of small nuclei/molecules into gradually larger particles. The fractionation data, amylose determination results, and the SEM images provide indirect support for the final growth/aggregation step. It is also plausible that the molecular type/solubility governed the initiation of starch nanoprecipitation when the AS/S ratio is increased. A similar trend of fractionation based on molecular weight/solubility was previously observed from the nanoprecipitation of lignin in aqueous ethanol solutions by adding water as antisolvent (Sipponen and others 2018), which supports these conclusions.

3.3.4. The effect of separation and drying methods on the formation of SNPs

Since a nanoparticle has a much smaller size and a greater Brownian diffusion against settling than a microparticle, the settling time of nanoparticles is much longer than that of microparticles. This could lead to nanoparticle coarsening due to Ostwald ripening and recrystallization. Therefore, a fast separation of produced nanoparticles away from ethanol-water system right after the mixing would be desirable. Fig. 3.7 shows FE-SEM images and PSD of SNPs collected by different separation and drying methods. A very high speed centrifugation could accelerate settling of SNPs. The preliminary trials indicated that a centrifugation speed of $48,000 \times g$ could settle more than 90% SNPs. However, it is highly energy-consuming and not suitable for a large-scale production.
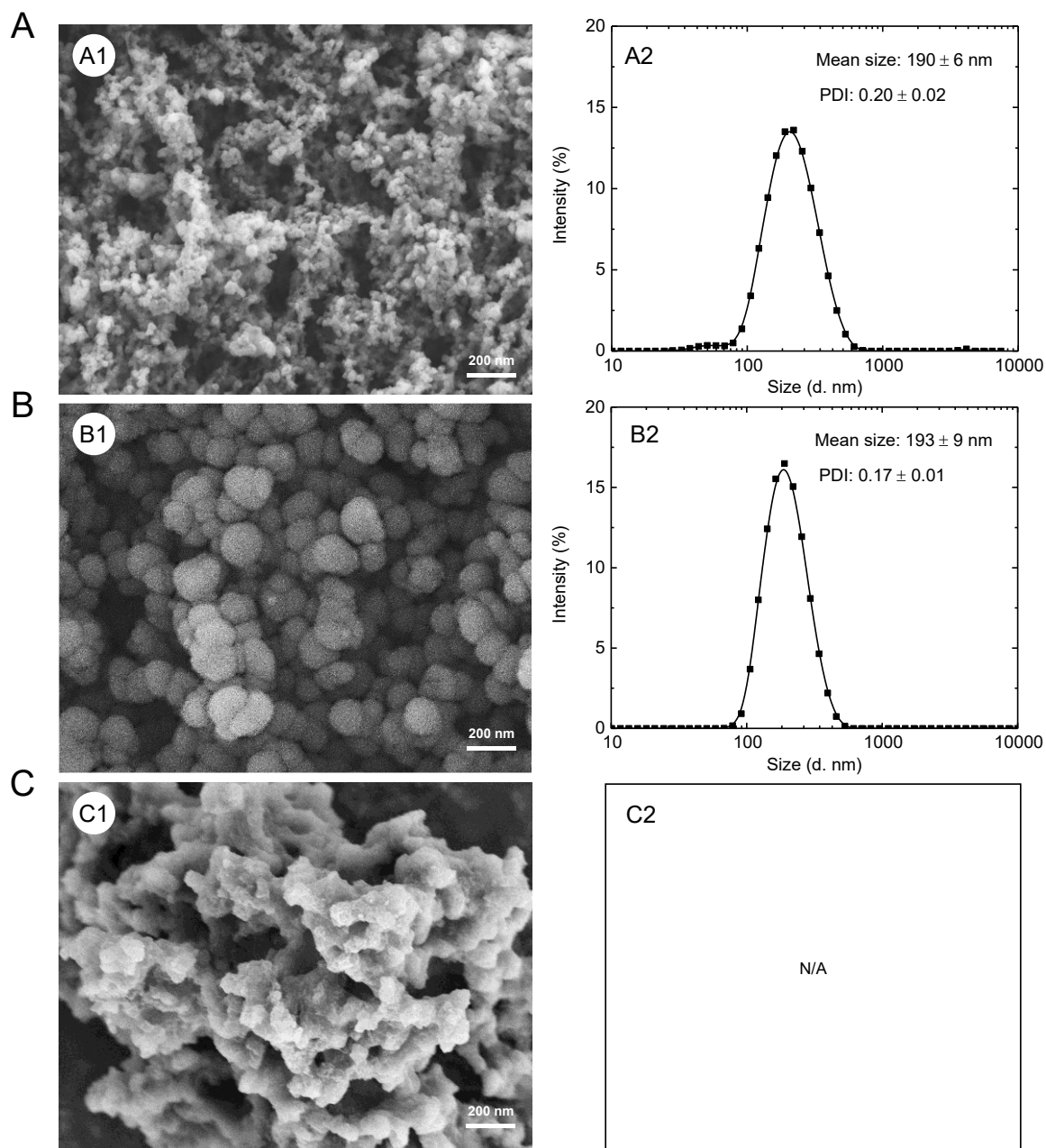
Fig. 3.7 (A1-C1) FE-SEM images, (A2-C2) mean particle size, PSD, and PDI values of: (A) freeze-dried SNP separated by solvent evaporation; (B) freeze-dried SNP separated by homogenization; (C) Oven-dried SNP (40 °C, overnight) separated by homogenization. All SNP were produced under the same conditions by rapid nanoprecipitation with 10 mg/mL diluted starch concentration at AS/S ratio of 1:1 (v/v).

More importantly, the colloidal SNPs obtained were not dispersible due to their very compact nature after centrifugation. Therefore, high speed centrifugation was not selected for the separation of SNPs in this study. Another widely used approach for polymer nanoparticle separation is solvent evaporation, but this method is time-consuming especially with large samples. According to a previous study (Cohen and others 2018), nanoparticles could rapidly aggregate and quickly settle under required sonication depending on the nanoparticle types. However, the mechanisms of this shear induced nanoparticle aggregation and settling remained unclear. The authors considered the balance of two opposing interfacial forces, where electrostatic repulsion and van der Waals attraction were closely related to the particle aggregation and colloidal stability. For particles in suspension, electrostatic repulsion is a major force against particle aggregation. In general, colloidal suspension with a zeta potential ranging from 0 to $\pm$ 5 mV will rapidly flocculate, while a zeta potential larger than $\pm$ 30 mV is considered the threshold beyond which the colloidal suspension has good stability. Suspended particles between $\pm$ 5 and $\pm$ 30 mV may either aggregate or stabilize in suspension (Everett 1988).

In the present study, the zeta potential of SNPs in ethanol-water mixture at the AS/S ratio of 1:1 was around -10 mV, and they remained stable in ethanol-water mixture for ~ 7 days and thereafter visible SNP aggregates were observed. The relatively weak electrostatic repulsive forces rendered the SNPs a high tendency to form aggregates rapidly upon shearing. Thus, it was proposed that applying appropriate shear would promote the settling of SNPs in the ethanol-water mixture. To test this, the effect of shearing on the settling of SNP in the ethanol-water mixture was studied. When applying shear by using a homogenizer at 8,000 rpm (minimum speed adapted) for 20, 40, and 60 s, SNPs in the mixture formed aggregates rapidly and then settled down at the bottom of

the container. The settled SNPs could be easily collected from the liquid mixture by centrifugation or filtration. The yield of SNPs recovered was up to 94% after homogenization for 60 s. When measuring the particle size and PDI values of the freshly prepared SNPs dispersed in Milli-Q water after separation without drying process, the mean particle size and PDI were 149 ± 12 nm and 0.28 ± 0.01, respectively, which were comparable to the data (mean size: 132 ± 9, PDI: 0.27 ± 0.01) measured by directly diluting an aliquot of resultant suspension after nanoprecipitation. The slight increase in mean particle size could be due to the aggregation during the redispersion procedure, but the difference was not significant.

The FE-SEM images of freeze-dried SNPs separated by shear induced recovery is presented in Fig. 3.7. For comparison, the FE-SEM images of the freeze-dried SNPs separated by evaporation and the sample separated by shear induced recovery with oven-drying were also incorporated in Fig. 3.7. All SNPs were formed from starch solution under identical conditions (starch concentration of 10 mg/mL at AS/S ratio 1:1). For the freeze-dried SNPs separated by solvent evaporation (Fig. 3.7A), most of the particles were irregular probably due to the long-time operation. The freeze-dried SNPs separated by the shear induced method (Fig. 3.7B) were more discrete than those separated by the solvent evaporation. Moreover, the freeze-dried SNPs separated by shear induced method were smoother in surface and more regular in shape. However, those SNPs separated by homogenization after oven drying (Fig. 3.7C) formed agglomerates. Different observations were found by other authors in a previous study (Uzun and Kokini 2014), in which corn SNPs were spherical in shape after vacuum oven drying, while losing their shape and forming a fibrous structure after freeze-drying. In another study, both oven-drying and freeze-drying had no obvious effect on the appearance of the amylose nanoparticles (Yan and others 2017). This could be

ascribed to the different drying conditions such as the temperature, humidity, drying time, as well as the starch type used (Uzun and Kokini 2014; Yan and others 2017).

In order to determine the dispersion characteristics of SNPs, the dry SNPs were redispersed in Milli-Q water. The mean particle size, PSD, and PDI of SNPs collected by different separation and drying methods are also presented in Fig. 3.7. Both freeze-dried samples separated by solvent evaporation and shear induced method show a nanoscale particle size and the PSD was narrow, while the sample produced with oven-drying was not able to redisperse in Milli-Q water. The freeze-dried SNPs were able to be dispersed in water. However, the mean particle size was larger than that measured before drying (see Fig. 3.8A), which was probably related to the aggregation of small particles (<100 nm) during drying procedure. Interestingly, the PDI was less after redispersion which means the PSD became narrower after freeze-drying (Fig. 3.7B2). A similar result was found for Hylon V and VII corn starch nanoparticles produced using acetone as an antisolvent (Sadeghi and others 2017). This could be related to the large content of amylose in Hylon V and VII as well as field pea starches, and the tendency of linear chain amylose in SNPs to form strong intra and/or inter molecular associations (i.e., hydrogen bonds) during drying, resulting in a strong network within the nanoparticles. Since the particle size was measured in Milli-Q water by DLS, the strong network would influence the hydration/swelling of freeze-dried SNPs compared to those without drying and thereby fewer large particles of freeze-dried SNPs distributed in the range of particle size > 500 nm. In general, based on the above observations, shear induced recovery of SNPs in ethanol-water mixture provides good means to quickly separate SNPs with high production efficiency and good particle characteristics.
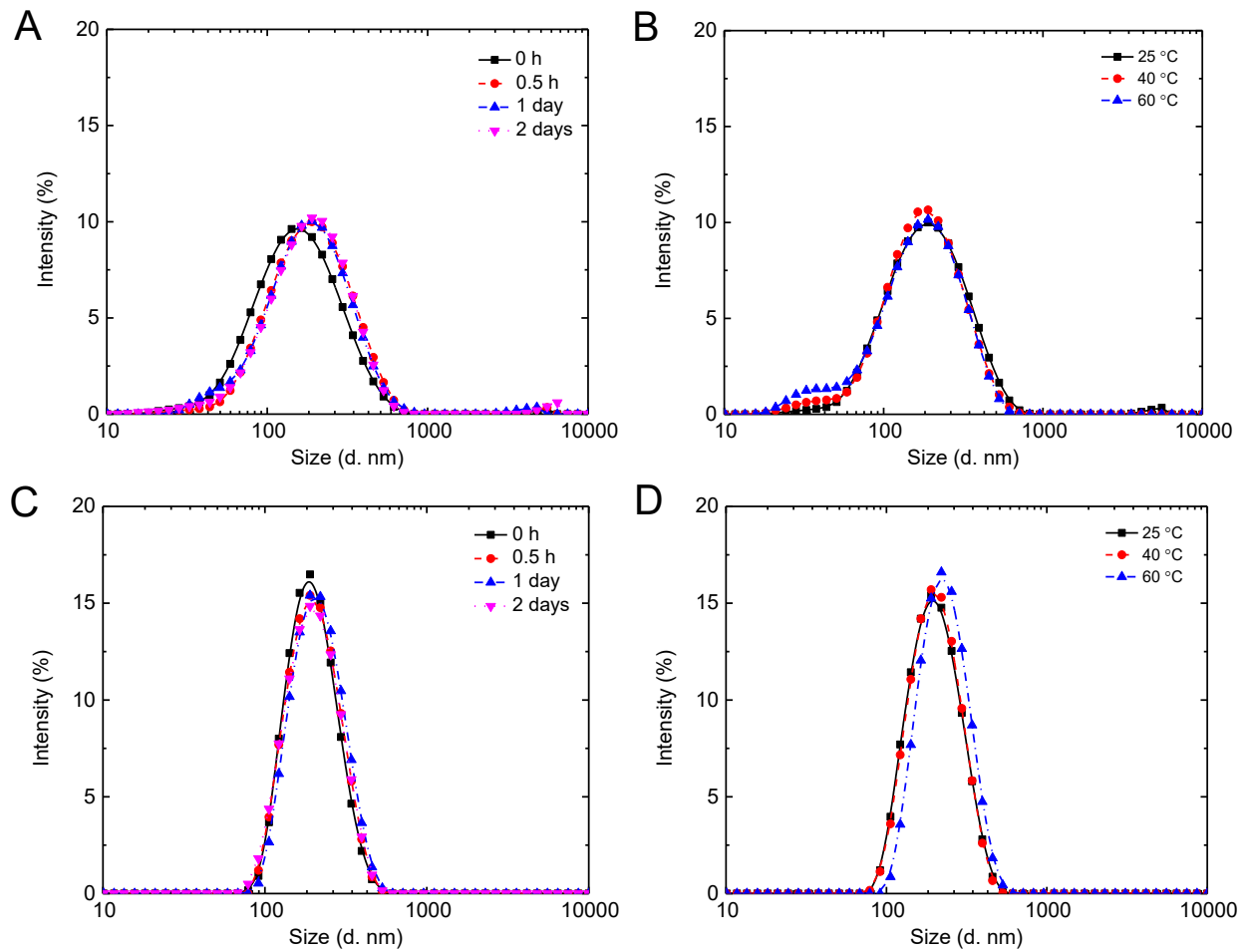
Fig. 3.8 Particle stability analysis of SNP resuspensions before (A and B) and after (C and D) freeze-drying: A and C shows the effect of storage time on particle size; B and D shows the effect of temperature on the particle size.

In order to further understand how shear induced recovery of SNPs work with other starch sources, different types of starch, including regular corn, wheat, faba bean, and potato, were investigated. Under identical conditions (starch concentration 10 mg/mL, AS/S ratio 1:1), only faba bean and potato starches formed the stable colloidal suspension in ethanol-water mixture. However, the rapid aggregation and settling of SNPs through homogenization were observed in faba bean starch but not in potato starch. This is probably because the potato SNPs suspension in ethanol-water system was very stable due to its high phosphorus content, giving potato SNPs more negative charge and interparticulate repulsion. This is consistent with a previous study (Cohen and others 2018), in which materials with lower zeta potential were likely to rapidly aggregate and settle at the bottom of the container upon ultrasonication. Since the different behaviors of starches were observed under identical SNP formation conditions, further research should focus on the influence of starch type on SNP formation.

3.3.5. Particle stability analysis

3.3.5.1. The effect of storage time

Effect of storage time on the particle size of SNPs before and after freeze-drying, and their size stability in aqueous suspension is presented in Fig. 3.8A and C. These SNPs were produced by rapid nanoprecipitation at 10 mg/mL (prepared by dilution of the stock solution) at the AS/S ratio of 1:1. As shown in Fig. 3.8A and C, the PSD of SNPs both before and after freeze-drying slightly shifted to larger size range within 0.5 h and then remained stable with storage time. The reason for this variation is that SNPs could absorb water and undergo certain extent of swelling during initial period. However, at longer storage time in aqueous suspension (for 0.5 h to 2 days), the size of SNPs remained unchanged. Therefore, SNPs seems to have a stable structure when they remain dispersed in water for a longer storage time.

3.3.5.2. The effect of temperature

The effect of temperature (up to 60 °C) on the stability of SNPs in water before and after freeze-drying were determined and presented in Fig. 3.8B and D. As shown in Fig. 3.8B, when the temperature was increased from 25 to 60 °C, the particle size of SNPs without drying decreased slightly probably due to the release of small particles from the incomplete growth of particles. However, for the SNPs redispersed after freeze-drying (Fig. 3.8D), the PSD remained unchanged with an increase in temperature from 25 to 40 °C and then a shift to larger size with further increase in temperature. The values of the mean particle size of freeze-dried SNPs after incubation at 25°C, 40°C, and 60°C were 191 ± 6, 190 ± 6, and 227 ± 19 nm, respectively. The significant increase in the mean particle size with an increase in temperature from 40 to 60°C was probably related to the swelling of SNPs at higher temperatures. However, the temperature increase was not sufficient to break the remaining hydrogen bonds in SNPs, and thus SNPs were stable and resisted the further increase in particle size (i.e., the particle size increased from 191 to 227 nm). These results further indicated the strong intra and/or inter molecular associations formed in SNPs after drying. This is in agreement with a previous study (Yan and others 2017), in which the authors revealed that amylose nanoparticles after drying exhibited a typical pattern of amorphous material with a short and/or intermediate range of structure, while those without drying did not show any diffraction peaks.

3.4. Conclusions

Field pea SNPs were successfully fabricated by optimizing the conditions of starch dissolution and nanoprecipitation. The SNP particle size and PSD were controlled by adjusting the processing parameters, such as starch stock solution concentration, ultrasonication amplitude, AS/S ratio, starch dilution concentration, as well as the SNP separation and drying technique. The optimum

ultrasonication amplitude was 60% with a starch concentration of 100 mg/mL in stock solution, followed by direct addition of ethanol to the diluted starch solution (10 mg/mL) at a ratio of 1:1 (v/v). With this technique, a suspension of SNPs with a mean particle size of about 130 nm was prepared with a narrow size distribution. Particle formation followed the classical nucleation/growth theory, and the molecular type (i.e., amylose, amylopectin) exerted a significant influence on the process of particle formation and growth. Application of shear mixing to the ethanol-water mixture containing SNPs facilitated SNP rapid aggregation and settling, which enabled easy collection of SNPs from the mixture. This newly identified SNP collection method is quick and effective when compared to conventional methods such as solvent evaporation or high-speed centrifugation, and thus shows commercial potential. The freeze-dried SNPs formed were spherical and could be well re-dispersed in water. The particle size of the freeze-dried SNPs in aqueous suspension were not affected by temperature within a 25-60 °C range, making them stable at body temperature and thus potentially suitable drug carriers for *in vivo* delivery.

Chapter 4: Preparation and characterization of nanoparticles from cereal and pulse starches by ultrasound-assisted dissolution and rapid nanoprecipitation

4.1. Introduction

The initial starch concentration, antisolvent/solvent (AS/S) ratio has been found to be crucial for the formation of SNPs by nanoprecipitation. A low starch concentration (1-8 mg/mL) is probably necessary to ensure that molecules are discrete in the solvent (Saari and others 2017). Ultrasonic treatment promotes the dissolution of starch molecules and gives smaller and more uniform particles with larger starch concentrations of up to 50 mg/mL by breaking the inter- and intra-molecular association of starch in the solvent. Preparing SNPs from a starch solution by nanoprecipitation using non-ultrasonication techniques have been reported for corn, wheat, rice, potato, sago, tapioca and other sources of starch. Ultrasonication methods have only been investigated with a few starch sources, such as pure amylose, potato, tapioca, chestnut, and lotus stem. The AS/S ratio has also been found to affect the formation of SNPs, where usually large ratios (10:1-30:1) are required to produce SNPs with desired size and shape, indicating the limitation of nanoprecipitation techniques where a large amount of antisolvent is used. In order to overcome this limitation, more recently, a rapid addition method by directly pouring ethanol into diluted starch solution was found to increase the production efficiency by using a small AS/S ratio 1:1 (Saari and others 2017). However, limited information is available regarding the effects of the starch source, starch concentration, and AS/S ratio on the formation and characterization of SNPs via this rapid nanoprecipitation technique. Furthermore, in Chapter 3, SNP produced from field pea starch through the combination of ultrasound-assisted dissolution and rapid nanoprecipitation showed that the formation of SNP was influenced to a large extent by the amylose molecules. However, there is dearth information on the molecular composition and structure of SNP produced

by nanoprecipitation. Therefore, the present study was designed to investigate the production and characterization of SNPs from pulse starches, faba bean and field pea, in comparison to those from commercial cereal starches, regular corn and wheat. The specific objectives are 1) to compare the effect of AS/S ratio and starch concentration on particle size of SNPs produced from native starches of different botanical origins; 2) to investigate the molecular composition and structure of SNPs obtained from pulse and cereal starches; and 3) to compare the morphology, molecular characteristics, crystalline structure, molecular order, and thermal properties of SNPs obtained from pulse starches to those from cereal starches.

4.2. Materials and methods

4.2.1. Materials

Regular corn, regular wheat, Faba bean, and field pea starches, amylose and amylopectin from potato starch were described in Chapter 3 section 3.2.1. Milli-Q water was used for all experiments. All other chemicals were of analytical grade.

4.2.2. Starch dissolution and rapid nanoprecipitation

The method development was based on two previous studies on dissolution (Chang and others 2017b) and nanoprecipitation (Saari and others 2017). Four types of native starch were individually dispersed in Milli Q water (50 mg/mL) and gelatinized in a boiling water bath for 30 min. The gelatinized starch paste was then cooled to 60 °C and sonicated for 10 min using a 20 kHz ultrasonic processer (FS-1200 N, Shanghai Sonxi Ultrasonic Instrument Co., Ltd., Shanghai, ZJ, China) equipped with a probe transducer and a flat tip of 13 mm. The probe was immersed into the samples during ultrasonication, which was carried out at an amplitude of 60% and 5/2 s on/off pulses were applied to minimize heat generation. The homogenous starch solution (50 mg/mL) was then diluted to concentrations of 2.5, 10, and 50 mg/mL before nanoprecipitation. The

nanoprecipitation was performed by pouring the antisolvent rapidly into a magnetically stirred starch solution. All experiments were completed using absolute ethanol as an antisolvent. The starch concentration and AS/S ratio were 2.5, 10, and 50 mg/mL and 1:1, 3:1, 5:1 (v/v), respectively. After thorough mixing, an aliquot of the colloidal suspension obtained was diluted with water for the analysis of the particle size, particle size distribution (PSD), and polydispersity index (PDI) by dynamic light scattering (DLS, see Chapter 3 Section 3.2.4). Finally, the colloidal suspension was homogenized to promote the precipitation of fine particles using a homogenizer at 8,000 rpm for 1 min (Heidolph Diax 900, Schwabath, Bavaria, Germany). The sediments were collected by centrifugation and then re-dispersed in water and frozen at -20 °C overnight in a freezer. The frozen samples were then freeze-dried (FreeZone 12, Labconco Corp., Kansas, MO, USA) at a sublimating temperature of −45 °C for 2 days.

4.2.3. Redispersion of SNPs

Freeze-dried SNPs were redispersed in Milli-Q water following the procedure described in Chapter 3 Section 3.2.3. The particle size, PSD, and PDI were measured by DLS as described in Chapter 3 Section 3.2.4.

4.2.4. Field emission scanning electron microscopy (FE-SEM)

The morphology and the size of freeze-dried SNP were observed followed the procedure as described in Chapter 3 Section 3.2.5.

4.2.5. Determination of the amylose content and molecular characteristics of native starches and SNP counterparts.

Apparent amylose content was measured using the iodine-blue method as described by Chrastil (1987). The weight-average molar mass (M_w), z-average radius (R_z) of gyration and molecular density (ρ) of native starch and SNP samples were evaluated using a high-performance size-

exclusion chromatography equipped with a multi angle laser light scattering and a differential refractive index detector (HPSEC-MALLS-RI) according to a previously reported method (Yoo 2002), with minor modification. In detail, samples (20 mg, dry basis) were dispersed in 1.5 mL of 90% (v/v) dimethyl sulfoxide (DMSO) and were then heated in a boiling water bath for 1 h with vortexing every 5 min. The solubilized starch solution was cooled to room temperature (22 °C) followed by the addition of absolute ethanol (10 mL) to precipitate starch. After maintaining at 4 °C for 2 h, the solution was then centrifuged at $6000 \times g$ for 10 min and the obtained pellet was washed with cold ethanol (5 mL). The pellet was re-dissolved by adding 2 mL 1 M NaOH and was then diluted with 15 mL 0.1 M $NaNO_3$. After the pH was adjusted to 6.7-6.9 using 1 M HCl, the diluted solution was made up to 20 mL using 0.1 M $NaNO_3$ to reach a starch concentration of 1 mg/mL. Afterward, the solution was heated in a boiling water bath for 30 min. The hot sample solution was filtered through a nylon membrane filter (5 μm) and 50 μL filtrate was injected into the HPSEC-MALLS-RI system.

The HPSEC-MALLS-RI system was equipped with an Agilent 1200 HPLC system (Agilent Technologies, Santa Clara, CA, USA) coupled with a multi-angle laser light scattering detector which had a laser wavelength of 658 nm (MALLS, DAWN-HELEOS II, Wyatt Technology, Santa Barbara, CA, USA), and a refractive index detector (RID, Agilent Technologies, Santa Clara, CA, USA). To separate amylopectin (AP) from amylose (AM), a guard column (Ultrahydrogel™, 6 × 40 mm, Waters Corporation, Milford, MA, USA) and an SEC column (Ultrahydrogel™ Linear, 7.8 × 300 mm, Waters Corporation, Milford, MA, USA) were connected to the HPLC system. The mobile phase was an aqueous solution of 0.1M $NaNO_3$ (0.1 M) and 5 mM NaN_3 with a flow rate of 0.5 mL/min. The column and RI detector temperatures were maintained at 40 °C and 35 °C,

respectively. A beta-glucan standard (Mw=2.65×10^5, 1 mg/mL) was used to test the chromatography system. The ASTRA software (Version 5.3.4.20, Wyatt Technology, Santa Barbara, CA, USA) was used to collect and analyze data from the HPSEC-MALLS-RI system. A refractive index increment (dn/dc value) of 0.146 mL/g for starch was applied in calculations using the Berry extrapolation model with a first-degree polynomial fit (Yoo 2002; Chen and Bergman 2007; Naguleswaran and others 2014). The M_w (g/mol) and R_z (nm) of AM and AP were automatically calculated by ASTRA, and the ρ ($\rho = M_w/R_z^3$ in g/mol/nm^3) of AP and AM was calculated according to the method of a previous study (Yoo 2002).

4.2.6. X-ray powder diffraction (XRD)

XRD patterns of the native starch and SNPs samples were obtained using a Rigaku Ultima IV multipurpose X-ray diffractometer (Rigaku America, Woodlands, TX, USA). The powder samples were placed on a zero-background plate, then scanned through a diffraction angle 2θ range of 5-90° at a speed of 2.0°/min, using a Co-Kα radiation generated at 38 kV and 38 mA. All data files were converted from cobalt (1.78899 Å) to copper (1.54059 Å) by changing the radiation wavelength.

4.2.7. Attenuated total reflectance-Fourier transform infrared (ATR-FTIR) spectroscopy

The molecular orders of native starch and SNPs were evaluated by an ATR-FTIR (Alpha, Bruker Optics Inc., Billerica, MA, USA). Dry starch and SNPs powder was used for spectral analysis. The ATR-FTIR spectra of samples was obtained using a 26 scan within a wavelength range of 4000-400 cm^{-1}. The spectra were then baseline-corrected and deconvoluted in the region from 1200-800 cm^{-1} with a half-band width of 20 cm^{-1} and an enhancement factor of 2.0 (using OMNIC 8.0). The absorbance intensities of the bands at about 1047, 1022 and 995

cm^{-1} were used to investigate the crystalline structures of native starch and SNPs (van Soest and others 1995; Zhang and others 2013).

4.2.8. Differential scanning calorimetry (DSC)

Gelatinization parameters of starches were measured using a differential scanning calorimeter (Q100, TA Instruments, New Castle, DE, USA) as described in the literature (Sang and others 2010). Water (15 µL) was added to native starch (3 mg, dry basis) initially placed in a stainless-steel DSC pan (PerkinElmer Inc., Shelton, CT, USA) which was then sealed, and allowed to equilibrate for 24 h at room temperature. The scanning temperature ranged from 10 to 200 °C and the heating rate was 10 °C/min. In all measurements, the thermogram was recorded with an empty sealed-steel pan as a reference. The thermal transitions of starch were defined in terms of temperature at T_o (onset), T_p (peak), and T_c (conclusion) and calculated from the thermograms. The value of T_c-T_o reflects the variation of crystalline stability. ΔH refers to the enthalpy of the transition and is expressed as per unit weight of dry starch (J/g).

4.2.9. Statistical analysis

All experiments were done in at least three replicates. Results are presented as mean ± standard deviation (SD). Analysis of variance (ANOVA) was performed, and the mean comparisons were performed by Tukey's HSD test using OriginPro software (OriginPro 9.0.0, OriginLab Northampton, MA, USA).

4.3. Results and discussion

4.3.1. The effect of starch concentration on particle size and morphology of SNP

The mean particle size and PDI (reflects on uniformity) of SNPs prepared from all four starches at three different starch concentrations (2.5, 10, 50 mg/mL) are presented in Table 4.1.

Table 4.1 Mean size and PDI of SNPs obtained using four types of starch at different operation conditions before and after freeze-drying

| Type of starch[a] | Operation parameters | | Before drying [b] | | After drying [c] | |
	Starch concentration (mg/mL)	AS/S ratio (v/v)	Mean size (d.nm)	PDI	Mean size (d.nm)	PDI
	2.5	1:1	166.9 ± 22.47	0.28 ± 0.01	232.5 ± 7.77	0.29 ± 0.03
	10	1:1	320.2 ± 48.7	0.52 ± 0.01	323.6 ± 19.9	0.37 ± 0.01
RC	50	1:1	669.4 ± 128.3	0.63 ± 0.17	1886.7 ± 75.7	0.46 ± 0.30
	10	3:1	358.5 ± 75.9	0.55 ± 0.03	482.9 ± 21.3	0.40 ± 0.06
	10	5:1	299.7 ± 61.2	0.54 ± 0.05	441.8 ± 58.3	0.59 ± 0.13
	2.5	1:1	217.9 ± 22.9	0.32 ± 0.03	239.2 ± 15.7	0.32 ± 0.03
	10	1:1	438.4 ± 35.0	0.55 ± 0.02	360.1 ± 18.3	0.38 ± 0.03
RW	50	1:1	806.0 ± 39.7	0.64 ± 0.05	1371.7 ± 54.9	0.72 ± 0.06
	10	3:1	238.7 ± 12.5	0.41 ± 0.01	264.4 ± 11.3	0.27 ± 0.03
	10	5:1	282.0 ± 39.3	0.52 ± 0.02	427.5 ± 54.5	0.51 ± 0.07
	2.5	1:1	133.6 ± 4.35	0.26 ± 0.01	184.5 ± 6.3	0.12 ± 0.02
	10	1:1	132.8 ± 6.0	0.27 ± 0.01	165.8 ± 6.9	0.17 ± 0.02
FB	50	1:1	333.8 ± 39.7	0.48 ± 0.01	341.7 ± 18.0	0.24 ± 0.02
	10	3:1	117.3 ± 6.0	0.28 ± 0.01	190.7 ± 13.0	0.15 ± 0.02
	10	5:1	107.6 ± 4.1	0.26 ± 0.01	152.5 ± 4.0	0.42 ± 0.02
	2.5	1:1	132.7 ± 5.9	0.27 ± 0.01	200.1 ± 4.4	0.14 ± 0.03
	10	1:1	122.6 ± 5.6	0.28 ± 0.02	189.5 ± 6.2	0.16 ± 0.01
FP	50	1:1	378.7 ± 80.9	0.48 ± 0.04	410.9 ± 23.5	0.22 ± 0.01
	10	3:1	126.0 ± 9.1	0.25 ± 0.01	266.3 ± 6.7	0.29 ± 0.01
	10	5:1	117.7 ± 11.0	0.25 ± 0.01	167.3 ± 6.2	0.80 ± 0.04

[a] RC (regular corn), RW (regular wheat), FB (faba bean), and FP (field pea)
[b] The mean particle size and PDI were measured using DLS, SNPs were dispersed in Milli-Q water after centrifugation without drying process
[c] The mean particle size and PDI were measured using DLS, Freeze-dried SNPs powder was dispersed in Milli-Q.
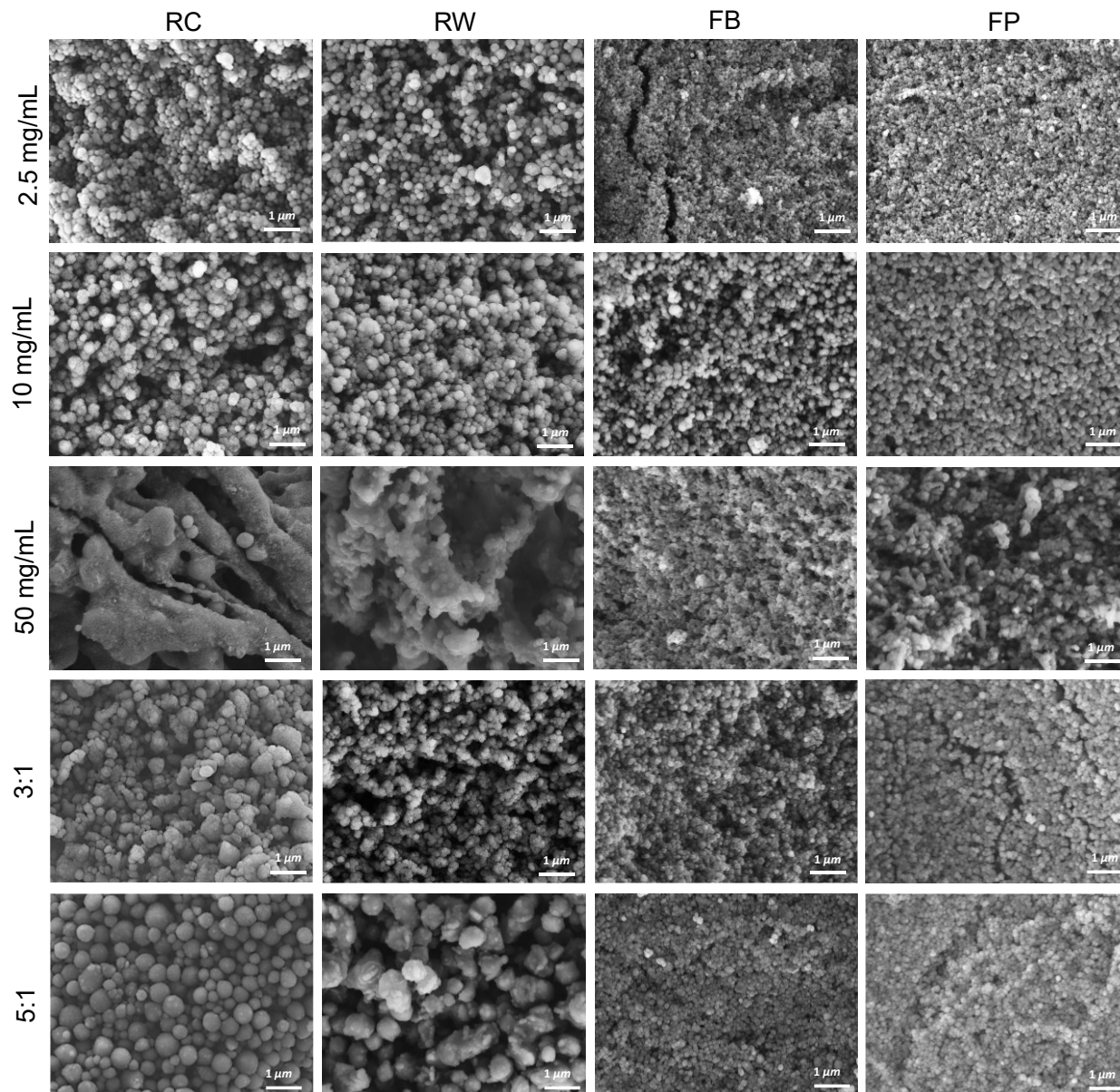
Fig. 4.1 Field emission scanning electron micrographs of samples prepared by rapid nanoprecipitation from RC (regular corn), RW (regular wheat), FB (faba bean), and FP (field pea) starch under different conditions. For different starch concentrations, SNPs were produced at AS/S (antisolvent-to-solvent) ratio of 1:1 (v/v) with starch concentration of 2.5, 10, and 50 mg/mL. For different AS/S ratio, SNPs were produced at AS/S ratio of 1:1, 3:1, 5:1 using starch concentration of 10 mg/mL.

The measurements were performed both before and after drying. The SNPs prepared from pulse starches were smaller and more uniform (lower PDI or narrower particle size distribution) compared to those from cereals at all investigated starch concentrations. In cereal starches, it was evident that the mean particle size and PDI progressively increased with the increasing starch concentration. The SNPs from wheat starch showed the largest mean particle sizes and the greatest PDI values. The FE-SEM images (Fig. 4.1) of freeze-dried SNPs prepared at different starch concentrations showed that the size of all SNPs are in the range of 50-150 nm, where a small fraction of SNPs was under 50 nm and a portion of small particles formed aggregates showing >150 nm in size. Under the same SNP preparation conditions, especially at starch concentration of 50 mg/mL, cereal starches with lower amylose contents formed larger and irregular sized aggregates when compared to pulse SNPs with higher amylose contents. This result is in good agreement with a previous study (Chang and others 2017b) where starch (potato) with high amylose content has been reported to show high potential to form smaller particles. However, in another study (Qin and others 2016), authors investigated the effect of starch type on the structural and morphological properties of SNPs through the nanoprecipitation method using seven native starches with low, medium, and high amylose contents. Their results showed that the starches with medium content of amylose (18.9-26.5%) were more suitable for the preparation of SNPs through nanoprecipitation because the prepared SNPs were more uniform in size. Compared to this study, there are obvious differences in the methodology used in the present study. In the present study, the starch dissolution in water was achieved by gelatinization and subsequent ultrasonication to form a homogeneous solution. This process might have been more effective in breaking inter-molecular H-bonds and possibly depolymerization in the native starch and solubilizing it thoroughly (Chang and others 2017b). In addition, nanoprecipitation method is also

91

different, where starch molecules were nano-precipitated by bulk pouring ethanol rapidly (adding ethanol at once) into starch solution in the present study. SNPs are usually generated by slow addition of antisolvent (ethanol) dropwise into starch solution or vice versa. According to a previous study (Sadeghi and others 2017), where ethanol was added dropwise into the starch solution, SNPs formed were unstable and lead to large aggregates, whereas SNPs remained small and stable (i.e. remained dispersed/discrete) when the starch solution was added into ethanol. This is consistent with the observations in a preliminary study, either addition of ethanol dropwise into starch solution or addition of starch solution dropwise into ethanol, SNPs remained in two phases as unstable large particles (precipitate or visible aggregates) and a stable colloidal dispersion. The extent of those two phases formed is affected by starch types, AS/S ratios, starch concentrations, as well as the addition techniques (i.e., addition rate, ethanol into starch solution or starch solution into ethanol, etc). However, it is found that the dispersion formed by rapid nanoprecipitation with four types of starch at different starch concentrations remained in one phase stable colloidal dispersion. The photographs of starch solution and antisolvent mixtures after mixing are presented in Fig. 4.2. Adding ethanol rapidly into starch solution at AS/S ratio of 1:1, cereal starch molecules formed a stable colloidal dispersion without visible aggregates at very low concentration (2.5 mg/mL), indicating the presence of small and uniform SNPs. With increasing starch concentration, unstable large particles/aggregates formed and rapidly settled down to the bottom of the tube. The RW starch settled down at lower starch concentration at 5 mg/mL, while RC starch settled at 10 mg/mL. However, for pulse, starch molecules formed a stable colloidal dispersion without visible aggregates at all three concentrations compared to cereal starches under the same conditions. These observations are consistent with the particle size measured objectively by DLS, where pulse starches show smaller SNP sizes and RW-SNP had the largest particle size. This is possibly

attributed to the variations observed in the molecular properties of starch molecules as determined

by HPSEC-MALLS-RI results (Table 4.2) and discussed under the section 4.3.4.
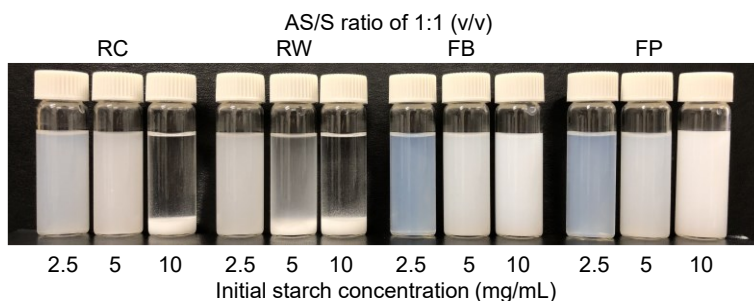
Fig. 4.2 Photographs of dispersions formed by rapid pouring of ethanol into starch solution. RC (regular corn), RW (regular wheat), FB (faba bean), and FP (field pea), AS/S (Antisolvent/solvent).

4.3.2. The effect of antisolvent-to-solvent (AS/S) ratio on particle size and morphology of SNP

The effect of different AS/S ratios on the formulation of SNPs was investigated since in previous

studies it was found that this ratio could significantly affect the particle size and final shape of the

SNPs. The ratios tested were 1:1, 3:1 and 5:1 with 10 mg/mL starch solution. Results are shown

in Table 4.1 and FE-SEM images are shown in Fig. 4.1. When AS/S ratio was changed from 1:1

to 5:1, the mean particle size of produced RC-SNPs remained unchanged around 300 nm. However,

the final morphology of the freeze-dried SNPs was dependent on the AS/S ratio. As shown in Fig.

4.1, at lower ratios, spherical SNPs with unsmooth surface were obtained due to the uncompleted

aggregation of small particles while smooth spheres were obtained when greater ratios were used

(5:1). This result is consistent with that previously reported by Wu and others (2016), who

observed that the RC SNPs were aggregated and with unclear shape when using AS/S of 5:1 while the obtained SNP were spherical in shape with distinct surface at AS/S ratio of 20:1 with particle sizes ranging from 300 to 400 nm. This observation was found under different AS/S ratios probably due to the different dissolution and nanoprecipitation methods used between the method here and the method elsewhere (Wu and others 2016). The method used in the present study significantly reduced the amount of antisolvent used (lower AS/S ratio). For RW starch, the particles became smaller when AS/S ratio increased to 3:1 while forming large aggregates at 5:1. The overgrowth of nanoparticles occurred because the supersaturation of starch molecules was too high for RW-SNP formation when using 10 mg/mL starch solution for nanoprecipitation at higher AS/S ratios. However, different observations were found for pulse starches. Pulse SNPs showed a slightly decrease in mean particle size, from 133 to 108 nm and from 123 to 117 nm for FB and FP, respectively, at higher AS/S ratios (Table 4.1). As shown in Fig. 4.1, the particles remained spherical in shape with smaller and uniform sizes. Considering the molecular structure of cereal and pulse starches, both contain amylose and amylopectin, which means the presence of two different sized molecules. Amylopectin was highly branched large molecule and amylose is a long chain molecule with just few branches. Therefore, how the SNPs formed with different sizes and shapes as shown in the FE-SEM images seems to be correlated with the structure of the pure starch molecules and amylose to amylopectin ratio of the starch granules (Qin and others 2016).

4.3.3. Re-dispersion of SNPs in Milli-Q water after freeze drying

Table 4.1 also shows particle size and PDI values of SNPs after freeze drying and re-dispersion in Milli-Q water. For cereal SNPs from RC and RW, particle size was slightly higher after drying and re-dispersion, but it was still close to the original size before freeze-drying when using starch concentration of less than 10 mg/mL. For pulse SNPs produced from FB and FP with starch

concentration range of 2.5-10 mg/mL, particle size was significantly increased after drying and re-dispersion. This could be explained by the highly packed small particles as shown in FE-SEM images which resulted in the presence of clusters of two or more nanoparticles in the re-dispersed SNPs suspension. Interestingly, for pulse SNPs produced at low AS/S ratio of 1:1, PDI values were lower after re-dispersion. This may be due to the aggregation of the very small particles (clusters of nanoparticles) which resulted in a larger mean particle size and narrower particle size distribution. Similar results were observed in a previous study on high amylose corn (Hylon V and VII) SNPs formulated with acetone as antisolvent (Sadeghi and others 2017). At higher AS/S ratios (3:1 and 5:1), all freeze-dried SNPs show larger particle sizes and greater PDI values than their sizes before freeze-drying, which were difficult to redisperse uniformly due to their very tightly packed nature. Based on the above findings, it could be concluded that the freeze-dried SNPs could be re-dispersed in water and larger size SNPs were much easier to redisperse than those SNPs with smaller particle sizes.

4.3.4. Molecular characteristics of SNPs determined by HPSEC-MALLS-RI

The molecular characteristics of AP and AM, such as weight-average molecular weight (M_w), z-average molecular size (R_z), dispersed-molecular density (ρ) are presented in Table 4.2. The M_w of AP in native starches ranged between 18.9×10^6 g/mol (FP) and 27.3×10^6 g/mol (RW). The R_z of AP was between 55.6 nm (FP) and 62.2 nm (RC). The R_z of AP in pulse starch was much smaller than those of cereal starches (Table 4.2). In comparison to AP, the M_w and molecular density (ρ) of AM were less and R_z was more. Since R_z is related to the volume occupied by a molecule in a solution, the observed smaller M_w and larger R_z of AM suggested AM chains are loosely packed (i.e., lower in density) with long and possibly unbranched chains. Whereas the larger M_w and smaller R_z of AP suggest AP chains are highly branched and higher in density (i.e., compactly

95

Table 4.2 Molecular characteristics of amylopectin and amylose of native starches and SNPs from regular corn (RC), regular wheat (RW), faba bean (FB), and field pea (FP).

Samples	Amylopectin				Amylose			
	Content (%)	M_w (×10^6) [b]	R_z (nm) [c]	ρ (g/mol/nm^3) [d]	Content (%)	M_w (×10^6)	R_z (nm)	ρ (g/mol/nm^3)
Native								
RC	73.8 ± 0.4 a	19.4 ± 0.5 c	62.2 ± 0.1 a	80.7 ± 2.0 d	26.2 ± 0.4 c	3.6 ± 0.1 b	70.8 ± 1.7 ab	10.1 ± 0.1 c
RW	71.2 ± 0.5 b	27.3 ± 0.4 a	61.6 ± 0.3 a	116.6 ± 1.6 b	28.8 ± 0.5 b	5.9 ± 0.5 a	73.2 ± 1.2 a	15.1 ± 0.8 b
FB	60.9 ± 0.3 c	21.6 ± 1.1 b	55.9 ± 0.4 b	123.7 ± 3.6 a	39.1 ± 0.3 a	6.6 ± 0.2 a	70.7 ± 2.1 ab	18.6 ± 0.6 a
FP	58.7 ± 0.5 d	18.9 ± 0.3 c	55.6 ± 0.2 b	109.7 ± 1.9 c	41.3 ± 0.5 a	6.2 ± 0.3 a	66.8 ± 2.0 b	20.8 ± 1.4 a
SNP								
RC	74.6 ± 0.7 a	8.6 ± 0.2 c	43.8 ± 0.8 c	102.3 ± 3.8 a	25.4 ± 0.7 c	1.9 ± 0.1 b	44.6 ± 0.1 c	21.8 ± 0.7 a
RW	71.7 ± 0.4 b	12.0 ± 0.1 a	53.9 ± 0.2 a	77.0 ± 1.7 c	28.3 ± 0.4 b	2.8 ± 0.4 a	56.7 ± 0.1 a	15.2 ± 2.0 b
FB	60.4 ± 0.3 c	10.0 ± 0.6 b	48.1 ± 0.1 b	89.7 ± 0.9 b	39.6 ± 0.3 a	1.3 ± 0.1 d	49.7 ± 0.2 b	10.9 ± 0.8 c
FP	59.9 ± 0.2 c	8.5 ± 0.2 c	47.4 ± 0.4 b	79.3 ± 3.2 c	40.1 ± 0.2 a	1.6 ± 0.1 c	48.2 ± 0.7 c	14.5 ± 0.7 b

Values are mean ± standard deviation (n = 3), and values with the same letters in the same column separately for native starch and SNP are not significantly different at p < 0.05.
[a] Weight-average molecular weight (g/mol).
[b] z-Average radius of gyration (nm).
[c] Dispersed-molecular density (g/mol/nm^3).

packed). This is consistent with a previous study (Naguleswaran and others 2014). In general, the molecular weight comparison of native starch and their SNP counterparts indicated depolymerization of amylose and amylopectin during SNP preparation. In other words, ultrasonic-assisted starch dissolution and rapid antisolvent nanoprecipitation significantly decreased the M_w and R_z of AP and AM in all starch types. This is possibly due to depolymerization of starch molecules by ultrasonication (a high shear process). This Mw reduction by ultrasonication was similar to that reported elsewhere (Chang and others 2017b). The extent of Mw reduction observed in AP was around 55% for all starch types, while this data for AM was much greater in pulse starches (i.e., 80% and 74% for FB and FP, respectively) than that in cereal starches (i.e., 46% and 53% for RC and RW, respectively). This is because pulse starches possess more linear and longer AM chains (~40%, Table 4.2) and thus the molecular network in a gelatinized starch solution is easily broken down and depolymerized by ultrasonication resulting in smaller M_w (Ahmad and others 2020).

Interestingly, across all starch types, the M_w of AP and AM in SNPs was smaller and more uniform than that of native starches. This indicated that SNPs produced from pulse starches consist of a larger amount of molecules (especially amylose) with smaller M_w than those from cereal starches. Considering such uniformity across the starch molecules as well as the same nanoprecipitation processing conditions resulting in significant variations in the nanoparticle size and uniformity between cereal and pulse SNPs suggested that the ratio between amylose and amylopectin possibly plays a very important role. Based on these findings, it can be postulated that a) the cavitation effect during ultrasonication promotes the dissolution of starch by breaking the hydrogen bonding among starch molecules as well as altering (i.e. decreasing) the molecular weight of starch to inhibit the formation of SNPs with larger particle size and inhomogeneous structure; b) pulse

starches with higher amylose content forms smaller SNPs with more uniform structure; c) the formation of inhomogeneous or larger particulate structure of SNPs may be attributed to the branched chains of amylopectin.

4.3.5. Long-range crystalline structure of SNPs by XRD

Samples analyzed by XRD include the four native starches and the corresponding SNPs obtained at an AS/S ratio of 1:1 and a starch concentration of 10 mg/mL. The XRD spectra and relative crystallinity of native starches and SNPs obtained are shown in Fig. 4.3 and Table 4.3, respectively. The A-type X-ray diffractions patterns were observed for RC and RW starch granules with peaks at Bragg angles (2θ) of 15°, 17°, 18° and 23°. Pulse starches exhibited the C-type crystalline pattern displaying the peaks at 15°, 17°, and 23° 2θ, a small peak around 5.6° 2θ and a shoulder peak around 18° 2θ. These results are in good agreement with previous studies (Chung and others 2009; Chung and others 2010; Li and others 2019). After SNPs formation, the major peaks of diffraction disappeared and whole structure appeared like amorphous hump. As shown in Fig. 4.3B, there were only weak diffraction peaks at 13°, 17° and 21° for cereal SNPs and 17°, 20° and 22° for pulse SNPs, suggesting that the SNPs possess the V-type crystalline structure. This is mainly attributed to the recrystallized crystallites from a single-helical structure made up of amylose and ethanol during SNP formation procedures (Qin and others 2016). The relative crystallinity of SNPs ranged from 8% to 12% which was much lower than their native counterpart (30-35%). These observations indicated that the SNPs do possess distinct short- to medium-range orders, but with very less crystalline long-range order. Similar results were observed from previous studies (Ahmad and others 2020; Gutiérrez and others 2020). Between the different starch sources, the relative crystallinity of SNPs from pulses was greater than that of SNPs from cereals. This was attributed

to the stronger ability of amylose to form a single-helical structure, leading to the formation of a more compact structure (Qiu and others 2016).
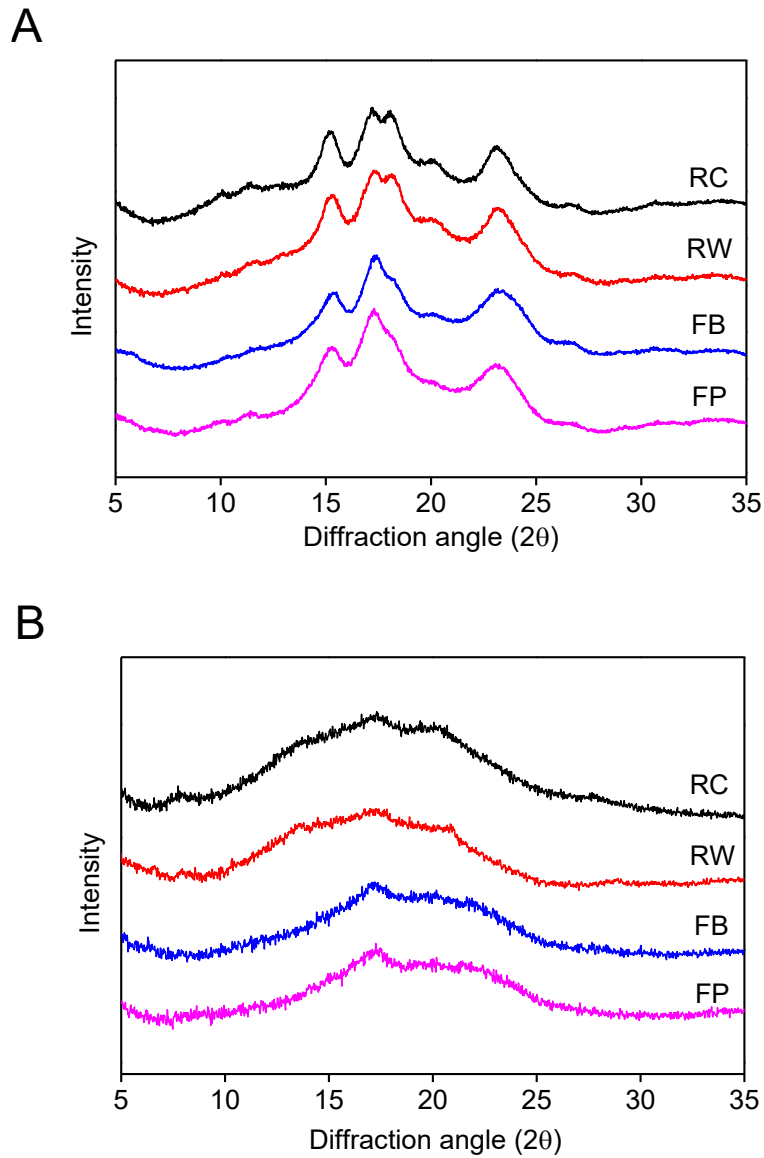
Fig. 4.3 X-ray diffraction patterns of (A) native starch and (B) SNPs from RC (regular corn), RW (regular wheat), FB (faba bean), and FP (field pea).

Table 4.3 Long-range crystallinity and short-range order of molecular order of native starch and SNPs quantified by XRD and ATR-FTIR, respectively.

Samples [a]	Long-range crystallinity by XRD (%)	Short-range order by ATR-FTIR	
		R (1047/1022)	R (995/1022)
Native			
RC	35.0 ± 0.65 a	0.58 ± 0.02 ab	1.12 ± 0.01 b
RW	30.90 ± 0.89 b	0.61 ± 0.01 ab	1.23 ± 0.01 a
FB	31.62 ± 0.62 b	0.62 ± 0.02 a	1.20 ± 0.01 a
FP	30.54 ± 0.46 b	0.61 ± 0.01 ab	1.19 ± 0.00 a
SNP			
RC	7.98 ± 0.40 d	0.50 ± 0.01 d	0.93 ± 0.01 d
RW	7.52 ± 0.21 d	0.52 ± 0.01 cd	0.96 ± 0.01 d
FB	12.18 ± 0.34 c	0.56 ± 0.01 bc	1.04 ± 0.01 c
FP	12.30 ± 0.28 c	0.59 ± 0.01 ab	1.02 ± 0.00 c

Values are mean ± standard deviation (n=3), and values with the same letters in the same column are not significantly different at $p < 0.05$.
[a] RC (regular corn), RW (regular wheat), FB (faba bean), and FP (field pea)

4.3.6. Short-range molecular order of SNPs by ATR-FTIR

The ATR-FTIR spectrum of starch has been shown to be sensitive to changes in the short-range molecular order of starch such as double helical structure, chain conformation, and the crystal form of starch (Wu and Seib 1990). The original and the deconvoluted ATR-FTIR spectra of the samples are presented in Fig. 4.4. As shown in Fig. 4.4A and C, all ATR-FTIR spectra of the samples were similar, which suggested there was no change in chemical composition changes in starch molecular structure caused by the size reduction process. However, the intensity of identical characteristic bands of SNP samples significantly increased/decreased in comparison to peaks of native starches. In the fundamental region, the spectra present a strong absorption peak around 3260-3280 cm^{-1} which is attributed to the -OH stretching and its width indicates the extent of formation of inter- and intra-molecular hydrogen bonds. In SNPs, the peak of -OH stretching shifted to a higher wavelength (~3310) for all samples (Fig. 4.4C). According to previous studies, this could be attributed to the loss of the crystalline structure and the exposure of -OH groups of the starch molecules during the process (Chun and others 2015; Ahmad and others 2020). Therefore, the new hydrogen bonds generated may be weaker than those in native starch granules. However, considering the smaller particle size of SNPs compared with starch granules as discussed in Section 4.3.4, the peak of -OH stretching shifted to a higher wavelength maybe not necessarily related to the weakness of the inter-molecular association in nanoparticles since the very high surface area also resulted in the exposure of more -OH groups on the surface of nanoparticles. In addition, for ATR-FTIR, the detection depth is generally 1-2 μm, which was the external layer of starch granules while the packing layer of SNPs clusters.
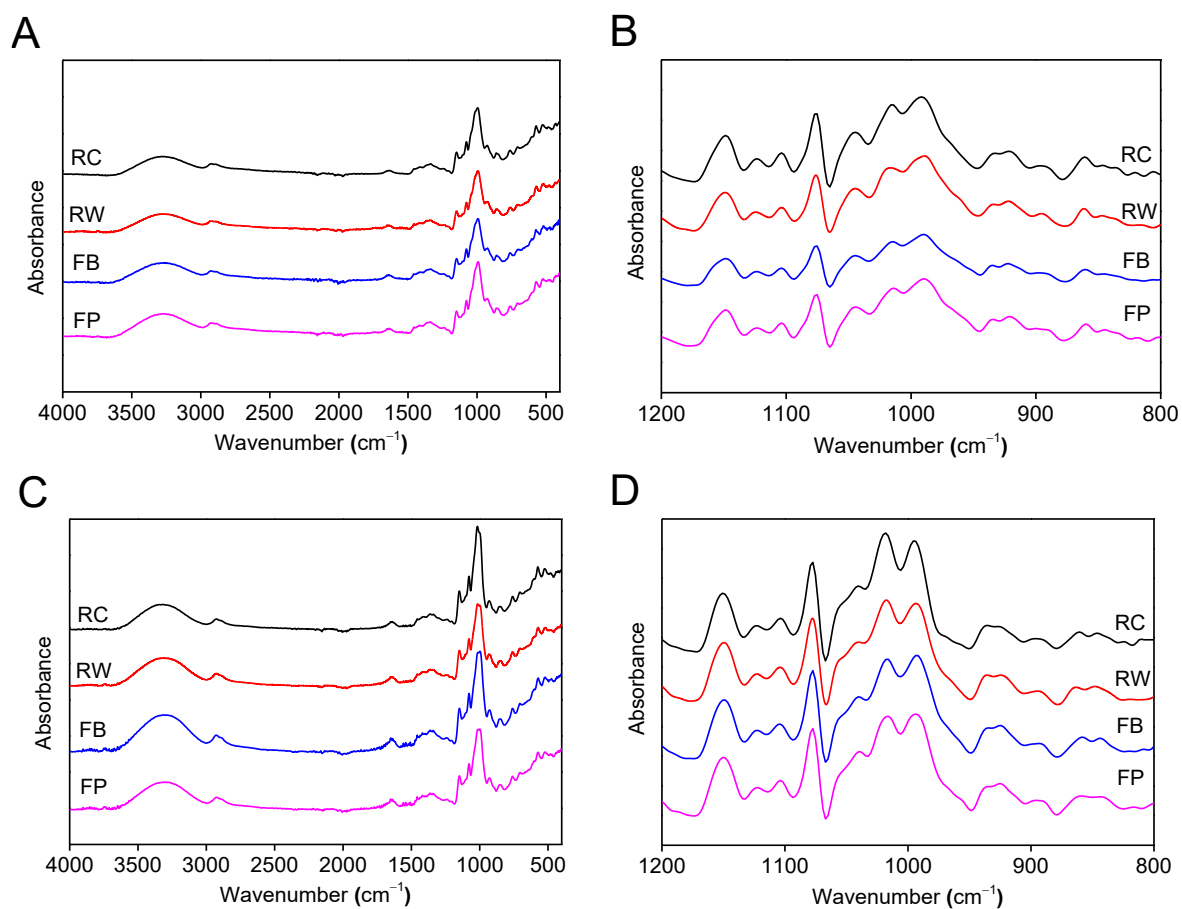
Fig. 4.4 (A, C) Original and (B, D) deconvoluted ATR-FTIR spectra of (A, B) native starches and (C, D) SNPs produced from RC (regular corn), RW (regular wheat), FB (faba bean), and FP (field pea), respectively.

The absorption peak observed around 2930 cm^{-1} can be ascribed to the asymmetric stretching of $-CH_2$ while the peaks observed at the wavelength of 1147, 1082 and 990 cm^{-1} are related to the stretching vibration of the C-O-C, C-O, and C-O-H groups in the glucose ring, respectively. The absorption around 1637 cm^{-1} was due to the presence of bound water in starch and it increased significantly in the peak intensity after SNP processing. These results were in good agreement with previous studies (Gutiérrez and others 2020; Ahmad and others 2020). The increased absorptions were less pronounced in cereal SNPs than pulses. This indicated that more bound water was present in pulse SNPs in comparison to other samples.

The deconvoluted ATR-FTIR spectra of native starches and SNPs in the range of 1200-800 cm^{-1} (Fig. 4.4B and D) could be used to determine the short-range molecular order of starch by characterizing the changes that occurred in the semi-crystalline and amorphous regions within starch granules (Gutiérrez and others 2020; Ahmad and others 2020). The band around 1047 cm^{-1} is sensitive to the amount of ordered or crystalline structure; the band at 1018 cm^{-1} is related to the amorphous structure; the band at 995 cm^{-1} is related to hydrogen bonding of the hydroxyl group at C-6 (van Soest and others 1995). Therefore, the absorbance ratio of 1047/1018 cm^{-1} and 995/1018 cm^{-1} can be used as a measure of the degree of order of starch. As shown in Fig. 4.4B and D, it could be noted that the absorbance peak at around 1047 cm^{-1} decreased significantly, while that at around 1018 cm^{-1} increased dramatically after SNP formation. Consequently, as shown in Table 4.3, both the ratio 1047/1018 and 995/1018 decreased after the SNP formation, indicating the decrease in crystalline structure of starch and the formation of its amorphous structure. This result was in good agreement with the XRD data (Fig. 4.3). Compared with cereal SNPs, these changes were less pronounced for pulse SNPs. The ratios for 1047/1018 and 995/1018

of cereal SNPs were less than those of pulse SNPs, indicating that the short-range structure of pulse SNPs was more ordered. In addition, the great absorbance intensity at around 995 cm^{-1} indicated a large amount of intramolecular hydrogen bonding of the hydroxyl groups at C-6, which was contributed to a greater degree of double helical order (short-range order). This indicated the regeneration of inter-molecular association in SNP possible through H-bonding. Based on the above findings, it can be concluded that the type of starch used for the formation of SNPs could produce some changes in the physicochemical structure of the resulting SNPs.

4.3.7. Thermal properties of starch nanoparticles

The thermal characteristics of native starches and SNPs were studied in excess water (with a starch concentration of 20%, w/v). The typical thermograms are shown in Fig. 4.5. The melting transition temperatures (T_o, T_p, and T_c) and the enthalpy ΔH are presented in Table 4.4. SNPs and starch granules show completely different thermograms with different thermal properties. As expected, the gelatinization thermogram of native starches showed a sharp endothermic peak in ranges of 68-79°C, 59-73 °C, 60-76 °C, and 61-76 °C, for RC, RW, FB, and FP, respectively (Table 4.4). However, all of the SNPs exhibited two melting regions: one small endothermic peak between 50-77 °C, with ΔH_1 from 4 to 6 J/g, and another temperature range of 120-162 °C, with ΔH_2 from 13 to 25 J/g. These two melting regions corresponded to the melting of amylopectin and the amylose crystals, respectively. This is consistent with a previous study (Ji and others 2018), where starch nanohydrogels were produced by reverse emulsification coupled with internal gelation. In comparison to native starches, the melting temperature and ΔH_1 of amylopectin crystals substantially decreased in SNPs due to the disruption of crystalline structure during heating and ultrasonication (Qin and others 2016; Chang and others 2017b). The second melting region existed only in SNP samples due to the reorganization of amylose molecules during SNP formation.

Among different starch sources, the T_o, T_p, and T_c of pulse SNPs were significantly greater than those of cereal SNPs. This could be related to the higher amylose content in pulse starches than that in cereal starches. However, the ΔH_2 of pulse SNPs was lower than that of cereal SNPs, which might be attributed to their smaller particle size/crystal size (Gutiérrez and others 2020). Therefore, the thermal properties of SNPs were influenced by their crystalline structure, molecular composition, and particle size.
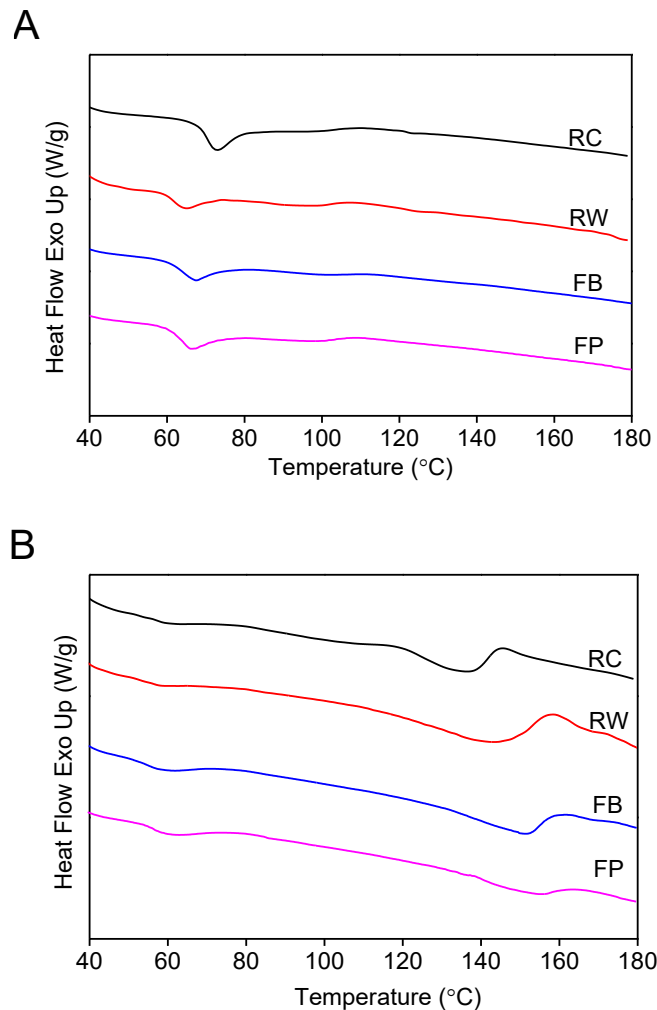
Fig. 4.5 Thermal analysis by Differential Scanning Colorimeter (DSC) of (A) native starches, and (B) SNPs produced from RC (regular corn), RW (regular wheat), FB (faba bean), and FP (field pea).

Table 4.4 Gelatinization onset (T_o), peak (T_p), and conclusion (T_c) temperatures and gelatinization enthalpy (ΔH) of native starches and SNPs.

Samples [a]	T_o	T_p	T_c	ΔH_1 (J/g)	T_o	T_p	T_c	ΔH_2 (J/g)
Native								
RC	68.24 ± 0.21 a	72.66 ± 0.28 a	79.32 ± 0.35 a	14.67 ± 0.14 b	/	/	/	/
RW	59.36 ± 0.23 c	63.80 ± 0.31 d	72.57 ± 0.24 f	11.38 ± 0.11 c	/	/	/	/
FB	60.40 ± 0.27 b	67.40 ± 0.17 b	76.10 ± 0.13 bc	15.10 ± 0.12 b	/	/	/	/
FP	60.82 ± 0.11 b	66.09 ± 0.13 c	75.56 ± 0.22 cd	15.80 ± 0.18 a	/	/	/	/
SNP								
RC	53.45 ± 0.30 e	61.10 ± 0.25 e	76.12 ± 0.17 bc	3.73 ± 0.07 e	120.04 ± 0.35 c	136.89 ± 0.42 c	143.85 ± 0.46 c	19.51 ± 0.24 b
RW	51.33 ± 0.23 f	58.06 ± 0.21 g	77.10 ± 0.14 b	5.83 ± 0.18 d	121.52 ± 0.44 c	144.93 ± 0.27 b	156.31 ± 0.41 b	24.75 ± 0.16 a
FB	50.37 ± 0.24 g	59.59 ± 0.23 f	73.45 ± 0.53 ef	6.15 ± 0.14 d	127.58 ± 0.60 b	151.62 ± 0.54 a	157.97 ± 0.73 b	16.45 ± 0.21 c
FP	54.52 ± 0.15 d	61.55 ± 0.31 e	74.47 ± 0.39 de	5.82 ± 0.11 d	135.15 ± 0.40 a	153.42 ± 0.59 a	162.39 ± 0.54 a	12.84 ± 0.20 d

Values are mean ± standard deviation (n=3), and values with the same letters in the same column are not significantly different at $p < 0.05$.
[a] RC (regular corn), RW (regular wheat), FB (faba bean), and FP (field pea)

4.4. Conclusion

SNPs were prepared via ultrasonic assisted-dissolution and rapid nanoprecipitation using regular corn, wheat, faba bean and field pea starch. The molecular weight comparison of native starch and their SNP counterparts indicated depolymerization of amylose and amylopectin during SNP preparation. This depolymerization seems to have enhanced the uniformity in starch molecular weights between cereal and pulse sources. However, greater amylose content resulted in the formation of smaller particles with uniform size distribution. Pulse starches, faba bean and field pea, with a high amylose content was superior to form uniform-distributed, spherical SNPs with a diameter of 130 nm using starch concentration of 10 mg/mL at low AS/S ratio of 1:1. Re-dispersibility of SNP was dependent on their starch composition, formation conditions (i.e., starch concentration, AS/S ratio) and particle size. Under identical conditions, pulse SNP exhibited a greater relative crystallinity and higher melting temperatures than cereal SNPs. The newly developed SNPs show future promise in a wide variety of applications for emulsions and delivery systems for water-soluble active ingredients and drugs.

Chapter 5: Rheology of starch nanoparticles prepared from pulse and cereal starches by rapid nanoprecipitation

5.1. Introduction

Because of the extremely small size, light weight, large surface area, low cost, abundance, renewability and biodegradability, SNP have attracted a lot of attention in various applications, including biodegradable composites, bioplastics and paper/paper board products, hydrogels, aerogels, emulsion stabilization, fat replacement and drug delivery (Salam and others 2013; Li and others 2014; Kim and others 2015; Chen and others 2019). The performances of SNP-based materials are strongly dependent on their characteristics, such as particle size, morphology, stability, dispersion microstructure, and rheological properties as well as how they change under different processing conditions (Saari and others 2017; Ge and others 2017). For instance, when SNPs are used as drug delivery systems, their stability can change with temperature, and the release of a drug from nanoparticle carriers is influenced by the rheological behavior as well (Schwarz and others 2012). Therefore, investigations on the particle size, morphology, stability, and rheological behavior of SNP under different conditions are of key scientific interest and practical significance.

Rheological measurements have recently been applied to characterize starch nanoparticles or microparticle suspensions (Shi and others 2012; Jiang and others 2016; Perez Herrera and others 2017). The rheological behavior of SNP were dependent on the processing technique (i.e. drying methods), characteristics of SNP (i.e. particle size and surface charge), and post-treatment (i.e. addition of NaCl) (Shi and others 2012; Jiang and others 2016; Perez Herrera and others 2017). Although some information on the rheological properties of SNP is available, comparative

research on the static and dynamic rheology of SNPs produced from different starch sources is very limited, especially for those SNP produced by nanoprecipitation. Most of the previous studies have focused on the rheological behavior of SNP produced by acid hydrolysis, or have solely dealt with individual SNP suspensions (Shi and others 2012; Shi and others 2013; Jiang and others 2016; Perez Herrera and others 2017). In Chapter 4, SNP from pulse and cereal starches were found to vary in their morphology, crystallinity and molecular size distribution. Pulse SNPs consisted of more linear chain amylose with smaller M_w than cereal SNPs. The difference in the molecular composition between pulse and cereal starches is expected to play an important role in the rheological behavior of aqueous SNP systems. Furthermore, most of the rheological studies of SNPs used cereal and tuber starches, such as corn, wheat, rice, oat, potato, and tapioca. The literature lacks information on the rheological properties of SNP prepared from starches of pulse origin (i.e., field pea, faba bean, etc). Pulse starches are not preferred in food and industrial applications primarily due to their high amylose content (~40%) and consequent high retrogradation capacity (Hoover and others 2010). Therefore, the rheological behavior of pulse SNPs was investigated to search for novel properties.

In the present study, SNP were formulated from two types of cereal starches, regular corn and wheat, and two types of pulse starches, faba bean and field pea, using a rapid and innovative nanoprecipitation technique (Saari and others 2017). The effect of starch source, concentration, and thermal stability on the viscosity and viscoelastic behavior of SNP suspensions were measured as a function of shear rate, frequency, and temperature. The aim of the study was to compare pulse and cereal SNPs with the following specific objectives: 1) to compare the PSD of SNP by dynamic light scattering methods and solid-state microscopy, 2) to evaluate the effect of temperature on the

PSD of SNP in aqueous suspensions, and 3) to determine the static and dynamic rheological properties of SNP suspensions as a function of shear, frequency and temperature. A more detailed understanding of these relationships provides us more fundamental guidance for the development of SNP-based materials to achieve desired rheological properties.

5.2. Materials and methods

5.2.1. Materials

Regular corn, regular wheat, faba bean, and field pea starches were described in Chapter 3 section 3.2.1. Milli-Q water was used for all experiments. All other chemicals were of analytical grade.

5.2.2. Preparation of SNP

5.2.2.1. Preparation of SNP suspensions

Starch samples were mixed with water and solubilized by heating/gelatinization and subsequent ultra-sonication (Iida and others 2008; Chang and others 2017b). Briefly, four types of native starch were dispersed in Milli-Q water (5%, w/v) and gelatinized in boiling water bath for 30 min with stirring on a vortex mixer every 5 min for 30 s. The gelatinized starch paste was then sonicated for 10 min using a 20 kHz ultrasonic processor (FS-1200 N, Shanghai Sonxi Ultrasonic Instrument Co., Ltd., Shanghai, ZJ, China) equipped with a probe transducer and a flat tip of 13 mm. The power output of 720 W and 5/2 s on/off pulses were applied to minimize heat generation. The viscosity of the starch paste was markedly decreased by ultra-sonication within 5 min. The homogenous starch solution (5%, w/v) was then diluted to concentrations of 1% (w/v) before nanoprecipitation. Nanoprecipitation was carried out by pouring absolute ethanol rapidly into the starch solution under constant stirring. The volume ratio of absolute ethanol to starch solution was 1:1. After thorough mixing, an aliquot of the colloidal suspension obtained was diluted with Milli-

Q water for the analysis of the particle size and PSD by dynamic light scattering (DLS, see Chapter 3 section 3.2.4.). Finally, the colloidal suspension was homogenized to promote the precipitation of fine particles using a homogenizer at 8,000 rpm for 1 min (Heidolph Diax 900, Schwabath, Bavaria, Germany). The precipitate was centrifugally separated and re-dispersed in Milli-Q water to prepare SNP suspensions with the desired concentrations for particle size, PSD, zeta potential, and rheological measurements.

5.2.2.2. Freeze-drying of SNP

Samples of 1% (w/v) SNPs in water suspension were frozen at -20 °C overnight in a freezer. The frozen samples were then freeze-dried (FreeZone 12, Labconco Corp., Kansas, MO, USA) at a sublimating temperature of -45 °C for 5 days.

5.2.3. Morphology of the starch nanoparticles

Microstructure and surface morphology of four types of starches and their freeze-dried SNP were observed using a field emission scanning electron microscopy (FE-SEM) (Zeiss Sigma 300 VP-FESEM, Zeiss, Oberkochen, Germany) at an accelerating voltage of 5 kV. Before observation, samples were mounted on circular aluminum stubs with a double-sided sticky tape and coated with carbon using a Nanotek SEM pre 2 sputter coater. The sizes of particles in the microscopy images were analyzed using the processing software ImageJ. The diameters of 200 particles (n = 200) from each sample were measured to determine the PSD.

5.2.4. Particle size and zeta potential analysis

The particle size, PSD, and zeta potential of the SNP in aqueous suspension were determined using a Zetasizer (Nano S, Malvern Instruments, Malvern, Worcestershire, UK) as described in Chapter 3 section 3.2.4. In order to evaluate the effect of temperature on PSD, SNP suspensions were

incubated at 25, 40, 60, 80, and 90 °C for 30 min, and then cooled down to room temperature. The particle size measurements for all SNP suspensions were conducted at 25 °C.

5.2.5. Measurement of static and dynamic rheological properties

SNP suspensions of 1%, 3% and 5% (w/v) were prepared according to the methodology described earlier under section 5.2.2.1 and then stored in a sealed glass container at 4 °C for 3 days to achieve sufficient hydration and interactions among particles. The samples were equilibrated at 25 °C for 30 min before each test. The rheological tests were measured using a stress-controlled rheometer (HR-3, TA Instrument, New Castle, DE, USA) with a cone and plate geometry (cone angle, 2°; diameter, 40 mm; truncation gap, 53 μm). The continuous shear tests were performed at 25 °C to measure the apparent viscosity. The shear rate range was from 0.01 to 100 s^{-1} in an upward sweep followed immediately by a downward sweep from 100 to 0.01 s^{-1}. Three sweep cycles were conducted consecutively in order to understand the relationship between the apparent viscosity and the shear rate of the SNP suspensions as well as their thixotropic behaviors. Strain amplitude sweep tests were performed to evaluate the linear viscoelastic range of the SNP suspensions at a frequency of 1 Hz with strain amplitudes ranging from 0.1% to 1000%. Frequency sweep tests were employed to evaluate the changes in the viscoelastic moduli as a function of angular frequency ranging between 0.1-10 rad/s. The temperature was set at 25 °C and oscillating strain of 2% was used. Strain amplitude sweep tests confirmed a 2% strain was within the linear viscoelastic region of all samples. Temperature ramp tests were carried out to determine the relationship between viscoelastic modulus and temperature. The tests were performed at a frequency of 1 Hz, oscillating strain of 2% and a heating rate of 2 °C/min from 25 °C to 90 °C. A solvent trap geometry and solvent trap cover were used to create a thermally stable environment and prevent moisture

loss from the samples during heating. Silica oil was placed in the solvent well. All rheological measurements were carried out in duplicates and the mean was reported.

5.2.6. Statistical analysis

All experiments were done in three replicates. Results are presented as mean ± SD (standard deviation). Analysis of variance (ANOVA) was performed, and the mean comparisons were performed by Tukey's HSD test at $p < 0.05$ with OriginPro software (OriginPro 9.0.0, OriginLab Northampton, MA, USA).

5.3. Results and discussion

5.3.1. Morphology and particle size of SNPs observed by FE-SEM

The morphology of native corn, wheat, faba bean and field pea starch granules and freeze-dried SNPs is presented in Fig. 5.1. Starch granules are mostly spherical, oval, and irregular in shape with a smooth surface and in a diameter range of 3-43 μm when evaluated using FE-SEM. As shown in Fig. 5.1, it can be clearly seen that the freeze-dried SNP are spherical in shape. They are loosely packed together and form SNP aggregates after freeze-drying. The mean size of freeze-dried SNP was determined from FE-SEM images as presented in Table 5.1. Compared to micro-scale native starch, the mean particle sizes of SNP were significantly reduced and mainly in a range of 50-500 nm. SNP obtained from pulse starches showed the significantly smaller particle size than those from cereal starches, with mean particle of 134 nm and 140 nm for faba bean starch and field pea starch, respectively. According to previous studies, polymeric nanoparticle size increases with increasing molecular weight (Saad and Prud'homme 2016; Lee and others 2020). Therefore, at identical process conditions, cereal starches with more AP (larger M_w) tend to form larger particulates than pulse starches.
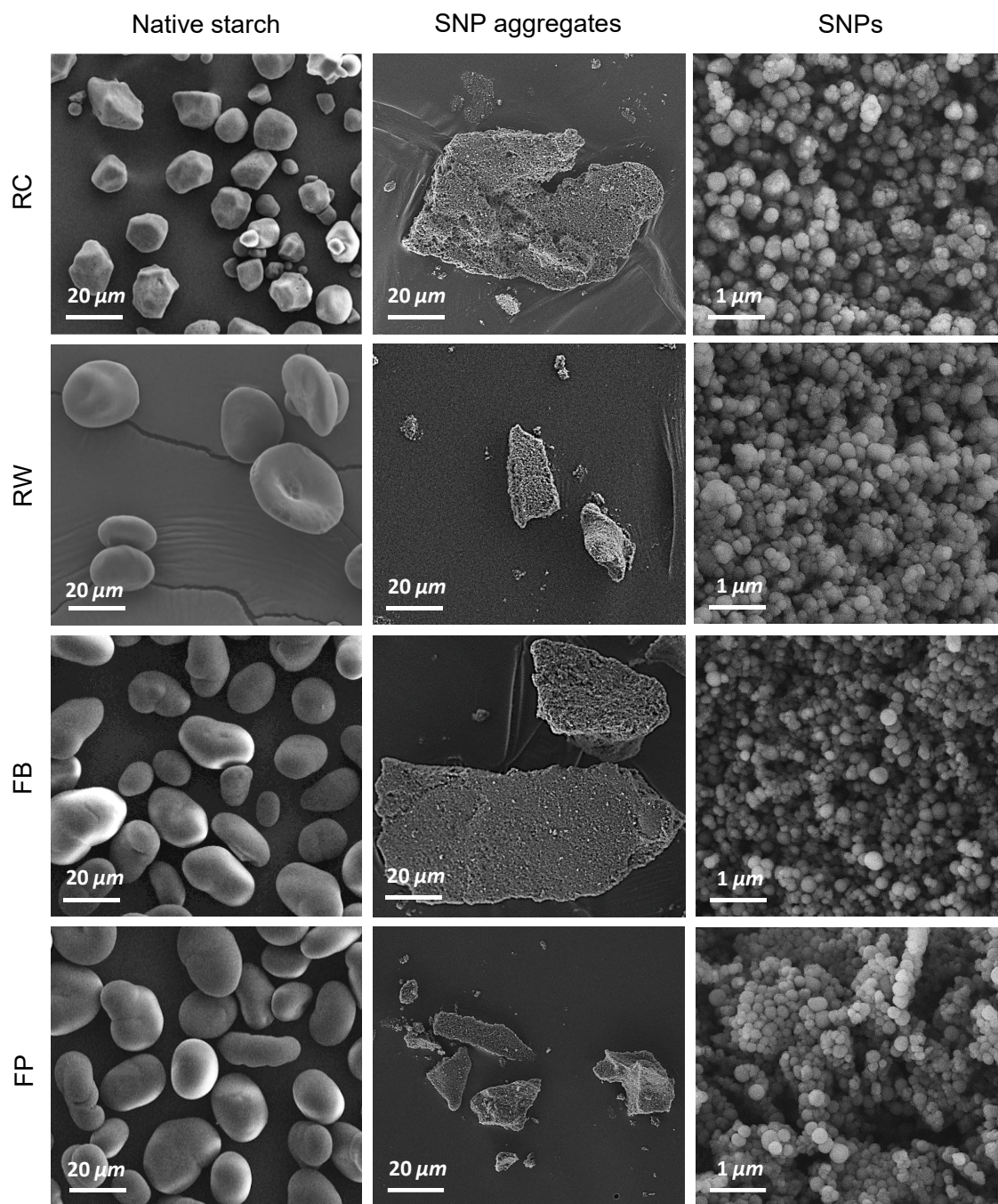
Fig. 5.1 Field emission scanning electron microscopy images of native starch and freeze-dried SNPs of regular corn, wheat, faba bean, and field pea. RC (regular corn); RW (regular wheat); FB (faba bean); FP-SNPs (field pea).

Table 5.1 Particle characteristics of SNPs obtained from regular corn, wheat, faba bean and field pea.

SNPs	FE-SEM Diameter [x] (d. nm)	DLS Hydrodynamic diameter (d. nm) [y]					Zeta potential [z] (mv)
		25 °C	40 °C	60 °C	80 °C	90 °C	
RC	238 ± 44 A	302 ± 22 Ba	353 ± 34 Ba	285± 26 Aa	130 ± 12 Bb	112 ± 8 Bb	−13.0 ± 1.7 A
RW	251 ± 31 A	438 ± 35 Aa	522 ± 49 Aa	316 ± 29 Ab	207 ± 19 Ac	195 ± 16 Ac	−10.2 ± 1.0 A
FB	134 ± 13 B	193 ± 15 Ca	165 ± 4 Cab	158 ± 20 Bab	151 ± 14 Bab	130 ± 10 Bb	−18.3 ± 1.1 B
FP	140 ± 12 B	210 ± 12 Ca	192 ± 20 Cab	180 ± 16 Bab	158 ± 5 Bb	150 ± 2 Bb	−18.6 ± 1.0 B

Values in the same row sharing a common letter are not significantly different (P < 0.05). Values in the same column sharing a capital are not significantly different (P < 0.05). RC (regular corn); RW (regular wheat); FB (faba bean); FP-SNPs (field pea).
[x] Nanoparticles in dry state were analyzed by FE-SEM at 25 °C.
[y] Hydrodynamic diameters were evaluated by DLS in regulated cell at 25 °C after incubated at the different temperatures.
[z] Zeta potential was measured by DLS in a U-shaped cuvette at 25 °C.

In addition, the morphology of freeze-dried nanoparticles has been reported to be significantly affected by suspension concentration, particle size, surface charge, and crystal structure (Han and others 2013). For example, during freeze-drying, cellulose nanoparticles reorganized to a lamellar structure at suspension concentrations of 0.5-1% (w/v) while ultrafine fibers were observed at concentrations of ~0.05% (w/v). Preliminary experiments in recovering SNPs by freeze-drying also showed that if suspension concentration remains high (more than 5%) SNP formed a lamellar structure, while large aggregates composed of nanosized particles were formed at low suspension concentration (< 5%); or even distinct individual nanoparticles at concentration < 0.1%. The particle size of freeze-dried SNPs in aqueous suspension also showed larger particle size than their particle size without drying, this trend was more significant with increasing the suspension concentration (data not shown). This is because at higher suspension concentrations, interparticle hydrogen bonding was enhanced on the surface of SNP due to the closer proximity, and these adjacent SNPs aligned along the freezing direction to form highly packed SNP aggregates. At diluted concentrations, due to the weakening of hydrogen bonding and interfacial attraction among the SNPs, SNPs were loosely packed and therefore showed separated uniform particles with spherical shape. The crystal structure of freeze-dried SNPs from all A- (corn and wheat), B- (potato) and C-type (pea) starches have been shown to exhibit V-type diffraction peaks (Qin and others 2016). The V-type crystallinity of SNPs could be attributed to the single-helical structure of amylose and ethanol that easily forms during nanoprecipitation i.e., addition of ethanol to solubilized starch. Therefore, the crystal structure of SNPs did not relate to the crystalline type of native starches. However, a previous study (Yan and others 2017) concluded that the V-type diffraction structure forms during the drying process instead of the nanoprecipitation step, because the XRD pattern of the SNPs without drying did not show any diffraction peaks. In the present

study, the morphology of freeze-dried SNP from cereal and pulse starches under identical conditions were demonstrated to compare their morphology and particle size.

5.3.2. Hydrodynamic particle size, particle size distribution, and zeta potential of SNPs

The particle size and PSD of the SNPs in aqueous suspension determined by DLS are presented in Table 5.1 and Fig. 5.2. DLS determines the hydrodynamic diameter of SNPs by measuring the Brownian motion of particles dispersed in solution. The values reported for DLS in Table 5.1 are the mean values (hydrodynamic diameter) of a size distribution curve. The average hydrodynamic diameter of SNPs varied significantly between starch types, particularly between pulses and cereals, which is consistent with the data from FE-SEM. RW-SNPs had the greatest average particle size (438 nm), followed by RC-SNPs (320 nm), FP-SNPs (210 nm), and then FB-SNPs (180 nm). Moreover, SNPs from pulse starches, FP and FB, had a single peak and a uniform PSD (PDI < 0.3) (Fig. 5.2A). However, those SNPs from cereals, RC and RW, had two peaks with greater PDI values (~0.5), suggesting that the PSD of cereal SNPs was not homogeneous. This means that pulse starches were superior to cereal starches for the formulation of SNPs through nanoprecipitation under the tested conditions. Furthermore, the hydrodynamic diameter of SNPs was substantially greater than the size of freeze-dried SNPs (FE-SEM). This was possibly due to the following reasons: a) the swelling of SNPs due to the hydration, b) the presence of the electrical double layer around the SNPs, and c) a tendency of two or more SNPs to aggregate together in the aqueous suspension (i.e. providing the size of clustered particles rather than individual particles) (Qin and others 2016; Perez Herrera and others 2017). The SNPs had negative zeta potential values of −13, −10, −18, and −19 mv for RC, RW, FP, and FB, respectively (Table 5.1). The hydroxyl groups on the surface of SNPs tend to ionize in water and result in the formation of negative surface charge and zeta potential (Liu and others 2009; Sadeghi and others 2017). The large zeta potential

117
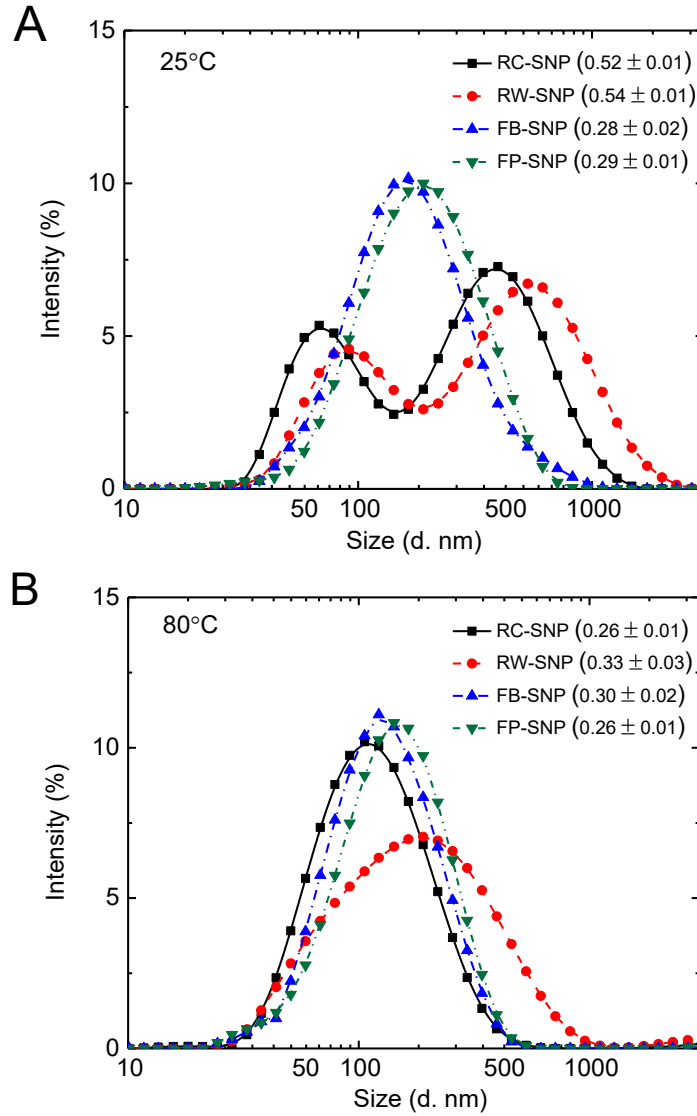
Fig. 5.2 Particle size distribution and polydispersity index (PDI in bracket) of SNP suspensions after incubation at: (A) 25 °C; and (B), 80 °C. RC-SNP (regular corn starch nanoparticles); RW-SNPs (regular wheat starch nanoparticles); FB-SNPs (faba bean starch nanoparticles); FP-SNPs (field pea starch nanoparticles)

increases the electrostatic repulsions between the particles, which results in a decrease in Van der Waals attraction. The Van der Waals forces are responsible for particle aggregation that eventually lead to clustering of particles (Schäfer and others 2010; Ahmad and others 2020). Therefore, the larger particle size and clustering of particles observed in cereal SNPs (Table 5.1 and Fig. 5.1) could be due to the lower zeta potential values. The zeta potential also reflected the stability of colloidal suspensions. As shown in Fig. 5.3, cereal SNPs flocculated to the bottom of vial within one week, while pulse SNPs were well dispersed in the aqueous solution until one month. According to a previous study (Perez Herrera and others 2017), the rheological properties of SNPs isolated by acid hydrolysis are influenced by the particle size, starch type, and temperature. Therefore, variation in the particle size and surface charge between pulses and cereals may play an important role in the thermal stability and rheological behavior of SNPs in aqueous suspension.
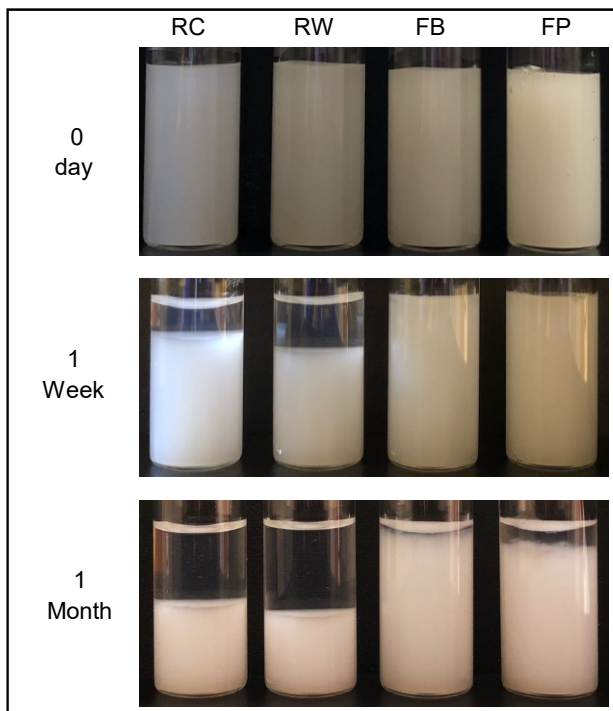
Fig. 5.3 Photographs of SNPs in aqueous suspensions at the concentration of 1% w/v at different storage times. RC (regular corn), RW (regular wheat), FB (faba bean), FP (field pea).

5.3.3. Thermal stability of SNP suspensions determined by DLS

The mean hydrodynamic diameters and PSD after incubation at elevated temperatures are presented in Table 5.1. The SNPs formulated from both pulses and cereals showed a decrease in the mean particle size with an increase in temperature, indicating significant heat sensitivity of SNPs. As shown in Table 5.1, following incubation at 40 °C, no significant change was observed for all SNPs. When temperature was increased to 60 °C, RW-SNPs showed a substantial decrease in size, while other SNPs remained unchanged, suggesting less thermal stability for RW-SNPs compared to other SNPs. However, when heated to 80 °C, all SNP diameters decreased, and the extent of decrease was more pronounced in cereal SNPs. For example, RC-SNPs showed a decrease in particle size from 302 to 130 nm, and the decrease was more pronounced than that in FP-SNPs (from 210 to 158 nm). Furthermore, after incubation at 90 °C, the SNP diameter of SNPs was 112, 130, 150, and 195 nm for RC, FB, FP and RW, respectively; the heat sensitivity of SNPs varied with starch source. The PSD of SNP suspensions after incubation at 25 °C and 80 °C (Fig. 5.2A and B) suggests that the thermal stability is greater for pulses (lower % size reduction) than that for cereals. The thermal degradation of SNPs was also visually evident by a change from a colloidal to a clear solution. Similar observations were found for SNC reported by previous studies (Wei and others 2014; Perez Herrera and others 2017). In SNPs, there are three possible molecular associations among AM and AP molecules, namely, the inter and intra-molecular hydrogen bonding between AM-AM, AM-AP, and AP-AP (Perez Herrera and others 2017). Since the M_w of linear AM are much smaller than the branched AP, AM tends to form smaller and tightly packed particles than AP. Therefore, it is plausible that those SNPs (i.e. cereal SNPs) formed mainly from the aggregation of AP molecules would thus have larger particle size and less thermal stability (Klucinec and Thompson 1999; Jane and others 1999). These differences observed in particle size

before and after heating are expected to influence the rheological and functional properties of SNP suspensions.

5.3.4. Apparent viscosity of SNP suspensions at different concentrations-From Newtonian to shear thinning and gel-like solutions

The effect of concentration on the apparent viscosity of SNPs from different starch sources was investigated. Initially, the viscosity of SNP suspensions after equilibration at room temperature (for 30 min) was observed visually by comparing the concentration of 1% and 5% (w/v). As shown in Fig. 5.4, with the field pea SNPs as a model sample, for a small concentration of 1%, the suspension exhibits a thin liquid which can easily flow, whereas for a larger concentration of 5%, it exhibits a gel-like behavior. The liquid-like behavior of SNP suspensions at small concentration (1%) is due to more free water molecules being present. At a larger concentration (5%), the gel-like behavior of SNP suspensions suggests the formation of a network, possibly due to the closer proximity among SNPs (i.e., the presence of a greater number of SNPs) and enhanced hydrogen bonding between the particles on the SNP surface (Angellier and others 2005).
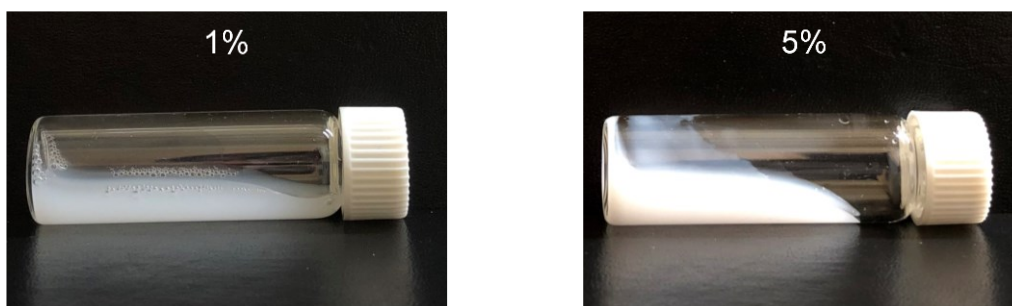
Fig. 5.4 Photographs of field pea SNP aqueous suspensions: 1% w/v, liquid-like behavior; and 5% w/v, gel-like behavior.

Fig. 5.5A and B present shear stress τ versus shear rate and viscosity η obtained as dividing the shear stress τ by the shear rate γ for SNP suspensions with different concentrations. For small concentration of 1%, SNP suspensions behave as Newtonian fluids as the viscosity is roughly constant. As the concentration increased to 3%, the Newtonian behavior remained unchanged for cereal SNP suspensions; however, for pulse SNP suspensions, the viscosity is no longer constant but various with shear and a shear-thinning behavior was observed, indicating a gel-like structure. At large concentration of 5%, all SNP suspensions showed shear-thinning behavior. The experimental data of shear stress τ versus shear rate γ (Fig. 5.5A) were fitted to the Bingham plastic, power-law and Herschel-Bulkley models as expressed by following equations:

$$\tau = \tau_0 + \eta_p \times \gamma \tag{5.1}$$

$$\tau = k \times \gamma^n \tag{5.2}$$

$$\tau = \tau_0 + k \times \gamma^n \tag{5.3}$$

respectively, where τ is the shear stress (N/m^2), η_p is the plastic viscosity, γ is the shear rate (s^{-1}), k is the consistency coefficient, n is the flow behavior index, and τ_0 is the yield stress (N/m^2) (extrapolated to zero shear rate γ).

The corresponding fit parameters are summarized in Table 5.2. For large concentrations, the flow curve is divided into two shear rate ranges. For high shear and high concentration, cereal SNP suspensions can be modeled using the power law model, while pulse SNP suspensions behave as Bingham fluid. However, for low shear and larger concentration, the rheological behavior of all cereal and pulse SNPs changes and the Herschel-Bulkley model becomes more relevant. As shown in Table 5.2, the flow behavior index n starts near 1 for low concentrations, which behave as Newtonian fluids and decreases with an increase in the concentration, indicating that the SNP
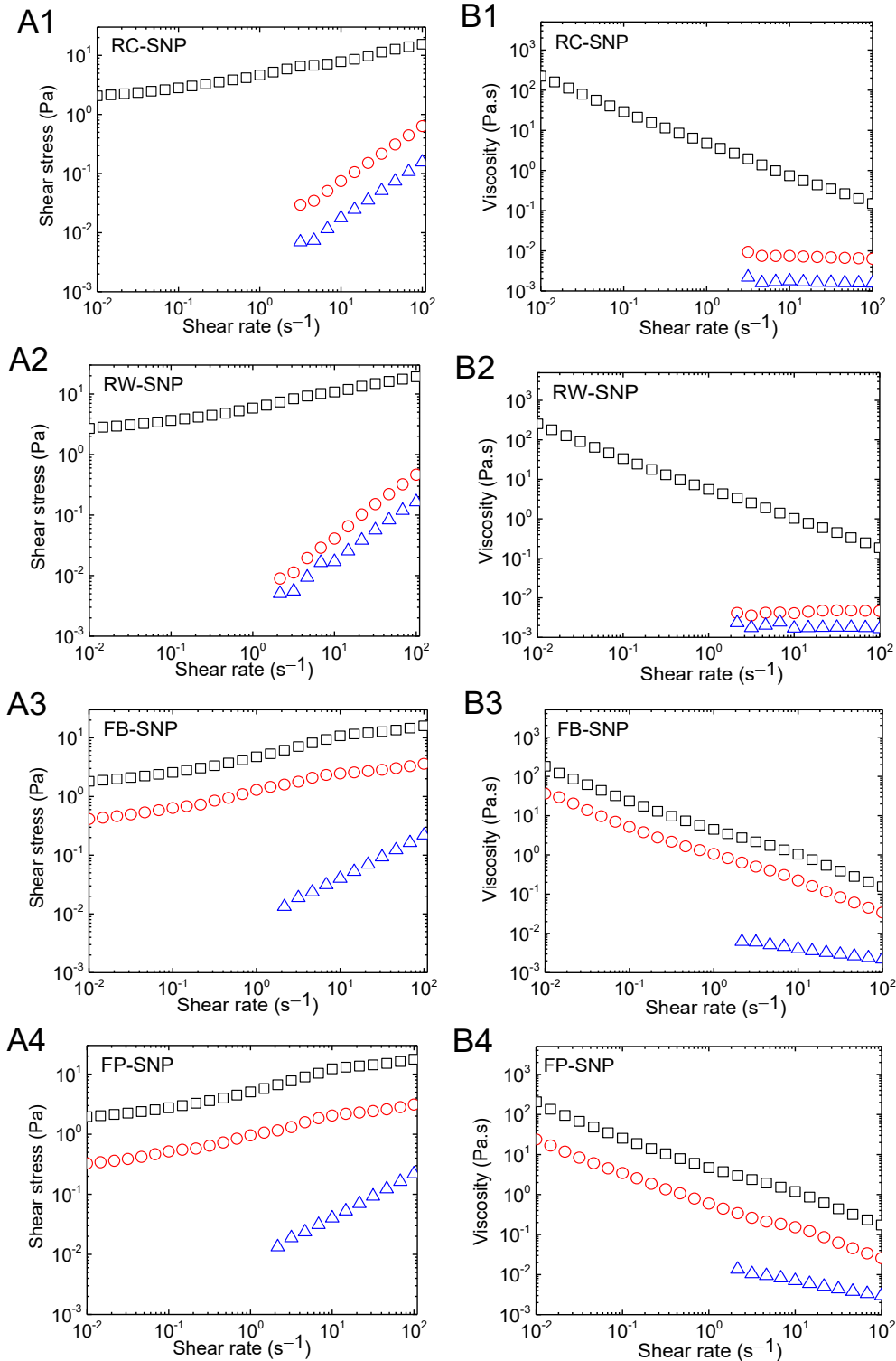
Fig. 5.5 Flow behavior of SNP suspension: (A) shear stress vs shear rate and (B) viscosity vs shear rate of SNP suspension at concentrations of 5 % (w/v, black squares), 3% (w/v, red circles), and 1% (w/v, blue triangles) at 25 °C. RC (regular corn), RW (regular wheat), FB (faba bean), FP (field pea).

Table 5.2 Bingham Plastic (BP), Herschel-Bulkley (HB), and Power Law (PL) model parameters obtained from the shear stress vs shear rate curves of SNP aqueous suspensions.

Samples*	Model	Shear rate range (s^{-1})	Yield stress τ_0 (Pa)	Flow behavior index n	Consistency coefficient k	R^2
5% SNP						
RC	HB	0.01-4.64	1.642 ± 0.083	0.424 ± 0.036	3.038 ± 0.147	0.997
	PL	4.64-100	0	0.300 ± 0.005	3.932 ± 0.270	0.996
RW	HB	0.01-10	1.796 ± 0.197	0.369 ± 0.030	4.122 ± 0.227	0.999
	PL	10-100	0	0.251 ± 0.007	6.122 ± 0.491	0.996
FB	HB	0.01-10	1.364 ± 0.057	0.443 ± 0.022	3.374 ± 0.046	0.999
	BP	10-100	11.015 ± 0.553	1	0.051 ± 0.001	0.994
FP	HB	0.01-10	1.541 ± 0.065	0.471 ± 0.024	3.569 ± 0.200	0.999
	BP	10-100	12.474 ± 0.520	1	0.053 ± 0.001	0.993
3% SNP						
RC	BP	3.16-100	0.007 ± 0.001	1	0.006 ± 0.000	0.998
RW	BP	3.16-100	0.002 ± 0.001	1	0.005 ± 0.000	0.998
FB	HB	0.01-10	0.258 ± 0.026	0.402 ± 0.012	0.955 ± 0.051	0.996
	BP	10-100	2.444 ± 0.137	1	0.012 ± 0.001	0.992
FP	HB	0.01-10	0.174 ± 0.017	0.398 ± 0.084	1.011 ± 0.131	0.995
	BP	10-100	2.068 ± 0.268	1	0.011 ± 0.002	0.993
1% SNP						
RC	BP	3.16-100	0.000 ± 0.001	1	0.002 ± 0.000	0.999
RW	BP	3.16-100	0.001 ± 0.001	1	0.002 ± 0.00	0.997
FB	PL	2.15-100	0	0.71 ± 0.03	0.01 ± 0.00	0.999
FP	PL	2.15-100	0	0.61 ± 0.06	0.02 ± 0.01	0.996

*RC (regular corn); RW (regular wheat); FB (faba bean); FP (field pea).

suspensions become more and more shear thinning. The value of n obtained in the Herschel-Bulkley regime depends mildly on concentration and has a value near 0.4. The increase in shear rate at which the change in model for a Herschel-Bulkley fluid to a power law or a Bingham fluid occurs is not constant and varies with starch type and concentration. According to previous studies (Perez Herrera and others 2017; Glasser and others 2019), this change in behavior may come from the fact that the hydroxyl groups on the surface of SNPs create inter-particulate hydrogen bonds (i.e. attractive surface forces) and that the yield stress is the result of these hydrogen bonds. Since the formation and breakdown of the structure are time-dependent, the SNPs will align themselves in the direction of flow quickly at high shear rates, and the structure force is broken at the same time. However, at the low shear rates, it is difficult to achieve the dynamic equilibrium of structure formation and destruction in a short time, because the structure force changes continuously with the extension of test time. This unsteady-continuous process leads to the change of flow behavior as a Herschel-Bulkley fluid at low shear rate.

Moreover, at concentrations of 1% and 3%, the greater viscosity of the pulse SNP suspension compared to that of cereal SNPs (Fig. 5.5B) suggested that the inter-particulate interactions (hydrogen bonds) were more for pulse SNPs. This can be attributed to the smaller particle size with more hydroxyl groups on the surface of pulse SNPs than that of cereal SNPs (Rubio-Hernández and others 2004). A similar observation was found in cellulose nanocrystal suspension with different aspect ratio (length/width) at low concentrations, where cellulose nanocrystal with smaller aspect ratio showed a greater viscosity at lower concentrations (Li and others 2015). In addition, the smaller particle size with more surface area of pulse SNPs produced more binding sites for water, and therefore more water would be immobilized in the SNP network, resulting in

125

greater viscosity (Mohaghegh and others 2006; Li and others 2015). However, at the higher concentration of 5%, the viscosity of SNP suspensions at 0.01 s^{-1} did not show significant differences between pulse and cereals. This indicates that both inter particulate interaction and hydration play major roles in the development of viscosity at greater concentrations. This was consistent with a previous study (Perez Herrera and others 2017), where the sample with the larger particle size contributed to the greater viscosity at a higher concentration. In the present study, FE-SEM and DLS measurements confirmed the larger particle size of cereal SNPs than pulse SNPs.

5.3.5. Flow behavior of SNP suspensions for three consecutive shear cycles

Starch pastes have been shown to have rheological instability (thixotropy/anti-thixotropy) depending on their source, concentration, pasting temperature, as well as storage temperature (Tattiyakul and Rao 2000; Wang and others 2010; Krystyjan and others 2016). In order to further examine and compare the rheological stability of SNP suspensions from different starch sources, three consecutive shear cycles were performed on both SNP suspensions and their native counterparts. Fig. 5.6A and B shows the viscosity versus shear rate curves of the 3% (w/v) starch pastes and 5% (w/v) SNP suspensions, respectively. The 3% (w/v) starch pastes were selected from preliminary experiments because pulse starch pastes of 5% (w/v) formed a very firm gel upon storage, which was not suitable for the rheological testing in the present study. As shown in Fig. 5.6A, all starch pastes exhibited a shear-thinning behavior, but with strong thixotropic behavior, where viscosities on the 1st downward curve were significantly lower than those on the upward curves, resulting in a hysteresis. This indicated that the structure of starch pastes was breaking down upon three cycles of shearing; pulse starches were breaking down more completely (Fig. 5.6A3 and A4), indicating a poor paste stability of pulse starches. Interestingly, the SNP suspensions were very stable, and their viscosity seemed to recover rapidly upon shearing. As
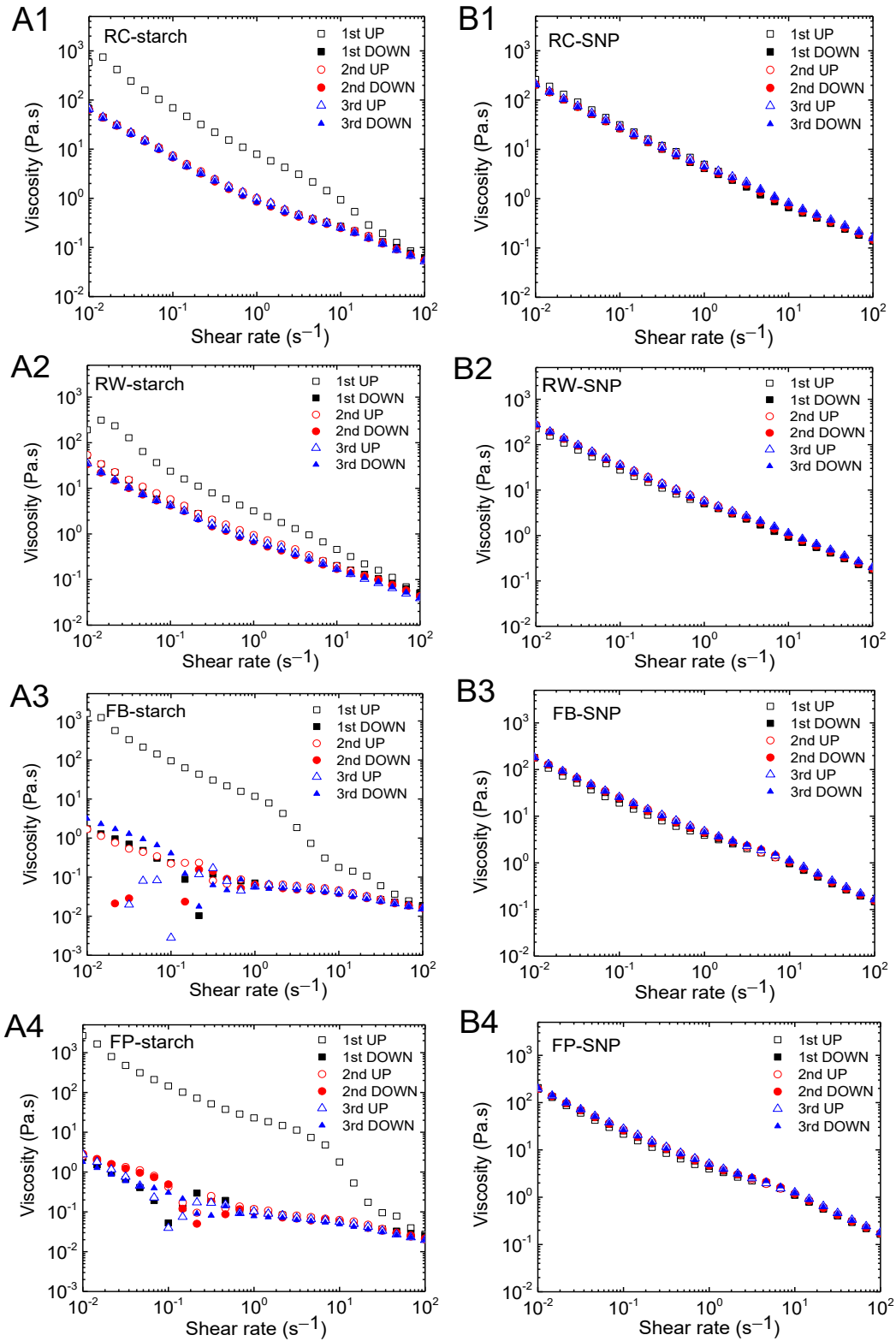
Fig. 5.6 Viscosity vs shear rate for upward and downward shear rate cycles of (A) native starch paste (3%, w/v) and (B) SNP suspension (5 %, w/v). RC (regular corn), RW(regular wheat), FB (faba bean), FP (field pea). (Open symbols, upward sweep; solid symbols, downward sweep.)

shown in Fig. 5.6B, SNPs exhibited a unique flow behavior during three full shear cycles. As shear rate increases, the gel-like network structure of the SNP breaks down, and the viscosity of the suspension decreases (upward curve). When the shear rate decreases, the viscosity recovers, and the structure rebuilds rapidly (downward curve). Only a slightly thixotropic/antithixotropic character can be seen at a lower shear rate in the downward curve versus the upward curve of the 1st cycle, where viscosity on the upward curve is slightly less for corn SNPs and more for other SNPs at the shear rate range of 0.01-1 s^{-1}. At the high shear rate, the apparent viscosity of all SNP samples slightly increases with each shearing cycle (upward and downward of 3rd cycle > upward and downward of 2nd cycle > upward and downward of 1st cycle), indicating a slight anti-thixotropic behavior; however, those differences were not significant. As discussed earlier, SNPs carry a large number of hydroxyl groups on the surface. These groups enable the SNPs to intensely interact with each other as well as the adjacent water molecules. Therefore, in the SNP suspension, the network is mainly composed of SNPs interacting at their surface through direct hydrogen bonding and/or water bridges (hydrogen bonds connecting water molecules) as well as immobilized water molecules. The network could be easily breakdown due to the weak forces of hydrogen bonding, resulting in a strong shear-thinning behavior upon upward shearing. However, due to the smaller particle size and well dispersibility of nanoparticles (i.e., a large number of hydroxyl groups as binding sites for water) the network can rebuild quickly on the downward curves. In addition, it is likely that more hydroxyl groups were exposed upon shearing and thus cause a slight increase in viscosity between shearing cycles as observed. Taken all together, nanoparticulation can significantly increase shear stability of starch pastes, particularly for pulse starches. This outcome suggests that SNP suspensions could readily be used for different applications, such as for drug delivery or as an emulsion stabilizer, where shear stability is critical.

5.3.6. Dynamic rheological properties

Oscillatory strain sweeps were performed at a frequency of 1 Hz with strain amplitudes ranging from 0.1% to 1000%. Frequency sweeps were performed at a fixed oscillation strain at an amplitude of 2% with frequency ranging from 0.1-10 rad/s. Storage modulus G′ and loss modulus G″ represent the elastic and viscous nature of the viscoelastic behavior, respectively. When G′ is higher than G″, a solid -like behavior will amplify, and this behavior is expected to intensify with increasing concentration (Glasser and others 2019). Viscoelastic behavior of SNP suspensions of different concentrations is shown in Fig. 5.7 and Fig. 5.8. Fig. 5.7A shows the dynamic moduli of RC-SNP suspension at a concentration of 5%. Linear viscoelastic response characterized by constant values of the G′ and G″ were obtained at strains below about 10%. The linear viscoelastic ranges of other SNP suspensions are summarized in Table 5.3. The average value of G′ and G″ within the linear viscoelastic range of SNP suspensions at different concentrations is presented in Fig. 5.7B. It was observed that all SNP suspensions become more elastic with increasing concentration. The G′ and G″ as a function of angular frequency ω of SNP suspensions at different concentrations are shown in Fig. 5.8. For SNP suspensions with high concentraitons (i.e., 5% for cereal SNP, 3% and 5% for pulse SNP), both G′ and G″ were independent of ω, and the G′ was much greater than G″ over the entire frequency range, indicating the solid-like structure of SNP suspensions. At relatively low concentrations of SNP suspensions (i.e., 1% and 3% for cereal SNP, 1% for pulse SNP), G′ and G″ increased with angular frequency. For the cereal SNP, as the concentration decreased, the slopes of G′ and G″ became steeper. Compared to cereal SNP suspensions, pulse SNP suspensions had much greater G′ values (i.e., a more elastic behavior than cereal SNP suspensions), revealing the more extensive inter-particulate associations on the surface of pulse SNPs. This is mainly due to pulse SNPs having a smaller particle size (large surface area),

greater amount of amylose with linear and long chains (denser and longer hairy layer), and thus more hydroxyl groups were exposed on the SNP surface. Similar observations were found for those SNP produced by acid hydrolysis, where potato SNP with smaller particle size resulted in greater elastic behavior than larger SNP from wheat, oat and barley (Perez Herrera and others 2017). Overall, in good agreement with the continuous shear test results, these dynamic rheological measurements also suggest the strong dependence of the rheological properties of SNP suspensions on the concentration and starch source. Pulse SNP with a smaller particle size are capable of forming more extensive inter-particulate associations and therefore providing a more elastic behavior than cereal SNP.
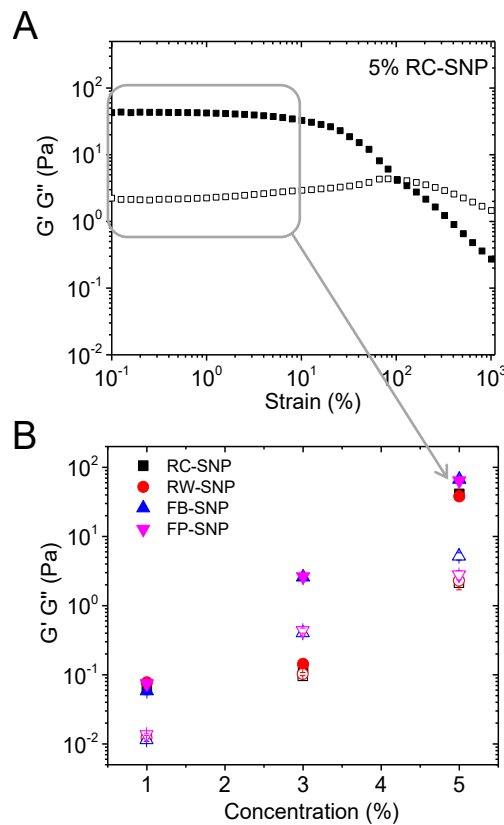
Fig. 5.7 Rheological behavior of SNP suspensions: (A) storage G′ (solid symbols) and loss G″ (open symbols) moduli vs oscillation strain for RC-SNP, 5% in water, at a frequency of 1 Hz and a temperature of 25 °C. (B) Average value of G′ (solid symbols) and G″ (open symbols) in the linear viscoelastic range (i.e., in the plateau region of Fig. 5.7A) vs concentration. RC (regular corn), RW(regular wheat), FB (faba bean), FP (field pea).
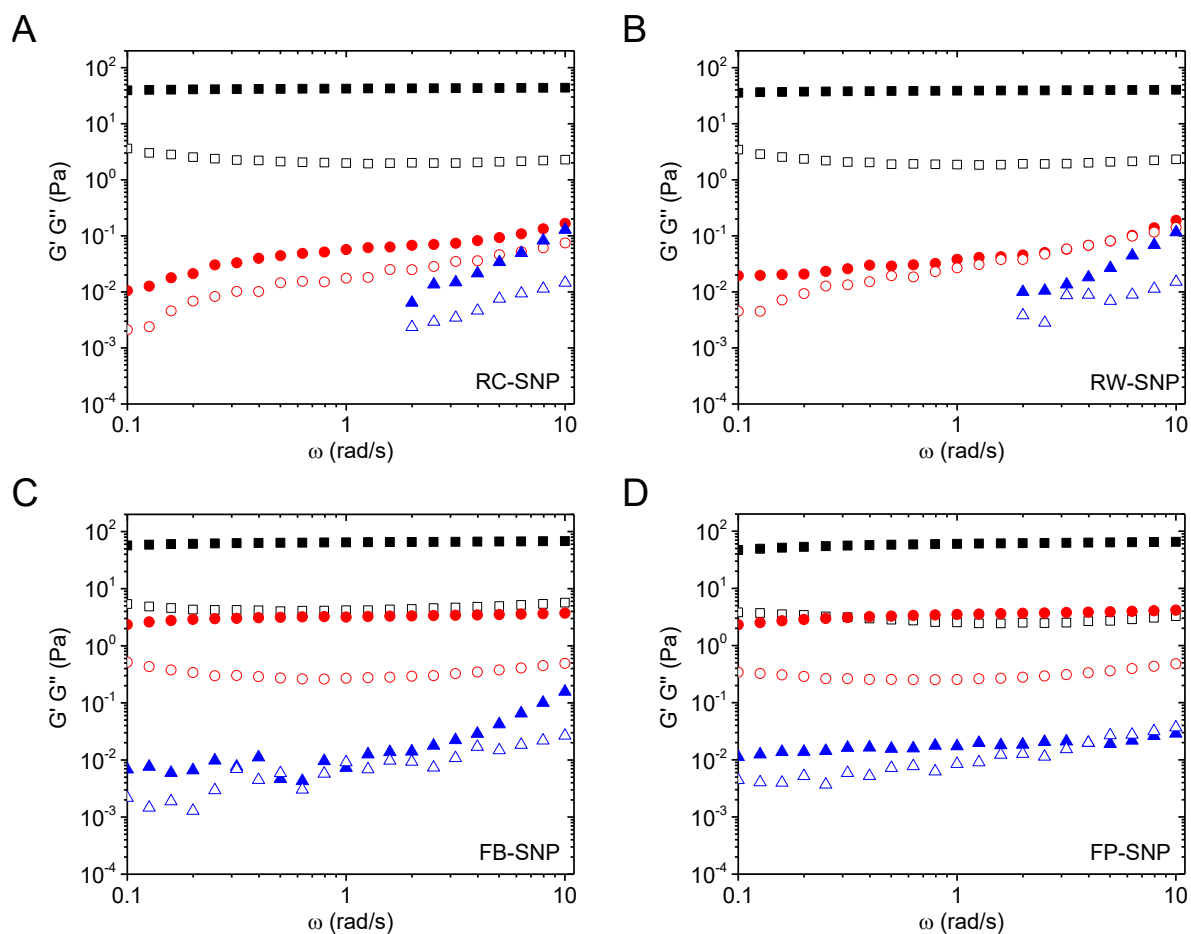
Fig. 5.8 Storage modulus G′ (solid symbols) and loss modulus G″ (open symbols) vs angular frequency ω of SNP suspensions with concentrations of 5% (w/v, black squares), 3% (w/v, red circles), and 1% (w/v, blue triangles) at 25 °C. RC (regular corn), RW (regular wheat), FB (faba bean), FP (field pea).

Table 5.3 Linear viscoelastic region of various concentrations of four different SNPs at 1 Hz

Samples*	Strain (%)		
	1%	3%	5%
RC-SNPs	100	20	10
RW-SNPs	100	10	10
FB-SNPs	100	10	10
FP-SNPs	100	10	10

*RC (regular corn), RW(regular wheat), FB (faba bean), FP (field pea)

5.3.7. The effect of temperature on dynamic rheological properties

In order to further understand how temperature affects the network of SNPs formed in aqueous suspensions, the viscoelastic behavior of SNP suspensions with different concentrations as a function of temperature was investigated. The results are shown in Fig. 5.9. A large variation in the temperature dependency of G' and G'' is observed among SNP suspensions depending on their concentration and starch source. At a larger concentration of 5%, all SNP suspensions behave like a more elastic gel ($G' > G''$) at all temperatures; G' and G'' remain independent of temperature at the lower temperature regions. However, with the increase in temperature, all SNP suspensions exhibited a drop in G' and G'', and the elastic gel structure seemed to breakdown. Finally, G' and G'' increased gradually with a further increase in temperature to 90 °C, which is probably due to the swelling, melting/solubilization of particles into their composite molecules and the consequent formation of a molecular network through an increase in starch molecule-water hydrogen bonding (Shi and others 2013). The decrease of G' and G'' which was gradually observed in cereal SNPs is probably due to the network breakdown and particle swelling overlapping in the middle temperature regions. As the concentration decreased to 3%, pulse SNP suspensions behaved like an elastic gel ($G' > G''$) at all the temperatures, while cereal SNPs behaved like a liquid ($G'' > G'$) at lower temperatures and transitioned to an elastic gel ($G' > G''$) above 48 °C and 40 °C for corn and wheat SNPs, respectively. In all samples at 1% the G' and G" values were greater with increasing temperature than those recorded at 25 °C, indicating new interactions in the suspensions were formed with increasing temperature (Jiang and others 2016). According to previous studies (Jiang and others 2016; Perez Herrera and others 2017), an initial decrease and then an increase in G' when SNPs are heated from 25 to 90 °C corresponds to the loss in the network aggregates and then SNP swelling and disrupting the intramolecular hydrogen bonds while increasing the

hydrogen bonding with water. In this study, it was proposed that at elevated temperatures, the decrease in G′ and G″ of SNPs suspensions with higher concentrations was due to two step phase transitions: 1) the breakdown of the particulate network into individual nanoparticles; 2) the swelling, and partial solubilization of particles into their composing molecules (disruption of inter and intra molecular hydrogen bonds), and the consequent formation of a molecular network (i.e. increase in starch molecule-water hydrogen bonding) that occludes SNPs. The extent of the overlapping of those two steps was varied for SNPs from different starch sources, depending on their thermal stability.
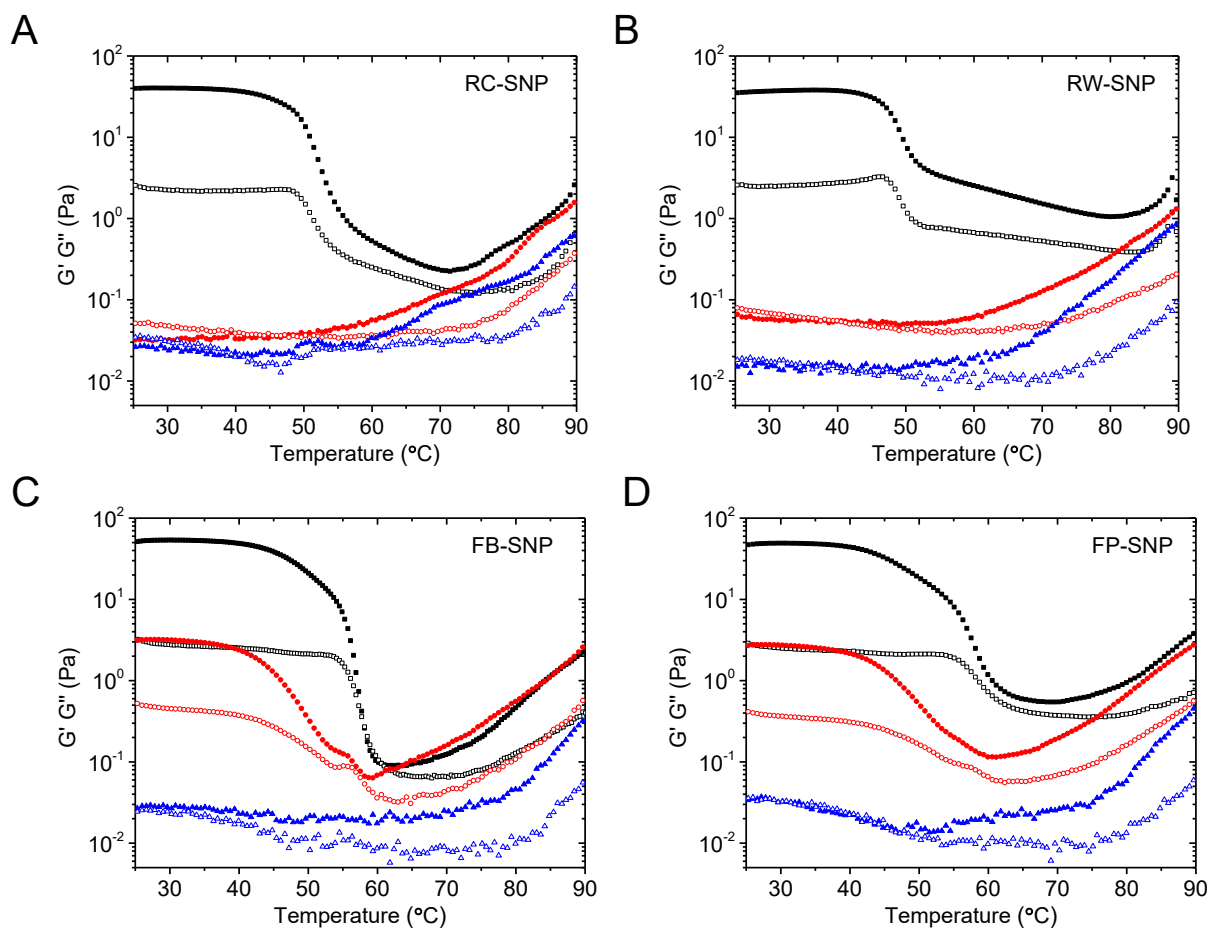
Fig. 5.9 Storage modulus G′ (solid symbols) and loss modulus G″ (open symbols) as a function of temperature: (A), RC-SNP (regular corn starch nanoparticles); (B), RW-SNP (regular wheat starch nanoparticles); (C), FB-SNP (faba bean starch nanoparticles); (D), FP-SNP (field pea starch nanoparticles) suspensions with concentrations of 5% (w/v, black squares), 3% (w/v, red circles), and 1% (w/v, blue triangles).

The complex viscosity of 1%, 3%, and 5% (w/v) SNP suspensions as a function of temperature is presented in Fig. 5.10. Complex viscosity η^* in oscillation rheology was found by dividing the complex modulus (G^*) by the angular frequency (ω). As shown in Fig. 5.10, at the beginning of the temperature ramp test (25 °C), pulse SNPs showed a greater complex viscosity for all concentrations compared to cereal SNPs; here cereal SNPs exhibited a very low viscosity at both 1% and 3% (liquid-like), which was consistent with the continuous shear test results (Fig. 5.5). For those SNP suspensions with gel-like behavior, their complex viscosity showed an initial decrease and then an increase with an increase in temperature. The initial decrease of complex viscosity could be explained by the breakdown of inter-particulate network into individual SNPs (liquid-like) (Li and others 2015; Perez Herrera and others 2017). However, the decrease was more gradual in pulse SNPs, as shown in Fig. 5.10A, indicating that the pulse SNP network was more stable to temperature changes than cereal SNPs. Similar results were reported by previous studies on SNPs produced by acid hydrolysis, where tuber SNP network broke down at higher temperatures than cereal SNPs (LeCorre and others 2012; Perez Herrera and others 2017). For the SNP suspensions with a liquid-like behavior, for example, at a concentration of 1%, as shown in Fig. 5.10C, the complex viscosity of all SNP suspensions was unchanged until temperature reached 70 °C for cereal SNPs, and 80 °C for pulse SNPs. The higher solubilization temperature observed in pulse SNP suspensions suggests a greater thermal stability of pulse SNPs than cereal SNPs. Here, the thermal stability of particles followed the order of FB > FP > RC > RW. This was consistent with thermal stability data measured by DLS (Table 5.1). Based on the above findings, pulse SNPs with smaller hydrodynamic diameters showed greater thermal stability and more elastic behavior than cereal SNPs. Therefore, pulse starch was superior in forming smaller particle

sizes of SNPs with greater thermal stability with the concurrent ability to form more extensive

inter-particle associations.
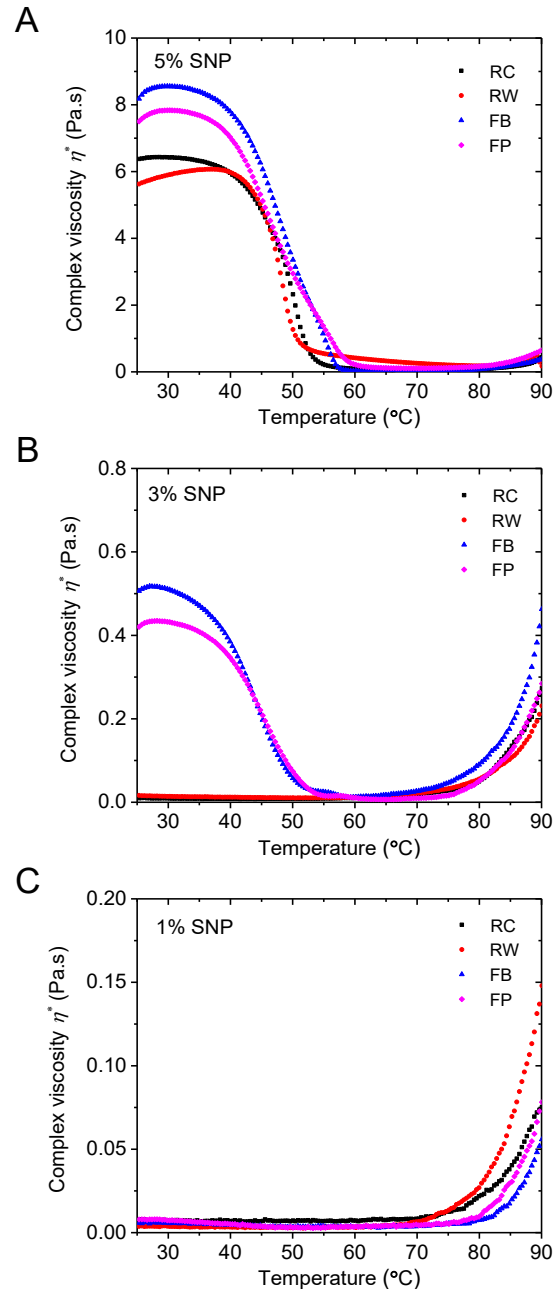
Fig. 5.10 Complex viscosity of A) 5% , B) 3%, C) 1% w/v SNP suspensions as a function of temperature. RC (regular corn), RW(regular wheat), FB (faba bean), FP (field pea).

5.3.8. Proposed mechanism for network formation of SNP suspensions

In order to better understand the difference in the dynamic rheological behavior of SNPs from different starch sources, the network of SNP suspensions was proposed, as illustrated in Fig. 5.11. After storage at a cool temperature (4 °C), the inter-particulate networks of concentrated SNP suspensions are enhanced and not reversible at room temperature. The network forms mainly through associations between surface hydroxyl groups through direct hydrogen bonding and water bridges (hydrogen bonding between SNPs and immobilized water molecules). The concentration, particle size and zeta potential of SNPs had significant influence on the network of SNP suspensions. At lower concentrations (i.e., 1%, w/v), the SNP suspension contained more free water molecules and less associations among SNP due to the surface charge and electrostatic repulsion of SNPs, which contributed to the observed viscous liquid-like rheological behavior. However, at greater concentrations (i.e., 5%, w/v), SNP suspensions contained more water bridges (immobilized water molecules) and SNP aggregations due to the closer proximity among SNPs and enhanced hydrogen bonding between "hairs" on the SNP surface network (Fig. 5.11), thus exhibiting elastic gel-like rheological behavior. The critical concentration of SNPs was different among the various starch sources presented here, with stronger inter particulate networks formed in pulse SNP suspensions at 3% compared to cereal SNP suspensions at the same concentration. It is possible that the greater amylose content and longer chain length of pulse starch molecules would lead to the formation of denser and longer hairy layer on the SNP surface. These SNPs would then carry a larger number of hydroxyl groups on the surface and enable the SNPs to better interact with each other as well as the adjacent water molecules. Upon shearing, three consecutive shear sweep cycles as presented in this study, the inter-particulate network (i.e., water bridges) breakdown into individual particles, represented by a sharp decrease in viscosity upon upward

136

Fig. 5.11 A schematic diagram showing SNP network at room temperature and the biphasic molecular network formation during heating of aqueous SNP suspensions. AM (amylose); AP (amylopectin) (Adapted and modified from Perez Herrera and others (2017).

shear sweep, but rebuilt instantaneously, represented by an increase in viscosity to the initial state rapidly upon downward shearing. However, upon heating, the inter-particulate network broke down and the intermolecular hydrogen bonds of SNPs were disrupted through swelling and solubilization, leading to the release of linear AM and branched AP molecules. Due to the different thermal stability between the AM crystals (highly packed) and AP crystals (loosely packed) (Jane and others 1999; Klucinec and Thompson 1999), it is plausible that the thermal stability of SNPs is greater when there is a greater content of amylose, translating to smaller SNPs or partially solubilized SNP residues. Thus, after heating, the network is composed of linear AM and branched AP, as a continuous phase, and small heat resistant SNP residues, as a dispersed phase represented by a molecular network that occludes SNPs. The thermal stability of SNP suspensions varies depending on their concentration, particle size and starch sources as discussed previously.

5.4. Conclusions

The SNPs produced from pulse and cereal starches were spherical in shape, however had significant differences in molecular characteristics, particle size distribution, rheological and thermal properties. The relationships between SNP concentration, molecular composition and structure, particle size, rheological and thermal properties were observed and discussed. The starch source and SNP concentration influenced the viscoelastic behavior of the aqueous SNP suspension. SNP suspensions exhibited elastic gel-like behavior at higher concentrations (i.e., 5% w/v) but exhibited a viscous liquid-like behavior at lower concentrations (i.e., 1% w/v). Pulse SNPs with smaller particle size could form more extensive inter-particulate associations, thereby having greater viscosities and possessing a more elastic gel-like behavior than cereal SNPs. During heating, SNP suspensions may undergo inter-particulate network breakdown, particulate swelling, and partial melting/solubilization, resulting in changes in average hydrodynamic diameter and

dynamic rheological behavior at elevated temperatures. Cereal SNPs in an aqueous suspension were less heat resistant than pulse SNPs. Cereal SNPs showed a greater extent of reduction in average hydrodynamic diameter measurements, network breakdown and swelling and melting/solubilization at lower temperatures. A schematic model was proposed and used to illustrate the SNP network formation at room temperature and heating in order to explain how processing conditions such as heating alter the particulate nature of SNPs. A careful selection of starch source and processing conditions, such as starch concentration, heating temperature, and shearing conditions, are required to achieve the desired rheological properties of SNPs in food and industrial applications.

Chapter 6: Scalable production of starch nanoparticles by continuous nanoprecipitation for food-grade Pickering emulsion

6.1. Introduction

Nanoprecipitation is a process in which nanoparticles are assembled from solublized molecules through kinetically controlled steps such as supersaturation, nucleation and then growth (D'Addio and Prud'homme 2011; Saad and Prud'homme 2016). The literature reports three widely used nanoprecipitation techniques as follows: conventional batch nanoprecipitation (BNP), flash nanoprecipitation (FNP), and microfluidic nanoprecipitation (MNP). The BNP is usually performed in a stirred tank reactor by the gradual addition of an antisolvent that is miscible with solvent in which solutes are dissolved (Chin and others 2011; Qin and others 2016). Efficient mixing between the solution and antisolvent is important for optimal nanoprecipitation. Thus, improved mixing techniques using micromixers have been developed and introduced to control nanoprecipitation. One that is based on turbulent mixing is called flash nanoprecipitation (FNP), and another is based on reducing molecular diffusion distance under laminar flow conditions and is called microfluidic nanoprecipitation (MNP) (Karnik and others 2008; Saad and Prud'homme 2016). FNP and MNP are usually operated in continuous flow, and thus can be easily scaled-up for industrial applications. Although several studies have reported the formation of SNPs from different starch types using BNP (Qin and others 2016; Saari and others 2017; Hedayati and others 2020), there is a lack of information regarding the production and characterization of SNPs using FNP and MNP techniques. Considering the advantages of FNP and MNP, this comparative study targeted here to evaluate their use in SNP formation was expected to generate useful information for future potential scale up of the process.

SNPs could be used in several applications such as nanocomposites, emulsification and encapsulation, but this study mainly focuses on the ability of these nanoparticles to stabilize Pickering emulsions. Pickering emulsions (Pickering 1907) are emulsions that are stabilized by solid particles, which accumulate at the interface between two immiscible liquids (i.e., oil and water phase) and stabilize droplets against coalescence. Recently, some biological and food-grade particles have drawn significant research interest since these solid colloids are uniquely biocompatible, biodegradable, and thus environmentally sustainable. Solid colloids can form an effective steric and electrostatic shield at the oil-water interface, which prevents the emulsion droplets from coalescence and thus improve the stability of emulsion (Tang and others 2014; Gong and others 2017). Starch, as an abundant, renewable, biodegradable, and biocompatible polymer, is therefore a good stabilizer candidate. Starch particles varying from nanometers to micrometers have been successfully used to stabilize emulsions, as is the case with corn, potato and tapioca SNPs (Ge and others 2017; Saari and others 2017), quinoa starch granules (Rayner and others 2012), and modified starch granules (Saari and others 2016). However, there is dearth information on the use of pulse SNPs for the production of a Pickering emulsion.

In the present study, high-purity field pea starch was used as a reference starch. SNPs were prepared using the batch process (BNP) and continuous processes (FNP and MNP). The main objective is to investigate continuous nanoprecipitation technologies for scale-up processing of SNPs and for their use in food-grade Pickering emulsions. The specific objectives are: 1) to investigate the optimum levels of starch concentration and antisolvent/solvent (AS/S) ratio using rapid batch nanoprecipitation (R-BNP) method with rapid injection of antisolvent and solvent to each other; 2) to evaluate the effect of flow rate on the formation of field pea SNPs using

continuous micromixers; 3) to compare the batch process (BNP) to continuous processes (FNP and MNP) for the production and characterization of field pea SNPs; 4) to produce Pickering emulsions using the resultant SNPs. This research will assist the industry to evaluate the potential of continuous nanoprecipitation techniques in the commercial production of SNPs for nutraceutical, food, and pharmaceutical applications.

6.2. Materials and methods

6.2.1. Materials

Field pea starch was used as described in Chapter 3 section 3.2.1. Milli-Q water was used for all experiments. All other chemicals were of analytical grade.

6.2.2. Starch dissolution

Starch solution was prepared according to a method described elsewhere (Iida and others 2008; Chang and others 2017b). Native field pea starch was dispersed in Milli Q water (50 mg/mL) and gelatinized in a boiling water bath for 30 min with stirring on a vortex mixer every 5 min. The gelatinized starch paste was then sonicated for 10 min using a 20 kHz ultrasonic processor (FS-1200 N, Shanghai Sonxi Ultrasonic Instrument Co., Ltd., Shanghai, ZJ, China) equipped with a probe transducer and a flat tip of 13 mm. The power output of 720 W and 5/2 s on/off pulses were applied to minimize heat generation. The temperature of the starch solution after the ultrasonic treatments was approximately 70 °C. The viscosity of the starch paste was markedly decreased by ultrasonication within 5 min, likely due to the destruction of the swollen starch granular network and quantitative solubilization of amylopectin and amylose molecules in the amorphous phase. The homogenous starch solution (50 mg/mL) was then diluted to concentrations of 2.5, 5, 10, 15, 30, and 50 mg/mL before nanoprecipitation.

6.2.3. Starch nanoprecipitation

Nanoprecipitation was achieved by a batch process (batch nanoprecipitation, BNP) as well as by two different continuous processes (flash nanoprecipitation, FNP, and microfluidic nanoprecipitation, MNP). In all three techniques, water and absolute ethanol were used as solvent and antisolvent, respectively. A schematic diagram showing the reactor designs for the batch (BNP) and continuous (FNP and MNP) processes is presented in Fig. 6.1. The BNP was performed by mixing solvent and antisolvent by adding one to the other dropwise or directly at once in a stirred reactor. The continuous processes used two types of micromixers as follows: a) Y-shaped confined impinging jet mixer (CIJM) for FNP and b) Y-shaped staggered herringbone mixer (HBM) for MNP. The Y shape was chosen rather than the T shape to minimize clogging of the tubes. The mixing of solvent and antisolvent takes place in the Y-junction of the two tube channels by pumping both liquids at the same time. The optimum levels of starch concentration and antisolvent-to-solvent (AS/S) ratio were selected based on the experiments performed by using BNP with direct mixing of solvent and antisolvent at once, which is easy and flexible to handle with low plugging probability. The continuous mixers were further used to fine tune and optimize the process parameters by manipulating inlet/outlet flows.

6.2.3.1. Batch nanoprecipitation (BNP)

Solutions of starch, with water as the solvent, were prepared according to the methodology described in section 6.2.2. All experiments were performed using absolute ethanol as the antisolvent (Fig. 6.1A). The production of SNPs consisted of mixing starch solution and ethanol under magnetic stirring by slow addition of one into the other, in either order, dropwise using a syringe pump (KD Scientific, Thermo Fisher scientific Inc, Mississauga, ON, Canada). The AS/S ratios (v/v) were 10:1 and 1:1. This dropwise slow BNP method is denoted as S-BNP. Alternatively,
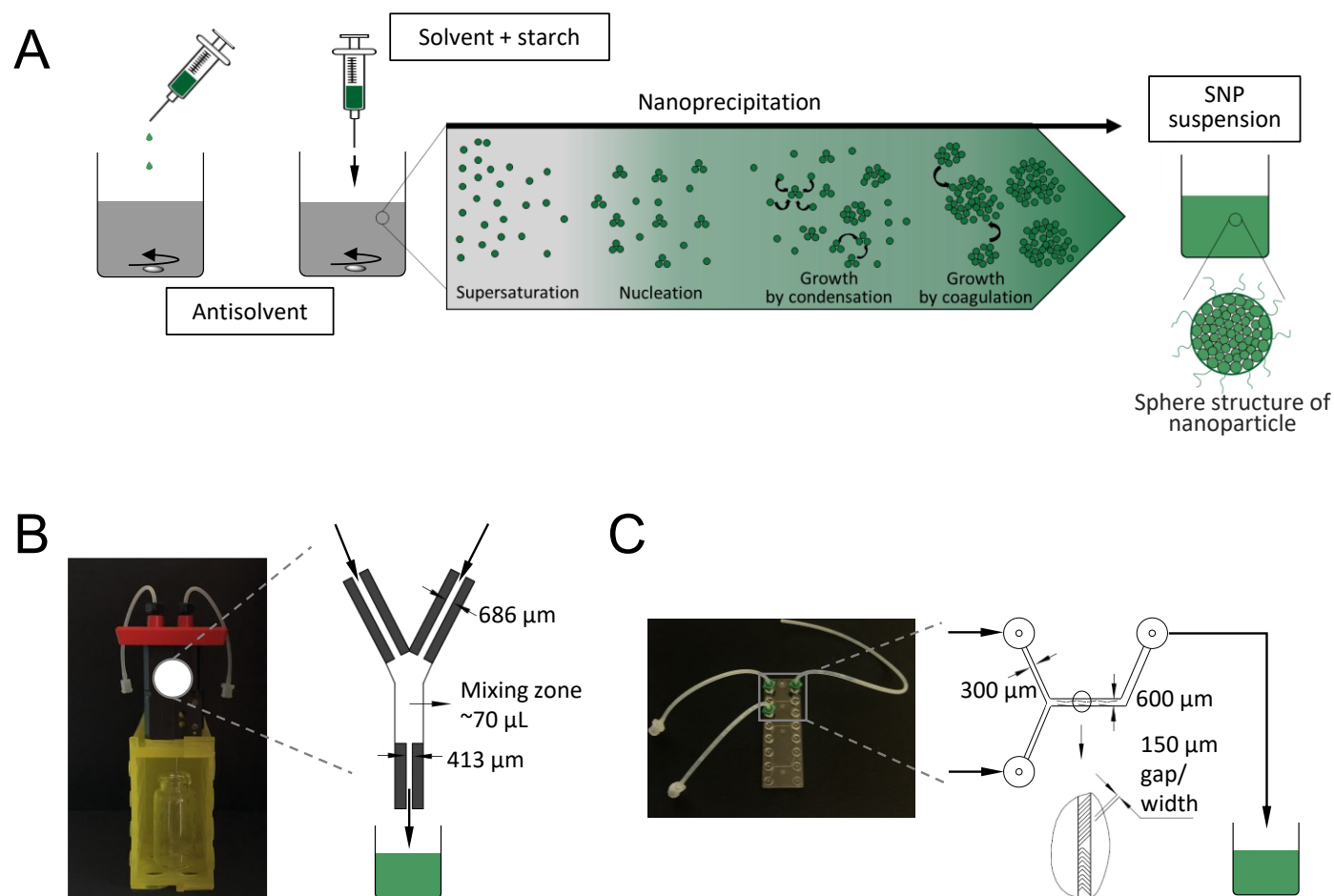
Fig. 6.1 A schematic diagram showing the reactor designs used for starch nanoprecipitation: (A) BNP (batch nanoprecipitation by dropwise mixing and directly mixing at once); (B) FNP (flash nanoprecipitation) by using a Y-shaped CIJM (confined impinging jet mixer); (C) MNP (microfluidic nanoprecipitation) by using a Y-shaped SHM (staggered herringbone mixer); FNP and MNP share the same principle of nanoprecipitation as BNP, but with improved mixing efficiencies. Condensation is the addition of single molecules to the particles surface. Coagulation is the adhesion of particles to each other's surface. (Adapted and modified from previous studies (Joye and McClements 2013; Kügler and Kind 2016; Martínez Rivas and others 2017; Lammari and others 2020).

a rapid BNP (R-BNP) mixing method was performed by pipetting the starch solution or ethanol into each other rapidly under magnetic stirring. The starch concentration and AS/S ratio ranged between 2.5-50 mg/mL and 10:1,1:1, respectively. After thorough mixing, an aliquot of the colloidal suspension was diluted with water for the analysis of the particle size, particle size distribution (PSD), and polydispersity index (PDI) by dynamic light scattering (DLS, see Section 6.2.5). Finally, the colloidal suspension was homogenized to promote the precipitation of fine particles using a homogenizer at 8,000 rpm for 1 min (Heidolph Diax 900, Schwabath, Bavaria, Germany). The sediments were collected by centrifugation and then re-dispersed in water and frozen at −20 °C overnight in a freezer. The frozen samples were then freeze dried (FreeZone 12, Labconco Corp., Kansas, MO, USA) at a sublimating temperature of −45 °C for 2 days.

6.2.3.2. Flash nanoprecipitation by a Y-shaped confined impinging jet mixer (CIJM)

FNP was performed by using a CIJM, which contains two inlet ports controlled by a digital multiple syringe pump and a single outlet port. The key part of the experimental setup is illustrated in Fig. 6.1B. The mixer has equal inlet diameters of 686 μm (inside diameter, ID), outlet diameter of 413 μm ID, 3 mm ID in the mixing zone and 10 mm length of mixing zone. In the experimental setup, the starch solution was loaded into a syringe and injected through one port while the other inlet stream contained absolute ethanol, at output flow rates of 20, 40, and 60 mL/min. The two streams were started at the same time and controlled by a multiple syringe pump (KD Scientific, Thermo Fisher scientific Inc, Mississauga, ON, Canada), for the volumetric ratio of AS/S 1:1. The rapid mixing of both liquid streams took place inside chamber, promoted by turbulence and the nanoprecipitation occurred immediately. Subsequently, an aliquot of the colloidal suspension obtained from the outlet was diluted with water for the analysis of particle size, PSD, and PDI by

DLS (see Section 6.2.5). After collecting the colloidal suspension, the procedure for recovering SNPs from suspension was performed as described in Section 6.2.3.1.

6.2.3.3. Microfluidic nanoprecipitation by a staggered herringbone mixer (SHM)

The microfluidic mixer chip used in the present study (Fig. 6.1C) is based on the idea of staggered herringbone mixer (SHM) design and was purchased from Darwin Microfluidics (Paris, France). The two inlet channels (Y-junction) are approximately 300 μm × 200 μm (width × depth), and its length is 10 mm. The cross-section of the mixing channel and outlet is 600 μm × 200 μm (width × depth), and their length is 10 mm. The starch solution and absolute ethanol were introduced into HBM at the same time by a multiple syringe pump (KD Scientific, Thermo Fisher scientific Inc, Mississauga, ON, Canada), for the volumetric ratio of AS/S 1:1. The rapid mixing of both liquid streams took place at the junction of the two channels (Y-junction) and the nanoprecipitation occurred instantly. Subsequently, an aliquot of the suspension obtained from the outlet was diluted with water for the analysis of particle size, PSD, and PDI by DLS (see Section 6.2.5.). After collecting the colloidal suspension, the procedure as described in section 6.2.3.1 was followed.

6.2.4. Production of Pickering emulsion

For Pickering emulsions, the aqueous phase was prepared by dispersing SNPs into Milli-Q water at concentrations of 10, 5, 2, 1, 0.5, 0.01 mg/mL, forming stable suspensions. Then, 1 mL of canola oil was added into 2 mL of SNP suspension, followed by sonication with a probe-type sonicator (Qsonica Sonicator Q55, Thermo Fisher Scientific Inc., Waltham, MA, USA) for 20 s to form a Pickering emulsion. To protect the samples from heating, a pulse function was used (5/5 s on/off). The emulsions prepared without SNPs under the same conditions were used for comparison.

6.2.5. Characterizations of SNPs

The particle size, PSD, and PDI of the SNPs in suspension were determined with a Zetasizer (Nano S, Malvern Instruments, Worcestershire, U.K.) following the procedure as described in Chapter 3 section 3.2.4. The morphology and the size of SNPs were observed using FE-SEM (Zeiss Sigma 300 VP-FESEM, Carl Zeiss NTS, Germany) following the procedure as described in Chapter 4 section 4.2.4. XRD patterns of the field pea starch and SNP samples were obtained using a Rigaku Ultima IV multipurpose X-ray diffractometer (Rigaku America, Woodlands, TX, USA) following the procedure as described in Chapter 4 section 4.2.6. The molecular orders of field pea starch and SNPs were evaluated by an ATR-FTIR (Alpha, Bruker, Berlin, Germany) following the procedure as described in Chapter 4 section 4.2.7.

6.2.6. Characterization of SNP stabilized Pickering emulsions

The droplet size of the SNP stabilized Pickering emulsions was characterized by the laser light scattering using a Mastersizer 2000 instrument (Malvern Instruments Ltd, Malvern, Worcestershire, UK). All measurements were carried out at room temperature in triplicate. For optical microscopic observation, a drop of the emulsion was placed on a glass slide, capped with a cover slip and was then observed using a ZEISS PrimoVert microscope (Carl Zeiss Microscopy GmbH, Göttingen, Germany).

6.2.7. Statistical analysis

All experiments were done in at least three replicates. Results are presented as mean ± SD (standard deviation). Analysis of variance was performed, and the mean comparisons were carried out by Tukey's HSD test (OriginPro 9.0.0, OriginLab Northampton, MA, USA).

6.3. Results and discussion

6.3.1. Effect of antisolvent-to-solvent ratio (AS/S) and addition methods

The production of SNPs by BNP method (using both S-BNP and R-BNP) was used as a control for this study. Initially, slow dropwise addition of starch solution (10 mg/mL) into absolute ethanol (i.e., S-BNP) under vigorous magnetic stirring to a final AS/S ratio of 10:1 was investigated. The SNPs formed by this method showed an average particle size of ~120 nm and a narrow PSD (i.e., PDI value of 0.22) (Fig. 6.2A and B). When SNP suspensions were diluted to a concentration of 0.02% (w/v) with Milli-Q water it showed a PDI <0.3, indicating the sample in water was in uniform colloidal suspension and therefore suitable for DLS measurements (Shi and others 2011; Dong and others 2015). The FE-SEM images show that the freeze-dried samples (Fig. 6.3A) had uniform smooth spheres, consistent with a previous study (Chin and others 2011), where a small volume of dilute starch solution (10 mg/mL) when mixed in excess of absolute ethanol (AS/S ratio 10:1, 15:1 and 20:1), nanoparticles formed instantaneously with a narrow PSD. The major shortcomings in this method are that it consumes a large amount of antisolvent (i.e., ethanol) and is slow to produce a unit quantity of SNPs. Therefore, the R-BNP method that involves direct mixing of the starch solution to absolute ethanol at once was investigated. The SNPs formed by R-BNP showed comparable particle size, PSD, PDI and morphology to that from S-BNP (Fig. 6.2A, B and Fig. 6.3B). This is attributed to the initial rapid supersaturation of molecules caused by the rapid molecular dehydration under high AS/S ratio (10:1, v/v) for both methods (Chin and others 2011; Qiu and others 2016).
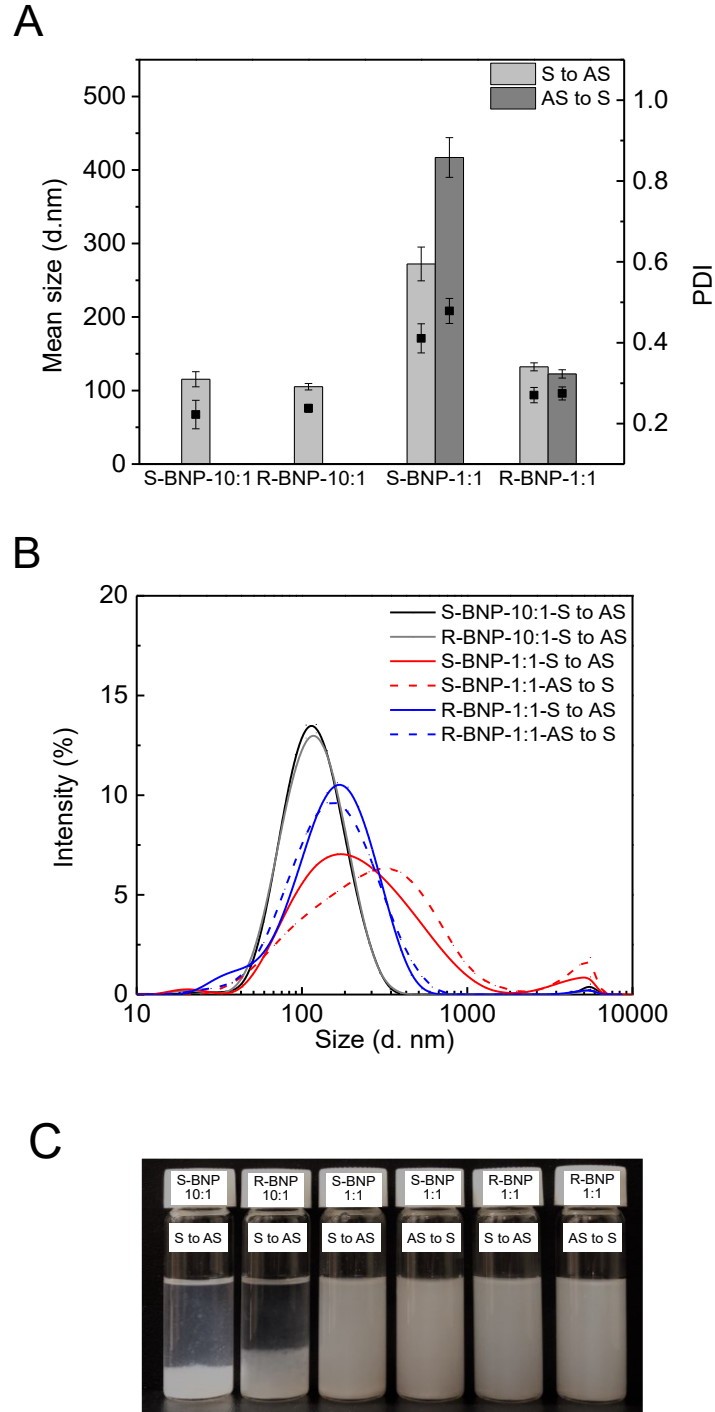
Fig. 6.2 Particle characteristics of the SNPs prepared by BNP with different mixing methods and different AS/S ratios at a fixed starch concentration of 10 mg/mL. A) Mean size (bar), PDI (solid square), B) particle size distribution, and C) Photographs of the suspensions formed after mixing.
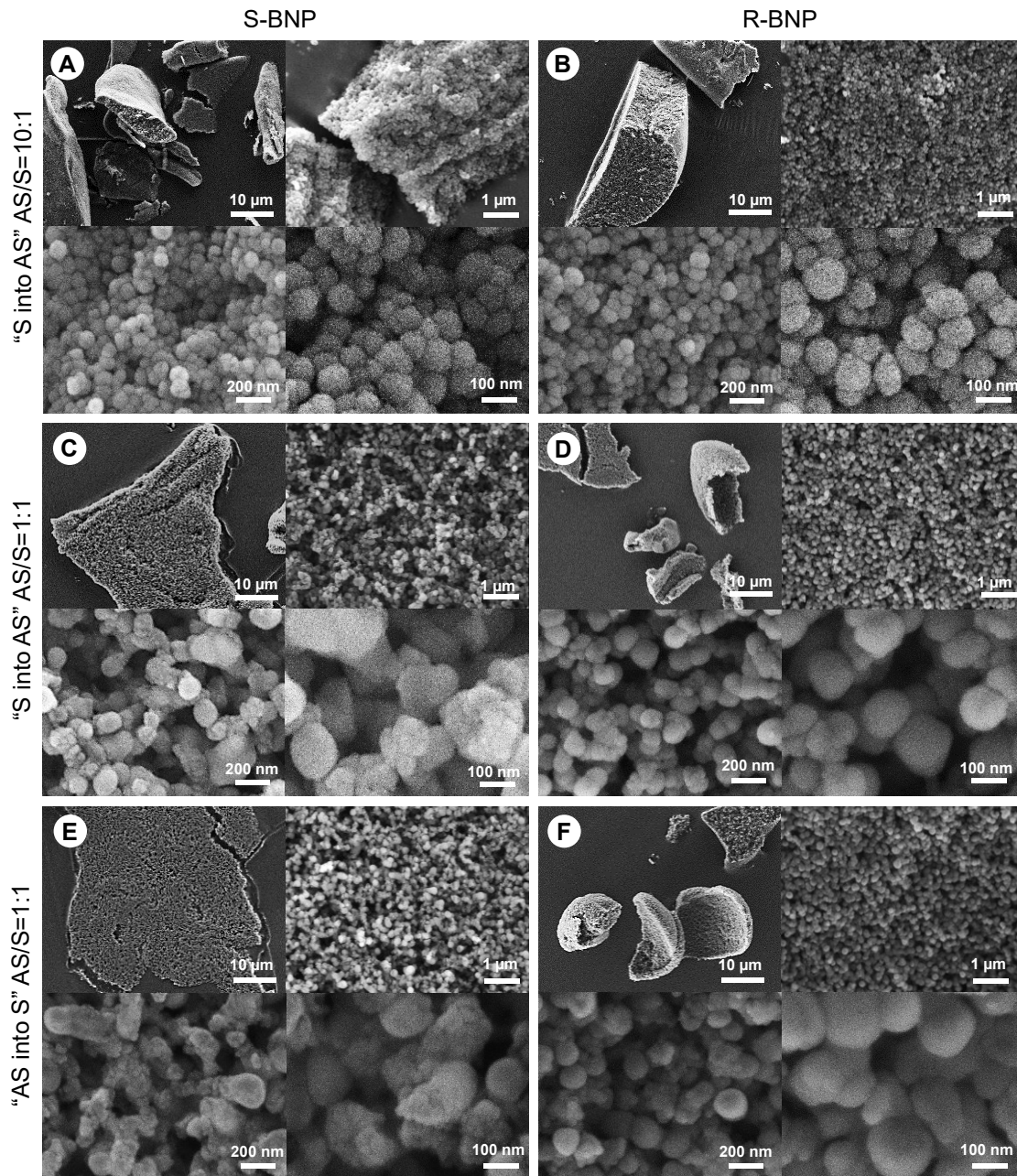
Fig. 6.3 The FE-SEM micrographs of the SNPs obtained from field pea starch by batch nanoprecipitation: S-BNP (Slow batch nanoprecipitation); R-BNP (Rapid batch nanoprecipitation); AS (antisolvent, absolute ethanol), S (solvent, starch in water). AS/S (antisolvent-to-solvent ratio, v/v). (The starch concentration was fixed at 10 mg/mL).

The reduction in the AS/S ratio from 10:1 to 1:1 (v/v) in both S-BNP and R-BNP increased the particle size, PSD and PDI values. This was consistent with previous reports, where the authors attributed their observations to the influence of supersaturation ratio on the rate of nucleation and particle size (Dong and others 2015; Kügler and Kind 2016; Qiu and others 2016). Interestingly though, R-BNP at 1:1 (v/v) ratio with direct mixing of "S into AS", gave a significantly smaller average particle size (~130 nm) and narrower PSD (PDI value of 0.27) compared to the S-BNP (average particle size ~270 nm, PDI value of 0.41). FE-SEM images also showed that particles prepared by the R-BNP were spherical and relatively uniformly distributed (Fig. 6.3D), while those by the S-BNP were less uniform with small nucleus and big aggregates being present (Fig. 6.3C). A similar observation was made when the SNPs were produced by the R-BNP at 1:1 (v/v) ratio with direct mixing of "AS into S" in comparison to the S-BNP (Fig. 6.2 and Fig. 6.3E and 6.3F). Furthermore, the R-BNP at 1:1 (v/v) ratio with direct mixing of "AS into S" showed a comparable particle size (~ 123 nm) and PSD (PDI value of 0.27) (Fig. 6.2A and 6.2B) and morphology (Fig. 6.3D and 6.3F) to that from direct mixing of "S into AS", whereas for the S-BNP at 1:1 (v/v) ratio with adding "AS into S" dropwise, showed much larger average particle size (~ 420 nm) with wider PSD (PDI value of 0.48) than that obtained by adding "S into AS" dropwise. This confirmed the influence of how antisolvent and solvent mixing impacts SNP formation. In the S-BNP method, due to slow dropwise addition of starch solution into ethanol (i.e., "S into AS"), the ethanol concentration in the reactor declined gradually from 100% to 50%. Thus, it was reasonable to expect the level of supersaturation of starch molecules would have also gradually decreased with time of addition. In contrast, as for the slow dropwise addition of ethanol into starch solution (i.e., "AS into S), the initial supersaturation of molecules would be very low and then gradually increased with time of addition as ethanol concentration increased gradually

from 0% to 50%. Thus, less uniform particle size (i.e., wider PSD) and larger PDI for S-BNP (both "AS into S" and "S into AS") were obtained when compared to that formed in a R-BNP reactor, where ethanol concentration would quickly change from 100% or 0% to 50%. In addition, the lower level of supersaturation of starch molecules in the batch reactor by slow dropwise addition of "AS into S" led to the formation of SNPs with larger particle size and broader PSD than that by slow dropwise addition of "S to AS" at AS/S ratio of 1:1. In this case, since the AS/S ratio was 1:1, the effect of mixing "S into AS" or "AS into S" did significantly affect the particle size of SNPs formed by R-BNP (Fig. 6.2). Similar observations were reported elsewhere (Saari and others 2017), where SNPs were formed from waxy corn starch (starch concentration of 8 mg/mL and 1:1 AS/S ratio), where R-BNP yielded a greater percentage (72%) of particles in the submicron range when compared to the S-BNP (65%). Despite the similar trends, Saari and others (2017) reported a larger particle size and wider PSD when compared to those obtained in the present study. This could be attributed to the nature of the different starch source (i.e., different molecular size, ratio between amylopectin/amylose, etc.) and larger volume of starch solution used, since larger volume would take longer to mix dropwise in the S-BNP method. Preliminary experiments also indicated (data not provided) that the particle size increased with increasing starch solution volume under the same starch concentration at a fixed AS/S ratio of 1:1. The BNP method has been reported in many studies in the literature. Thus, simple variations within this methodology could be attributed to the contradictory information reported in the literature regarding particle characteristics of SNPs formed.

In addition, as shown in Fig. 6.2C, clear differences were observed in the appearance of the suspensions formed after mixing in different ways. All SNPs formed at AS/S of 10:1 (v/v) precipitated instantaneously due to the greater amount of AS used. When mixing AS and S at a

ratio of 1:1 (v/v), a colloidal suspension was produced instantaneously with fine particles dispersed inside. There were no visible sediments in the suspension formed by R-BNP through mixing "S into AS" or "AS into S", while some sediments and visible particles were observed in that formed by S-BNP. This also indicated the more uniform kinetics generated by R-BNP compared to that generated by S-BNP at low AS/S ratio of 1:1 (v/v).

These outcomes suggested that very fast mixing could make it possible to reach the supersaturation intended by minimizing mixing effects on supersaturation built up at a lower AS/S ratio, 1:1 (v/v) for instance. Therefore, BNP could be achieved in a shorter time with a smaller particle size and narrower PSD using R-BNP at a AS/S ratio of 1:1 (v/v) compared to S-BNP.

6.3.2. Effect of starch concentration

Freshly prepared starch solution (i.e., stock solution, 50 mg/ml) was diluted to different concentrations: 2.5, 5, 10, 15, 30, and 50 mg/mL and used in the nanoprecipitation experiment. The effect of starch concentration on the PSD, mean particle size and PDI was investigated by adapting the R-BNP method with "AS to S" mixing at a fixed AS/S ratio 1:1 (v/v). As shown in Fig. 6.4, coagulation of particles was visually observed beyond 30 mg/mL starch concentrations from the photograph (Fig. 6.4A). The PSD, mean particle size and PDI of SNPs increased with starch concentration, but not in a linear fashion (Fig. 6.4B and 6.4C). Increasing the starch concentration from 2.5 to 10 mg/mL led to a decrease in the mean particle size from 135 nm to 123 nm, which could be attributed to enhanced molecular supersaturation and consequent greater nucleation rate. There was no significant difference between PDI (all values <0.3) with increasing starch concentration from 2.5 to 10 mg/mL, indicating SNPs formed had a narrow PSD and were thus more uniform in nature (Fig. 6.4B and 6.4C). However, the particle size remarkably increased
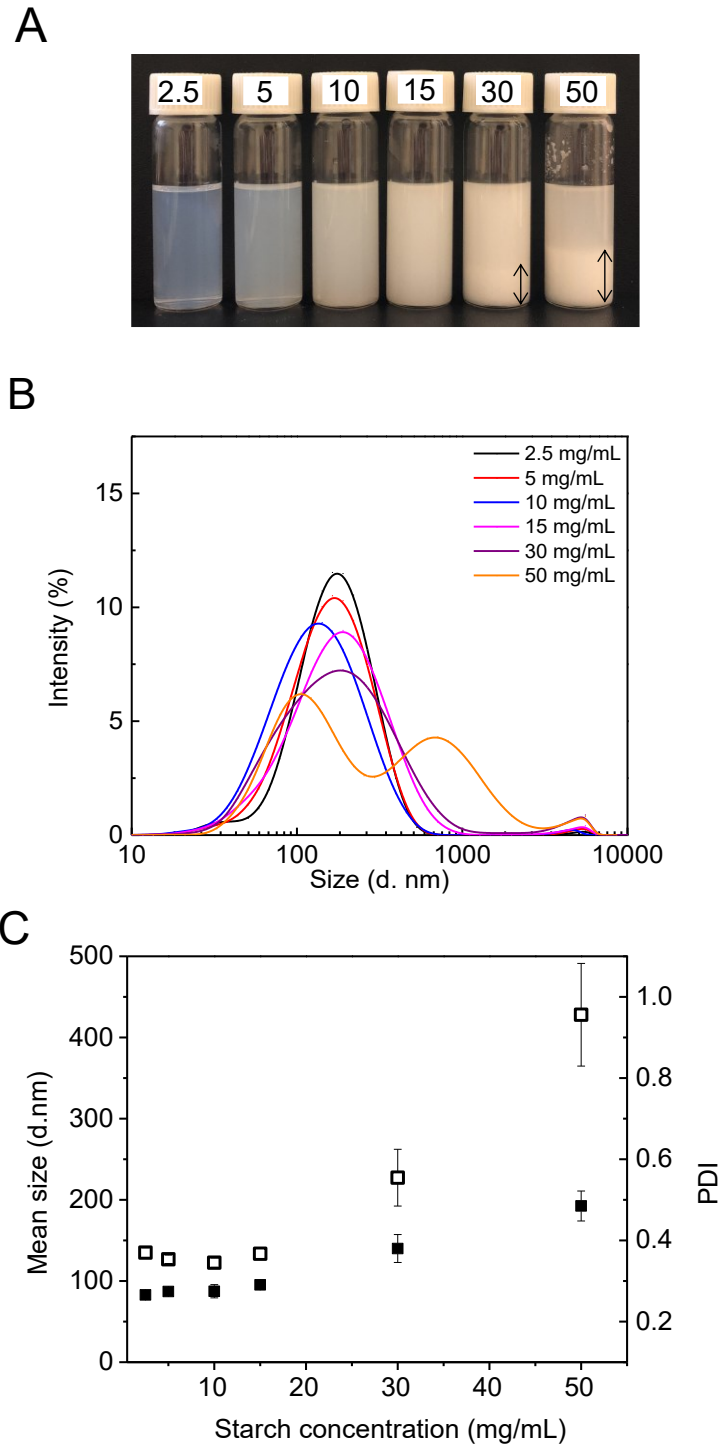
Fig. 6.4 The particle characteristics of the SNPs prepared by R-BNP with different initial starch concentrations at AS/S ratio of 1:1. A) Photographs of suspensions, (B) particle size distribution, and C) mean sizes (open square) and PDI (solid square)

from ~120 to more than 400 nm with further increase in concentration from 10 to 50 mg/mL, where the PDI correspondingly increased up to 0.5. This could be due to the increasing viscosity of the "AS and S" mixture with increasing starch concentration. The greater viscosity of solution with increasing starch concentration could have hindered the diffusion between starch solution and ethanol, and thus lead to non-uniform molecular supersaturation, nucleation and growth, resulting in larger particles with a broader PSD. This phenomenon was also observed with a preliminary experiment, in which nanoparticles would not form with gelatinized starch solution/paste with high viscosity (data not shown) when prepared without ultrasonication, even at a concentration as low as 10 mg/mL. The swollen starch granules are primarily composed of an amylopectin network and are responsible for the gelatinized starch viscosity. Disruption of this network and possible molecular depolymerization caused by ultrasonication can lead to viscosity loss as well as complete molecular dispersion. This process can render the starch molecules to discretely distribute in the solution, facilitating better molecular supersaturation and nucleation processes. These observations were in agreement with previous studies (Tan and others 2009; Saari and others 2017), where lower concentrations were required to ensure that the polymer molecules were in a dispersed state and could be separated into nanodomains by adding the antisolvent. Saari and others (2017) found that starch concentrations of less than 8 mg/mL were preferable as the PSD was narrower, while the increase in the starch concentration led to a rapid increase broader PSD, and coagulation occurred at concentrations above 20 mg/mL. This may be attributed to the growth of nucleus resulting in small particles at lower concentrations, but beyond an optimum concentration the continued growth of nucleus leads to particle enlargement towards micro size and coagulation (Tan and others 2009; Saari and others 2017). Therefore, careful selection of starch concentration and molecular size are important to precisely control molecular

supersaturation and nucleation rates and to produce SNPs with desirable particle characteristics, such as low mean particle size, PDI < 0.3 and a narrow PSD. In the present study, the data suggested that a starch concentration of 10 mg/mL was the optimal choice for producing SNPs with lower mean particle size and narrower PSD from field pea starch using R-BNP at AS/S ratio of 1:1 (v/v).

6.3.3. Continuous nanoprecipitation

The optimum levels of starch concentration and antisolvent-to-solvent (AS/S) ratio were selected based on the experiments performed by using BNP with direct mixing of solvent and antisolvent at once, which is easy and flexible to handle with low plugging probability. Two different continuous flow micromixers, CIJM and HBM for FNP and MFP, respectively, were investigated for the SNP preparation at a fixed starch concentration of 10 mg/mL and AS/S ratio of 1:1 (v/v) in order to compare SNP characteristics. The rapid micromixing of starch solution and antisolvent (absolute ethanol) facilitates better environment for SNP formation, where the individual starch molecules first fold/collapse into spherical globule and then start aggregating to minimize the contact area with the surrounding solvent (water) (Nikoubashman and others 2016). Therefore, the individual flow rates of the AS and S, as well as the overall merged flow rate of the mixture (i.e., AS and S mixture) are crucial for controlling micromixing efficiency. Hence, the present study investigated the effect of micromixing time on SNP characteristics by adjusting the overall merged flow rate.

The effect of overall merged flow rate of starch solution and ethanol mixture on the particle characteristics of SNPs formed by CIJM at a fixed AS/S ratio of 1:1 (v/v) is presented in Fig. 6.5A and B. The average particle size decreased from 179 to 111 nm with the increased overall flowrate
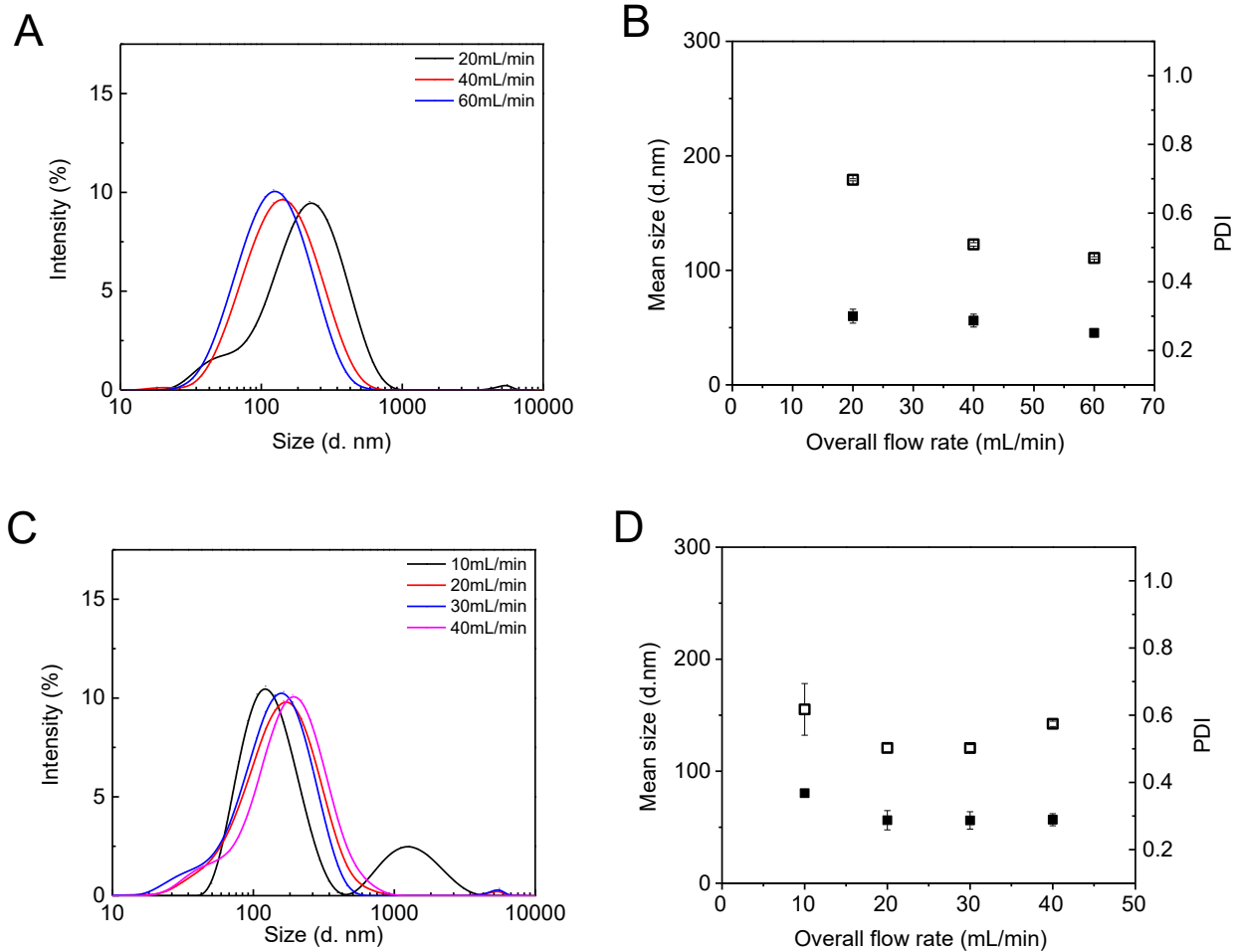
Fig. 6.5 The particle characteristics of SNPs prepared by (A, B) CIJM and (C, D) SHM with different overall flow rates at a fixed starch concentration (10 mg/mL) and AS/S ratio (1:1). (A, C) Particle size distribution, (B, D) mean size (open square) and PDI (solid square).

from 20-60 mL/min. The CIJM model that was used in this study accommodates a maximum overall flow rate of 60 mL/min. In a CIJM (Fig. 6.1B), starch solution and ethanol were injected into the inlets at high flow rate to form liquid jet streams that collided inside the chamber to create a turbulent and rapid mixing. This efficient mixing provides a better environment for supersaturation, nucleation, and growth of nucleus (Saad and Prud'homme 2016). The decrease in mean particle size (Fig. 6.5B) with increasing flow rate can be attributed to the efficient mixing in the CIJM that ensured a uniform starch molecular distribution in the mixing zone (Fig. 6.1B), facilitating the formation of smaller and uniform SNPs. In addition, the configuration/dimension of the micromixer (CIJM) can be proportionally increased and optimized to increase the SNP production rate. The increase of flow rate towards the production of smaller nanoparticles was also demonstrated previously for polystyrene, drug polymer, protein nanoparticles as well as carboxymethyl cellulose (Johnson and Prud'homme 2003; Zhu and others 2010; Li and others 2014; Nikoubashman and others 2016; Bteich and others 2017). Thus, CIJM can potentially be used for preparing SNPs with consistent quality and high production rate at commercial scale without clogging the channels.

Fig. 6.5C and D presents the effect of overall flow rate on the particle size of SNPs formed by HBM at a fixed AS/S ratio of 1:1 (v/v). With the increase of the overall flow rate from 10-40 mL/min, the mean particle size initially decreased from 155 (10 mL/min) to 121 nm (30 mL/min) and then increased to 142 nm (40 mL/min). The initial particle size decrease could be explained by the faster mixing between starch and ethanol with the increasing overall flow rate (i.e., fast diffusion of starch solution into the ethanol). However, the observed increase in particle size when the flow rate exceeds 30 mL/min could be explained by the shorter residence time that led to

insufficient mixing at a greater flow rate, resulting in a non-uniform supersaturation and thereby generating larger particles with wider PSD. The efficient mixing of the starch solution and ethanol is therefore very crucial to the formation of smaller SNPs in the SHM used in this study. Similar observations were found in the cefuroxime axetil nanoparticles formulation in a microfluidic device, where larger particles with broader PSDs were obtained due to the induced incomplete mixing at a greater flow rate (Wang and others 2010). Therefore, optimum flow rate need to be adjusted based on the dimension of the microfluidic apparatus. However, in the present study the micromixer CIJM showed more efficient mixing and much greater production rate (with overall follow rate 60 mL/min) than SHM (with overall follow rate 30 mL/min). Under these optimized conditions, the particles formed by CIJM were smaller with narrower PSD than those formed by SHM. This was consistent with previous reports (Kim and others 2012; Ding and others 2016) that SHM displayed slightly larger particles with a greater PDI compared to CIJM when those two micromixers were used for nanoparticle fabrication. This can be explained by the different working principles as well as the configurations of the micromixers (Fig. 6.1B and C). According to a previous study (Stroock and others 2002), SHM used the grooves on channel walls to drive chaotic advection in microchannels. Alternating groove patterns resulted in two rotational flows in opposite directions, through the interactions between the two in recirculation. This structure greatly increased the rate of mixing between streams. SHM has found wide application in microfluidic nanoprecipitation due to its simplicity; here it only requires grooves on the channel wall. However, it usually shows relatively lower productivity due to small internal volume and low flow rates when compared with CIJM, a turbulence-based micromixer, usually with a larger mixing chamber inside the mixer. The diameter of the chamber is 3 mm and is much larger than the diameters of both inlet and outlet channels. The mixing time and residence time could be

controlled by changing the dimensions of inlet and outlet channels. Smaller nanoparticle size can be obtained with a narrower inlet channel. Thus, the configuration of CIJM, when compared to SHM makes it possible to achieve sufficient mixing at greater overall flow rate.

6.3.4. Physicochemical characteristics of SNPs prepared by batch and continuous nanoprecipitation techniques

The characteristics of SNPs prepared by conventional batch methods (S-BNP and R-BNP) as well as continuous methods (CIJM and SHM) at a starch concentration of 10 mg/mL and AS/S ratio of 1:1 were compared. The optimized flow rate was used for CIJM and SHM. The SNP produced by S-BNP and R-BNP at AS/S ratio 10:1 was used as control samples.

6.3.4.1. Particle size and morphology

The DLS and FE-SEM results showed a narrower PSD indicating that the particles obtained by CIJM and SHM were much smaller and more uniform than those prepared by S-BNP and R-BNP at AS/S of 1:1. The particle sizes followed the order: CIJM < SHM < R-BNP < S-BNP. The FE-SEM images also showed that particles prepared by the CIJM were spherical and uniformly distributed (Fig. 6.6A), while those from S-BNP were not uniform with small nucleus and aggregates (Fig. 6.3C). The SNPs formed by R-BNP (Fig. 6.3D) were relatively more uniform than those from S-BNP (Fig. 6.3C). However, it was found that at greater AS/S ratios (10:1, v/v) there were no remarkable differences in the particle size and morphology between SNPs prepared by R-BNP and S-BNP under the same conditions, where both techniques yielded small and spherical SNPs (Fig. 6.3A and B). According to previous studies (Dong and others 2015; Saari and others 2017), the particle size of SNPs increased with reducing AS/S ratio to 1:1 for both R-BNP and S-BNP methods. In the present study, SNPs prepared by CIJM at AS/S ratio of 1:1 showed comparable particle size and morphology with those obtained by either S-BNP or R-BNP

at a greater AS/S ratio of 10:1 (Fig. 6.3A, B and Fig. 6.6A). Thus, SNPs prepared by CIJM is superior to other methods in terms of productivity and particle morphology. The spherical SNPs showed a large specific surface area and can be easily dispersed or packed in food matrix (Kim and others 2015). The more uniform, nano-size and spherical morphology of SNPs from CIJM would be a more suitable method than the BNP to produce SNPs for different applications.
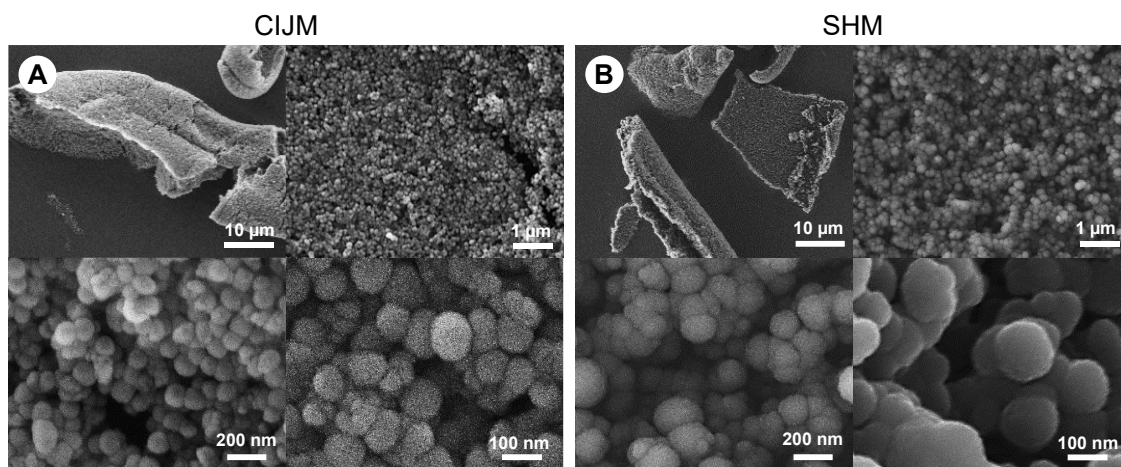
Fig. 6.6 FE-SEM micrographs of the SNPs obtained from the field pea starch by continuous nanoprecipitation at a fixed starch concentration (10 mg/mL) and AS/S ratio (1:1): A) CIJM (confined impinging jet mixer) at an overall flow rate of 60 mL/min; B) SHM (staggered herringbone mixer) at an overall flow rate of 30 mL/min.

6.3.4.2. Crystalline/amorphous structure

The crystalline/amorphous characteristics of selected SNPs have been determined by XRD analysis as shown in Fig. 6.7. Native field pea exhibited a typical C-type crystalline structure with strong diffraction peaks at around 15°, 17°, and 23° 2θ, a small peak at around 5.6° 2θ and a shoulder peak at around 18° 2θ (Fig. 6.7a). However, instead of strong crystalline peaks, SNPs exhibited a "halo" pattern, typical of an amorphous material, with very weak diffraction peaks at around 17° and 21° 2θ. The typical diffraction peaks from C-type crystallites almost disappeared, which was expected as a result of solubilization of starch during gelatinization and ultrasonication steps. The broad and diffused peak at around 2θ = 7-35° was caused by a random arrangement of starch molecules in SNPs. The very weak diffraction peaks at 17° and 21° 2θ were mainly attributed to the amylose-ethanol complexes and recrystallized crystallites during SNP formation procedures (Qin and others 2016). This indicated that the SNPs do possess distinct short- to medium-range orders, but with less crystalline long-range order. These results proved that the whole structure of SNP powder was almost amorphous. Similar results were observed from previous studies where there was a decrease in crystalline structure after gelatinization, sonication, as well as some other methods like alkalization, heat moisture treatment, and microwave degradation of starch (Chung and others 2009; Bel Haaj and others 2013; Zhou and others 2019; Ahmad and others 2020). The decrease in relative crystallinity could be related to the increase in amorphous regions of starch after nanoparticulation. This was consistent with previous studies (Wang and others 2010; Sipponen and others 2018; Ahmad and others 2020; Gutiérrez and others 2020), where nanoprecipitation was normally used to formulate colloidal nanoparticles with a mostly amorphous structure. A previous study (Yan and others 2017) also suggested that the V-type diffraction structure formed during the drying process instead of the nanoprecipitation process,

because the XRD pattern of the SNPs without drying did not show any diffraction peaks. Moreover, it was also reported that the low crystallinity was not necessarily related to poorly ordered starch molecules in SNPs but may be the result of small size crystallites in the particles (Gutiérrez and others 2020). Therefore, the small particle size of SNPs observed in the present study could explain the XRD results. Thus, the different peak intensities among SNPs were probably caused by the different particle size, PSD, as well as different arrangement/interaction of starch molecules.
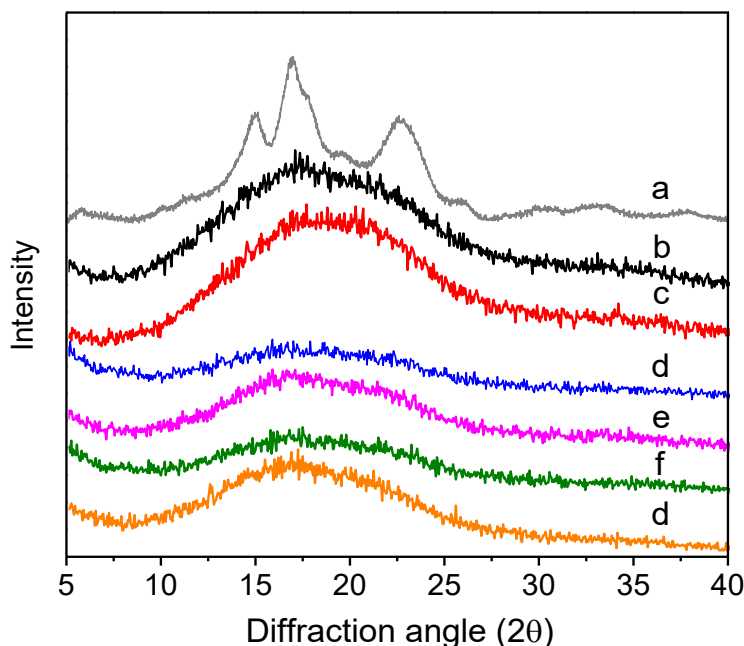
Fig. 6.7 X-ray diffraction pattern of (a) native field pea starch, (b) SNPs produced by S-BPN (batch nanoprecipitation by slow dropwise addition of starch solution into ethanol) at AS/S (antisolvent/solvent) ratio 10:1, (c) SNPs produced by R-BPN (batch nanoprecipitation by rapid pipetting of starch solution into ethanol all at once) at AS/S ratio 10:1, (d) SNPs produced by S-BPN at AS/S ratio 1:1, (e) SNPs produced by R-BPN at AS/S ratio 1:1, (f) SNPs produced by continuous nanoprecipitation using CIJM (confined impinging jet mixer) at AS/S ratio 1:1, and (g) SNPs produced by continuous nanoprecipitation using SHM (staggered herringbone mixer) at AS/S ratio 1:1.

6.3.4.3. Short-range molecular order characteristics

The ATR-FTIR spectrum of starch has shown to be sensitive to changes in the short-range molecular order of starch such as double helical structure, chain conformation, and the crystal form of starch (Wu and Seib 1990). The original and the deconvoluted ATR-FTIR spectra of the samples are presented in Fig. 6.8. As shown in Fig. 6.8A, all the ATR-FTIR spectra of the samples were similar, which suggested there was no change in chemical composition in starch molecular structure caused by the nanoprecipitation process. However, the intensity of identical characteristic bands of SNP samples significantly increased/decreased in comparison to peaks of native field pea starch. In the fundamental region, the spectra present a strong absorption peak around 3260 cm^{-1} which was attributed to the -OH stretching and its width indicated the extent of formation of inter- and intra-molecular hydrogen bonds. In SNPs, the peaks of -OH stretching shifted to a larger wavelength for all samples. This shift indicated that hydrogen bonds generated in the SNPs became weaker than those in starch granules. This could be attributed to the disruption of the crystalline structure and the exposure of -OH groups of the starch molecules due to gelatinization and ultrasonication process (Chun and others 2015; Ahmad and others 2020). The new hydrogen bonds generated during SNP processing, including nanoprecipitation (supersaturation, nucleation, and growth) and drying procedure, were not as strong as that in native starch granules. Similar results were obtained for SNPs obtained by S-BNP from corn starches with different amylose contents (Gutiérrez and others 2020; Ahmad and others 2020). In the present study, the peaks of -OH stretching shifted to 3328 and 3338 cm^{-1} for SNPs formed at AS/S ratio 10:1 by S-BNP and R-BNP, respectively. As the AS/S ratio (v/v) reduced from 10:1 to 1:1 in both methods, the peaks of -OH stretching shifted to even higher wavelength (3351 cm^{-1}) for S-BNP, while there was no significant change for R-BNP (3331 cm^{-1}). This indicated that the
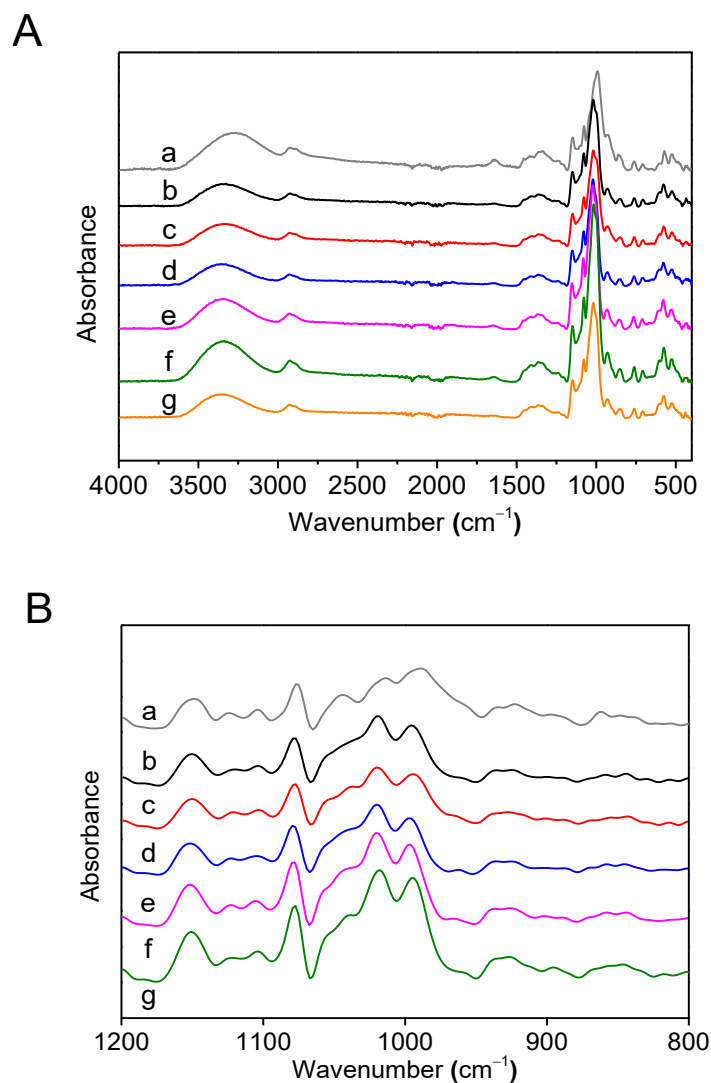
Fig. 6.8 (A) Original and (B) deconvoluted ATR-FTIR spectra of (a) native field pea starch, (b) SNPs produced by S-BPN (batch nanoprecipitation by the slow dropwise addition of starch solution into ethanol) at AS/S (antisolvent/solvent) ratio 10:1, (c) SNPs produced by R-BPN (batch nanoprecipitation by rapid pipetting starch solution into ethanol all at once) at AS/S ratio 10:1, (d) SNPs produced by S-BPN at AS/S ratio 1:1, (e) SNPs produced by R-BPN at AS/S ratio 1:1, (f) SNPs produced by continuous nanoprecipitation using CIJM (confined impinging jet mixer) at AS/S ratio 1:1, and (g) SNPs produced by continuous nanoprecipitation using SHM (staggered herringbone mixer) at AS/S ratio 1:1.

hydrogen bonds in SNPs formed by R-BNP were significantly stronger than those formed by S-BNP at AS/S ratio 1:1. When compared to continuous nanoprecipitation at AS/S ratio 1:1, SNPs formed in CIJM showed comparable result as R-BNP, in which peaks of -OH stretching at 3339 cm^{-1}, whereas those SNPs formed in SHM showed similar result as S-BNP (peaks of -OH at 3360 cm^{-1}). The absorption at around 1637 cm^{-1} was due to the presence of bound water in starch and it decreased significantly in peak intensity after SNP processing. These results were in good agreement with previous studies (Gutiérrez and others 2020; Ahmad and others 2020). The decrease in absorptions were less pronounced in R-SNP-1 and CIJM. This indicated that more bound water was present in those two SNP samples in comparison to other samples.

The deconvoluted ATR-FTIR spectra of the samples in the range of 1200-800 cm^{-1} (Fig. 6.8B) could be used to determine the short-range molecular order of starch by characterizing the changes that occurred in the semi-crystalline and amorphous regions within starch granules/particles. The band at around 1047 cm^{-1} is sensitive to the amount of ordered or crystalline structure; the band at 1022 cm^{-1} is related to the amorphous structure; the band at 995 cm^{-1} is related to hydrogen bonding of the hydroxyl group at C-6 (van Soest and others 1995). Therefore, the absorbance ratio 1047/1022 can be used to measure the change of ordered starch to amorphous starch, and the absorbance ratio 995/1022 can be used as a measure of the degree of double helices. A greater absorbance ratio at 1047/1022 indicated a greater degree of order/crystallinity and a greater ratio of absorbance at 995/1022 indicates a greater degree of double helix. Thus, the intensity of the FTIR bands at 1047, 1022, and 995 cm^{-1} were determined, and then the absorbance ratios at 1047/1022 and 1022/995 were calculated (Table 6.1). As shown in Fig. 6.8B, it could be noted that the absorbance peak at around 1047 cm^{-1} decreased significantly, while that at around 1022 cm^{-1} increased dramatically after nanoparticulation. Consequently, as shown in Table 6.1, both

Table 6.1 Short-range molecular order of the native field pea starch and SNPs by attenuated total reflectance Fourier transform infrared spectroscopy (ATR-FTIR).

Samples	R (1047/1022)	R (995/1022)
Native starch	0.61 ± 0.01 a	1.19 ± 0.00 a
S-BNP-10	0.53 ± 0.01 cd	0.85 ± 0.01 c
R-BNP-10	0.53 ± 0.01 bc	0.88 ± 0.01 c
S-BNP-1	0.57 ± 0.01 b	0.79 ± 0.01 d
R-BNP-1	0.54 ± 0.01 bc	0.86 ± 0.01 c
CIJM	0.50 ± 0.01 d	0.92 ± 0.01 b
SHM	0.54 ± 0.01bc	0.85 ± 0.01 c

Data are means ± standard deviation (n = 3). Means within columns not sharing a common letter are significantly different at $p < 0.05$. R (1047/1022) (ratio 1047/1022 cm^{-1}, a measure of the amount of ordered starch to amorphous starch); R (995/1022) (ratio 995/1022 cm^{-1}, a measure of the degree of double helices); S-BNP-10 (Slow batch nanoprecipitation at AS/S ratio 10:1); R-BNP-10 (Rapid batch nanoprecipitation at AS/S ratio 10:1); S-BNP-1 (Slow batch nanoprecipitation at AS/S ratio 1:1); R-BNP-1 (Rapid batch nanoprecipitation at AS/S ratio 1:1); CIJM (Confined impinging jet mixer at AS/S ratio 1:1); SHM (Staggered herringbone mixer at AS/S ratio 1:1).

the ratio 1047/1022 and 995/1022 decreased after the SNP formation, indicating the decrease in crystalline structure of starch and the formation of its amorphous structure. This result was in agreement with the XRD total relative crystallinity data, indicating that gelatinization disrupted not only the long-range crystallites but also the short-range molecular order of field pea starch. The SNPs formed were mostly in an amorphous phase. These results were also consistent with those reported in a previous study (van Soest and others 1995), when changing starch from semi-crystalline to amorphous starch, the specific molecular surroundings become lost and as a result the spectra of amorphous starches show changes in band shape and intensity. The great absorbance intensity at around 994 cm^{-1} indicated a large amount of intramolecular hydrogen bonding of the hydroxyl groups at C-6, which contributed to a greater degree of double helical order (short-range order). This suggested that starch molecules in SNPs were still linked via hydrogen bonding. The absorbance ratios at 995/1022 cm^{-1} were similar for SNPs formed by S-BNP and R-BNP at AS/S ratio 10:1. When reducing AS/S to 1:1, this value did not change significantly for R-BNP, while decreased significantly for S-BNP, indicating the loosely packed starch molecules inside the particle. This was consistent with the results from DLS and FE-SEM, where SNPs obtained from S-BNP at AS/S ratio 1:1 show broader PSD due to less uniform kinetics during particle formation than those from R-BNP. SNPs from SHM exhibited a comparable degree of double helix with R-BNP at AS/S ratio 1:1, while those from CIJM show significantly greater degree of double helix than all other SNPs probably due to the greater mixing rate.

6.3.5. SNP-stabilized emulsions

As shown in Fig. 6.9, the particles produced using the FNP method developed in this work can be used to stabilize emulsions. The emulsions produced with 10 mg/mL SNPs had a size distribution from 0.4 to 45 μm with an average droplet size of 3 μm and had an emulsion index (EI, the volume
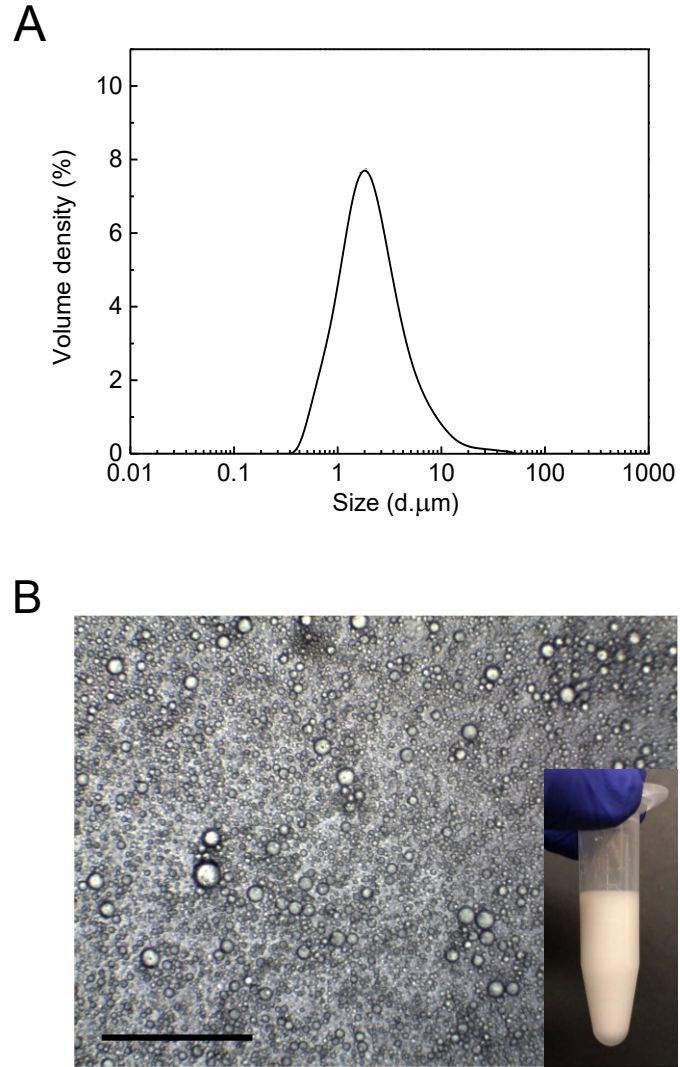
Fig. 6.9 (A) Droplet size distribution and (B) Optical microscopic image of Pickering emulsion stabilized by 10 mg/mL SNPs (based on water fraction) at water to oil ratio 2:1 (v/v, scale bar: 100 μm). Inserted is a photograph of the emulsion. SNPs were prepared from flash nanoprecipitation at overall flow rate 60 mL/min with starch concentration 10mg/mL at antisolvent to solvent (AS/S) ratio of 1:1 (v/v).

of the emulsion phase compared to total volume) of 1 (on day zero). An EI of 1 means that the emulsion is a space-filling system, with no creaming or sedimentation. The emulsions were also visualized by optical microscopy. As shown in Fig. 6.9B, the emulsions stabilized by SNPs were homogeneous without any bulk aggregates formed. This can be compared to previous results for an emulsion of SNPs produced by batch nanoprecipitation (Saari and others 2017; Ge and others 2017). Thus, it is clear that the SNPs produced by FNP in this study can be used to form emulsions with a much smaller droplet size than is possible with native starch granules (granular size of 6-43 µm) from field pea. This is probably a result of the fact that as the particle size decreases the available surface area per unit mass of starch increases.

In order to investigate the effect of SNP concentration on the droplet size of emulsions, a series of dilution of SNPs (from 10 mg/mL to 5, 3, 1, and 0.5 mg/mL) was used to prepare the Pickering emulsions and compared to the emulsion prepared without SNPs. As shown in Fig. 6.10, with the presence of SNPs, the droplet size sharply decreased with an increase of SNP concentration (0.5-10 mg/mL) until a plateau value of around 3 µm was reached in the concentration range from 5.0 mg/mL to 10 mg/mL. However, when there is no SNPs present, the emulsion reaches maximum droplet size equivalent to what free oil gives when it is pumped through the static light scattering equipment. The size is around 200 µm. A SNP concentration of 1 mg/mL is able to create droplets of 10 µm size whereas a starch concentration of 0.5 mg/mL and below is not sufficient in covering the oil droplets. The emulsions produced with SNP concentration above 3 mg/mL were stable, maintaining an EI of 1 for up to 1 week.
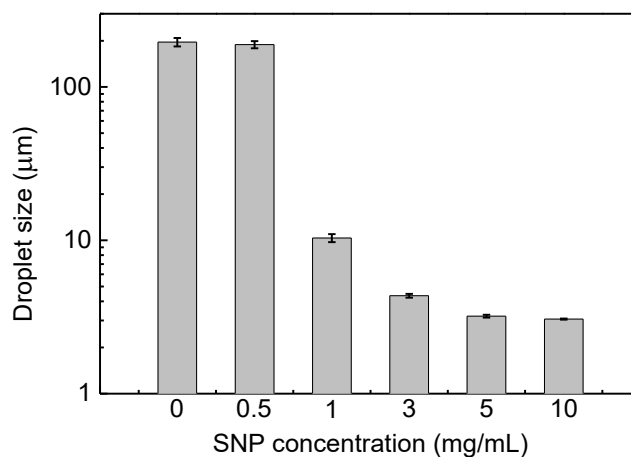
Fig. 6.10 The effect of SNP concentration (based on water fraction) on the mean droplet size of emulsions produced at water to oil ratio 2:1 (v/v).

6.4. Conclusions

Mixing conditions were critical in SNP formation, where substantial variation in particle size and PDI was observed to be influenced by AS/S ratio, starch concentration, mixing technique, and flow rate. Size-controllable SNPs could be produced by fine tuning the mixing parameters. The FNP involving CIJM mixer design showed the best SNP characteristics without channel-clogging during processing. This shows that the continuous production of SNPs through FNP involving CIJM mixer design is a simple and economic way to prepare SNPs with tunable sizes and meets the requirement for scale-up processing with consistent quality without technical challenges. The resultant SNPs could be used as a stabilizer to produce Pickering emulsions with reduced emulsion droplet size.

Chapter 7: Effect of phosphorylation techniques on structural, thermal, and pasting properties of pulse starches in comparison with corn starch

7.1. Introduction

Phosphorylation, a starch cross-linking technique, is the most commonly used chemical modification in food-grade starch production. Crosslinking occurs by forming an intra- and/or intermolecular cross-linkage of one phosphate linked between hydroxyl groups in starch molecules in the amorphous region (Landerito and Wang 2005; Shukri and others 2015). The main purpose of cross-linking is to eliminate the shortcomings of native starch and thus improve starch textural properties, thermal/shear resistance, and acid stability, as well as paste stability (Hoover and others 2010). Therefore, it is possible to control starch functional properties through changing the degree of crosslinking with different modification techniques. However, due to regulatory constraints, only a limited number of chemical reagents and modification techniques have been introduced and permitted in the last several decades. In regard to starch modified by phosphorylation, food-grade starches are regulated in the USA to not exceed 0.4% add-on phosphorus based on the chemical reagents used on a dry matter basis. This indicates the importance of understanding the ability to use different chemical reagents and existing modification techniques to effectively manipulate starch functionality. Chemical reagents for phosphorylation include phosphoryl chloride ($POCl_3$), sodium trimetaphosphate (STMP), sodium tripolyphosphate (STPP), and their mixtures (STMP/STPP) (Woo and Seib 2002; Hoover and others 2010). Currently, the most widely used commercial phosphorylated starches are prepared primarily by adding $POCl_3$ to an aqueous starch slurry (~35%) at pH 8-12 ($POCl_3$-aqueous), or prepared by reacting a starch with a mixture of 5-12% STMP/STPP (99/1, w/w) in slurry (~35%) at pH 10-12 (STMP-aqueous) (Woo and Seib 2002; Hirsch and Kokini 2002; Sui and others 2013). In addition, starch can be cross-linked by reacting

starch with STMP and/or STPP at pH 10-11, drying at 40 °C to less than 20% moisture content, then roasting at 120-140 °C (STMP-semidry) (Lim and Seib 1993; Sang and Seib 2006).

To date, comparative studies on the effects of different phosphorylation techniques on the structural characteristics and physicochemical properties of starch are limited. The relevant studies available in literature were generally performed by applying a limited number of treatments (i.e. one or two phosphorylations on a single starch; one single phosphorylation on starches from a variety of botanical origins), making it difficult to obtain and compare data for the modification of starch structural and physicochemical properties under different phosphorylation techniques and conditions. Most of these studies were performed with corn, tapioca, potato, barley, wheat, and rice starches (Woo and Seib 2002; Shukri and others 2015; Ashwar and others 2018; Wang and others 2018; Shen and others 2019). Very limited information is available regarding the effectiveness of different phosphorylation techniques on pulse starches, and how that would influence their structural and physicochemical properties. Therefore, the objective of this study was to investigate the effects of three different phosphorylations (POCl$_3$-aqueous, STMP-semidry, STMP-aqueous) with faba bean and field pea starches on structural, thermal and pasting properties. Since chemical modification of corn starches has been widely researched and commercially used, the study compared the properties of the native and modified pulse starches to those of corn starch counterparts. The results obtained are expected to provide a theoretical basis for a better understanding of structure-phosphorylation-functional relationships of both pulse and corn starches. This will represent a foundation for the food industry to intelligently design novel starch materials with more precisely selected phosphorylation techniques for a given botanical starch origin.

7.2. Materials and methods

7.2.1. Materials

Regular corn, faba bean, field pea starches, pure amylose and amylopectin from potato starch were obtained as described in Chapter 4 section 4.2.1. Sodium trimetaphosphate (STMP, >95% purity), sodium tripolyphosphate (STPP, >98% purity), sodium sulfate (>99% purity), and phosphoryl chloride (POCl$_3$, >99% purity) was obtained from Millipore Sigma Canada Co, Oakville, ON, Canada. All other chemicals were of analytical grade.

7.2.2. Starch phosphorylation

7.2.2.1. Slurry phosphorylation with phosphoryl chloride (POCl$_3$-aqueous)

Phosphorylation of starch with POCl$_3$ was done by a slightly modified method (Woo and Seib 2002; Sui and others 2013). Native starch (20.0 g, db) was dispersed in distilled water (30 mL) with stirring at 25 °C, and 10% sodium sulfate based on starch (w/w, sb) was added. The pH of the slurry was adjusted to 11.2 with 1 M NaOH dropwise. POCl$_3$ (1%, 2%, v/w, sb) was added into the slurry dropwise. The reaction was maintained at pH 11.2 with stirring for 1 h at 25 °C. After reaction, the reaction mixture was neutralized to pH 6.5 with 1 M HCl. The modified starch was recovered by centrifugation (3000 × g, 10 min), washed 4 times with distilled water and then washed twice with ethanol and dried in a fume hood.

7.2.2.2. Semidry phosphorylation with STMP/STPP (STMP-semidry)

Semidry reaction with STMP/STPP was done with the modified method of previous studies (Lim and Seib 1993; Woo and Seib 2002). Native starch (20.0 g, db) was dispersed in distilled water (30 mL) with stirring at 25 °C. The pH of the slurry was adjusted to 11.0 with 1 M NaOH dropwise before adding a solution (10 mL) containing sodium sulfate (5 %, w/w, sb) and a 99:1 mixture of

STMP/STPP (2%, 4%, w/w, sb). The reaction mixture was maintained at pH 11.0 for 1 h with stirring at 25 °C and then dried to 10-15% moisture in a dish at 40 °C using a forced-air oven. The mixture with 10-15% moisture was transferred to a sealed container and heated at 130 °C for 2 h. After cooling to room temperature, the starch was dispersed in 40 mL of distilled water. The reaction mixture was neutralized to pH 6.5 with diluted HCl, and then followed the procedure as described in section 7.2.2.1 was followed.

7.2.2.3. Slurry phosphorylation with STMP/STPP (STMP-aqueous)

Starch (20 g, db) was dispersed in distilled water (30 mL) containing sodium sulfate (10%, w/w, sb) and a 99:1 mixture of STMP/STPP (5, 10, and 12%, w/w, sb)(Woo and Seib 2002). The dispersion was adjusted to pH 11.5 with 1 M NaOH solution and kept at 45 °C in a shaking water bath for 3 h at 100 rpm. After cooling to room temperature, the reaction mixture was neutralized to pH 6.5 with diluted HCl and then the procedure as described in section 7.2.2.1 was followed.

7.2.3. Chemical composition analysis

Native corn, field pea, and faba bean starches were analyzed for moisture (925.45)   and   ash (942.05) according to the methods of the Association of Official Analytical Chemists (AOAC, 2000). The nitrogen content of the samples was determined by using a LECO TruSpec CN Elemental Determinator (LECO Co., St. Joseph, MI, USA). The nitrogen value obtained was multiplied by 6.25 to convert it to crude protein. Starch lipid was determined by the procedure outlined in an earlier publication (Vasanthan and Hoover 1992). Starch content was estimated according to the total starch assay kit of Megazyme (Megazyme International Ireland Ltd., Bray, County Wicklow, Ireland). Apparent amylose content was measured by iodine-blue method as described by Chrastil (1987).

7.2.4. Determination of phosphorus content and degree of crosslinking

Phosphorus content (P%, w/w) was measured by using ammonium molybdate and vanadate spectrophotometric method (Smith and Caruso 1964) with a slight modification. A mixture of starch sample (0.3 g) with 0.5 mL 10% zinc acetate solution was heated until dry and then ashed for 3 h at 550 °C and cooled down. The ash was dissolved in 1 mL (w/v) HNO_3 (29%, w/v), then ashed again for another 1 h, cooled down, dissolved in 1 mL 20% HCl, and mixed well. Then 0.2 mL of supernatant was taken, mixed with 1 mL HNO_3 (29%), 1 mL ammonium vanadate (0.25%), and 1 mL ammonium molybdate (5%) and volume was adjusted to 10 mL with distilled water. After 10 min, the absorbance was measured at 435 nm against a sample blank. A calibration curve (0-20 μg phosphorus per mL) was made using potassium dihydrogen phosphate.

The degree of crosslinking (DC) of crosslinked starch is expressed as moles of phosphorus per mole of anhydrous glucose unit, which was calculated by the percentage increase of the phosphorus content (P%, w/w) in modified starch compared to native starch as follows:

$$DC = 162n_p / (m - 102\, n_p) = 162\, P / (3100 - 102\, P) \quad (7.1)$$

Where n_p, mole phosphorus ($n_p = P/31$); 162, the molar mass of anhydroglucose; m, mass of dry sample; 102, the molar mass of $NaPO_3^{2-}$, and P, percentage increase of the phosphorus content in modified starch compared to native starch.

7.2.5. Determination of pasting properties

The pasting properties of native and modified starches were determined using a Rapid Visco-Analyzer (RVA-4500, Perten Instruments, Kungens, Sweden), according to a previous method with slight modification (Han and BeMiller 2007). Firstly, the starch slurry was prepared by dispersing (3.0 g, db) starch into distilled water in an RVA aluminum container (sample + water = 28.0 g). The slurries were held at 50 °C for 60 s, then heated to 95 °C within 222 s, held at 95 °C

for 150 s, cooled to 50 °C within 228 s and held at 50 °C for 120 s, while keeping the speed of paddle at 160 rpm. At the beginning of 10 s, the paddle speed was 960 rpm.

The percentage reduction of peak viscosity was calculated by using Eq. (7.2):

$$Percentage\ reduction\ of\ peak\ viscosity\ (\%)\ =\ (A-B)/A \times 100 \qquad (7.2)$$

where A is the peak viscosity of the unmodified sample, and B is the peak viscosity of the cross-linked starch.

7.2.6. Thermal properties by differential scanning calorimetry (DSC)

Gelatinization parameters of starches were measured as described in Chapter 4 section 4.2.8.

7.2.7. X-ray diffraction (XRD)

X-ray diffraction analysis of native and crosslinked starches (~10% moisture content) was performed using a Rigaku Ultima IV multipurpose X-ray diffractometer (Rigaku America, Woodlands, TX, USA) as described in Chapter 4 section 4.2.6.

7.2.8. Attenuated total reflectance-Fourier transform infrared (ATR-FTIR) spectroscopy

ATR-FTIR spectra of native and cross-linked starches were recorded following the procedure as described in Chapter 4 section 4.2.7.

7.2.9. Statistical analysis

All experiments were done in three replicates. Results are presented as mean ± SD (standard deviation). Analysis of variance (ANOVA) was performed, and the mean comparisons were carried out by Duncan's range test at $P < 0.05$ using the SPSS statistical software (Version 22, SPSS Inc., Chicago, IL, USA).

7.3. Results and discussion

7.3.1. Chemical composition and reaction efficiency

The chemical compositions of native regular corn, faba bean, and field pea starches are shown in Table 7.1. All three starches had high purity (>96%) with very low contents of residual protein, lipid, and phosphorus (0.02-0.27%, 0.02-0.69% and 0.01-0.02%, respectively). The apparent amylose content of regular corn starch was 26.2%, whereas those of pulse starches for faba bean and field pea, accounted for 39.1% and 41.3%, respectively.

Table 7.1 Chemical composition (%, db) of native starches.

Composition (%, db)	Regular corn	Faba bean	Field pea
Starch	98.52 ± 0.21 a	96.33 ± 0.93 a	97.30 ± 0.95 a
Protein	0.27 ± 0.02 a	0.12 ± 0.02 b	0.02 ± 0.00 c
Lipid	0.69 ± 0.00 a	0.09 ± 0.00 b	0.02 ± 0.00 c
Ash	0.24 ± 0.01 a	0.10 ± 0.01 b	0.06 ± 0.01 b
Apparent amylose	26.18 ± 0.37 b	39.06 ± 0.26 a	41.30 ± 0.54 a
Phosphorus	0.02 ± 0.00 a	0.01 ± 0.00 ab	<0.01 b

Data are means ± standard deviation (n = 3). Means within rows not sharing a common letter are significantly different at $p < 0.05$.

The reaction efficiency of a crosslinked starch is represented by DC, which indicates the mole number of phosphates crosslinked into the anhydroglucose entity. Native starch contains certain amounts of phosphate monoesters and thus the DC of modified starch was calculated by subtracting the endogenous P% of native starch. As shown in Table 7.2, The DC of modified starches varied with phosphorylation techniques and starch origin. Under the same reaction conditions, the influence of cross-linking on pulse starches was greater than that on the corn starch. Among treatments, the highest DC was reached by treatment with STEP-semidry-4% (0.0071, 0.0089, 0.0099 for RC, FB, and FP, respectively). Different DC values indicated different reaction efficiency among crosslinked starches, which could be due to different crystalline type of starch structure (C-type pulse vs A-type cereal) and chain length of starch molecules, as well as the different reaction patterns of crosslinking reagents in different cereal and pulse starches (Fannon and others 2004; Shukri and others 2015). Particularly, the larger amount of amylose in pulse starch could preferentially form more cross linkages between AM-AP. This is consistent with previous reports that amylose was cross-linked to amylopectin when granular starch was subjected to crosslinking reaction (Jane and others 1992; Kou and Gao 2018; Shen and others 2019). Furthermore, the higher content of amylose being interspersed among amylopectin molecules in pulse starches may also lead to formation of mono-starch esters along the amylose chains more than that in corn starch (Jane and others 1992). Thus, more phosphorus can be incorporated in pulse starches. In addition, the DC increased with increasing concentration of cross-linking reagent. Among phosphorylation techniques, STMP-semidry involving heat treatment yielded the highest DC followed by STMP-aqueous and POCl$_3$-aqueous. Compared to the STMP-aqueous method, STMP-semidry method showed more phosphorus binding (Table 7.2), indicating that phosphorylation is promoted by STMP/STPP with heating (130 °C) at low moisture (10-15%).

Table 7.2 Degree of crosslinking (DC) and percentage peak viscosity reduction of phosphorylated regular corn, faba bean and field pea starches.

Treatment	Degree of crosslinking			Percentage reduction of peak viscosity (%)		
	RC	FB	FP	RC	FB	FP
POCl$_3$-aqueous-1	0.0034 ± 0.0001 Cc	0.0041 ± 0.0000 Db	0.0044 ± 0.0000 Da	99.56 ± 0.07 Aa	99.67 ± 0.01 Aa	99.50 ± 0.03 Aa
POCl$_3$-aqueous-2	0.0053 ± 0.0004 Bb	0.0062 ± 0.0001 Ba	0.0064 ± 0.0002 Ca	99.56 ± 0.07 Aa	99.67 ± 0.00 Aa	99.52 ± 0.03 Aa
STMP-semidry-2	0.0058 ± 0.0004 Bb	0.0062 ± 0.0002 Bab	0.0066 ± 0.0002 Ca	97.07 ± 0.48 Aa	70.63 ± 1.93 Db	27.59 ± 4.37Dc
STMP-semidry-4	0.0071 ± 0.0003 Ac	0.0086 ± 0.0002 Ab	0.0099 ± 0.0004 Aa	99.52 ± 0.07 Aa	99.67 ± 0.02 Aa	99.46 ± 0.03 Aa
STMP-aqueous-5	0.0009 ± 0.0002 Db	0.0018 ± 0.0001 Ea	0.0020 ± 0.0001 Ea	98.14 ± 0.34 Aa	85.56 ± 0.60 Cb	47.94 ± 3.14 Cc
STMP-aqueous-10	0.0034 ± 0.0001 Cc	0.0053 ± 0.0001 Cb	0.0067 ± 0.0001 Ca	99.12 ± 0.13 Aa	95.08 ± 0.99 Bb	95.39 ± 0.28 Bb
STMP-aqueous-12	0.0067 ± 0.0001 Bb	0.0065 ± 0.0003 Bb	0.0077 ± 0.0002 Ba	99.54 ± 0.04 Aa	98.44 ± 0.02 Aa	96.90 ± 0.19 ABa

Data are means ± standard deviation (n=3). DC of crosslinked starch is expressed as moles of phosphorus per mole of anhydrous glucose unit, which was calculated by the percentage increase of the phosphorus content (P%, w/w) in modified starch compared to native starch. Values in the same raw sharing a common letter are not significantly different ($P < 0.05$). Values in the same column sharing a capital letter are not significantly different ($P < 0.05$). RC (regular corn starch); FB (faba bean starch); FP (field pea starch); POCl$_3$-aqueous (1% and 2% POCl$_3$ in aqueous slurry at 25 °C); STMP-semidry (2% and 4% STMP/STPP [99:1. w/w] in a semidry state at 130 °C); STMP-aqueous (5%, 10%, and 12% STMP/STPP [99:1. w/w] in aqueous slurry at 45 °C)

7.3.2. Effect of phosphorylation techniques on pasting property of starch

The pasting profiles of native and crosslinked starches are presented in Fig. 7.1. Peak viscosity is considered to verify the equilibrium point between swelling and rupture of starch granules. The swelling of starch granules, accompanied with amylose leaching, increased the viscosity and further heating, broke down the granular structure and resulted in reduced viscosity. During cooling of the starch pastes, leached amylose molecules rapidly associate with each other and this reassociation is responsible for the final viscosity. The pasting temperatures of faba bean and field pea starches (71.9 and 71.0 °C, respectively) were significantly lower than that of regular corn starch (76.7 °C). Faba bean and field pea showed greater peak viscosity (7.2 and 5.3 Pa.s, respectively), setback (4.53 and 6.12 Pa.s, respectively), and final viscosities (9.16 and 9.94 Pa.s, respectively) when compared with regular corn starch (4.77, 2.19, and 5.18 Pa.s of peak, breakdown, setback and final viscosities, respectively). The remarkably higher pasting temperature and lower peak viscosity of regular corn starch may be due to amylose-lipid complex formation that restricted the swelling of starch granules during heating (Li and others 2019). The greater final viscosity of pulse starches could be attributed to their higher amylose content (Table 7.1). These results are consistent with previous reports, where pasting properties of regular cereal starch differed from that of waxy cereal, and other tuber and root starches (Srichuwong and others 2005; Li and others 2019). In addition, the pasting properties of starches have been reported to be influenced by many other factors, such as granular size, rigidity, amylose to amylopectin ratio, as well as pasting parameters (e.g. starch concentration, heating/cooling rate)(Cai and others 2014; Wang and others 2018).
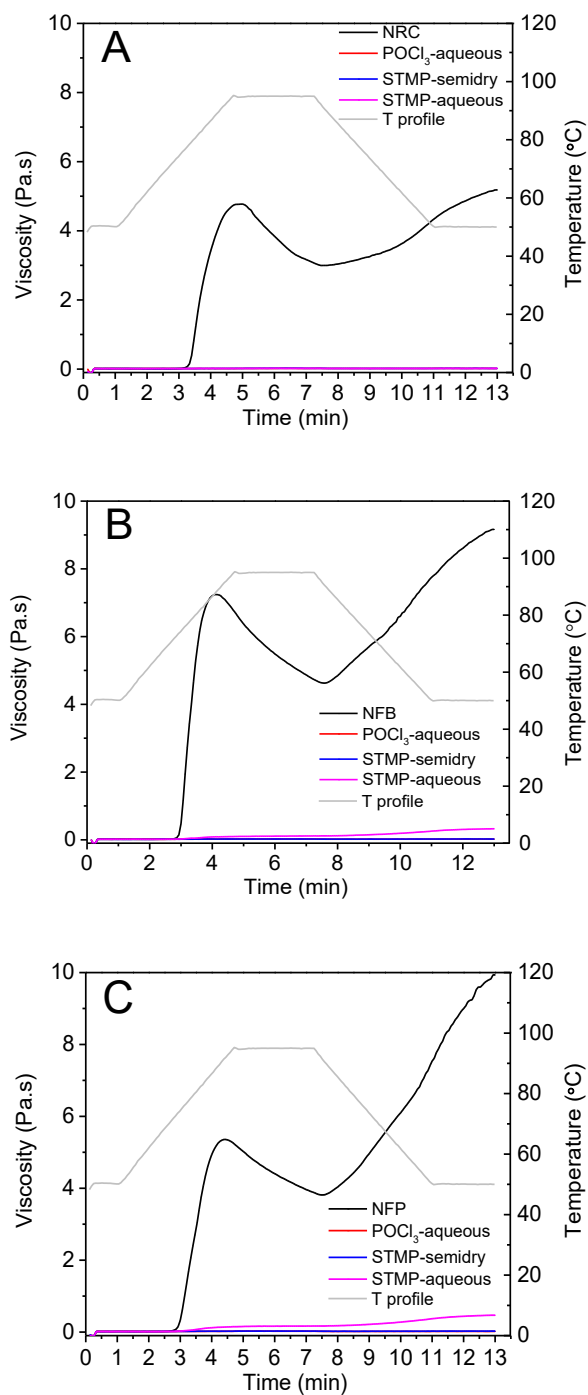
Fig. 7.1 Pasting profiles of native and phosphorylated A) regular corn, B) faba bean, and C) field pea starches, at total starch concentration 10.0%. NRC (native regular corn starch); NFB (native faba bean starch); NFP (native field pea starch); POCl₃-aqueous (2% POCl₃ in aqueous slurry at 25 °C); STMP-semidry (4% STMP/STPP [99:1. w/w] in a semidry state at 130 °C); STMP-aqueous (12% STMP/STPP [99:1. w/w] in aqueous slurry at 45 °C); T profile (Temperature profile).

182

Crosslinking reaction influences starch pasting properties especially the peak viscosity that is mainly dictated by starch granule swelling and amylose leaching. Research studies (Steeneken 1989; Kou and Gao 2018) have shown that lightly crosslinking with lower reagent levels, depending on starch type and crosslinking technique used, can increase starch granules swelling and peak viscosity during heating in excess water. However, heavily crosslinking substantially reduce swelling of the granules and increase the overall granule stability and strength (Steeneken 1989; Kou and Gao 2018). In this study, three types of starches were heavily crosslinked by three different techniques, therefore, the percentage reduction of peak viscosity (Table 7.2) was calculated to investigate how different crosslinking techniques influence the pasting properties. As shown in Table 7.2, increasing concentrations of phosphorylating reagent from 2% to 4% for STMP-semidry, and 5% to 12% for STMP-aqueous increased the percentage reduction of peak viscosity. However, high percentage reduction of peak viscosity (> 99.5%) occurred for $POCl_3$-aqueous-1% treatment. The $POCl_3$-aqueous method also showed higher percentage reduction of peak viscosity when compared to both STMP methods with similar DC, for example, all crosslinked field pea starches at DC of ~0.0065, showed the percentage reduction of peak viscosity following the order as $POCl_3$-aqueous-2% (99.5%) > STMP-aqueous-10% (95.4%) > STMP-semidry-2% (27.6%). These results indicated that $POCl_3$-aqueous was the most efficient crosslinking method for altering the pasting properties of starch compared with STMP-semidry and STMP-aqueous. This is probably due to the high reactivity of $POCl_3$, cross-linkages predominate on the outer layer, and/or interior channels of the crosslinked granules, forming more rigid granule surface than other crosslinking treatment (Huber and BeMiller 2001).

Compared to pulse starches, all crosslinked corn starches obtained by three phosphorylation methods showed high percentage reduction of peak viscosity ranging from 97.1 to 99.6% (DC ranged from 0.0009 to 0.0071), indicating that the effect of crosslinking on pasting properties of corn starch was more pronounced than that of pulse starches. This further indicated that the location and distribution of phosphate groups may be quite different among starches due to the particular starch structure and phosphorylation reaction condition. In addition, phosphorylated starches prepared by both STMP methods (STMP-semidry and STMP-aqueous) may exist in both cross-linked and substituted forms. This is in accordance with a previous study, where ^{31}P-NMR showed phosphorylated wheat starch (0.38% P) prepared under the same conditions contained 63% of phosphorus as di-starch monophosphate ester and 37% of phosphorus as mono-starch monophosphate ester (Sang and others 2007). It is important to note that crosslinking (i.e. di-starch esters) and substitution (i.e. mono-starch esters) influence the starch viscosity development in opposite ways depending on the degree of crosslinking and substitution (Shukri and Shi 2017). This is consistent with the results discussed in section 7.3.1, where more phosphorus can be incorporated in pulse starches probably due to the substitution reaction.

The outcomes indicated the reduction of viscosity varied with starch source, crosslinking agent, and crosslinking method. The pasting profiles of crosslinked starch with the highest level of crosslinking are presented in Fig. 7.1. All three starches with the highest level of reagents did not show well-developed viscosity in RVA curves (Fig.7.1) even at 10% (w/v) total starch concentration. This can be attributed to the higher degree of cross-linking and the additional phosphate linkage (covalent bonds) restricting the swelling of starch granules and thus enabling the granules to withstand the heating temperature (95 °C). The impact of crosslinking on pasting

properties was higher in corn starch under the same reaction conditions than that in the pulse starches. However, pulse starches show higher processability which can be easily processed in a controlled manner to obtain crosslinked starch with different viscosities. In order to investigate the influence of different crosslinking methods on thermal and structural properties of starch, the crosslinking with highest reagent levels were selected for further study, where viscosity was no longer developed in RVA at the test starch concentration (10%, w/v).

7.3.3. Effect of phosphorylation techniques on thermal properties of starch

The crosslinked starch samples with the highest DC were selected to investigate the impact of three phosphorylation techniques on thermal properties of the three starches. The gelatinization transition temperature (onset [T_o], peak [T_p], and conclusion [T_c]), gelatinization transition temperature range (T_c-T_o), and gelatinization enthalpy (ΔH) of native and crosslinked starches are presented in Table 7.3 and Fig. 7.2. The gelatinization temperatures of the three native starches ranged from 60.0 to 67.7 °C for T_o, from 66.1 to 72.5 °C for T_p, and from 77.8 to 80.3 °C for T_c. Corn had the highest T_o, T_p and T_c values compared to faba bean and field pea starches, which may be due to the more compact crystal arrangement of cereal starch, which is an A-type polymorph, compared to the C-type polymorph of pulse starches. In the granules of C-type pulse starches, such as faba bean and field pea, the B-type polymorphs are in the inner layer of starch granules and surrounded by the A-type polymorphs (Fannon and others 2004; Cai and others 2014). During heating in excess water, the gelatinization of C-type starch granules is initiated from the central hilum region, and B-type polymorphs start melting at lower temperature than A-type polymorphs due to their loose packing. This is in agreement with the trend in pasting temperature (Fig. 7.1). The lower T_o, T_p, and T_c for native pulse starches also reflect their lower amylopectin contents (Table 7.1), however, the higher T_c-T_o reflects their greater variation in crystalline stability. The

Table 7.3 Gelatinization parameters of native and modified starches from regular corn, faba bean and field pea.

Starch	T_o (°C)	T_p (°C)	T_c (°C)	T_c-T_o (°C)	ΔH (J/g)
NRC	67.7 ± 0.1 c	72.5 ± 0.2 d	80.3 ± 0.1 c	12.6 ± 0.1 b	14.6 ± 0.3 a
POCl₃-aqueous	72.0 ± 0.1 a	77.3 ± 0.1 a	84.0 ± 0.3 a	11.9 ± 0.3 b	13.9 ± 0.3 a
STMP-semidry	67.2 ± 0.2 d	75.2 ± 0.1 b	82.1 ± 0.2 b	15.0 ± 0.3 a	11.9 ± 0.7 b
STMP-aqueous	69.2 ± 0.0 b	74.5 ± 0.0 c	82.4 ± 0.5 b	13.3 ± 0.5 b	14.2 ± 0.1 a
NFB	61.4 ± 0.1 b	66.4 ± 0.1 c	77.1 ± 0.5 d	15.7 ± 0.5 d	15.9 ± 0.3 a
POCl₃-aqueous	63.4 ± 0.3 a	71.0 ± 0.1 b	83.8 ± 0.7 b	20.4 ± 0.7 b	15.7 ± 0.6 a
STMP-semidry	54.6 ± 0.7 c	74.9 ± 0.9 a	86.1 ± 1.0 a	31.5 ± 1.7 a	13.5 ± 1.1 b
STMP-aqueous	60.7 ± 0.0 b	66.3 ± 0.0 c	79.3 ± 0.3 c	18.6 ± 0.3 c	15.8 ± 0.1 a
NFP	60.0 ± 0.1 b	66.1 ± 0.0 c	77.8 ± 0.7 c	17.8 ± 0.8 d	15.5 ± 0.4 a
POCl₃-aqueous	62.2 ± 0.1 a	71.3 ± 0.0 b	82.9 ± 0.1 b	20.8 ± 0.1 c	14.5 ± 0.4 ab
STMP-semidry	53.0 ± 0.0 c	76.7 ± 0.1 a	88.0 ± 0.5 a	35.0 ± 0.5 a	13.1 ± 0.8 b
STMP-aqueous	60.3 ± 0.1 b	65.8 ± 0.6 c	82.6 ± 0.3 b	22.3 ± 0.3 b	15.4 ± 0.1 a

Values not sharing a common letter in the same column within each starch are significantly different ($P < 0.05$). T_o (onset temperature); T_p (peak temperature); T_c (conclusion temperature); T_c-T_o (gelatinization temperature range); ΔH (gelatinization enthalpy); NRC (native regular corn starch); NFB (native faba bean starch); NFP (native field pea starch); POCl₃-aqueous (2% POCl₃ in aqueous slurry at 25 °C); STMP-semidry (4% STMP/STPP [99:1. w/w] in a semidry state at 130 °C); STMP-aqueous (12% STMP/STPP [99:1. w/w] in aqueous slurry at 45 °C).
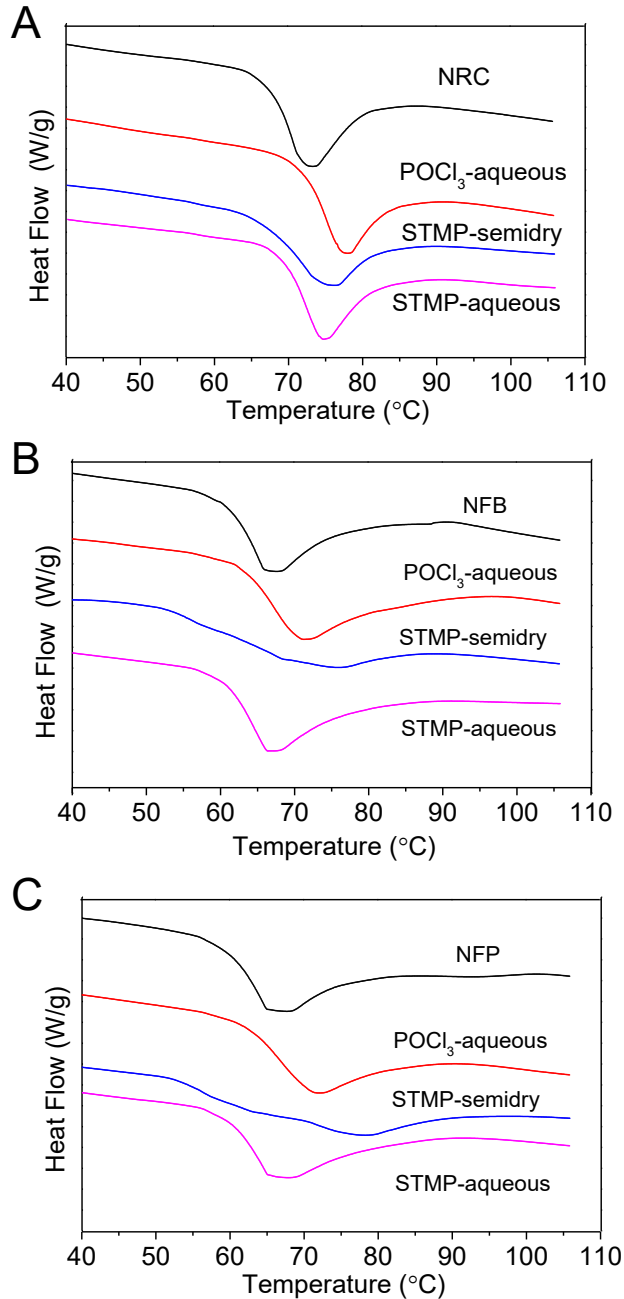
Fig. 7.2 DSC thermograms of native and crosslinked (A) regular corn, (B)faba bean, and (C) field pea starches. NRC (native regular corn starch); NFB (native faba bean starch); NFP (native field pea starch); POCl$_3$-aqueous (2% POCl$_3$ in aqueous slurry at 25 °C); STMP-semidry (4% STMP/STPP [99:1. w/w] in a semidry state at 130 °C); STMP-aqueous (12% STMP/STPP [99:1. w/w] in aqueous slurry at 45 °C).

enthalpy of gelatinization represents the amount of energy required to melt double helices in starch during the gelatinization process. Faba bean starch exhibited the highest gelatinization enthalpy change (15.9 J/g), followed by field pea (15.2 J/g), and regular corn (14.6 J/g) starches. The more narrow T_c-T_o range and lower ΔH in corn starch than in pulse starches reflected that corn starch contains a higher proportion of crystallites but are smaller in size, which are formed from short double helices of amylopectin molecular chains and are less stable, and therefore less energy would be required to melt those double helices during gelatinization (Chung and others 2009). In addition, gelatinization behaviors of native starches are also influenced by some minor components in starch such as protein and lipid. The higher level of lipid in regular corn starch may inhibit swelling under conditions when AM-lipid complexes are likely to be formed, and thus would show a higher gelatinization temperature (Tester and Morrison 1990). However, no AM-lipid complex was present to affect the gelatinization behavior of pulse starches in this study because only trace quantities of lipids were associated with starch granules of faba bean and field pea starches (Table 7.1).

Crosslinking caused significant changes in the gelatinization parameters of all three starches (Table 7.3). As shown in Fig. 7.2, the peak of DSC curves shifted toward the right side on $POCl_3$-aqueous crosslinked starches, which indicated an increase in transition temperature (T_o, T_p, and T_c) of crosslinked starches. The extent of increase in T_o, T_p, and T_c varied with starch and crosslinking techniques. As shown in Table 7.3, $POCl_3$-aqueous significantly increased T_c-T_o of faba bean and field pea starches but did not show significant influence on T_c-T_o of corn starch. It is notable that $POCl_3$-aqueous has a greater influence on the increase in T_o than STMP-semidry and STMP-aqueous, since T_o represents melting of the weakest crystallites. The increase of T_o indicated that

crosslinking by $POCl_3$-aqueous stabilized crystalline structure in starch granules that were more resistant to gelatinization. This influence was more pronounced in corn starch (T_o increased from 67.7 to 72.0 °C), which could be attributed to the stabilization of its higher proportion of short chains with less swelling capability. The previous study reported that crystalline and double helical melting during gelatinization were assisted by hydration and swelling of amorphous regions in the starch granule (Donovan 1979). The swelling of the amorphous regions imparts a stress on the crystalline regions, leading to a disruption of hydrogen bonds linking adjacent double helices in the crystalline regions (crystalline melting) (Donovan 1979). Phosphate crosslinks between AP-AP and/or AM-AP chains would suppress the mobility of the amorphous regions. Consequently, the amorphous regions of crosslinked starch would require a higher temperature to incur adequate swelling that could contribute to the disruption of the crystalline regions. Therefore, the increase in T_o, T_p, and T_c could reflect the formation of AM-AP and/or AP-AP crosslinks in $POCl_3$-aqueous starch. In addition, greater increases in T_c and T_c-T_o were found for pulse starches than that for corn starch. This may be attributed to the higher proportion of phosphate crosslinks between AM-AP in their phosphorylated counterpart. This study supports that the stabilization of crystallites due to crosslinking is mainly contributed by strengthening of AM-AP, which could happen between amorphous and crystalline regions of starch granules (Jane and others 1992).

In all starches, STMP-semidry decreased T_o but significantly increased T_p and T_c as compared to their native counterparts. The extent of changes in T_o, T_p, and T_c followed the order: field pea > faba bean > regular corn. The T_c-T_o was widened (field pea > faba bean > regular corn) and ΔH was decreased (regular corn > faba bean > field pea) on STMP-semidry. The increase in T_p, T_c, and T_c-T_o on STMP-semidry could be attributed to interactions between AM-AP and/or AP-AP by

crosslinking. The same factors influencing T_p, T_c and T_c-T_o on POCl$_3$-aqueous could also be responsible for the increase in T_p, T_c and T_c-T_o on STMP-semidry, being higher in faba bean and field pea starches than in corn starch. It was interesting to note that STMP-semidry show a greater influence on the increase in T_c (represents melting of very stable crystallites) when compared to POCl$_3$-aqueous in pulse starches, while an opposite trend was found in corn starch. This may be due to the different diffusion patterns of crosslinking reagent between pulse and cereal starches, and thus different location and distribution of phosphate linkages (Fannon and others 2004; Shukri and others 2015). In addition, STMP-semidry induced lower ΔH values as compared to the native starches (Table 7.3), suggesting that less thermal energy was required to melt the double helices of STMP-semidry crosslinked starches. According to a previous study, starches with higher transition temperatures often showed higher ΔH and the ΔH mainly reflects the loss of molecular order within the internal structure of starch granules (Cooke and Gidley 1992). In this study, starches were linked by not only hydrogen bonds but also crosslinking molecules, and therefore, the internal structure of crosslinked starches was more complex and amorphous, which may cause the decrease of ΔH values of crosslinked starches compared to that of native starches. Compared to POCl$_3$-aqueous and STMP-aqueous starches, the extent of decreases in ΔH was more pronounced in STMP-semidry starches. This result suggested that the high temperature (130 °C) involved during crosslinking by STMP-semidry may have increased the mobility of double helices, leading to the disruption of some hydrogen bonds linking adjacent double helices. Decreased ΔH has also been reported in pea, lentil, navy bean, and jack bean starches, as well as cereal starches modified by heat moisture treatment (HMT), where high temperatures (100-120 °C) were also involved (Chung and others 2009).

STMP-aqueous in this study showed less pronounced effect than POCl$_3$-aqueous and STMP-semidry on increasing crystalline stability of crosslinked starches. STMP-aqueous significantly increased T$_o$, T$_p$, T$_c$ in corn starch, but only increased T$_c$ in pulse starches, indicating influences of crosslinking agent and crosslinking method on different starches. In general, all three crosslinking methods exhibited significant influence on increasing crystalline stability in all three starches. This influence varied with starch source, crosslinking agent, and crosslinking method. For example, STMP-semidry with the highest DC in pulse starches also showed the greatest increase of crystalline stability (STMP-semidry > POCl$_3$-aqueous > STMP-aqueous), whereas in corn starches, POCl$_3$-aqueous had lowest DC showing highest influence on increasing the crystalline stability. STMP-aqueous showed less influence on thermal stability than STMP-semidry and POCl$_3$-aqueous in all starches (Corn > filed pea ~ faba bean). This is consistent with the result obtained from RVA analysis.

7.3.4. Effect of phosphorylation techniques on crystalline order characteristics

The XRD patterns of native and crosslinked regular corn, faba bean, and field pea starches are shown in Fig. 7.3. Native regular corn starch displayed a distinctive A-type XRD pattern with strong diffraction peaks at around 15° and 23° 2θ and an unresolved doublet at around 17° and 18° 2θ. According to previous studies, B-type starch gives the strongest diffraction at around 17° 2θ, a few small peaks at around 15°, 20°, 22°, 24° 2θ, and a characteristic diffraction reflection at around 5.6º 2θ (Zhang and others 2013). Compared with corn starch, faba bean and field pea starches had strong diffraction reflections at around 15°, 17°, and 23° 2θ, a small peak at around 5.6° 2θ and a shoulder peak at around 18° 2θ, exhibiting typical C-type diffraction patterns (a mixture of A and B-type crystalline). The relative crystallinities were determined by the ratio of diffraction peak area to total peak area (Table 7.4). The relative crystallinity in native starches
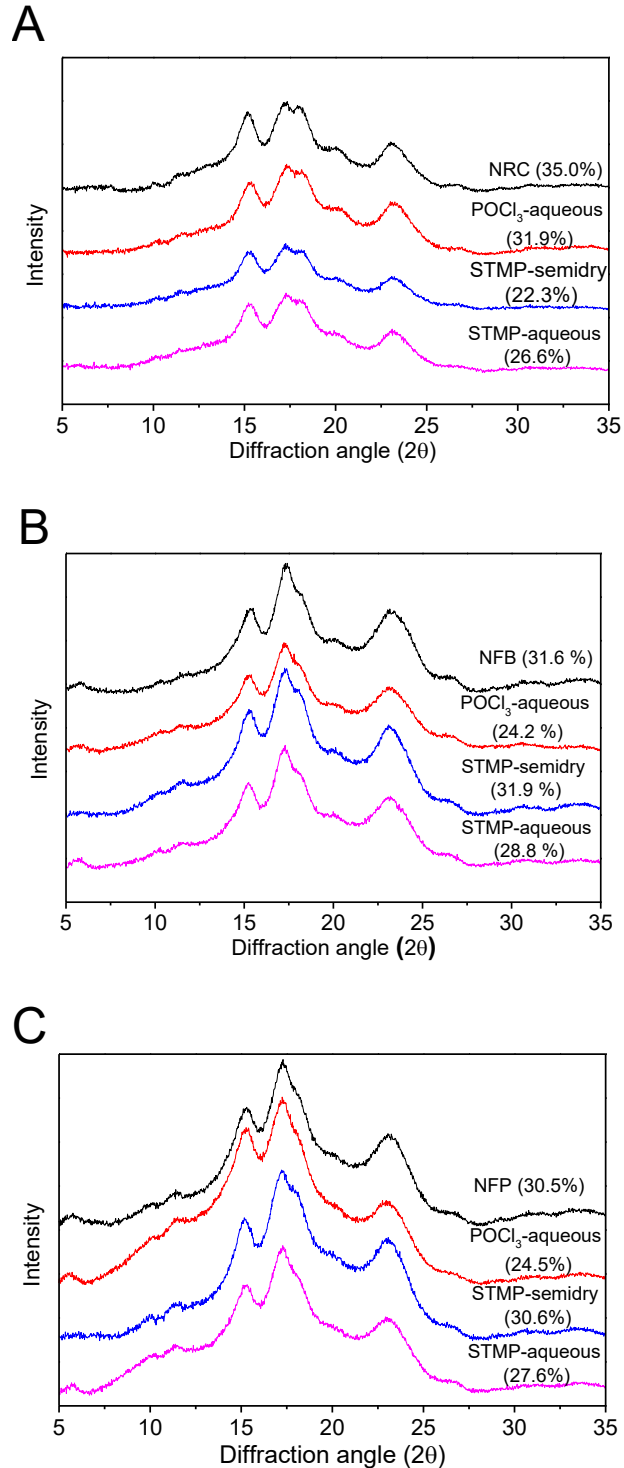
Fig. 7.3 X-ray diffraction patterns and relative crystallinity (numbers in the bracket) of native starches and phosphorylated corn (A), faba bean (B), and field pea (C) starches. NRC (native regular corn starch); NFB (native faba bean starch); NFP (native field pea starch); POCl$_3$-aqueous (2% POCl$_3$ in aqueous slurry at 25 °C); STMP-semidry (4% STMP/STPP [99:1. w/w] in a semidry state at 130 °C); STMP-aqueous (12% STMP/STPP [99:1. w/w] in aqueous slurry at 45 °C).

192

Table 7.4 Parameters of crystallinity and molecular order of the native and phosphorylated starches by X-ray diffraction (XRD) and attenuated total reflectance-fourier transform infrared spectroscopy (ATR-FTIR).

Samples	Crystallinity by XRD (%)	R (1047/1022) by ATR-FTIR	R (1047/1035) by ATR-FTIR
NRC	34.95 ± 0.67 a	0.6111 ± 0.0011 a	1.0994 ± 0.0013 a
POCl$_3$-aqueous	31.92 ± 0.92 b	0.6026 ± 0.0013 b	1.0628 ± 0.0015 c
STMP-semidry	22.28 ± 0.49 d	0.6041 ± 0.0009 b	1.0761 ± 0.0011 c
STMP-aqueous	26.60 ± 0.38 c	0.5946 ± 0.0030 c	1.0747 ± 0.0041 c
NFB	31.62 ± 0.61 a	0.6166 ±0.0004 a	1.0770 ± 0.0006 a
POCl$_3$-aqueous	24.22 ± 0.34 c	0.6028 ± 0.0023 c	1.0288 ± 0.0025 d
STMP-semidry	31.93 ± 0.53 a	0.6104 ± 0.0030 b	1.0441 ± 0.0019 c
STMP-aqueous	28.82 ± 1.04 b	0.6074 ± 0.0010 b	1.0634 ± 0.0009 b
NFP	30.54 ± 0.46 a	0.6182 ± 0.0040 a	1.0830 ± 0.0055 a
POCl$_3$-aqueous	24.46 ± 0.79 b	0.5860 ± 0.0022 c	1.0247 ± 0.0048 c
STMP-semidry	30.62 ± 1.00 a	0.6079 ± 0.0009 b	1.0433 ± 0.0008 b
STMP-aqueous	27.60 ± 0.97 a	0.6132 ± 0.0011 ab	1.0414 ± 0.0009 b

Means (n=3) in the same column within same type of starch sharing a common letter are not significantly different at P< 0.05. NRC (native regular corn starch); NFB (native faba bean starch); NFP (native field pea starch); R (1047/1022) (ratio 1047/1022 cm^{-1}, a measure of the amount of ordered starch to amorphous starch); R (1047/1035) (ratio 1047/1035 cm^{-1}, a measure of the amount of ordered starch); POCl$_3$-aqueous (2% POCl$_3$ in aqueous slurry at 25 °C); STMP-semidry (4% STMP/STPP [99:1. w/w] in a semidry state at 130 °C); STMP-aqueous (12% STMP/STPP [99:1. w/w] in aqueous slurry at 45 °C);

followed this order: regular corn (35.0%) > faba bean (31.6%) > field pea (30.5%). Similar values of relative crystallinity for corn and pulse starches have been reported (Chung and others 2009; Chung and others 2010; Li and others 2019). The highest degree of crystallinity in starch granules of regular corn starch is due to the organization of amylopectin molecules.

As shown in Fig. 7.3A, the overall crystalline patterns of all crosslinked regular corn starches were similar to native corn starch, which showed that the crosslinked corn starches shared the same A-type X-ray patterns as the native starch. But the relative crystallinity of corn starch was decreased in crosslinked starches following the order $POCl_3$-aqueous (31.9%) > STMP-aqueous (26.6%) > STMP-semidry (22.3%). As compared to corn starch, the relative crystallinity of crosslinked pulse starch followed the opposite trend (Table 7.4), where STMP-semidry showed the highest relative crystallinity. The XRD spectra of both STMP-semidry faba bean and field pea starches showed that the peak at 2θ 5.6° disappeared, the peak at 2θ 18° and 23.0° became stronger and sharper, which indicated that STMP-semidry pulse starches gave more A-type crystallinities. This revealed the possible conversion of crystal types from C-type to A-type in C-type starch. This is due to the B-type polymorphs that were disrupted during the process of STMP-semidry, where a high temperature (130 °C) was involved. This was in agreement with previous reports that B-type polymorph in the C-type starches was degraded faster than A-type polymorph during the process of acid modification (Cai and others 2014). The STMP-aqueous only slightly decreased the crystallinity in pulse starches, while significantly decreased that in corn starch from 35% to 26.6%. $POCl_3$-aqueous did not change the X-ray patterns of pulse starch but significantly decreased the relative crystallinity.

These diverse results indicate that the influence of crosslinking on the starch crystallinity depends on the type of starch and phosphorylation method used. Generally, crosslinking by $POCl_3$-aqueous and STMP-aqueous had no pronounced effect on the XRD patterns of all starches (A-type for regular corn, C-type for pulse starches); it seems that the phosphate cross-links must have occurred in the amorphous regions of the starch granules. This is consistent with the previous study by Koo and others (2010). However, the reduction of crystallinity after crosslinking indicated the action of crosslinking disrupted the crystallinity of starch. The different behaviors of these two crosslinking methods among corn and pulse starches may be due to the different crosslinking reagent and level used, as well as the different reaction patterns between pulse and corn starches. This is probably because of the lack of channels in pulse starch granules which, when present, offer a quick rate of penetration into the amorphous region of the granule. Literature also reported that when a higher concentration of $POCl_3$ was used, some starch granules appeared to be crosslinked on or near the surface of both channels and central cavity and in the region surrounding the central cavity (Huber and BeMiller 2001). This indicates that a non-uniform reaction with $POCl_3$ occurs preferentially at the granule surfaces, both those at the granule periphery and those of interior channels and cavities (Huber and BeMiller 2001; Fannon and others 2004). Accordingly, when pulse starch was reacted with $POCl_3$ (very reactive), it appeared that the rate of reaction was greater than its rate of diffusion into granules, and thus was mainly surface oriented, forming a hard shell. It is notable that the very organized/crystalline structures are usually present in the outer layers of starch granules. Therefore, the influence of $POCl_3$-aqueous on crystallinity in pulse starch was more pronounced than in corn starch. In contrast, STMP-aqueous had more influence on the crystallinity of corn starch than that of pulse starch (Table 7.4). This is because the reagent of STMP/STPP reacts at a much slower rate than $POCl_3$ does and has time to penetrate the entire

granule before reacting, meanwhile, the channels in corn starch facilitate the penetration of STMP/STPP to the entire granule faster than with pulse starches. Furthermore, the long reaction time of starch at high pH and temperatures lead to the reduction of crystallinity. In addition, the hard shell of $POCl_3$-aqueous starch may also contribute to inhibition of swelling of individual starch granules and thus result in lower viscosity of starch paste than the softer, more deformable STMP/STPP at even lower DC (Table 7.3).

7.3.5. Effect of phosphorylation techniques on short-range molecular order characteristics

The ATR-FTIR spectrum of starch has been shown to be sensitive to changes in the short-range molecular order of starch such as double helical structure, chain conformation, and the crystal form of starch (Wu and Seib 1990). Furthermore, ATR-FTIR only provides the structural characteristics of starch near the granule surface, since the IR beam penetrates only to a depth of 2 µm into the granule (van Soest and others 1995; Sevenou and others 2002). Hence, the ATR-FTIR technique was used to further explore the external structural organization of starches as influenced by three different phosphorylation techniques. The original and deconvoluted ATR-FTIR spectrum of native and crosslinked starches are presented in Fig. 7.4. The fundamental region of all starch samples presents the broad bands around 3264 cm^{-1} which was attributed to inner- and intro hydroxyl groups (O-H) stretching vibration; the sharp bands around 2926 cm^{-1} can be ascribed to the asymmetric stretching of carbon-hydrogen bond (C-H). The absorption at around 1640 cm^{-1} was ascribed to adsorbed water i.e. H-O-H bending vibrations on the amorphous regions of starch, which was a typical characteristic absorption band of starch (Bernardino-Nicanor and others 2017). The bands around 1363 cm^{-1} and 1338 cm^{-1} were assigned to C-H stretch in alkane, and 1242 cm^{-1} was attributed to the C-OH stretching of CH_2OH. The peaks in the region 1160-1100 cm^{-1} were mainly attributed to asymmetrical stretching of C-O-C, whereas in 1077-928 cm^{-1} were

assigned to C-O stretch of C-O-H in starch.
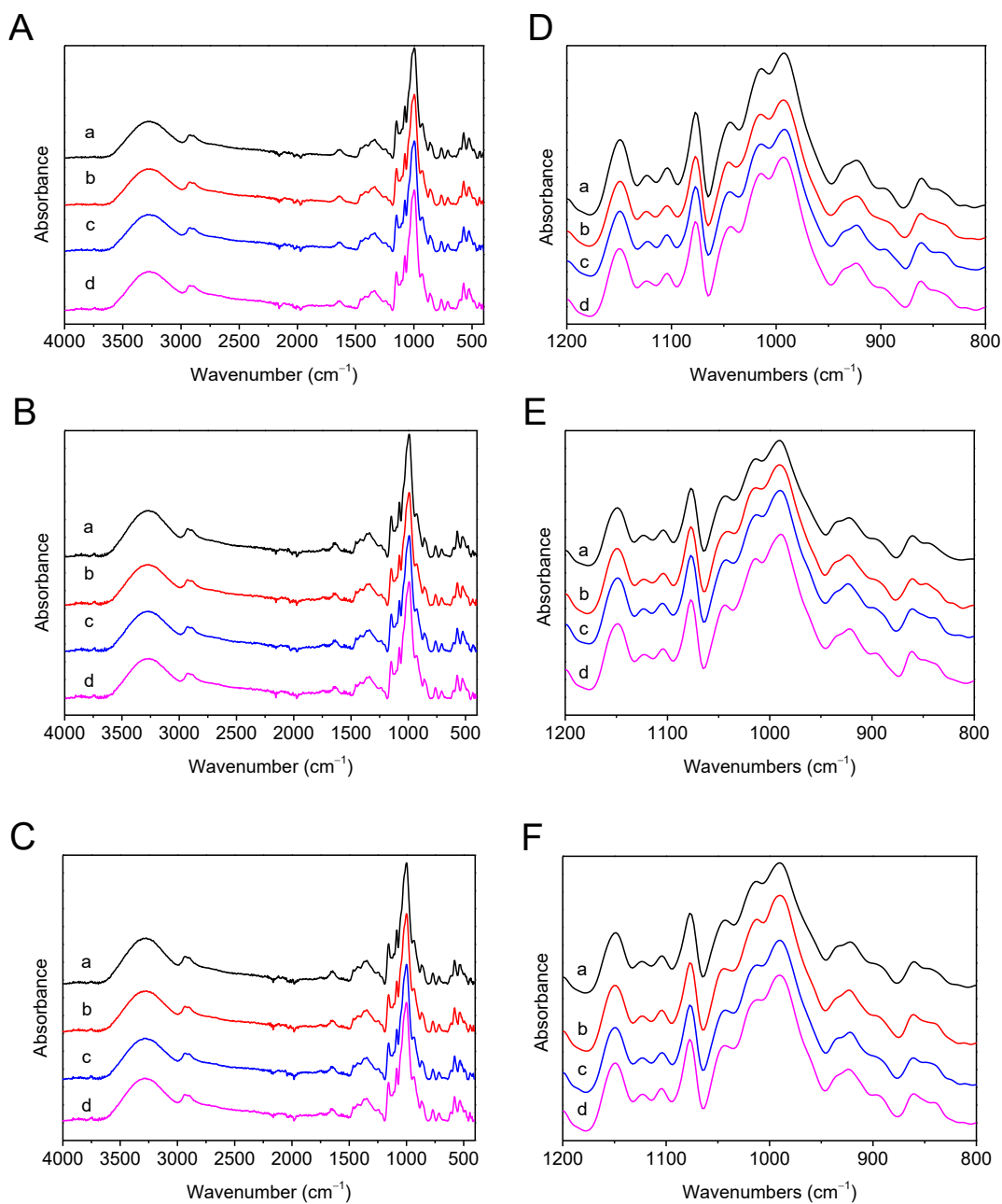
Fig. 7.4 Original (A-C) ATR-FTIR spectrum and deconvoluted (D-F) ATR-FTIR spectrum of native and phosphorylated (A, D) corn, (B, E) faba bean, and (C, F) field pea starches. a, native starch; b, POCl₃-aqueous (2% POCl₃ in aqueous slurry at 25 °C); c, STMP-semidry (4% STMP/STPP [99:1. w/w] in a semidry state at 130°C); d, STMP-aqueous (12% STMP/STPP (99:1. w/w) in aqueous slurry at 45 °C).

It is clear that there is no distinct difference among the vibration bands of O-H, C-H, and C-O in all native and crosslinked starches. This could be due to the fact that the basic chemical structures of native and crosslinked starches are similar which is reflected in their similar absorption peaks. However, a slight decrease in absorption at 3264 cm^{-1} (corresponding to hydroxyl), 1640 cm^{-1} (corresponding to the intra-molecular hydrogen bond), as well as 994 cm^{-1} (corresponding to intramolecular hydrogen bonding of hydroxyl groups at C-6) was observed for all crosslinked starches. This may be due to the breaking of hydrogen bonds and phosphate groups being introduced between hydroxyl groups of the crosslinked starch sample. The similar spectral results for cross-linked corn and rice starches have been reported earlier (Shalviri and others 2010; Ashwar and others 2017). Meanwhile, the slight increase of characteristic absorptions found in cross-linked starches were at around 836 cm^{-1} and 889 cm^{-1}, which may be related to the P-O-C bond. And the slight increase of absorption in the region of 1150-1300 cm^{-1} was assigned to symmetrical stretching of phosphorus-oxygen bond (P=O) (Shalviri and others 2010). However, the intensity of characteristic adsorption peaks did show significant differences among the cross-linked starch samples, which could be attributed to the low content of phosphorus bonded in these crosslinked starch samples. These outcomes suggested the structure of starch was not broken but phosphate cross-linked groups formed after cross-linking.

The deconvoluted ATR-FTIR spectrum in the region of 1200-800 cm^{-1} of native and crosslinked starches from regular corn, faba bean, and field pea are presented in Fig. 7.4 (D-F). The bands at around 1047 and 1022 cm^{-1} are related to the crystalline and amorphous areas of starch, respectively (van Soest and others 1995). Therefore, the absorbance ratio 1047/1022 can be used to measure the change of ordered starch to amorphous starch, and the absorbance ratio 1047/1035

(the valley at 1035 cm^{-1}) can be used as a measure of the amount of ordered starch. The ratio 1047/1022 and 1047/1035 of starch samples are shown in Table 7.4. The ratio 1047/1022 of native regular corn, faba bean, and field pea starches were 0.6111, 0.6166 and 0.6182, respectively. However, after cross-linking, the absorbance ratios of all crosslinked starches were reduced as compared with their native counterparts. For instance, the ratio 1047/1022 of POCl$_3$-aqueous, STMP-aqueous, and STMP-semidry FP starches were reduced to 0.5860, 0.6079 and 0.6132, respectively (Table 7.4). These results indicated that the short-range molecular order in the region near the starch granules' surfaces may be disrupted by cross-linking reaction, which was in accordance with the results of XRD. This slight decrease may have been due to double helical reorientation within crystalline domains and/or the disruption of the hydrogen bonds linking adjacent double helices on the surface of granules by the reaction of cross-linking. Similar with the XRD result, in pulse starches, POCl$_3$-aqueous showed the lowest peak viscosity with lowest DC (Fig. 7.3) but showed a relatively higher extent of decrease in the ratio 1047/1022 as compared to STMP methods; however, this trend was not observed in corn starch. The ratio 1047/1035 had a similar trend as that of 1047/1022, suggesting that crosslinked starches show less short-range order than their native counterparts. This also indicated the disruption of the hydrogen bonds on the surface of granules by the reaction of cross-linking, and the influence was more pronounced in POCl$_3$-aqueous starch than in STMP-semidry and STMP-aqueous starches. This was probably due to the different reaction pattern of those two chemical reagents between corn and pulse starches as discussed in section 7.3.4, where cross-links predominate on the surface of POCl$_3$-aqueous pulse starch granules due to the higher reactivity of POCl$_3$ and the lack of channels on pulse starch granules.

7.4. Conclusion

Three phosphorylation techniques were applied to modify regular corn, faba bean, and field pea starches. Their effects on the structural, thermal, and pasting properties changes of starches were monitored. Cross-linking by phosphorylation significantly increased pasting temperature, decreased breakdown, increased gelatinization temperature and thermal stability to different extents, which could enable a wide range of applications. XRD and ATR-FTIR spectra confirmed the crystalline structure and crystallinity of starch was slightly changed and new cross-linked groups (phosphate groups) formed after cross-linking by all three phosphorylation techniques. The influence of $POCl_3$-aqueous on the crystalline structure of starch was more pronounced in pulse starches, faba bean and field pea, than in corn starch; while STMP-aqueous had less influence on the crystalline structure of pulse starch; STMP-semidry preferentially disrupted the B-type polymorph in C-type pulse starches. The extent of changes in physicochemical and structural properties of three starches which differed with the three phosphorylation techniques were possibly due to the differences in amylose content and molecule size, molecular structure of amylopectin, crosslinking agent, reaction conditions, as well as the location and distribution of phosphate groups in starch granules. This study contributes to a theoretical understanding of structure-phosphorylation-functional property relationships of pulse and corn starches and may benefit a methodical and strategic industrial design of novel starch materials using a strategic selection of phosphorylation techniques and starch sources.

Chapter 8: Amylase resistance of corn, faba bean, and field pea starches as influenced by three different phosphorylation (cross-linking) techniques

8.1. Introduction

The rate of starch digestibility is a very important aspect of the human nutrition and health. In humans, starch is digested predominantly by amylase in the small intestine, and based on the "rate of digestibility" starch has been classified into three major fractions: rapidly digestible starch (RDS), slowly digestible starch (SDS) and resistant starch (RS) (Englyst and others 1992). Based on the amylase resistance, starch is classified into 5 types of resistant starch: physically entrapped starch (RS1), amylopectin crystals in native granular starch (RS2), amylose crystals in retrograded starch (RS3), chemically modified starch (RS4), and lipid complexed starch (RS5) (Birt and others 2013).

Chemically modified starch increases starch amylase resistance (AR). Chemical substitution such as hydroxylpropylation, acetylation, and oxidation decreases the susceptibility of starch to α-amylase and increases the RS content in cooked and uncooked starches (Chung and others 2008). However, contradictory information exists in literature regarding the effect of crosslinking by phosphorylation on starch amylase resistance. Some researchers have reported that the cross-linking with phosphorylation may reduce the rate of digestion (Woo and Seib 2002; Shukri and others 2015), whereas others have observed only minor effect on starch digestibility (Hoover and Sosulski 1986; Park and others 2018). Most chemical modification studies were done with corn, wheat, and rice starches (Woo and Seib 2002; Shukri and others 2015; Ashwar and others 2018). However, an increasing global demand for plant protein has enhanced the pulse processing activities in Canada, including the production of protein isolates/concentrates from field pea and

faba bean. Crude starch is the major byproduct (~50%, w/w) of pulse processing, and therefore the interest in pulse starch refining and utilization has been growing. In Chapter 7, three phosphorylation techniques, $POCl_3$-aqueous, STMP-semidry, and STMP- aqueous were applied to modify regular corn, faba bean, and field pea starches. The results indicated that the influence of phosphorylation on physicochemical and structural properties of three starches differed with the three phosphorylation techniques, which may be due to the differences in amylose content and molecule size, molecular structure of amylopectin, crosslinking agent, reaction conditions, as well as the location and distribution of phosphate groups in starch granules. These differences among starches is expected to influence the amylase resistance of native and modified starches. In addition, pulse starches from field pea, faba bean, and lentil have greater amylase resistance compared to cereal starches like corn and wheat. However, this is true only in their uncooked forms. Since starches in most food applications are used in the cooked form, a preliminary study in the laboratory has shown that cooked and gelatinized starches from field pea, faba bean, corn and wheat had high and comparable digestibility (~90% RDS). Therefore, to reflect the actual practical situation, the present study investigated the effect of chemical modifications on starch amylase resistance in both the uncooked and cooked forms. The objective was to establish the correlation between degree of crosslinking (DC), % P and AR, of starch in gelatinized form, as well as to explore the mechanism of AR in type 4 resistant starch. This will permit a better understanding of how starch types (corn, faba bean and field pea) and the three different phosphorylation methods play a role in starch digestibility.

8.2. Materials and methods

8.2.1. Materials

Regular corn, faba bean, field pea starches, pure amylose and amylopectin from potato starch were obtained as described in Chapter 4 section 4.2.1. Sodium trimetaphosphate (STMP, >95% purity), sodium tripolyphosphate (STPP, >98% purity), sodium sulfate (>99% purity), and phosphoryl chloride (POCl$_3$, >99% purity) was obtained from Millipore Sigma Canada Co, Oakville, ON, Canada. The Assay Kit for amylase resistance determination was purchased from Megazyme (Megazyme International Ireland Ltd., Bray, County Wicklow, Ireland). All other chemicals were of analytical grade.

8.2.2. Starch phosphorylation

Starch was modified using three different phosphorylation techniques as described in Chapter 7 section 7.2.2.

8.2.3. Determination of reaction efficiency by phosphorus content

Considering the low content of phosphorus (% P) in starch, the commonly used ammonium molybdate and vanadate spectrophotometric method (Smith and Caruso 1964) had to be modified to reach a greater sensitivity. Starch samples (0.3 g) with 0.5 mL 10% zinc acetate solution were heated until dry and then ashed for 3 h at 550 °C and cooled down. The ash was dissolved in 1 mL 29% (w/v) HNO$_3$, then ashed again for another 1 h, cooled down, dissolved in 1 mL 20% HCl, mixed well, then 0.2 mL of supernatant was taken, mixed with 1 mL HNO$_3$ 29%, 1 mL ammonium vanadate (0.25%), and 1 mL ammonium molybdate (5%) and the volume was adjusted to 10 mL with distilled water. After 10 min, the absorbance was measured at 435 nm against a sample blank. A calibration curve (0-20 µg phosphorus per mL) was prepared using potassium dihydrogen phosphate. P levels are the P incorporated by chemical treatment (total P in phosphorylated starch

minus the endogenous P in native starch).

8.2.4. Degree of crosslinking calculated by percentage of amylose crosslinked

DC of modified starch was also measured by colorimetric procedure with slight modification according to a recent report (Kou and Gao 2018). Briefly, starch (100 ± 0.1 mg, db) was mixed with 1 mL ethanol added for sufficient dispersion, then 10 mL 1 M NaOH solution was added to ensure a homogeneous solution. The above solution was kept for 1 h at room temperature, after that, the whole solution was diluted to 50 mL with distilled water. 2.5 mL of the above chemical gelatinized starch solution was transferred into another 100 mL volumetric flask (with 50 mL distilled water inside), HCl was added to neutralize the solution, then 2 mL KI/I_2 was added and diluted to 100 mL for the colour reaction. After 30 min, the absorbance of the native starch (A_0) and the crosslinked starches (A_1) were measured against a blank solution. The DC% was determined by the following equation:

Percentage of amylose crosslinked % $= \frac{A_0 - A_1}{A_0} \times 100\%$ (8.1)

Where percentage of amylose crosslinked % is the crosslinking degree calculated by the colorimetric method mentioned above, A_0 is the absorbance of the native starch, A_1 is the absorbance of the crosslinked starches.

8.2.5. Amylase resistance

8.2.5.1. Ungelatinized starch

The digestibility profile of starches was determined by the procedure of Englyst and others (1992) with minor modifications. The Megazyme Assay Kit (AOAC 2002.2, AACC method 32-40.01, CODEX Type II method) was used. Briefly, starch samples (100 mg) were incubated in a simulated intestinal solution (4 mL, 30 U/mL α-amylase, 3 U/mL amyloglucosidase, and 100 mM

sodium maleate phosphate buffer, pH 6.0) in a shaking water bath (37 °C, 200 strokes/min). After a 20 min, 120 min, and 16 h incubation period, the enzymatic reaction was stopped with 4 mL of 99% ethanol, vortexed and centrifuged (1500 × g, 10 min), the residue was washed twice with 8 mL 50% ethanol, vortexed and centrifuged. The supernatant solutions were combined, and the volume was adjusted with 100 mM sodium acetate buffer (pH 4.5). An aliquot of this solution (0.1 mL) was incubated with 10 μL dilute amyloglucosidase solution (300 U/mL, 20 min, at 50 °C). The glucose released was measured via a glucose oxidase peroxidase diagnostic kit (Megazyme, Ireland) by taking the absorbance of samples against the reagent at 510 nm using UV/VIS spectrophotometer.

Starch was classified as rapidly digestible starch (RDS), slowly digestible starch (SDS), very slowly digestible starch (VSDS), and resistant starch (RS) based on the rate of hydrolysis: RDS was hydrolyzed within 20 min of incubation, SDS was digested between 20 and 120 min, VSDS was digested between 2 and 16 h, and RS did not hydrolyze within 16 h.

Then, the content of RS was calculated by differences (RS = 100 − RDS − SDS − VSDS).

8.2.5.2. Gelatinized starch

The native and modified starches (100 mg) and 3 mL 100 mM sodium maleate phosphate buffer, pH 6.0 were added to 15 mL screw-capped polypropylene centrifuge tubes and mixed by vortexing. The tubes were heated in boiling-water bath for 15 min, vortexed every 2 min. After heating, the tubes were placed in 37 °C water bath and equilibrated for 10 min. Then, 1 mL of enzyme solution was added to the tube (total enzyme concentration was equivalent to the above solution in section 8.2.5.1). Then followed the same procedure as described in section 8.2.5.1 (Englyst and others 1992).

8.2.6. Field emission scanning electron microscopy (FE-SEM)

The morphology of native starch and crosslinked phosphorylated starches, as well as enzymatically digested starch residues were observed followed the procedure as described in Chapter 3 section 3.2.5. The enzymatically hydrolyzed ungelatinized starch residues after 20 min, 120 min, and 16 h were recovered with the addition of anhydrous ethanol followed by centrifugation (Fisher Scientific accuSpin™ 400 bench top centrifuge, Osterode am Harz, Germany) at $3000 \times g$ for 10 min.

8.2.7. Statistical analysis

All experiments were done in three replicates. Results are presented as mean ± SD (standard deviation). Analysis of variance (ANOVA) was performed, and the mean comparisons were carried out by Duncan's range test at $P < 0.05$ using the SPSS statistical software (Version 22, SPSS Inc., Chicago, IL, USA).

8.3. Results and discussion

8.3.1. Granule morphology of native and modified starches

The purity of the starches was verified on the basis of high total starch content (> 95%) with low content of residual protein (<0.3%), lipid (<0.7%) and ash (< 0.3%) (Table 7.1) and microscopic observation (Fig. 8.1), where the granules appeared smooth and free of other grain components. Typical morphological features of corn starch (polygonal shapes with well-defined edges and smooth surface) and pulse starches (round to oval shapes with smooth surface) were observed (Fig. 8.1). Granular shape and surface features of phosphorylated starches showed no remarkable change when compared to their native counterparts. Only very few fissures and smooth indentations could be seen on some starch granules. Previous studies also reported no major differences in the morphological structure of native and cross-linked rice and oat starches (Mirmoghtadaie and others 2009; Ashwar and others 2017). In addition, some larger starch

granules were observed in crosslinked rice starch, which may be formed by the STMP/STPP mixture (Ashwar and others 2017). Cross-linked corn starch granules with different degree of cross-linking prepared with the mixture STMP/STPP exhibited a slightly rough surface and had black zones on the surface, indicating a slight fragmentation and the formation of a deep groove in the starch granules (Koo and others 2010). Overall, crosslinking is a reaction that occurs at molecular level, where changes in the morphology of the intact granules are usually not observed.
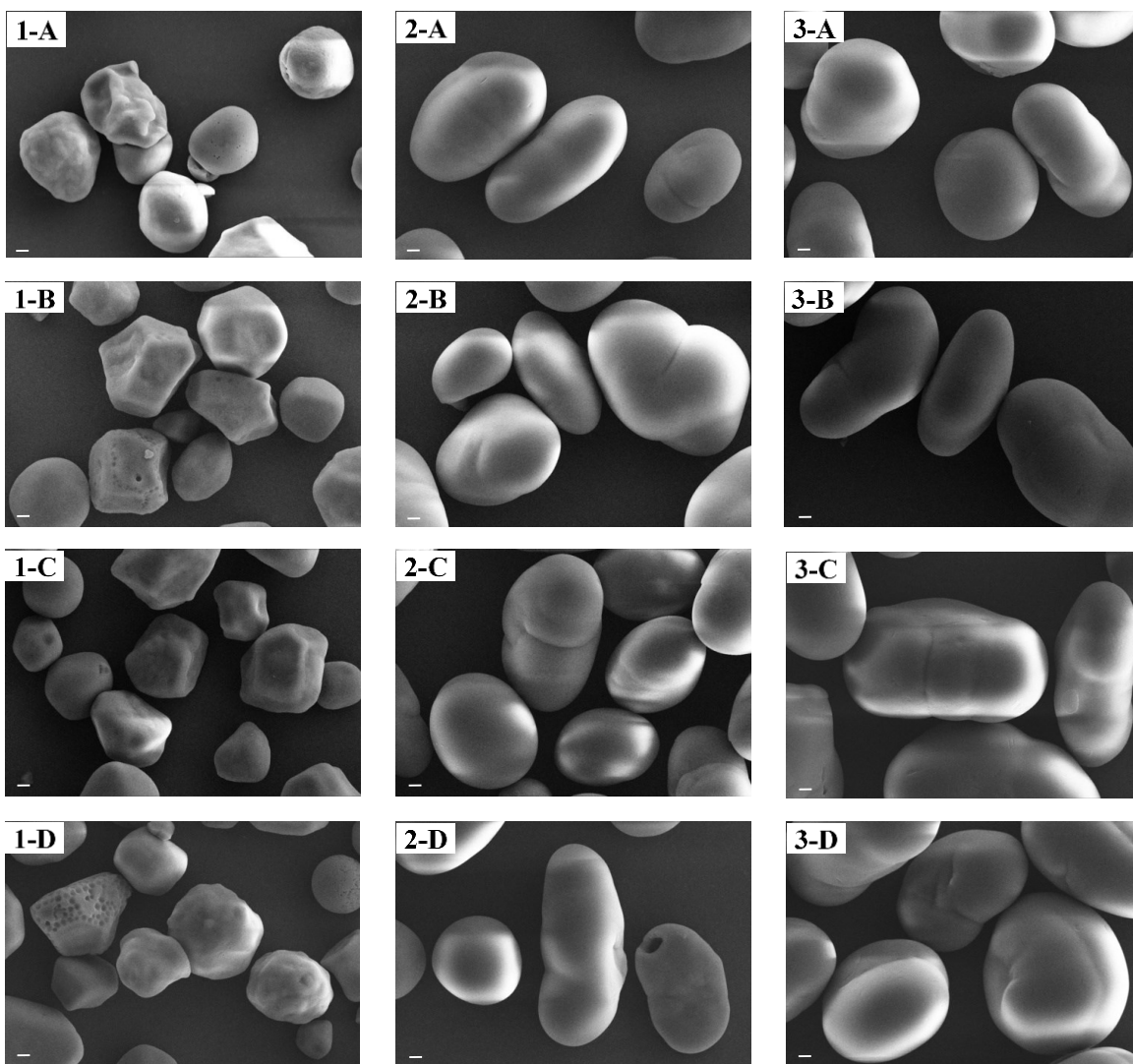
Fig. 8.1 The morphology of native and phosphorylated starches (1, Regular corn; 2, Faba bean; 3, Field pea; A, Native starch; B, POCl$_3$-aqueous modified starch; C, STMP-semidry modified starch; D, STMP-aqueous modified starch) (Scale bar=2μm).

8.3.2. Phosphorus content of cross-linked starch

Phosphorus content (%P) is widely used to interpret the degree of crosslinking, which reflects the reaction efficiencies of different crosslinking methods. The %P incorporated in modified starches were calculated by subtracting the endogenous %P content of native starches (Table 8.1). In the phosphorylated starches, the %P is influenced by different phosphorylation techniques. STMP-semidry involving heat treatment yielded the greatest %P followed by STMP-aqueous and $POCl_3$-aqueous. The %P increased as the concentration of phosphorylating agent increased from 1 to 2% of $POCl_3$ for $POCl_3$-aqueous, 2 to 4% of STMP/STPP for STMP-semidry, and 5 to 12% of STMP/STPP for STMP-aqueous. Compared to STMP-aqueous method (at 25 °C), STMP-semidry method (at 130 °C) showed more phosphorus binding, where lower levels of chemicals were used. Among the modified starches, FP showed the highest %P up to 0.19 % followed by FB and RC that indicated better reaction efficiency of pulse starches. A previous study with different corn genotypes (waxy, regular and high amylose) proposed that amylopectin could be more effective in the crosslinking process due to higher levels of retained phosphorylating salts in the branched regions of amylopectin (Shukri and others 2015). However, in the present study FB and FP starches with higher amylose contents (AM, 39% and 41%, respectively) showed more phosphorus binding when compared to RC (higher amylopectin content, AP, ~74%). This may be due to different crystalline types of starches ("C-type" pulse vs "A-type" cereal) and chain length of starch molecules (i.e. AP and AM from pulse starches show higher degree of polymerization), as well as the different reaction pattern of crosslinking reagent between pulse and cereal starches, and thus different location and distribution of phosphate linkages (Fannon and others 2004; Shukri and others 2015). This is because phosphorylation reagents enter and react readily in the less ordered, amorphous regions (Fannon and others 2004). In "B-type" (tuber and high amylose starches) and

208

Table 8.1 Phosphorus content (% P, w/w) and percentage amylose crosslinked of modified starches by three different phosphorylation techniques

Treatment	Phosphorus content (%)			Percentage amylose crosslinked (%)		
	RC	FB	FP	RC	FB	FP
POCl$_3$-aqueous-1	0.07 ± 0.00Cc	0.08 ± 0.00Cb	0.09 ± 0.00Da	96.85 ± 0.92Aa	96.58 ± 1.12Aa	98.33 ± 0.69ABa
POCl$_3$-aqueous-2	0.10 ± 0.01Bb	0.12 ± 0.00Ba	0.12 ± 0.00Ca	99.63 ± 0.16Aa	99.08 ± 0.19Aa	99.30 ± 0.39Aa
STMP-semidry-2	0.11 ± 0.01Bb	0.12 ± 0.00Bab	0.13 ± 0.00Ca	78.70 ± 1.31Ca	79.21 ± 0.65Da	77.16 ± 1.18Da
STMP-semidry-4	0.14 ± 0.01Ac	0.16 ± 0.00Ab	0.19 ± 0.01Aa	95.93 ± 1.70Aa	96.97 ± 0.93Aa	97.91 ± 0.20ABa
STMP-aqueous-5	0.02 ± 0.00Db	0.03 ± 0.00Da	0.04 ± 0.00Ea	75.74 ± 0.52Cb	80.26 ± 0.56Da	79.25 ± 1.38Dab
STMP-aqueous-10	0.06 ± 0.00Cb	0.12 ± 0.02Ba	0.13 ± 0.00Ca	84.63 ± 1.44Bb	88.95 ± 0.74Ca	92.62 ± 0.59Ca
STMP-aqueous-12	0.11 ± 0.02Bb	0.12 ± 0.01Bb	0.15 ± 0.00Ba	96.30 ± 1.57Aa	92.50 ± 0.37Ba	95.26 ± 1.08Ba

Data are means ± standard deviation (n=3). Means within columns not sharing a capital letter and means within rows not sharing a common letter are significantly different at $p < 0.05$. RC (regular corn); FB (faba bean); FP (field pea); POCl$_3$-aqueous (1% and 2% POCl$_3$ in aqueous slurry at 25 °C); STMP-semidry (2% and 4% STMP/STPP [99:1. w/w] in a semidry state at 130 °C); STMP-aqueous (5%, 10%, and 12% STMP/STPP [99:1. w/w] in aqueous slurry at 45 °C).

"C-type" (a mixed A and B types; legume starches) crystalline structures, branch points are mostly found in amorphous region and thereby may retain higher levels of phosphorylation chemicals in the branched regions than "A-type" (cereal), where branch linkages also exist in the crystalline lamella (Jane and others 1997; O'Brien and Wang 2008). In addition, the diffusion pattern of phosphorylation reagents into the starch granules are different between pulse starch and corn starch, mainly due to the lack of channels in pulse starch granules. This is consistent with the FE-SEM images (Fig. 8.3) that treatment with amylolytic enzymes enlarged the channels of corn starch granules, while that of pulse starch showed opening/splitting of granules along grooves. Furthermore, the different reaction efficiencies between pulse and corn starches may be due to the higher amylose content of pulse starches, where AM-AP cross linkages are likely to dominate. This is consistent with the view that amylose molecules are interspersed among amylopectin molecules and are crosslinked to amylopectin during reaction (Jane and others 1992; Kou and Gao 2018; Shen and others 2019). In addition, the higher content of amylose being interspersed among amylopectin molecules in pulse starches may also lead to formation of mono-starch esters (i.e., substitution reaction) along the amylose chains more than that in corn starch. Thus, more phosphorus can be incorporated into pulse starches.

8.3.3. Degree of crosslinking (DC) by percentage amylose crosslinked

A new approach to characterize the DC% based on amylose-iodine complexing was used as described in a recent study (Kou and Gao 2018). According to literature, crosslinking preferentially occurs between chains of amylopectin (AP-AP) and then between amylose and amylopectin (AM-AP), while it may not occur between amylose molecules (AM-AM) due to lack of proximity (Jane and others 1992). Therefore, when an amylose molecule crosslinks with an amylopectin molecule, the new amylose-amylopectin complex structure would not be able to complex with iodine to form

the blue color. Thus, the measured true amylose content decreases. Increasing concentrations of crosslinking reagent from 2 to 4% for STMP-semidry, and 5 to 12% for STMP-aqueous method significantly increased DC (Table 8.1). It was observed that the DC increased to the range of 92.5%-97.9% at higher levels of crosslinking reagents at 4% for STMP-semidry and 12% for STMP-aqueous. However, all starches showed high DC (> 96%) for $POCl_3$-aqueous treatment. This indicated that $POCl_3$-aqueous was a very efficient crosslinking method to bind amylose molecules with amylopectin molecules of native starch. Moreover, pulse starch, FB and FP showed a better reaction efficiency than RC starch upon all phosphorylation techniques except $POCl_3$-aqueous, where no significant difference was shown among starch types. This may be due to the different starch polymorph of pulse starch ("C-type" crystalline) and corn starch ("A-type" crystalline). This result was in agreement with a previous report which suggested "C-type" starch reacted more quickly than A-type starch upon crosslinking by STMP-aqueous method (Kou and Gao 2018). The same factors influencing P% are also responsible for the difference in DC, being higher in pulse starches than in corn starch as discussed in section 8.3.2.

8.3.4. Amylase resistance of ungelatinized phosphorylated starches

Amylase resistance (AR) of modified starches tends to be influenced by different types of starches and the crosslinking phosphorylation techniques. The amount of rapidly digestible (RDS), slowly digestible (SDS), very slowly digestible (VSDS) and resistant (RS) starch in native and modified granular starches are presented in Fig. 8.2 (A-C). The extent of digestion (after 120 min) among native starches followed the order: RC (51.27%) > FP (48.20%) > FB (34.42 %) (Fig. 8.2 A-C). The high AR of native pulse starches could be explained by their higher amylose content and longer amylose and amylopectin chain lengths as well as starch polymorph type ("C-type" vs "A-type") (Chung and others 2009). This is in coincidence with previous reports, which have proposed
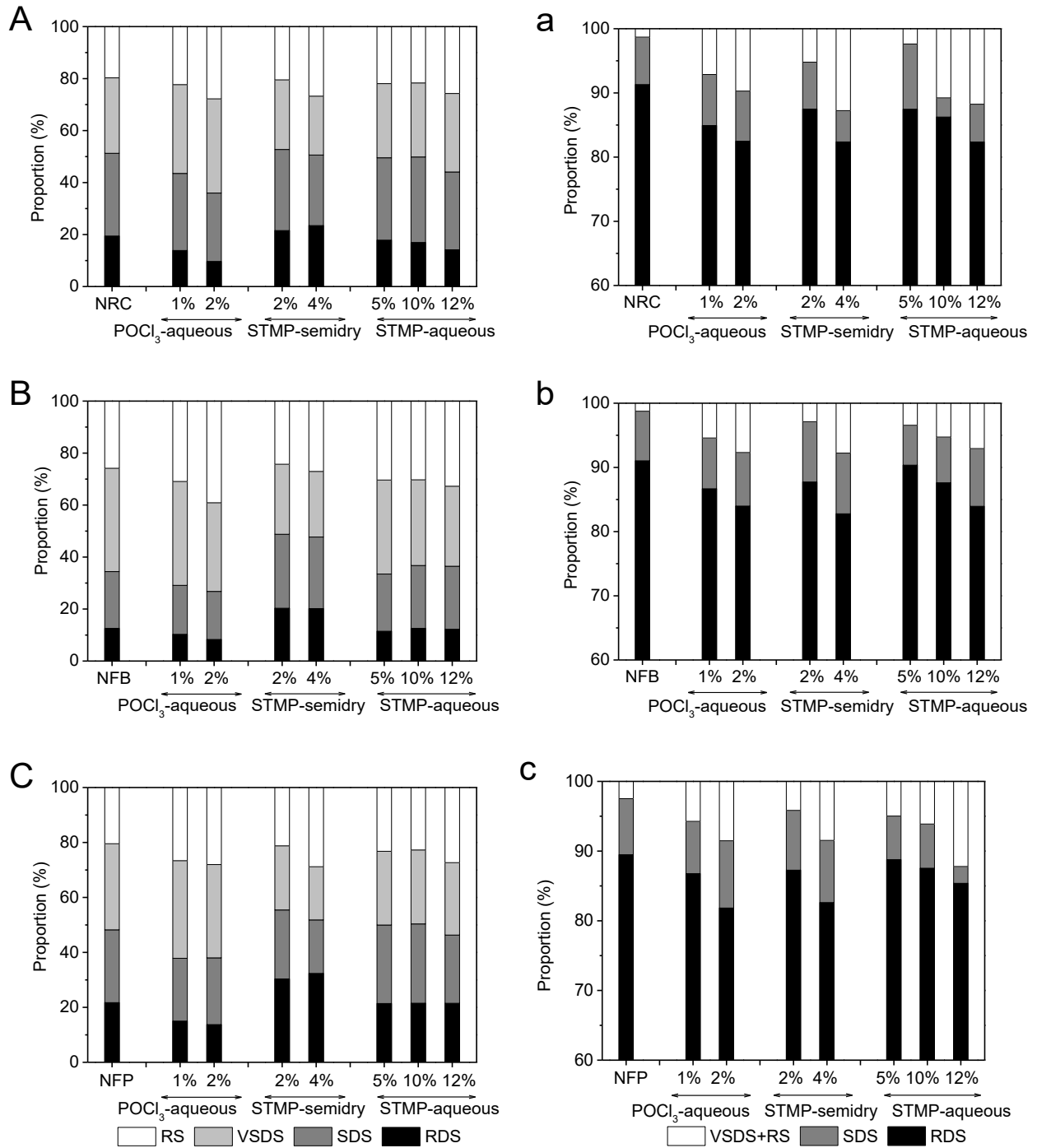
Fig. 8.2 Digestion profiles of native and phosphorylated starches before (A-C) and after gelatinization (a-c). RDS (rapidly digestible starch); SDS (slowly digestible starch); VSDS (very slowly digestible starch); RS (resistant starch); VSDS+RS (very slowly digestible starch + resistant starch);NRC (native regular corn starch); NFB (native faba bean starch); NFP (native field pea starch); POCl$_3$-aqueous (1% and 2% POCl$_3$ in aqueous slurry at 25 °C); STMP-semidry (2% and 4% STMP/STPP [99:1. w/w] in a semidry state at 130 °C); STMP-aqueous (5%, 10%, and 12% STMP/STPP [99:1. w/w] in aqueous slurry at 45 °C).

that AR of starch is affected by the size and arrangement of AM and AP molecules in the amorphous and crystalline structure as well as their interactions with non-starch molecules/components (i.e. phosphate) (Jane and others 1997; O'Brien and Wang 2008; Shrestha and others 2012; Dhital and others 2017). The presence of branch linkages in the crystalline structure of "A-type" (cereal) starches produced 'weak' points that are more susceptible to amylolysis. Whereas, in "B-type" (tuber and high amylose starches) and "C-type" (a mixed A and B types; legume starches) more branch points were found in the amorphous region and thereby provide a more superior crystalline structure that increased the AR (Jane and others 1997; Chung and others 2009). In addition, pulse starches possess a larger granular size (i.e., less surface area/unit mass) when compared to corn starch, which may also contribute to their lower digestibility (i.e., higher AR). This is consistent with previous studies, where larger granules have been reported to have lower amylolysis rates as compared to smaller counterparts (Naguleswaran and others 2012).

Phosphorylation with $POCl_3$ significantly decreased the RDS and SDS, while increased the VSDS and RS levels in all ungelatinized modified starches. For instance, the RDS content of pea starch was 21.7% ± 0.5%, 15.0% ± 0.8%, and 13.7% ± 0.4%, and RS content was 20.5% ± 0.8%, 26.6% ± 0.5%, and 28.0% ± 1.4% in native FP, 1% $POCl_3$-aquoues FP, and 2% $POCl_3$-aquoues FP starch, respectively. The extent of these changes was more pronounced with 2% $POCl_3$, since more phosphorus binding occurred than with 1% $POCl_3$ (Table 8.1). The decrease in RDS and the increase in RS levels of crosslinked starches indicated that interactions between starch chains (AP-AP and/or AP-AM) were enhanced by phosphate group, thus improving the AR of starch.

STMP-semidry increased RDS and RS and decreased SDS and/or VSDS levels in all three ungelatinized starches (Fig. 8.2A-C). STMP-semidry modified starches were rapidly digested compared with native starch at the early stages (within 20 min); however, digestion was more pronounced in native starches after 120 min. For instance, native RC, 2% STMP-semidry RC and 4% STMP-semidry RC were digested to the extent of 19.4% ± 0.1%, 21.5% ± 0.7%, and 23.5% ± 0.4%, respectively, after 20 min. Whereas, after 16 h, native RC, 2% STMP-semidry RC and 4% STMP-semidry RC were digested to the extent of 80.3% ± 1.5%, 79.53% ± 2.6%, and 73.3% ± 3.0%, respectively. The increase in RDS could be explained by the heating procedure involved. The heating procedure may have led to the disruption of double helices of crystalline structure which was critical for defining the rate and extent of amylase hydrolysis (Gunaratne and Hoover 2002; Chung and others 2009). Consequently, the crystalline disruption of STMP-semidry starch may facilitate the rapid entry of amylase into granule interiors. The increase in RS on STMP-semidry indicated the enhanced starch chain interaction by crosslinking.

STMP-aqueous method decreased the RDS and increased RS level in RC starch; however, it did not show significant change in pulse starch, especially at lower chemical concentration. At a chemical concentration of 12%, RS levels increased from 19.7% ± 1.1% to 25.7% ± 1.1%, 25.8% ± 0.4% to 32.8% ± 0.7%, and 20.46% to 27.3% ± 1.1% in RC, FB, and FP, respectively. Among both STMP methods, STMP-semidry with 4% STMP/STPP mixture, although disrupted the crystalline structure of starch, increased RS level compared to that of STMP-aqueous with 12% STMP/STPP mixture. As shown earlier, the %P was higher in 4% STMP-semidry starch than 12% STMP-aqueous starch, therefore, in ungelatinized phosphorylated starches, their AR was influenced not only by phosphorylation but also the crystalline structure of starches.

The morphological and granular architectural changes of native and crosslinked starches caused by the synergistic action of α-amylase and amyloglucosidase, at 20 min, 2 h, and 16 h, is presented in FE-SEM micrographs (Fig. 8.3). The surface of starch granules from RC showed pores that lead to channels inside the granules (Fig. 8.3A, D, G). The pores and channels facilitate amylase access into the granules, which leads to rapid digestion of granules "inside out" (Shrestha and others 2012; Naguleswaran and others 2012; Naguleswaran and others 2013). With increasing hydrolysis time from 20 min (Fig. 8.3A) to 120 min (Fig. 8.3D), the pores on the surface of RC starch granules enlarged (Fig. 8.3A, D, G). After 16 h digestion, the starch granules fragmented, while some intact starch granules still existed (Fig. 8.3G). The granules of FB and FP starches also showed digestion patterns "inside-out". However, the splitting of the granules was observed along the grooves (Fig. 8.1) that seemed to have facilitated easy enzyme access to the interior of granules as shown in Fig. 8.3 B, E, H and Fig. 8.3 C, F, I. The growth rings were remarkably visible after 120 min (Fig. 8.3 E, F) of digestion than 20 min (Fig. 8.3 B, C). These observations differ from that of potato starch ("B-type" crystalline), where the enzymes initiate the digestion from the surface towards the granule interior in an "outside in" pattern (Gallant and others 1992). This could be possibly explained by the view that in "C-type" starches, "B-type" polymorphs exist in the interior and is surrounded by the A-type polymorphs at the periphery of starch granules (Cai and others 2014).

In all starches, crosslinking did not change the nature of digestion pattern (Fig. 8.3). However, the extent of amylase attack was observed to be different at all time intervals (Fig. 8.3 J-R shows micrographs only for residues after 120 min of digestion). This was remarkably visible in RC starch, where crosslinking by POCl$_3$-aqeous and STMP-aqueous inhibited the enlargement of pores on the granule surface (Fig. 8.3 J, P, respectively). In pulse starches, it was interesting to
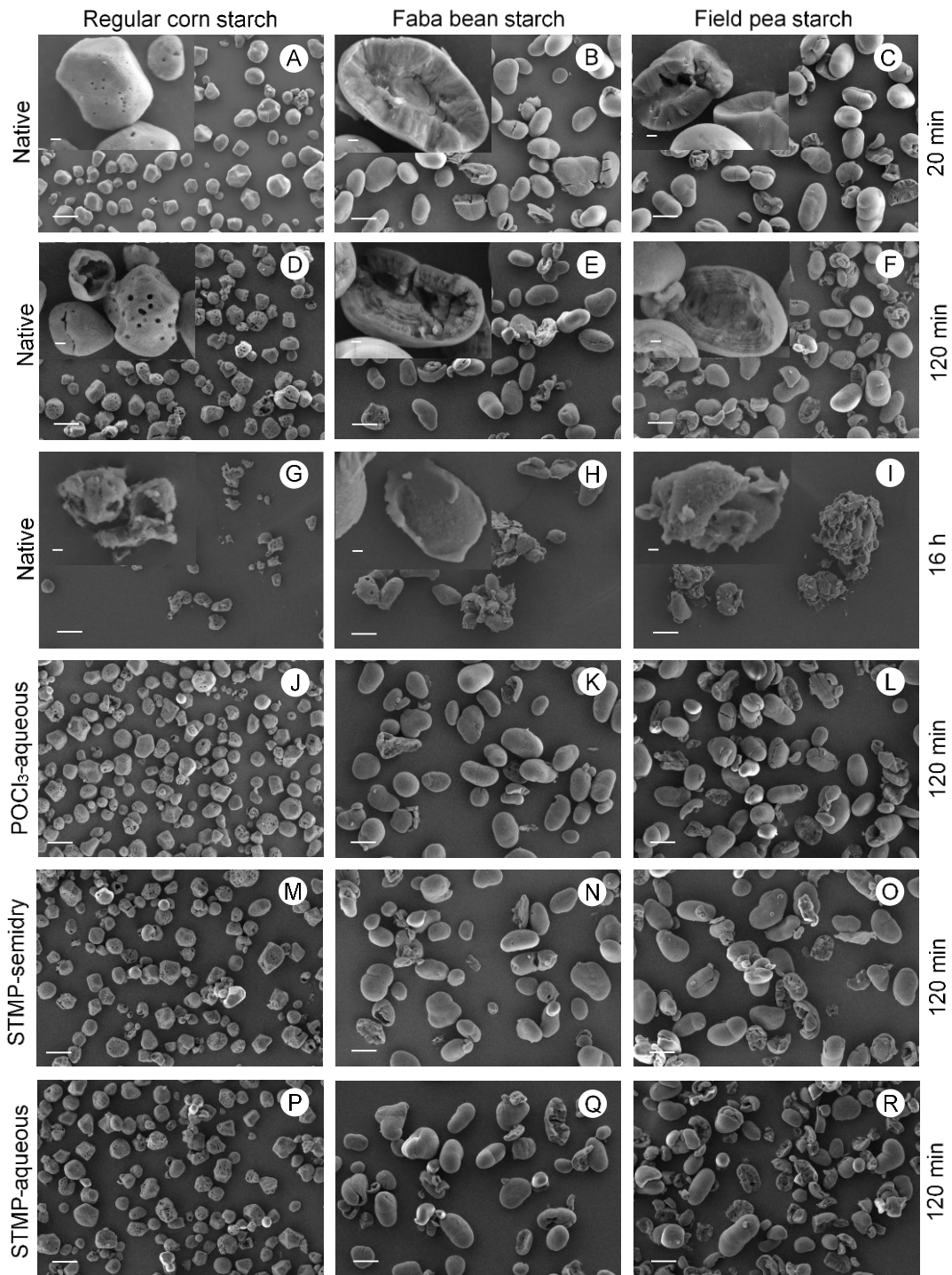
Fig. 8.3 Morphology of enzyme hydrolyzed starch residue of native starches after 20 min (A-C), 120 min (D-F), 16 h (G-I); POCl$_3$-aqueous modified starches after 120 min (J-L); STMP-semidry modified starches after 120 min (M-O); STMP-aqueous modified starches after 120 min (P-R) (×500, scale bar = 20 μm). Insets in A-I were at ×2000, scale bar = 2μm.

note that the extent of splitting was mitigated by cross-linking, but highly prominent in POCl$_3$-aqueous modified samples, where split regions were clearly observed, and the split-halves of the granules remained together. This may be possibly due to the instantaneous nature of the POCl$_3$ reaction, leading to more surface-oriented cross-linking along the grooves. This is also true for RC, where minimal enlargement of pores was observed.

8.3.5. Amylase resistance of gelatinized phosphorylated starches

Studies have clearly demonstrated that the rate of starch digestion is influenced by a number of factors in their native/uncooked state, such as granular size, starch granular architecture, non-starch components and molecular structure. However, in the present study, in order to reflect the true end use scenario of starches (i.e., food use), the amylase action on gelatinized/cooked starches was focused, where the effect on amylolysis by the granular-structural attributes of uncooked starch is mostly eliminated by cooking. The amylase digestibility profiles of native and phosphorylated starches after gelatinization are presented in Fig. 8.2 a-c. As expected, all gelatinized native starches showed higher RDS, which was up to 92% (i.e., at 20 min digestion), and the extent of digestion did not increase after 120 min. Therefore, the values for VSDS and RS fractions together (denoted as VSDS+RS) were presented. The high RDS values of gelatinized starches, both native and modified, were due to the disruption of the crystalline structures of starch granules by gelatinization which enhanced enzyme accessibility to starch and accelerated digestibility. However, cross-linking decreased the RDS content and increased the "VSDS+RS" levels when compared to their native counterparts. Furthermore, changes to RDS and "VSDS+RS" levels on modified starch for all starch types were more pronounced at higher concentrations of chemicals (2% POCl$_3$ for POCl$_3$-aqueous, 4% and 12% STMP/STPP mixture for STMP-semidry and STMP-aqueous, respectively). For instance, when the starch was phosphorylated with 2% POCl$_3$, the RDS

content decreased as compared to gelatinized native starch by 8.8%, 7.0%, and 7.64%, and the "VSDS+RS" content increased by 8.4%, 6.4%, and 6.0% for RC, FB, and FP starches, respectively. Compared with uncooked starches (Fig. 8.2 A-C), after gelatinization (Fig. 8.2 a-c), STMP-semidry starches had different behavior, which exhibited lower RDS content among all starch samples than their native counterpart. This was because the influence of heating procedure involved in this method on the crystalline structure could be eliminated by gelatinization and the influence of phosphorylation on RDS content was shown. Comparing the two STMP methods, STMP-semidry method with lower concentration of chemical used showed comparable AR than STMP-aqueous methods after gelatinization. This could be explained by the higher %P and DC in STMP-semidry starches (Table 8.1).

The increase in thermo-stable "VSDS + RS" suggested that the interactions formed between starch molecules (phosphate linkages between AP-AP and/or AP-AM) during modification may have survived after gelatinization, thereby restricting accessibility of certain starch chains to amylolysis. However, in contrast to the earlier studies that were mainly performed on wheat starch (Woo and Seib 2002; Shukri and others 2013; Shukri and others 2015), the observed increase in the present study in AR, determined on phosphorylated starches after gelatinization, although significant, is not substantial enough to be commercially appealing. This could be explained by the difference of *in vitro* method used for measurement of AR, as *in vitro* levels of RS are method dependent; it is debatable which methods should be used, and consequently, contradictory information was found in literature as mentioned earlier.

8.3.6. Effect of phosphorus content and degree of crosslinking on amylase resistance of gelatinized starch

In order to understand how phosphorylation affects AR, the correlations between %P vs AR and DC vs AR were investigated. The correlations were performed only within gelatinized starches in order to avoid the influence of starch crystalline structure in granular starches. The % change in RDS, SDS, and "VSDS+RS" content as well as %P and DC for each gelatinized native starch (i.e. control) and their gelatinized modified (i.e. phosphorylated by 3 different methods) (Kou and Gao 2018) counterparts are presented in Fig. 8.4. Amongst the starch types, corn responded better than pulses to all phosphorylation methods (i.e., % change in RDS and "VSDS+RS"). Furthermore, within each starch type and phosphorylation methodology, the RDS decreased and "VSDS+RS" increased with increasing %P and DC. However, phosphorylated pulse starches, although showed higher %P and DC, showed lower % decrease in RDS and increase in "VSDS+RS". This could be explained by the higher amylose content of pulse starches. As mentioned earlier, crosslinking occurs primarily between amylopectin molecules and that between amylopectin and amylose molecules is secondary (Jane and others 1992; Kou and Gao 2018). This was because the amorphous regions of amylopectin were more rigid and structured than the free amylose molecules, which may require extensive steric positioning for efficient cross-linking. Since the amylose content of pulse starches is higher than corn, the proportion of AP-AM crosslinks are expected to be more in pulses. In other words, starch from corn would have had more AP-AP cross-links when compared to pulses. Thus, the observed increase in AR was more in phosphorylated corn than pulse starches, which indicates that AP-AP crosslinking is dominantly influencing AR. Furthermore, higher %P and lower DC observed in both STMP modified starches indicates that STMP modified starches had undergone more phosphorous substitution (i.e. mono starch

phosphate) when compared to POCl₃ modified starch, where the effect of substitution on AR would be minimal (Sang and others 2010).
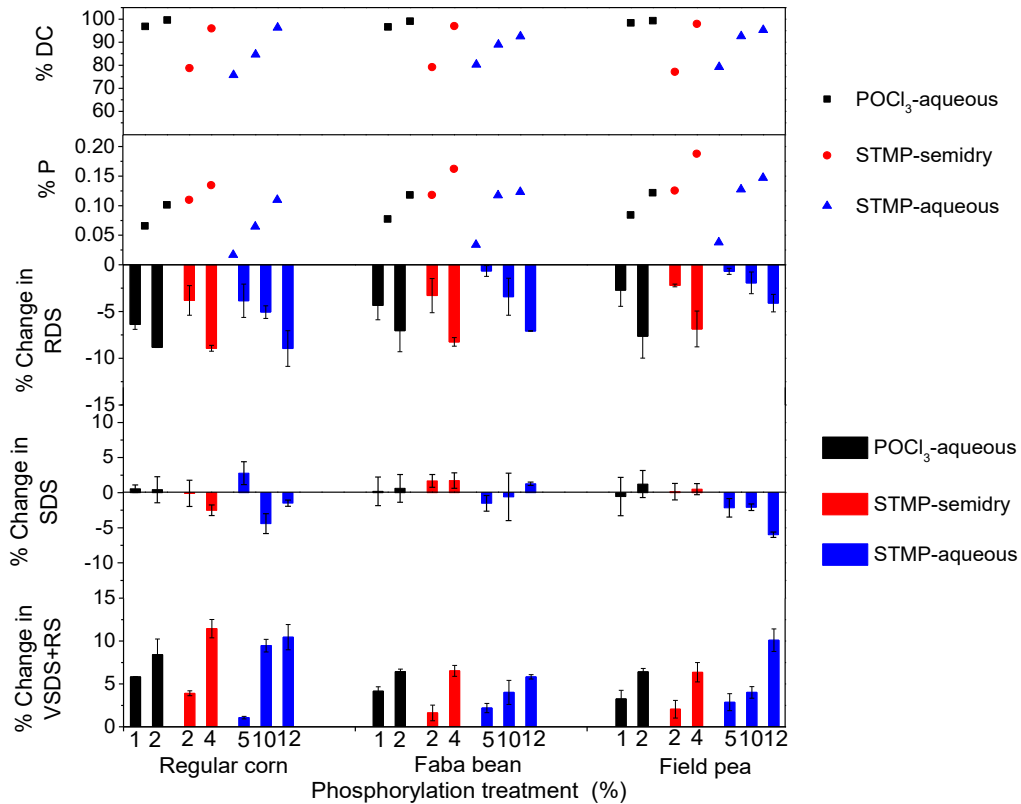
Fig. 8.4 The % change in RDS, SDS, and "VSDS+RS" content, as well as phosphorus content (% P, w/w) and degree of crosslinking (DC, %) for phosphorylated starches after gelatinization. RDS (rapidly digestible starch); SDS (slowly digestible starch); VSDS (very slowly digestible starch); RS (resistant starch); VSDS+RS (very slowly digestible starch+ resistant starch); NRC (native regular corn starch); NFB (native faba bean starch); NFP (native field pea starch); POCl₃-aqueous (1% and 2% POCl₃ in aqueous slurry at 25 °C); STMP-semidry (2% and 4% STMP/STPP [99:1. w/w] in a semidry state at 130 °C); STMP-aqueous (5%, 10%, and 12% STMP/STPP [99:1. w/w] in aqueous slurry at 45 °C).

The graphs of %P or DC vs % change in "RDS" / "VSDS+RS" for all 3 starch types and 3 phosphorylation methods is presented in Fig. 8.5. The %P or DC had an inversely proportional correlation with % change in RDS, and a directly proportional correlation with the % change in "VSDS+RS", but with moderate correlation coefficients. This may be due to the interplay between different starch sources and phosphorylation methods. The correlation coefficients observed between DC vs % change in RDS was significantly higher than that between phosphorus content vs % change in RDS (r = -0.6790 and -0.4604, respectively, p<0.05). A similar trend was observed in "VSDS+RS" (r = 0.6050 and 0.4126, respectively, p<0.05). Therefore, DC measured by amylose-iodine binding method maybe a better parameter than merely the phosphorous content to show the effect of phosphorylation on AR. This may be attributed to the fact that during phosphorylation, both substitution and cross-linking reactions occur simultaneously but to different extents, where these reactions influence AR differently (Sang and others 2007; Sang and others 2010; Shukri and Shi 2017). This result is in accordance with previous studies that reported wheat starch phosphorylated with STMP under different conditions to similar amount of %P (~0.4%) gave a wide variation in the extent of AR, where higher levels of cross-linking resulted in higher AR (Sang and others 2007; Sang and others 2010).
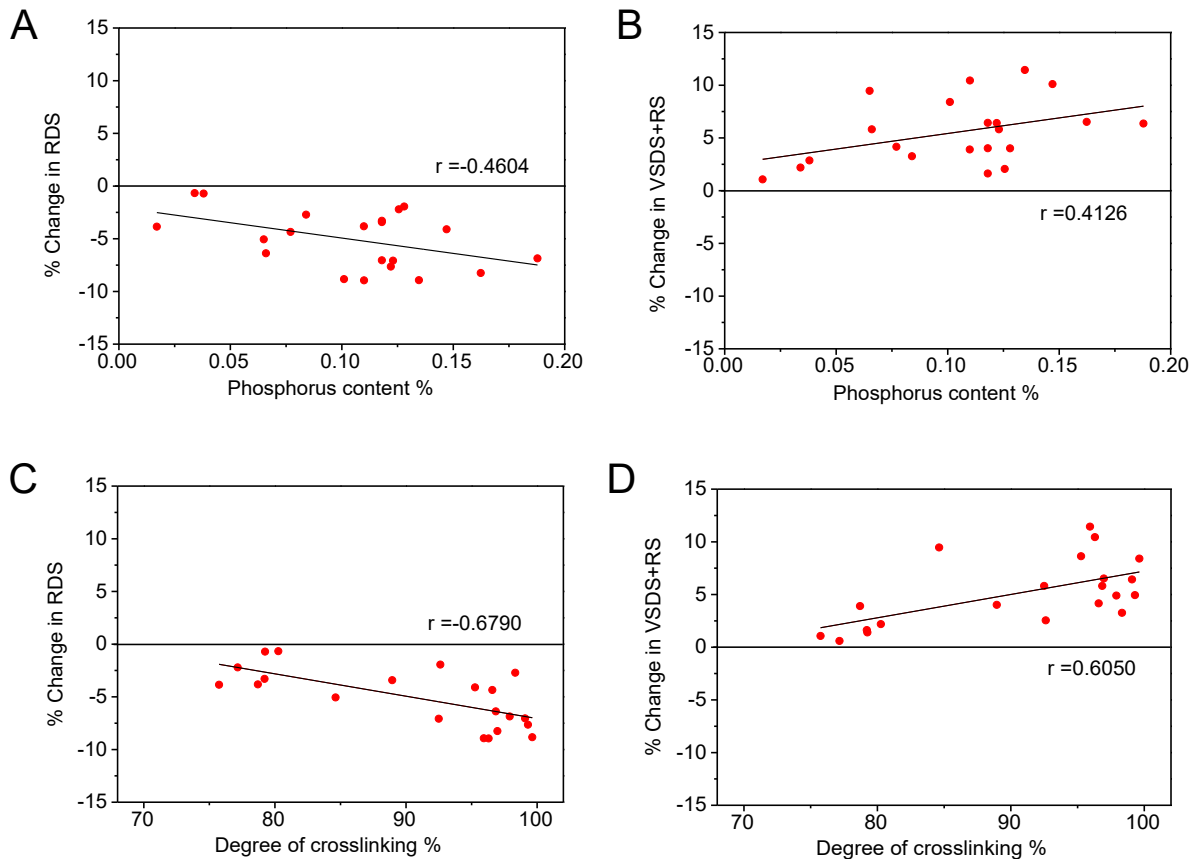
Fig. 8.5 Linear regression of: A) phosphorus content and % change in RDS, B) phosphorus content and % change in "VSDS+RS", C) degree of crosslinking and % change in RDS, and D) degree of crosslinking and "VSDS+RS" of phosphorylated starches prepared by three different phosphorylation techniques after gelatinization. r values within different graphs ac or bd not sharing a common letter are significantly different at p < 0.05. RDS (rapidly digestible starch), "VSDS+RS" (very slowly digestible starch + resistant starch).

8.3.7. The effects of starch types and phosphorylation methods on amylase resistance

The correlation coefficient between DC vs AR (represented by both % change in RDS and VSDS+RS) was significantly higher than that between % P vs AR (Fig. 8.5). Therefore, the effect of starch types and phosphorylation methods on starch AR was evaluated by plotting the graphs of DC vs AR individually for each type of starch and phosphorylation methods (Fig. 8.6a-f). As shown in Fig. 8.6a-c, different phosphorylation techniques significantly influenced the relationship between DC and AR of starch (represented by the % change in VSDS+RS), where extent of the influence was the greatest in FP starch followed by RC and FB starch (r=0.627, 0.724, 0.910, respectively, p<0.05). The influence of starch type on the relationship for different phosphorylation techniques followed the order: $POCl_3$-aqueous (r=0.590) > STMP-aqueous (r=0.716) > STMP-semidry (r=0.799) with significant difference (p<0.05) (Fig. 8.6d-f). Thus, it is evident that interaction between starch type and phosphorylation method plays an important role in the relationship between DC and AR. This may be attributed to the location and distribution of phosphate cross-linkages formed in different starches differing with phosphorylation methods. Similar trends were also observed with DC vs AR of starch (represented by % change in RDS, data were not shown). Those results suggested that different starch behaved differently during phosphorylation and may play a major role in influencing the effect of phosphorylation on starch AR.
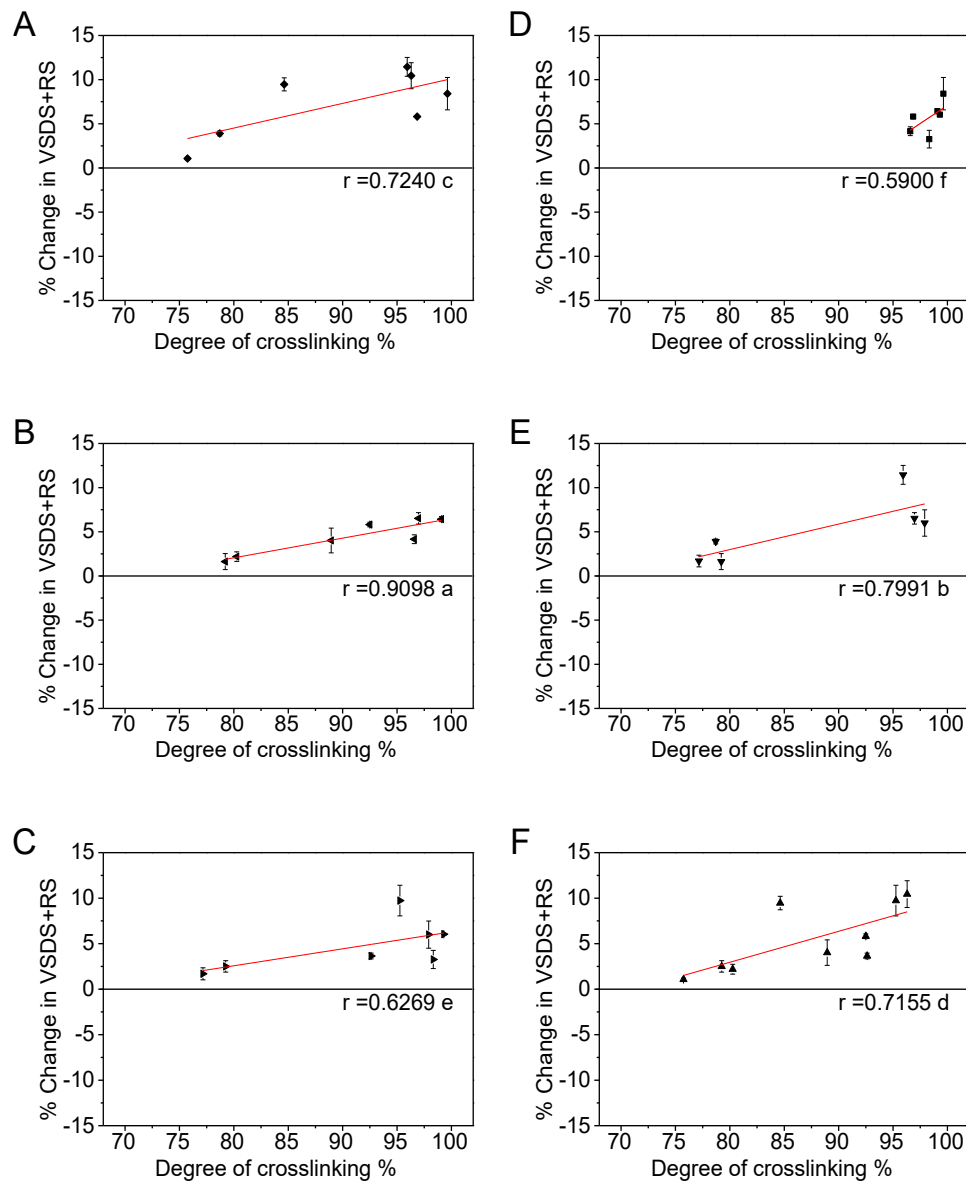
Fig. 8.6 Linear regression of degree of crosslinking and % change in "VSDS+RS" (very slowly digestible starch+ resistant starch) of phosphorylated starches prepared by three different phosphorylation techniques to show the effect of phosphorylation method and starch type on amylase resistance after gelatinization: data for each starch phosphorylated by three methods: (A) RC (regular corn), (B) FB (faba bean), (C) FP (field pea); data for each method with three starch types: (D) $POCl_3$-aqueous (1% and 2% $POCl_3$ in aqueous slurry at 25 °C), (E) STMP-semidry (2% and 4% STMP/STPP [99:1. w/w] in a semidry state at 130 °C), (F) STMP-aqueous (5%, 10%, and 12% STMP/STPP [99:1. w/w] in aqueous slurry at 45 °C). r values not sharing a common letter are significantly different at $p < 0.05$.

8.3.8. Proposed mechanism for phosphorylation increasing RS4

The phosphorylation reaction and the bonding of phosphate to starch in various forms indicates that phosphorylation converts a portion of rapidly digestible amorphous regions of native starch to RS4. As shown in Fig. 8.7, native starch has crystalline and amorphous regions, where the crystalline region is amylase resistant due to tight molecular packing, and the amorphous region is free starch and thus is rapidly digestible. During chemical modification, the phosphorylating reagent preferentially binds to the amorphous region and thus starch structure is modified. Therefore, a certain amount of RDS is converted into RS4, which is resistant starch. Upon the cooking/gelatinization of unmodified and phosphorylated starches, crystalline regions would melt and increase the RDS content. However, in modified/phosphorylated starch, RS4 increases because some of the RDS fraction of native starch is already converted into resistant starch by the phosphate cross-linkages during modification. The observed decrease in RDS and increase in "VSDS+RS" may be attributed to this mechanism. Therefore, these results suggest that few but strong residual phosphorus interactions and thermally stable starch structure after crosslinking may have contributed to produce RS4 after gelatinization. In other words, the combination of starch crystalline structure and phosphate cross-linkages in uncooked starch increased the AR (i.e., both RS2 and RS4), whereas in gelatinized starch only the RS4 remained undigested. These RS4 fractions can remain solubilized within the digested solution, but not available for enzyme digestion and thus can be considered as soluble dietary fiber. Further studies are required to verify the molecular characteristics of this soluble RS4 portion.
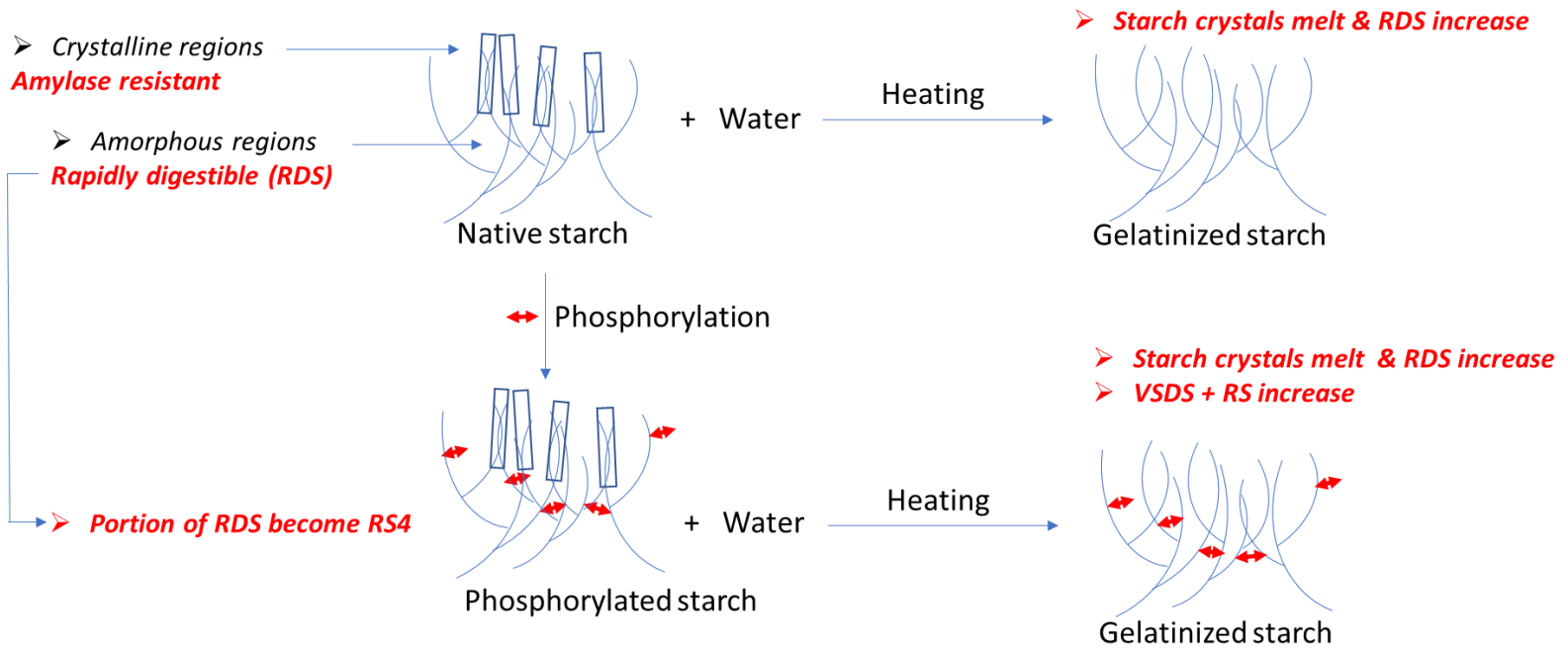
Fig. 8.7 The proposed mechanism of phosphorylation for increasing RS4.

8.4. Conclusion

Crosslinking of starch by all three phosphorylation methods did not remarkably influence the morphology of starch. The phosphorylation efficiencies of isolated pulse starches were significantly higher than of regular corn. The pattern of amylase action was observed to be different between pulse (splitting) and corn (channeling) starches. AR of modified starches when determined after gelatinization enabled the understanding of the effect of phosphorylation in the absence of granular architectural features such as granular size and crystalline structure. In all ungelatinized/granular starches, $POCl_3$-aqueous method showed the highest % increase in AR when compared to STMP-semidry and STMP-aqueous. In gelatinized starches, all phosphorylation techniques reduced RDS and increased "VSDS+RS". Phosphorylation influences AR of corn starch better than pulse starches, despite the lower % P content of modified corn starches. The correlation between DC vs AR was significantly higher than that between % P content vs AR. In general, AR of crosslinked phosphorylated starch is influenced more by the types of starch than by phosphorylation techniques. This implies that industry needs to precisely control the starch source in order to supply modified starch with consistent AR properties. In contrast to the earlier reports, the present study found that the increase in AR of gelatinized phosphorylated starches, although significant, but was not substantial enough to be commercially appealing. Further research is warranted to determine the ratio of crosslinking vs substitution in different starch sources during phosphorylation by different techniques, and how the ratio influences AR.

Chapter 9: Conclusions and perspectives

9.1. Summary and significance of research

Pulse grains are rich in nutritionally superior protein. The fast-increasing demand for plant protein has triggered the development of many pulse grain fractionation and refining operations across the world. However, native pulse starches are not preferred in food and industrial applications primarily due to their high amylose content (~40%) and their high capacity for retrogradation (Hoover and others 2010). In other words, pulse starches are not stable when cooked in water to solubilize and form a starch paste, and the texture of the paste quickly becomes a hard gel upon storage. The modification of pulse starch using chemical, physical, and/or enzymatic methods to improve their inherent properties becomes essential for developing wider food and industrial applications. Starch nanoparticles (SNPs) represent a potential natural and environmentally sustainable nanomaterial to be used in food and non-food applications. Nanoprecipitation is a promising method in the production of nanoparticles from biopolymers due to its simplicity and pragmatic potential for scale up processing. To date, SNPs from waxy corn and potato have been subjected to intense research related to their production, characterization and applications especially in polymer nanocomposites and bioplastics. However, the use of pulse starches as the raw material for SNP extraction has received little attention and thus presents a research opportunity. Furthermore, phosphorylation is the most commonly used chemical modification to eliminate the shortcomings of native starch and thus improve starch textural properties, thermal/shear resistance, and acid stability, as well as paste stability (Hoover and others 2010). However, limited information is available on pulse starch phosphorylation. Therefore, finding novel applications to pulse starches by nanoparticulation and chemical modification will positively impact the Canadian grain industry.

The present thesis addresses some of the research gaps on the pulse starches nanoparticulation and chemical modification. This body of work contributes to the foundation of growing research necessary to fully utilize pulse starches, through both nanoparticulation and chemical modification, in food and other industries. Through developing and evaluating a novel method involving ultrasound-assisted dissolution and rapid nanoprecipitation, the potential of SNPs novel characteristics in comparison to cereal starches was demonstrated. The formation and physicochemical properties of SNPs can vary according to: a) the processing conditions, such as ultrasonic amplitude, starch concentration, antisolvent-to-solvent (AS/S) ratio, the mode of antisolvent addition, and nanoparticle recovery methods, etc., b) the starch source, c) amylose content, d) morphology, e) particle size, and f) thermal stability. With regards to the mechanism of SNP formation using anti-solvent nanoprecipitation, this study indicated amylose molecules likely formed the initial critical nuclei. Subsequently, the role of amylose and amylopectin in SNP formation was established. Through three different phosphorylation techniques, the structure-phosphorylation-functional property relationships of pulse and corn starches was demonstrated. The extent of changes in physicochemical and structural properties of starch significantly differed among phosphorylation techniques and starch sources, which were possibly due to the differences in amylose content and molecule size, molecular structure of amylopectin, phosphorylation agent, reaction conditions, as well as the location and distribution of phosphate groups in starch granules. The above findings confirmed there is a strong relationship between the structure and function of modified starch, in particular in amylose containing starches such as corn, wheat, faba bean and field pea. Thus, proper selection of the raw starch material and the processing protocol can be used to control the functionality of modified starches for different food and non-food applications.

In Chapter 3, SNPs from field pea starch were obtained by the combination of ultrasound-assisted dissolution and rapid nanoprecipitation. The effects of processing parameters, such as duration and amplitude of ultrasonication, AS/S ratio, starch concentration, separation and drying techniques were investigated. The results indicated that there was an optimal AS/S ratio (1:1, v/v) and starch concentration (10 mg/mL) that would reliably give rise to smaller SNPs with a narrower PSD. The formation of SNPs was found to follow a kinetically controlled nucleation-growth/aggregation mechanism in which amylose molecules likely formed the initial critical nuclei. Apart from the AS/S ratio and starch concentration, the ultrasonication amplitude and separation and drying techniques significantly influenced the size and morphology of SNPs. The application of moderate shear to the synthesized SNPs in ethanol-water mixture facilitated rapid aggregation and precipitation of SNPs which were easily recovered by centrifugation and preserved with freeze drying. The freeze-dried SNPs were able to disperse quickly and quantitatively in water, and were stable in water as demonstrated by retaining their particle characteristics at temperature ranges of 25-60 °C.

The protocol developed in Chapter 3 was further applied and investigated in Chapter 4 for the production of SNPs from other starch sources, including two types of cereal starch (regular corn and wheat) and two types of pulse starches (faba bean and field pea). The effect of starch type, amylose content, starch concentration, and AS/S ratio on the formation of SNPs were investigated. The molecular composition and size, crystalline structure, molecular order, and thermal properties of the SNPs formed were also characterized and compared under identical formation conditions in Chapter 4. The experimental results revealed that pulse starches were superior in forming smaller, uniform spherical SNPs with respect to operational conditions. All freeze-dried SNPs could be

redispersed in water. Compared with cereal SNPs, pulse SNPs with higher amylose content and smaller molecular weight showed a greater relative crystallinity, more ordered short-range structure, and better thermal stability.

In Chapter 5, static and dynamic rheological properties of the aqueous SNP suspensions were investigated by rotational and oscillatory rheometry. The viscosity and viscoelastic behavior of SNP suspensions were determined as a function of shear, frequency and temperature, and were dependent on starch source and SNP concentration. The SNP suspensions exhibited a viscous liquid-like behavior at smaller concentrations (i.e., 1% w/v), but an elastic solid-like behavior at high concentrations (i.e., 5% w/v). Interestingly, at 5% (w/v) concentration, SNP suspensions showed an non-thixotropic behavior demonstrating the capacity of the suspension to instantaneously recover from the applied shear deformation. However, pulse SNPs displayed relatively greater viscosities and more elastic behavior than cereal SNPs, indicating their potential to form extensive inter-particulate associations. A schematic diagram (Fig. 5.11) was developed to explain the observed rheological behaviors, predicting inter-particulate network formation at room temperature and the biphasic molecular network formation during heating of aqueous SNP suspensions. The careful selection of starch type and processing conditions, such as temperature and shearing conditions, is required to achieve a desired functionality for SNPs for the food industry, particularly in applications such as thickening and texture modification.

Although scalable production of SNPs has not been widely explored, the successful production of SNPs using the rapid nanoprecipitation process would make it possible to use continuous processing devises. Therefore, in Chapter 6, SNPs were prepared from field pea starch by

continuous nanoprecipitation, flash nanoprecipitation (FNP) and microfluidic nanoprecipitation (MNP). Their morphological and physicochemical characteristics were determined and compared to counterparts made from batch nanoprecipitation (BNP). The effects of operation parameters on the particle characteristics were investigated, such as AS/S ratio, starch concentration, mixing technique and flow rate. SNPs with smaller particle sizes and narrower distributions could be prepared by BNP at a starch concentration of 10 mg/mL and AS/S ratio 1:1, in a shorter time by rapid-addition (R-BNP) than by slow-addition (S-BNP). Under the same conditions, FNP involving confined impinging jet mixer (CIJM) at an overall flow rate of 60 mL/min, had a uniform spherical shape with a particle size of ~100 nm, which was superior to all other techniques investigated. Regardless of the techniques used, all SNPs had an amorphous structure with short-range molecular order. This shows that the continuous production of SNPs through FNP involving CIJM mixer design is a simple and economic way to prepare SNPs with tunable sizes. This then meets the requirement for scale-up processing with consistent quality without technical challenges. For the application of SNPs, based on their physicochemical properties, they could be used as thickening, bulking and texturizing ingredients, as well as emulsion stabilizers and drug delivery carriers. In Chapter 6, the ability of SNPs to be used as a stabilizer in a Pickering emulsion was also investigated. Indeed, SNPs were used as a stabilizer to produce Pickering emulsions with a reduced emulsion droplet size. The emulsion produced using SNPs had a droplet size ranged 0.4 and 45 μm with an average droplet size of 3 μm. This small size contributed to their stability against creaming.

In Chapters 7 and 8, native starch was chemically modified using three different phosphorylation techniques based on the widely used commercial processing. The effects of three different

phosphorylations on the structural, thermal, and pasting properties and amylase resistance of starch were investigated. The results indicated cross-linking by phosphorylation significantly increased pasting temperature, decreased breakdown, increased gelatinization temperature and thermal stability and amylase resistance to different extents, which could enable a wide range of applications.

9.2. Future work and recommendations

More research is warranted to make the formation of SNPs commercially appealing. With regards to antisolvent nanoprecipitation, the yield (> 90%) is significantly greater compared to acid hydrolysis (< 15%). The starch concentration used could increase up to 50 mg/mL using pulse starches as a precursor, which then minimizes the amount of antisolvent and water used. Those improvements make this process more economically feasible and environmentally sustainable at a large commercial scale. However, the thermal stability of SNPs needs improvement to facilitate different applications. Since SNPs are mostly amorphous in structure with short range molecular order, increasing the crystalline content after formation would improve their stability. This may be achieved by incorporating a treatment with annealing or including a heat moisture treatment (HMT) after SNP formation. Annealing and HMT have been shown to increase the crystallinity in different starch types and promote crystal growth and stability (Gunaratne and Hoover 2002; Lan and others 2008; Chung, Liu and others 2009). Furthermore, food-grade modification including grafting and cross-linking either towards native starch or SNPs should be investigated to modify the surface reactive groups in SNPs. The aim would be to promote or inhibit intermolecular interactions with different food ingredients. For example, the presence of phosphate would increase the surface charge and provide excellent suspension stability to the resultant SNPs. For the application in a Pickering emulsion, since some of SNP-stabilized emulsion droplets are submicron in size, the ability of SNPs to form nano-emulsions need to be further investigated by reducing the particle size and improving the stability of SNPs. Finally, in the area of

encapsulation, the use of flash nanoprecipitation has been investigated to form hybrid biomaterials using different biopolymers simultaneously (Martínez Rivas and others 2017). This technique can be applied here to produce functional ingredients using SNPs as a delivery system, such as for water-insoluble nutraceutical or drug components. In addition, more research is required to establish potential effect of starch-based nanoparticles on human health by toxicology tests.

References

Abidin MNZ, Goh PS, Ismail AF, Said N, Othman MHD, Hasbullah H, Abdullah MS, Ng BC, Kadir, Siti Hamimah Sheikh Abdul, Kamal F. 2018. Highly adsorptive oxidized starch nanoparticles for efficient urea removal. Carbohydrate Polymers 201:257-63.

Ahmad M, Gani A, Hassan I, Huang Q, Shabbir H. 2020. Production and characterization of starch nanoparticles by mild alkali hydrolysis and ultra-sonication process. Scientific reports 10(1):3533.

Ai Y, Medic J, Jiang H, Wang D, Jane J. 2011. Starch characterization and ethanol production of sorghum. Journal of Agricultural and Food Chemistry 59(13):7385-92.

Ambigaipalan P, Hoover R, Donner E, Liu Q, Jaiswal S, Chibbar R, Nantanga KKM, Seetharaman K. 2011. Structure of faba bean, black bean and pinto bean starches at different levels of granule organization and their physicochemical properties. Food Research International 44(9):2962-74.

Angellier H, Molina-Boisseau S, Dufresne A. 2005. Mechanical properties of waxy maize starch nanocrystal reinforced natural rubber. Macromolecules 38(22):9161-70.

Angellier H, Molina-Boisseau S, Lebrun L, Dufresne A. 2005. Processing and structural properties of waxy maize starch nanocrystals reinforced natural rubber. Macromolecules 38(9):3783-92.

Angellier H, Choisnard L, Molina-Boisseau S, Ozil P, Dufresne A. 2004. Optimization of the preparation of aqueous suspensions of waxy maize starch nanocrystals using a response surface methodology. Biomacromolecules 5(4):1545-1551.

Angellier-Coussy H, Putaux J, Molina-Boisseau S, Dufresne A, Bertoft E, Perez S. 2009. The molecular structure of waxy maize starch nanocrystals. Carbohydrate Research 344(12):1558-66.

Ao Z, Jane J. 2007. Characterization and modeling of the A- and B-granule starches of wheat, triticale, and barley. Carbohydrate Polymers 67(1):46-55.

Ashwar BA, Gani A, Shah A, Masoodi FA. 2017. Physicochemical properties, in-vitro digestibility and structural elucidation of RS4 from rice starch. International Journal of Biological Macromolecules 105:471-7.

Ashwar BA, Gani A, Gani A, Shah A, Masoodi FA. 2018. Production of RS4 from rice starch and its utilization as an encapsulating agent for targeted delivery of probiotics. Food Chemistry 239:287-94.

Aubry J, Ganachaud F, Cohen Addad J, Cabane B. 2009. Nanoprecipitation of polymethylmethacrylate by solvent shifting: 1. boundaries. Langmuir 25(4):1970-9.

Baldwin PM, Adler J, Davies MC, Melia CD. 1998. High resolution imaging of starch granule surfaces by atomic force microscopy. Journal of Cereal Science 27(3):255-65.

Ball S, Guan H, James M, Myers A, Keeling P, Mouille G, Buléon A, Colonna P, Preiss J. 1996. From glycogen to amylopectin: a model for the biogenesis of the plant starch granule. Cell 86(3):349-52.

Barreras-Urbina CG, Ramírez-Wong B, López-Ahumada GA, Burruel-Ibarra SE, Martínez-Cruz O, Tapia-Hernández JA, Rodríguez Félix F. 2016. Nano- and micro-particles by nanoprecipitation: possible application in the food and agricultural industries. International Journal of Food Properties 19(9):1912-23.

Bel Haaj S, Thielemans W, Magnin A, Boufi S. 2016. Starch nanocrystals and starch nanoparticles from waxy maize as nanoreinforcement: A comparative study. Carbohydrate Polymers 143:310-7.

Bel Haaj S, Magnin A, Pétrier C, Boufi S. 2013. Starch nanoparticles formation via high power ultrasonication. Carbohydrate Polymers 92(2):1625-32.

Bernardino-Nicanor A, Bernardino-Nicanor A, Acosta-García G, Acosta-García G, Güemes-Vera N, Güemes-Vera N, Montañez-Soto J, Montañez-Soto J, de los Ángeles Vivar-Vera, María, de los Ángeles Vivar-Vera, María, González-Cruz L, González-Cruz L. 2017. Fourier transform infrared and Raman spectroscopic study of the effect of the thermal treatment and extraction methods on the characteristics of ayocote bean starches. Journal of Food Science and Technology 54(4):933-43.

Birt DF, Boylston T, Hendrich S, Jane J, Hollis J, Li L, McClelland J, Moore S, Phillips GJ, Rowling M, Schalinske K, Scott MP, Whitley EM. 2013. Resistant starch: promise for improving human health. Advances in Nutrition 4(6):587-601.

Blazek J, Copeland L. 2008. Pasting and swelling properties of wheat flour and starch in relation to amylose content. Carbohydrate Polymers 71(3):380-7.

Bogracheva TY, Morris VJ, Ring SG, Hedley CL. 1998. The granular structure of C-type pea starch and its role in gelatinization. Biopolymers 45(4):323-32.

Brick MC, Palmer HJ, Whitesides TH. 2003. Formation of colloidal dispersions of organic materials in aqueous media by solvent shifting. Langmuir 19(16):6367-80.

Bteich J, McManus SA, Ernsting MJ, Mohammed MZ, Prud'homme RK, Sokoll KK. 2017. Using flash nanoprecipitation to produce highly potent and stable cellax nanoparticles from amphiphilic polymers derived from carboxymethyl cellulose, polyethylene glycol, and cabazitaxel. Molecular Pharmaceutics 14(11):3998-4007.

Bu X, Wang X, Dai L, Ji N, Xiong L, Sun Q. 2020. The combination of starch nanoparticles and Tween 80 results in enhanced emulsion stability. International Journal of Biological Macromolecules 163:2048-59.

Buléon A, Colonna P, Planchot V, Ball S. 1998. Starch granules: structure and biosynthesis. International Journal of Biological Macromolecules 23(2):85-112.

Cai J, Cai C, Man J, Zhou W, Wei C. 2014. Structural and functional properties of C-type starches. Carbohydrate Polymers 101:289-300.

Chang Y, Yan X, Wang Q, Ren L, Tong J, Zhou J. 2017a. Influence of ultrasonic treatment on formation of amylose nanoparticles prepared by nanoprecipitation. Carbohydrate Polymers 157:1413-8.

Chang Y, Yan X, Wang Q, Ren L, Tong J, Zhou J. 2017b. High efficiency and low cost preparation of size controlled starch nanoparticles through ultrasonic treatment and precipitation. Food Chemistry 227:369-75.

Chen M, Bergman CJ. 2007. Method for determining the amylose content, molecular weights, and weight- and molar-based distributions of degree of polymerization of amylose and fine-structure of amylopectin. Carbohydrate Polymers 69(3):562-78.

Chen Y, Dai G, Gao Q. 2019. Starch nanoparticles–graphene aerogels with high supercapacitor performance and efficient adsorption. ACS Sustainable Chemistry & Engineering 7(16):14064-73.

Chen Y, Cao X, Chang PR, Huneault MA. 2008. Comparative study on the films of poly(vinyl alcohol)/pea starch nanocrystals and poly(vinyl alcohol)/native pea starch. Carbohydrate Polymers 73(1):8-17.

Chin SF, Pang SC, Tay SH. 2011. Size controlled synthesis of starch nanoparticles by a simple nanoprecipitation method. Carbohydrate Polymers 86(4):1817-9.

Chin SF, Akmar SN, Yazid M, Pang SC. 2014. Preparation and characterization of starch nanoparticles for controlled release of curcumin. International Journal of Polymer Science 2014(1):1-8.

Chrastil J. 1987. Improved colorimetric determination of amylose in starches or flours. Carbohydrate Research 159(1):154-8.

Chun A, Lee H, Hamaker BR, Janaswamy S. 2015. Effects of ripening temperature on starch structure and gelatinization, pasting, and cooking properties in rice (*oryza sativa*). Journal of Agricultural and Food Chemistry 63(12):3085-93.

Chung H, Liu Q, Hoover R. 2010. Effect of single and dual hydrothermal treatments on the crystalline structure, thermal properties, and nutritional fractions of pea, lentil, and navy bean starches. Food Research International 43(2):501-8.

Chung H, Hoover R, Liu Q. 2009. The impact of single and dual hydrothermal modifications on the molecular structure and physicochemical properties of normal corn starch. International Journal of Biological Macromolecules 44(2):203-10.

Chung H, Liu Q, Hoover R. 2009. Impact of annealing and heat-moisture treatment on rapidly digestible, slowly digestible and resistant starch levels in native and gelatinized corn, pea and lentil starches. Carbohydrate Polymers 75(3):436-47.

Chung H, Liu Q, Donner E, Hoover R, Warkentin TD, Vandenberg B. 2008. Composition, molecular structure, properties, and in vitro digestibility of starches from newly released canadian pulse cultivars. Cereal Chemistry 85(4):471-9.

Cohen JM, Beltran-Huarac J, Pyrgiotakis G, Demokritou P. 2018. Effective delivery of sonication energy to fast settling and agglomerating nanomaterial suspensions for cellular studies: Implications for stability, particle kinetics, dosimetry and toxicity. NanoImpact 10:81-6.

Cooke D, Gidley MJ. 1992. Loss of crystalline and molecular order during starch gelatinisation: origin of the enthalpic transition. Carbohydrate Research 227:103-12.

D'Addio SM, Prud'homme RK. 2011. Controlling drug nanoparticle formation by rapid precipitation. Advanced Drug Delivery Reviews 63(6):417-26.

Dai L, Li C, Zhang J, Cheng F. 2018. Preparation and characterization of starch nanocrystals combining ball milling with acid hydrolysis. Carbohydrate Polymers 180(Supplement C):122-7.

Danilovas PP, Navikaite V, Rutkaite R. 2014. Preparation and characterization of potentially antimicrobial polymer films containing starch nano- and microparticles. Medžiagotyra 20(3):283-8.

Dhital S, Warren FJ, Butterworth PJ, Ellis PR, Gidley MJ. 2017. Mechanisms of starch digestion by α-amylase—Structural basis for kinetic properties. Critical Reviews in Food Science and Nutrition 57(5):875-92.

Ding S, Anton N, Vandamme TF, Serra CA. 2016. Microfluidic nanoprecipitation systems for preparing pure drug or polymeric drug loaded nanoparticles: an overview. Expert Opinion on Drug Delivery 13(10):1447-60.

Dong Y, Chang Y, Wang Q, Tong J, Zhou J. 2015. Effect of operating conditions on size and morphology of amylose nanoparticles prepared by precipitation. Starch - Stärke 67(3-4):365-72.

Donovan JW. 1979. Phase transitions of the starch–water system. Biopolymers 18(2):263-75.

Dufresne A. 2014. Crystalline starch based nanoparticles. Current Opinion in Colloid & Interface Science 19(5):397-408.

Eerlingen RC, Delcour JA. 1995. Formation, analysis, structure and properties of type III enzyme resistant starch. Journal of Cereal Science 22(2):129-38.

El-Naggar ME, El-Rafie MH, El-sheikh MA, El-Feky GS, Hebeish A. 2015. Synthesis, characterization, release kinetics and toxicity profile of drug-loaded starch nanoparticles. International Journal of Biological Macromolecules 81:718-29.

Englyst HN, Kingman SM, Cummings JH. 1992. Classification and measurement of nutritionally important starch fractions. European Journal of Clinical Nutrition 46(SUPPL. 2):S33-s50.

Everett DH. 1988. Basic principles of colloid science. London: Royal Soc. of Chemistry.

Fannon JE, Gray JA, Gunawan N, Huber KC, BeMiller JN. 2004. Heterogeneity of starch granules and the effect of granule channelization on starch modification. Cellulose 11(2):247-54.

Franco CML, Wong K, Yoo S, Jane J. 2002. Structural and functional characteristics of selected soft wheat starches. Cereal Chemistry 79(2):243-8.

Gallant DJ, Bouchet B, Buleon A, Perea S. 1992. Physical characteristics of starch granules and susceptibility to enzymatic degradation. European Journal of Clinical Nutrition 46:3-16.

Gallant DJ, Bouchet B, Baldwin PM. 1997. Microscopy of starch: evidence of a new level of granule organization. Carbohydrate Polymers 32(3):177-91.

Gao J, Vasanthan T, Hoover R. 2009. Isolation and characterization of high-purity starch isolates from regular, waxy, and high-amylose hulless barley grains. Cereal Chemistry 86(2):157-63.

Ge S, Xiong L, Li M, Liu J, Yang J, Chang R, Liang C, Sun Q. 2017. Characterizations of Pickering emulsions stabilized by starch nanoparticles: Influence of starch variety and particle size. Food Chemistry 234:339-47.

Gidley MJ. 1989. Molecular mechanisms underlying amylose aggregation and gelation. Macromolecules 22(1):351-8.

Glasser A, Cloutet E, Hadziioannou G, Kellay H. 2019. Tuning the rheology of conducting polymer inks for various deposition processes. Chemistry of Materials 31(17):6936-44.

Godet MC, Buléon A, Tran V, Colonna P. 1993. Structural features of fatty acid-amylose complexes. Carbohydrate Polymers 21(2-3):91-5.

Gomand SV, Verwimp T, Goesaert H, Delcour JA. 2011. Structural and physicochemical characterisation of rye starch. Carbohydrate Research 346(17):2727-35.

Gong X, Wang Y, Chen L. 2017. Enhanced emulsifying properties of wood-based cellulose nanocrystals as Pickering emulsion stabilizer. Carbohydrate Polymers 169:295-303.

Gunaratne A, Hoover R. 2002. Effect of heat–moisture treatment on the structure and physicochemical properties of tuber and root starches. Carbohydrate Polymers 49(4):425-37.

Gunasekera, S. U. A. K, Stoddard FL, Marshall DR. 1999. Variation in faba bean amylose content. Starch - Stärke 51(7):259-62.

Guo L, Deng Y, Lu L, Zou F, Cui B. 2019. Synergistic effects of branching enzyme and transglucosidase on the modification of potato starch granules. International Journal of Biological Macromolecules 130:499-507.

Gutiérrez G, Morán D, Marefati A, Purhagen J, Rayner M, Matos M. 2020. Synthesis of controlled size starch nanoparticles (SNPs). Carbohydrate Polymers 250:116938.

Haase NU, Shi HL. 1991. A characterization of faba bean starch (*Vicia fabaL.*). Starch - Stärke 43(6):205-8.

Hall C, Hillen C, Garden Robinson J. 2017. Composition, nutritional value, and health benefits of pulses. Cereal Chemistry 94(1):11-31.

Han J, Zhou C, Wu Y, Liu F, Wu Q. 2013. Self-assembling behavior of cellulose nanoparticles during freeze-drying: effect of suspension concentration, particle size, crystal structure, and surface charge. Biomacromolecules 14(5):1529-40.

Han J, BeMiller JN. 2007. Preparation and physical characteristics of slowly digesting modified food starches. Carbohydrate Polymers 67(3):366-74.

Hebeish A, El-Rafie M, EL-Sheikh M, El-Naggar M. 2014. Ultra-fine characteristics of starch nanoparticles prepared using native starch with and without surfactant. Journal of Inorganic and Organometallic Polymers and Materials 24(3):515-24.

Hedayati S, Niakousari M, Mohsenpour Z. 2020. Production of tapioca starch nanoparticles by nanoprecipitation-sonication treatment. International Journal of Biological Macromolecules 143:136-42.

Hirsch JB, Kokini JL. 2002. Understanding the mechanism of cross-linking agents (POCl₃, STMP, and SPI) through swelling behavior and pasting properties of cross-linked waxy maize starches. Cereal Chemistry 79(1):102-7.

Hizukuri S. 1986. Polymodal distribution of the chain lengths of amylopectins, and its significance. Carbohydrate Research 147(2):342-7.

Hoover R. 1995. Starch retrogradation. Food Reviews International 11(2):331-46.

Hoover R, Ratnayake WS. 2002. Starch characteristics of black bean, chick pea, lentil, navy bean and pinto bean cultivars grown in Canada. Food Chemistry 78(4):489-98.

Hoover R, Sosulski F. 1986. Effect of cross-linking on functional properties of legume starches. Starch - Stärke 38(5):149-55.

Hoover R, Hadziyev D. 1981. Characterization of potato starch and its monoglyceride complexes. Starch - Stärke 33(9):290-300.

Hoover R, Hughes T, Chung HJ, Liu Q. 2010. Composition, molecular structure, properties, and modification of pulse starches: A review. Food Research International 43(2):399-413.

Huang J, Schols HA, Jin Z, Sulmann E, Voragen AGJ. 2007. Characterization of differently sized granule fractions of yellow pea, cowpea and chickpea starches after modification with acetic anhydride and vinyl acetate. Carbohydrate Polymers 67(1):11-20.

Huber KC, BeMiller JN. 2001. Location of sites of reaction within starch granules. Cereal Chemistry 78(2):173-80.

Iida Y, Tuziuti T, Yasui K, Towata A, Kozuka T. 2008. Control of viscosity in starch and polysaccharide solutions with ultrasound after gelatinization. Innovative Food Science & Emerging Technologies 9(2):140-6.

Jane J, Wong K, McPherson AE. 1997. Branch-structure difference in starches of A- and B-type X-ray patterns revealed by their Naegeli dextrins. Carbohydrate Research 300(3):219-27.

Jane J, Xu A, Radosavljevic M, Seib PA. 1992. Location of amylose in normal starch granules. I. Susceptibility of amylose and amylopectin to cross-linking reagents. Cereal Chemistry 69 (4): 405-9.

Jane J, Chen YY, Lee LF, McPherson AE, Wong KS, Radosavljevic M, Kasemsuwan T. 1999. Effects of amylopectin branch chain length and amylose content on the gelatinization and pasting properties of starch. Cereal Chemistry 76(5):629-37.

Javidi F, Razavi SMA, Mohammad Amini A. 2019. Cornstarch nanocrystals as a potential fat replacer in reduced fat O/W emulsions: A rheological and physical study. Food Hydrocolloids 90:172-81.

Jeong O, Shin M. 2018. Preparation and stability of resistant starch nanoparticles, using acid hydrolysis and cross-linking of waxy rice starch. Food Chemistry 256:77-84.

Ji N, Qin Y, Li M, Xiong L, Qiu L, Bian X, Sun Q. 2018. Fabrication and characterization of starch nanohydrogels via reverse emulsification and internal gelation. Journal of Agricultural and Food Chemistry 66(35):9326-34.

Jiang S, Liu C, Han Z, Xiong L, Sun Q. 2016. Evaluation of rheological behavior of starch nanocrystals by acid hydrolysis and starch nanoparticles by self-assembly: A comparative study. Food Hydrocolloids 52:914-22.

Johnson BK, Prud'homme RK. 2003. Flash nanoprecipitation of organic actives and block copolymers using a confined impinging jets mixer. Australian Journal of Chemistry 56(10):1021-4.

Joye IJ. 2019. Starch. In: Melton L, Shahidi F, Varelis P, editors. Encyclopedia of Food Chemistry. Oxford: Academic Press. p 256-64.

Joye IJ, McClements DJ. 2013. Production of nanoparticles by anti-solvent precipitation for use in food systems. Trends in Food Science & Technology 34(2):109-23.

Jung J, Kasi G, Seo J. 2018. Development of functional antimicrobial papers using chitosan/starch-silver nanoparticles. International Journal of Biological Macromolecules 112:530-6.

Karnik R, Gu F, Basto P, Cannizzaro C, Dean L, Kyei-Manu W, Langer R, Farokhzad OC. 2008. Microfluidic platform for controlled synthesis of polymeric nanoparticles. Nano Letters 8(9):2906-12.

Kaur J, Kaur G, Sharma S. 2019. Corn starch nanoparticles: Preparation, characterization, and utilization as a fat replacer in salad dressing. Acta Alimentaria (Budapest) 48(2):204-12.

Kim H, Lee JH, Kim J, Lim W, Lim S. 2012. Characterization of nanoparticles prepared by acid hydrolysis of various starches. Starch - Stärke 64(5):367-73.

Kim H, Park SS, Lim S. 2015. Preparation, characterization and utilization of starch nanoparticles. Colloids and Surfaces B: Biointerfaces 126:607-20.

Kim JH, Park DH, Kim J. 2017. Effect of heat-moisture treatment under mildly acidic condition on fragmentation of waxy maize starch granules into nanoparticles. Food Hydrocolloids 63:59-66.

Kim J, Park D, Lim S. 2008. Fragmentation of waxy rice starch granules by enzymatic hydrolysis. Cereal Chemistry 85(2):182-7.

Kim Y, Lee Chung B, Ma M, Mulder WJM, Fayad ZA, Farokhzad OC, Langer R. 2012. Mass production and size control of lipid–polymer hybrid nanoparticles through controlled microvortices. Nano Letters 12(7):3587-91.

Klucinec JD, Thompson DB. 1999. Amylose and amylopectin interact in retrogradation of dispersed high-amylose starches. Cereal Chemistry 76(2):282-91.

Koo SH, Lee KY, Lee HG. 2010. Effect of cross-linking on the physicochemical and physiological properties of corn starch. Food Hydrocolloids 24(6):619-25.

Kou T, Gao Q. 2018. New insight in crosslinking degree determination for crosslinked starch. Carbohydrate Research 458-459:13-8.

Kristo E, Biliaderi CG. 2007. Physical properties of starch nanocrystal-reinforced pullulan films. Carbohydrate Polymers 68(1):146-58.

Krystyjan M, Sikora M, Adamczyk G, Dobosz A, Tomasik P, Berski W, Łukasiewicz M, Izak P. 2016. Thixotropic properties of waxy potato starch depending on the degree of the granules pasting. Carbohydrate Polymers 141:126-34.

Kügler RT, Kind M. 2016. Experimental study about plugging in confined impinging jet mixers during the precipitation of strontium sulfate. Chemical Engineering and Processing: Process Intensification 101:25-32.

Lammari N, Louaer O, Meniai AH, Elaissari A. 2020. Encapsulation of essential oils via nanoprecipitation process: overview, progress, challenges and prospects. Pharmaceutics 12(5):431.

Lan H, Hoover R, Jayakody L, Liu Q, Donner E, Baga M, Asare EK, Hucl P, Chibbar RN. 2008. Impact of annealing on the molecular structure and physicochemical properties of normal, waxy and high amylose bread wheat starches. Food Chemistry 111(3):663-75.

Landerito NA, Wang Y. 2005. Preparation and properties of starch phosphates using waxy, common, and high-amylose corn starches. II. reactive extrusion method. Cereal Chemistry 82(3):271-6.

Le Corre D, Angellier-Coussy H. 2014. Preparation and application of starch nanoparticles for nanocomposites: A review. Reactive & Functional Polymers 85:97-120.

Le Corre D, Bras J, Dufresne A. 2010. Starch nanoparticles: a review. Biomacromolecules 11(5):1139-53.

LeCorre D, Bras J, Dufresne A. 2012. Influence of native starch's properties on starch nanocrystals thermal properties. Carbohydrate Polymers 87(1):658-66.

LeCorre D, Bras J, Dufresne A. 2011. Influence of botanic origin and amylose content on the morphology of starch nanocrystals. Journal of Nanoparticle Research : an Interdisciplinary Forum for Nanoscale Science and Technology 13(12):7193-208.

Lee D, Park EY, Lim S. 2019. Effects of partial debranching and storage temperature on recrystallization of waxy maize starch. International Journal of Biological Macromolecules 140:350-7.

Lee JH, Park SY, Choi I, Choi JW. 2020. Investigation of molecular size effect on the formation of lignin nanoparticles by nanoprecipitation. Applied Sciences 10(14):4910.

Li C, Sun P, Yang C. 2012. Emulsion stabilized by starch nanocrystals. Die Stärke 64(6):497-502.

Li J, Shin GH, Lee IW, Chen X, Park HJ. 2016. Soluble starch formulated nanocomposite increases water solubility and stability of curcumin. Food Hydrocolloids 56:41-9.

Li K, Zhang X, Huang Q, Yin S, Yang X, Wen Q, Tang C, Lai F. 2014. Continuous preparation of zein colloidal particles by Flash NanoPrecipitation (FNP). Journal of Food Engineering 127:103-10.

Li L, Yuan TZ, Setia R, Raja RB, Zhang B, Ai Y. 2019. Characteristics of pea, lentil and faba bean starches isolated from air-classified flours in comparison with commercial starches. Food Chemistry 276:599-607.

Li M, Wu Q, Song K, Lee S, Qing Y, Wu Y. 2015. Cellulose nanoparticles: structure–morphology–rheology relationships. ACS Sustainable Chemistry & Engineering 3(5):821-32.

Li Y, Liu C, Tan Y, Xu K, Lu C, Wang P. 2014. In situ hydrogel constructed by starch-based nanoparticles via a Schiff base reaction. Carbohydrate Polymers 110: 87-94.

Lim S, Seib PA. 1993. Preparation and pasting properties of wheat and corn starch phosphates. Cereal Chemistry 70(2):137-44.

Lin N, Huang J, Dufresne A. 2012. Preparation, properties and applications of polysaccharide nanocrystals in advanced functional nanomaterials: a review. Nanoscale 4(11):3274-94.

Lin N, Yu J, Chang PR, Li J, Huang J. 2011. Poly(butylene succinate)-based biocomposites filled with polysaccharide nanocrystals: Structure and properties. Polymer Composites 32(3):472-82.

Liu C, Qin Y, Li X, Sun Q, Xiong L, Liu Z. 2016. Preparation and characterization of starch nanoparticles via self-assembly at moderate temperature. International Journal of Biological Macromolecules 84:354-60.

Liu C, Ge S, Yang J, Xu Y, Zhao M, Xiong L, Sun Q. 2016. Adsorption mechanism of polyphenols onto starch nanoparticles and enhanced antioxidant activity under adverse conditions. Journal of Functional Foods 26:632-44.

Liu D, Wu Q, Chen H, Chang PR. 2009. Transitional properties of starch colloid with particle size reduction from micro- to nanometer. Journal of Colloid and Interface Science 339(1):117-24.

Liu M, Zhang X, Yang B, Li Z, Deng F, Yang Y, Zhang X, Wei Y. 2015. Fluorescent nanoparticles from starch: Facile preparation, tunable luminescence and bioimaging. Carbohydrate Polymers 121:49-55.

Lu K, Miao M, Ye F, Cui SW, Li X, Jiang B. 2016. Impact of dual-enzyme treatment on the octenylsuccinic anhydride esterification of soluble starch nanoparticle. Carbohydrate Polymers 147:392-400.

Mahmoudi Najafi SH, Baghaie M, Ashori A. 2016. Preparation and characterization of acetylated starch nanoparticles as drug carrier: Ciprofloxacin as a model. International Journal of Biological Macromolecules 87:48-54.

Martínez Rivas CJ, Tarhini M, Badri W, Miladi K, Greige-Gerges H, Nazari QA, Galindo Rodríguez SA, Román RÁ, Fessi H, Elaissari A. 2017. Nanoprecipitation process: From encapsulation to drug delivery. International Journal of Pharmaceutics 532(1):66-81.

McPherson AE, Jane J. 1999. Comparison of waxy potato with other root and tuber starches. Carbohydrate Polymers 40(1):57-70.

Mirmoghtadaie L, Kadivar M, Shahedi M. 2009. Effects of cross-linking and acetylation on oat starch properties. Food Chemistry 116(3):709-13.

Miskeen S, Hong JS, Choi H, Kim J. 2021. Fabrication of citric acid-modified starch nanoparticles to improve their thermal stability and hydrophobicity. Carbohydrate Polymers 253: 117242.

Mohaghegh SMS, Barikani M, Entezami AA. 2006. The effect of grafted poly(ethylene glycol monomethyl ether) on particle size and viscosity of aqueous polyurethane dispersions. Colloids and surfaces. A, Physicochemical and Engineering Aspects 276(1-3):95-9.

Morrison WR, Laignelet B. 1983. An improved colorimetric procedure for determining apparent and total amylose in cereal and other starches. Journal of Cereal Science 1(1):9-20.

Mua JP, Jackson DS. 1997. Fine Structure of Corn Amylose and Amylopectin Fractions with Various Molecular Weights. Journal of Agricultural and Food Chemistry 45(10):3840-7.

Naguleswaran S, Vasanthan T, Hoover R, Bressler D. 2014. Amylolysis of amylopectin and amylose isolated from wheat, triticale, corn and barley starches. Food Hydrocolloids 35: 686-93.

Naguleswaran S, Vasanthan T, Hoover R, Bressler D. 2013. The susceptibility of large and small granules of waxy, normal and high-amylose genotypes of barley and corn starches toward amylolysis at sub-gelatinization temperatures. Food Research International 51(2):771-82.

Naguleswaran S, Li J, Vasanthan T, Bressler D, Hoover R. 2012. Amylolysis of large and small granules of native triticale, wheat and corn starches using a mixture of α-amylase and glucoamylase. Carbohydrate Polymers 88(3):864-74.

Nallasamy P, Ramalingam T, Nooruddin T, Shanmuganathan R, Arivalagan P, Natarajan S. 2020. Polyherbal drug loaded starch nanoparticles as promising drug delivery system: Antimicrobial, antibiofilm and neuroprotective studies. Process Biochemistry 92:355-64.

Narayanan D, Nair S, Menon D. 2015. A systematic evaluation of hydroxyethyl starch as a potential nanocarrier for parenteral drug delivery. International Journal of Biological Macromolecules 74:575-84.

Nikoubashman A, Lee VE, Sosa C, Prud'homme RK, Priestley RD, Panagiotopoulos AZ. 2016. Directed assembly of soft colloids through rapid solvent exchange. ACS Nano 10(1):1425-33.

O'Brien S, Wang Y. 2008. Susceptibility of annealed starches to hydrolysis by α-amylase and glucoamylase. Carbohydrate Polymers 72(4):597-607.

Park EY, Kim M, Cho M, Lee JH, Kim J. 2016. Production of starch nanoparticles using normal maize starch via heat-moisture treatment under mildly acidic conditions and homogenization. Carbohydrate Polymers 151:274-82.

Park EY, Ma J, Kim J, Lee DH, Kim SY, Kwon D, Kim J. 2018. Effect of dual modification of HMT and crosslinking on physicochemical properties and digestibility of waxy maize starch. Food Hydrocolloids 75:33-40.

Paul T, Chatterjee S, Bandyopadhyay A, Chattopadhyay D, Basu S, Sarkar K. 2015. A simple one pot purification of bacterial amylase from fermented broth based on affinity toward starch-functionalized magnetic nanoparticle. Preparative Biochemistry & Biotechnology 45(6):501-14.

Perera C, Lu Z, Sell J, Jane J. 2001. Comparison of physicochemical properties and structures of sugary‐2 cornstarch with normal and waxy cultivars. Cereal Chemistry 78(3):249-56.

Perez Herrera M, Vasanthan T, Chen L. 2017. Rheology of starch nanoparticles as influenced by particle size, concentration and temperature. Food Hydrocolloids 66:237-45.

Perez Herrera M, Vasanthan T, Hoover R. 2016. Characterization of maize starch nanoparticles prepared by acid hydrolysis. Cereal Chemistry 93(3):323-30.

Perez Herrera M, Vasanthan T, Hoover R, Izydorczyk M. 2017. Molecular size distribution and amylase resistance of maize starch nanoparticles prepared by acid hydrolysis. Cereal Chemistry 94(2):262-9.

Pérez S, Bertoft E. 2010. The molecular structures of starch components and their contribution to the architecture of starch granules: A comprehensive review. Starch - Stärke 62(8):389-420.

Pickering SU. 1907. CXCVI.- Emulsions. Journal of the Chemical Society Transactions. 91:2001-21.

Pilling E, Smith AM. 2003. Growth ring formation in the starch granules of potato tubers. Plant Physiology 132(1):365-71.

Putaux J, Molina-Boisseau S, Momaur T, Dufresne A. 2003. Platelet nanocrystals resulting from the disruption of waxy maize starch granules by acid hydrolysis. Biomacromolecules 4(5):1198-202.

Qin Y, Liu C, Jiang S, Xiong L, Sun Q. 2016. Characterization of starch nanoparticles prepared by nanoprecipitation: Influence of amylose content and starch type. Industrial Crops and Products 87:182-90.

Qiu C, Qin Y, Zhang S, Xiong L, Sun Q. 2016. A comparative study of size-controlled worm-like amylopectin nanoparticles and spherical amylose nanoparticles: Their characteristics and the adsorption properties of polyphenols. Food Chemistry 213:579-87.

Qiu C, Yang J, Ge S, Chang R, Xiong L, Sun Q. 2016. Preparation and characterization of size-controlled starch nanoparticles based on short linear chains from debranched waxy corn starch. LWT 74:303-10.

Ratnayake WS, Hoover R, Shahidi F, Perera C, Jane J. 2001. Composition, molecular structure, and physicochemical properties of starches from four field pea (*Pisum sativum L.*) cultivars. Food Chemistry 74(2):189-202.

Rayner M, Timgren A, Sjöö M, Dejmek P. 2012. Quinoa starch granules: a candidate for stabilising food-grade Pickering emulsions. Journal of the Science of Food and Agriculture 92(9):1841-7.

Rubio-Hernández FJ, Carrique F, Ruiz-Reina E. 2004. The primary electroviscous effect in colloidal suspensions. Advances in Colloid and Interface Science 107(1):51-60.

Saad WS, Prud'homme RK. 2016. Principles of nanoparticle formation by flash nanoprecipitation. Nano Today 11(2):212-27.

Saari H, Fuentes C, Sjöö M, Rayner M, Wahlgren M. 2017. Production of starch nanoparticles by dissolution and non-solvent precipitation for use in food-grade Pickering emulsions. Carbohydrate Polymers 157:558-66.

Saari H, Heravifar K, Rayner M, Wahlgren M, Sjöö M. 2016. Preparation and characterization of starch particles for use in pickering emulsions. Cereal Chemistry 93(2):116-24.

Sadeghi R, Daniella Z, Uzun S, Kokini J. 2017. Effects of starch composition and type of non-solvent on the formation of starch nanoparticles and improvement of curcumin stability in aqueous media. Journal of Cereal Science 76:122-30.

Salam A, Lucia LA, Jameel H. 2013. Synthesis, characterization, and evaluation of chitosan-complexed starch nanoparticles on the physical properties of recycled paper furnish. ACS Applied Materials & Interfaces 5(21):11029-37.

Sang Y, Seib PA. 2006. Resistant starches from amylose mutants of corn by simultaneous heat-moisture treatment and phosphorylation. Carbohydrate Polymers 63(2):167-75.

Sang Y, Prakash O, Seib PA. 2007. Characterization of phosphorylated cross-linked resistant starch by 31P nuclear magnetic resonance (31P NMR) spectroscopy. Carbohydrate Polymers 67(2):201-12.

Sang Y, Seib PA, Herrera AI, Prakash O, Shi Y. 2010. Effects of alkaline treatment on the structure of phosphorylated wheat starch and its digestibility. Food Chemistry 118(2):323-7.

Schäfer B, Hecht M, Harting J, Nirschl H. 2010. Agglomeration and filtration of colloidal suspensions with DVLO interactions in simulation and experiment. Journal of Colloid and Interface Science 349(1):186-95.

Schwarz JC, Weixelbaum A, Pagitsch E, Löw M, Resch GP, Valenta C. 2012. Nanocarriers for dermal drug delivery: Influence of preparation method, carrier type and rheological properties. International Journal of Pharmaceutics 437(1-2):83-8.

Sevenou O, Hill SE, Farhat IA, Mitchell JR. 2002. Organisation of the external region of the starch granule as determined by infrared spectroscopy. International Journal of Biological Macromolecules 31(1):79-85.

Shabana S, Prasansha R, Kalinina I, Potoroko I, Bagale U, Shirish SH. 2019. Ultrasound assisted acid hydrolyzed structure modification and loading of antioxidants on potato starch nanoparticles. Ultrasonics Sonochemistry 51:444-50.

Shafiei-Sabet S, Hamad WY, Hatzikiriakos SG. 2012. Rheology of nanocrystalline cellulose aqueous suspensions. Langmuir 28(49):17124-33.

Shalviri A, Liu Q, Abdekhodaie MJ, Wu XY. 2010. Novel modified starch–xanthan gum hydrogels for controlled drug delivery: Synthesis and characterization. Carbohydrate Polymers 79(4):898-907.

Shen Y, Zhang N, Xu Y, Huang J, Yuan M, Wu D, Shu X. 2019. Physicochemical properties of hydroxypropylated and cross-linked rice starches differential in amylose content. International Journal of Biological Macromolecules 128:775-81.

Shi A, Wang L, Li D, Adhikari B. 2013. Suspensions of vacuum-freeze dried starch nanoparticles: Influence of NaCl on their rheological properties. Carbohydrate Polymers 94(2):782-90.

Shi A, Li D, Wang L, Adhikari B. 2012a. The effect of NaCl on the rheological properties of suspension containing spray dried starch nanoparticles. Carbohydrate Polymers 90(4):1530-7.

Shi A, Li D, Wang L, Adhikari B. 2012b. Rheological properties of suspensions containing cross-linked starch nanoparticles prepared by spray and vacuum freeze-drying methods. Carbohydrate Polymers 90(4):1732-8.

Shi A, Wang L, Li D, Adhikari B. 2012c. The effect of annealing and cryoprotectants on the properties of vacuum-freeze dried starch nanoparticles. Carbohydrate Polymers 88(4):1334-41.

Shi A, Li D, Wang L, Li B, Adhikari B. 2011. Preparation of starch-based nanoparticles through high-pressure homogenization and miniemulsion cross-linking: Influence of various process parameters on particle size and stability. Carbohydrate Polymers 83(4):1604-10.

Shrestha AK, Blazek J, Flanagan BM, Dhital S, Larroque O, Morell MK, Gilbert EP, Gidley MJ. 2012. Molecular, mesoscopic and microscopic structure evolution during amylase digestion of maize starch granules. Carbohydrate Polymers 90(1):23-33.

Shukri R, Shi Y. 2017. Structure and pasting properties of alkaline-treated phosphorylated cross-linked waxy maize starches. Food Chemistry 214:90-5.

Shukri R, Seib PA, Maningat CC, Shi Y. 2013. *In vitro* enzymatic testing method and digestion mechanism of cross-linked wheat starch. In: Anonymous Resistant Starch. Hoboken, NJ, USA: John Wiley & Sons, Inc. p 145-66.

Shukri R, Zhu L, Seib PA, Maningat C, Shi Y. 2015. Direct in-vitro assay of resistant starch in phosphorylated cross-linked starch. Bioactive Carbohydrates and Dietary Fibre 5(1):1-9.

Silverio J, Fredriksson H, Andersson R, Eliasson A-, Åman P. 2000. The effect of temperature cycling on the amylopectin retrogradation of starches with different amylopectin unit-chain length distribution. Carbohydrate Polymers 42(2):175-84.

Singh N, Singh S, Isono N, Noda T, Singh AM. 2009. Diversity in amylopectin structure, thermal and pasting properties of starches from wheat varieties/lines. International Journal of Biological Macromolecules 45(3):298-304.

Sipponen MH, Lange H, Ago M, Crestini C. 2018. Understanding lignin aggregation processes. a case study: budesonide entrapment and stimuli-controlled release from lignin nanoparticles. ACS Sustainable Chemistry & Engineering 6(7):9342-51.

Smith RJ, Caruso J. 1964. Determination of phosphorus. Methods in Carbohydrate Chemistry 4: 42-6.

Song D, Thio YS, Deng Y. 2011. Starch nanoparticle formation via reactive extrusion and related mechanism study. Carbohydrate Polymers 85(1):208-14.

Srichuwong S, Sunarti TC, Mishima T, Isono N, Hisamatsu M. 2005. Starches from different botanical sources II: Contribution of starch structure to swelling and pasting properties. Carbohydrate Polymers 62(1):25-34.

Steeneken PAM. 1989. Rheological properties of aqueous suspensions of swollen starch granules. Carbohydrate Polymers 11(1):23-42.

Stroock AD, Dertinger SKW, Ajdari A, Mezić I, Stone HA, Whitesides GM. 2002. Chaotic mixer for microchannels. Science 295(5555):647.

Sufi-Maragheh P, Nikfarjam N, Deng Y, Taheri-Qazvini N. 2019. Pickering emulsion stabilized by amphiphilic pH-sensitive starch nanoparticles as therapeutic containers. Colloids and surfaces, B, Biointerfaces 181:244-51.

Sui Z, Huber KC, BeMiller JN. 2013. Effects of the order of addition of reagents and catalyst on modification of maize starches. Carbohydrate Polymers 96(1):118-30.

Sun Q. 2018. Starch nanoparticles. In: Malin Sjöö, Lars Nilsson, editors. Starch in Food. Woodhead Publishing. p 691-745.

Sun Q, Gong M, Li Y, Xiong L. 2014. Effect of retrogradation time on preparation and characterization of proso millet starch nanoparticles. Carbohydrate Polymers 111:133-8.

Sun Q, Li G, Dai L, Ji N, Xiong L. 2014. Green preparation and characterisation of waxy maize starch nanoparticles through enzymolysis and recrystallisation. Food Chemistry 162:223-8.

Tan Y, Xu K, Li L, Liu C, Song C, Wang P. 2009. Fabrication of Size-Controlled Starch-Based Nanospheres by Nanoprecipitation. ACS Applied Materials & Interfaces 1(4):956-9.

Tang J, Lee MFX, Zhang W, Zhao B, Berry RM, Tam KC. 2014. Dual responsive pickering emulsion stabilized by poly[2-(dimethylamino)ethyl methacrylate] grafted cellulose nanocrystals. Biomacromolecules 15(8):3052-60.

Tattiyakul J, Rao MA. 2000. Rheological behavior of cross-linked waxy maize starch dispersions during and after heating. Carbohydrate Polymers 43(3):215-22.

Tester RF, Morrison WR. 1990. Swelling and gelatinization of cereal starches. I. Effects of amylopectin, amylose, and lipids. Cereal Chemistry. 67(6):551-7.

Tester RF, Karkalas J, Qi X. 2004. Starch—composition, fine structure and architecture. Journal of Cereal Science 39(2):151-65.

Thielemans W, Belgacem MN, Dufresne A. 2006. Starch nanocrystals with large chain surface modifications. Langmuir 22(10):4804-10.

Tyler RT, Youngs CG, Sosulski FW. 1981. Air classification of Legumes. I. separation efficiency, yield, and composition of the starch and protein fractions. Cereal Chemistry 58(2):144-8.

Uzun S, Kokini JL. 2014. Preparation and characterization of starch nanoparticles by desolvation method. Technical Proceedings of the 2014 NSTI Nanotechnology Conference and Expo, NSTI-Nanotech 2:297-300.

Valodkar M, Thakore S. 2010. Isocyanate crosslinked reactive starch nanoparticles for thermo-responsive conducting applications. Carbohydrate Research 345(16):2354-60.

van Soest JJG, Tournois H, de Wit D, Vliegenthart JFG. 1995. Short-range structure in (partially) crystalline potato starch determined with attenuated total reflectance Fourier-transform IR spectroscopy. Carbohydrate Research 279:201-14.

Varatharajan V, Hoover R, Liu Q, Seetharaman K. 2010. The impact of heat-moisture treatment on the molecular structure and physicochemical properties of normal and waxy potato starches. Carbohydrate Polymers 81(2):466-75.

Vasanthan T, Hoover R. 1992. Effect of defatting on starch structure and physicochemical properties. Food Chemistry 45(5):337-47.

Waduge RN, Xu S, Seetharaman K. 2010. Iodine absorption properties and its effect on the crystallinity of developing wheat starch granules. Carbohydrate Polymers 82(3):786-94.

Waigh TA, Gidley MJ, Komanshek BU, Donald AM. 2000. The phase transformations in starch during gelatinisation: a liquid crystalline approach. Carbohydrate Research 328(2):165-76.

Wang B, Li D, Wang L, Özkan N. 2010. Anti-thixotropic properties of waxy maize starch dispersions with different pasting conditions. Carbohydrate Polymers 79(4):1130-9.

Wang J, Zhang Q, Zhou Y, Shao L, Chen J. 2010. Microfluidic synthesis of amorphous cefuroxime axetil nanoparticles with size-dependent and enhanced dissolution rate. Chemical Engineering Journal 162(2):844-51.

Wang J, Hu P, Chen Z, Liu Q, Wei C. 2017. Progress in high-amylose cereal crops through inactivation of starch branching enzymes. Frontiers in Plant Science 8:469.

Wang L, Wang Y. 2001. Structures and Physicochemical Properties of Acid-Thinned Corn, Potato and Rice Starches. Starch - Stärke 53(11):570-6.

Wang W, Guan L, Seib PA, Shi Y. 2018. Settling volume and morphology changes in cross-linked and unmodified starches from wheat, waxy wheat, and waxy maize in relation to their pasting properties. Carbohydrate Polymers 196:18-26.

Wei B, Hu X, Li H, Wu C, Xu X, Jin Z, Tian Y. 2014. Effect of pHs on dispersity of maize starch nanocrystals in aqueous medium. Food Hydrocolloids 36:369-73.

Woo KS, Seib PA. 2002. Cross-linked resistant starch: preparation and properties. Cereal Chemistry 79(6):819-25.

Wu X, Chang Y, Fu Y, Ren L, Tong J, Zhou J. 2016. Effects of non-solvent and starch solution on formation of starch nanoparticles by nanoprecipitation. Die Stärke 68(3-4):258-63.

Wu Y, Seib PA. 1990. Acetylated and hydroxypropylated distarch phosphates from waxy barley: paste properties and freeze-thaw stability. Cereal Chemistry 67(2):202-8.

Xiao Z, Wang L, Lv C, Guo S, Lu X, Tao L, Duan Q, Yang Q, Luo Z. 2020. Preparation and characterization of pH-responsive Pickering emulsion stabilized by grafted carboxymethyl starch nanoparticles. International Journal of Biological Macromolecules 143:401-12.

Yan X, Chang Y, Wang Q, Fu Y, Zhou J. 2017. Effect of drying conditions on crystallinity of amylose nanoparticles prepared by nanoprecipitation. International Journal of Biological Macromolecules 97:481-8.

Yang J, Li F, Li M, Zhang S, Liu J, Liang C, Sun Q, Xiong L. 2017. Fabrication and characterization of hollow starch nanoparticles by gelation process for drug delivery application. Carbohydrate Polymers 173:223-32.

Yoo S. 2002. Molecular weights and gyration radii of amylopectins determined by high-performance size-exclusion chromatography equipped with multi-angle laser-light scattering and refractive index detectors. Carbohydrate Polymers 49(3):307-14.

Yu J, Ai F, Dufresne A, Gao S, Huang J, Chang PR. 2008. Structure and Mechanical Properties of Poly(lactic acid) Filled with (Starch nanocrystal)-graft-poly(ε-caprolactone). Macromolecular Materials and Engineering 293(9):763-70.

Zhang B, Li X, Liu J, Xie F, Chen L. 2013. Supramolecular structure of A- and B-type granules of wheat starch. Food Hydrocolloids 31(1):68-73.

Zheng H, Ai F, Chang PR, Huang J, Dufresne A. 2009. Structure and properties of starch nanocrystal-reinforced soy protein plastics. Polymer Composites 30(4):474-80.

Zhou D, Ma Z, Yin X, Hu X, Boye JI. 2019. Structural characteristics and physicochemical properties of field pea starch modified by physical, enzymatic, and acid treatments. Food Hydrocolloids 93:386-94.

Zhu Z, Margulis-Goshen K, Magdassi S, Talmon Y, Macosko CW. 2010. Polyelectrolyte stabilized drug nanoparticles via flash nanoprecipitation: a model study with β-carotene. Journal of Pharmaceutical Sciences 99(10):4295-306.

Zobel HF. 1988. Molecules to granules: a comprehensive starch review. Starch - Stärke 40(2):44-50.